Universidade de Aveiro Departamento de Ciências Médicas
2017

Joana Fernandes da Rocha

Caracterização das funções neurotróficas da Proteína Precursora de Amilóide de Alzheimer

Characterizing Alzheimer's Amyloid Precursor Protein (APP) neurotrophic functions

Universidade de Aveiro Departamento de Ciências Médicas
2017

Joana Fernandes da Rocha

Caracterização das funções neurotróficas da Proteína Precursora de Amilóide de Alzheimer

Characterizing Alzheimer's Amyloid Precursor Protein (APP) neurotrophic functions

Tese apresentada à Universidade de Aveiro para cumprimento dos requisitos necessários à obtenção do grau de Doutor em Biomedicina, realizada sob a orientação científica da Doutora Sandra Isabel Vieira, Professora Auxiliar Convidada do Departamento de Ciências Médicas da Universidade de Aveiro e da Doutora Odete da Cruz e Silva, Professora Auxiliar Convidada com Agregação do Departamento de Ciências Médicas da Universidade de Aveiro

Este trabalho é financiado por Fundos FEDER através do Programa Operacional Factores de Competitividade – COMPETE e por Fundos Nacionais através da FCT – Fundação para a Ciência e a Tecnologia no âmbito do projeto «PTDC/SAU-NMC/111980/2009»; por Fundos da FCT e do programa POPH/FSE no âmbito bolsa individual «SFRH/BD/ 78507/2011»; e pelo Instituto de Biomedicina – iBiMED «UID/BIM/04501/2013».

Dedico este trabalho às minhas sobrinhas Francisca e Clara.

o júri

presidente

Professor Doutor Luís António Ferreira Martins Dias Carlos
professor catedrático do Departamento de Física da Universidade de Aveiro

Doutor Uwe Konietzko
investigador sénior do Instituto de Medicina Regenerativa (IREM), Universidade de Zurique, Suíça

Doutora Cláudia Guimas de Almeida Gomes
investigadora auxiliar do Centro de Estudos de Doenças Crónicas (CEDOC), Faculdade de Ciências Médicas da Universidade Nova de Lisboa

Professora Doutora Ana Gabriela da Silva Cavaleiro Henriques
professora auxiliar convidada do Departamento de Ciências Médicas da Universidade de Aveiro

Professora Doutora Sandra Isabel Moreira Pinto Vieira
professora auxiliar convidada do Departamento de Ciências Médicas da Universidade de Aveiro

agradecimentos

Aos meus pais, por todos os sacríficos que fizeram para que pudesse usufruir de educação superior.

À Professora Sandra Vieira e à Professora Odete da Cruz e Silva pela oportunidade de trabalhar neste projeto e pela orientação científica.

À Joana Vieira, amiga e colega de casa de tantos anos, e ao Miguel por evitarem que eu enlouquecesse a formatar este documento. Fico eternamente grata.

Aos meus colegas de trabalho desde o CBC ao iBiMED, a grande recompensa deste doutoramento. Um especial agradecimento aos meus colegas de doutoramento Filipa Martins, Joana Oliveira, e Roberto Dias. Ao Igor pelo suporte aos dramas informáticos. Aos alunos de mestrado que acompanhei mais de perto Regina, Lili, Páti, Ana, Luísa, Catarina, Soraia, Joana, Marlene, e Patrícia. Às colegas e vizinhas que nunca recusaram ajuda, Juliana e Maria. Aos colegas mais velhos pela partilha de conhecimentos, especialmente à Mariana. À minha (ex)"work wife" Sara.

To Uwe Konietzko and his team members Sarina, Sabine, and Sonja for their warm welcome and generosity.

Aos colegas de faculdade que me acompanharam mais de perto neste percurso Carina, Sofia, Ritinha, e Guida.

Às minhas amigas Sofia, Beatriz, Joana, Andreia, Ana. Num mundo dominado por aparências e materialismo, obrigada por me proporcionarem o prazer de uma longa e verdadeira amizade!

Ao Luís, o meu melhor amigo, por acreditar em mim mesmo quando eu própria duvidei.

palavras-chave

proteína precursora de amilóide de Alzheimer, fosforilação (S655), células SH-SY5Y, diferenciação neuronal, via do factor de crescimento epidermal, interacções proteína-proteína, sinalização intracelular.

resumo

A Proteína Precursora de Amilóide (APP) é uma proteína membranar mais conhecida por ser precursora do péptido Amilóide β, tendo por isso um papel central na doença de Alzheimer. Não obstante, a APP tem sido reconhecida como neuromodulador do sistema nervoso central. Alterações nos níveis ou na atividade da APP e seus fragmentos estão implicadas em diferentes doenças neurológicas. As relações entre o seu transporte intracelular, modificações pós-traducionais, corte proteolítico, e proteínas com as quais interage são complexas e multifacetadas. Talvez por isso, estudos focados no papel fisiológico da APP apresentem resultados contraditórios e muitas questões em aberto. O objetivo deste trabalho consistiu na caracterização do papel fisiológico da APP na diferenciação neuronal. Particularmente, focámo-nos nos mecanismos mediados pela APP e fragmento sAPP, e a fosforilação da APP no resíduo serina 655.

Inicialmente, caracterizámos a proteína APP ao longo da diferenciação de células SH-SY5Y com ácido retinóico (RA). A análise sistemática deste modelo permitiu delimitar uma resposta bifásica: na primeira fase (D0-D4), um pico de sAPP/APP acompanha o aparecimento de novos processos e o crescimento a neurites; na segunda fase (D4-D8) o aumento nos níveis da APP suporta o crescimento e manutenção das neurites.

Caracterizámos posteriormente a relação entre a APP e a via de sinalização EGF-EGFR-ERK na diferenciação neuronal. Demonstrámos, pela primeira vez, que a APP interage com o proEGF, e confirmámos a sua ligação ao EGFR. Adicionalmente, observámos que a APP e o EGF têm um efeito sinérgico na diferenciação tipo-neuronal e aumento da ativação da ERK1/2, e que a APP afeta os níveis e transporte do EGFR. Estes mecanismos são modulados pela fosforilação da APP na S655, que favorece a dendritogénese em neurónios corticais de ratinho.

Por último, focámo-nos na identificação de proteínas interatoras da APP dependentes da fosforilação em S655 e com função na diferenciação neuronal. Usando células SH-SY5Y diferenciadas e a sobrexpressar a APPWt ou fosfomutantes da S655, imunoprecipitámos as diferentes APPs e seus interatores, posteriormente identificados por espectrometria de massa. O interatoma da APP desfosforilada é enriquecido em funções associadas à organização do citoesqueleto, levando a uma maior reorganização da actina. O interatoma da APP fosforilada incluí proteínas envolvidas na regulação de sobrevivência e diferenciação, e em várias vias de sinalização, o que se correlaciona com o favorecimento de neurites nestas células.

Com este trabalho esperamos ter contribuído para uma melhor compreensão do papel neurotrófico da APP e dos mecanismos subjacentes a este.

keywords

Alzheimer's Amyloid Precursor Protein, (S655) phosphorylation, SH-SY5Y cells, neuronal differentiation, epidermal growth factor pathway, protein-protein interactors, intracellular signaling

abstract

The Amyloid Precursor Protein (APP) is a type 1 membrane glycoprotein, mainly known as the precursor of the amyloid β-peptide, a central player in Alzheimer's disease. Nevertheless, APP has been established as a neuromodulator of developing and mature nervous system. Alterations in the level or activity of APP and APP fragments seem to play a critical role in several neurodegenerative and neurodevelopment disorders. APP is a complex molecule due to the intricate relationships between its intracellular trafficking, posttranslational modifications, proteolytic cleavages, and multiple protein interactors. Various studies currently address the physiological roles of APP and its fragments, but there are contradictory results and missing pieces that need further work. The main objective of this thesis was to contribute to the characterization of the role of APP in neuronal differentiation. Particularly, we focused on mechanisms mediated by APP, its fragment sAPP, and APP phosphorylation at serine 655.

First, we characterized the APP protein in Retinoic Acid (RA)-induced SH-SY5Y cell differentiation. The comprehensive analysis of this model exposed a biphasic temporal response: a first early phase (D0-D4), where a sAPP/APP peak assists the emergence of new processes and their elongation into neurites; and a second phase (D4-D8) when increased holoAPP protein levels are necessary to sustain neuritic elongation and stabilization.

In line with our main aim, we subsequently characterized the relationship between APP and the neurotrophic EGF-EGFR-ERK signaling pathway. We showed, for the first time, that APP interacts with proEGF, and confirmed the interaction with EGFR. Furthermore, we showed that combined APP and EGF have a synergistic effect on neuronal-like differentiation, related to enhanced ERK1/2 activation, and observed that APP modulates EGFR expression levels and trafficking. Both ERK1/2 activation and EGFR seem to be modulated by the APP S655 phosphorylation state, and phosphorylation at this residue favours dendritogenesis in mice cortical neurons.

Finally, we focused on discovering APP protein interactors dependent on S655 phosphorylation and with a role in neuronal differentiation. SH-SY5Y differentiated cells, overexpressing APPWt or S655 phosphomutants, were used to immunoprecipitate the specific APP proteins and their respective interacting partners, later identified by mass spectrometry. The dephosphoS655 APP interactome was enriched in functions associated with cytoskeleton organization, and these cells were particularly associated with actin remodeling. The phosphoS655 APP interactome included proteins involved in the regulation of survival and differentiation, and in various signaling pathways, correlating well with an enhanced neurite outgrowth displayed by these cells.

We hope that the knowledge here gathered can contribute to a better comprehension of APP-driven neurotrophic roles and underlying mechanisms.

Table of Contents

Table of Figures

Table of Supplementary Figures

Table of Tables

Table of Supplementary Tables

Abbreviations

AD	Alzheimer's disease
ADAM	A disintegrin and metalloproteinase
ADP	Adenosine 5′-diphosphate
AICD	APP intracellular C-terminal domain
ANOVA	analysis of variance
APL-1	Beta-amyloid-like protein (C. elegans)
APLP1	Amyloid-like protein 1
APLP2	Amyloid-like protein 2
APP	Amyloid Precursor Protein
APP-BP1	Amyloid beta precursor protein-binding protein 1/ NEDD8-activating enzyme E1 regulatory subunit
APPL	Beta-amyloid-like protein (D. melanogaster)
APPL1	Adapter protein containing PH domain, PTB domain and leucine zipper motif 1/ DCC-interacting protein 13-alpha
ATP	Adenosine-5´-triphosphate
Aβ	amyloid β-peptide
BACE	beta-site APP-cleavage enzyme
BDNF	brain-derived neurotrophic factor
BMPs	bone morphogenetic proteins
BP	bipolar
BSA	Bovine Serum Albumin
CBD	Collagen binding domain
CBL	E3 ubiquitin-protein ligase Casitas B-lineage lymphoma
cDNA	complementary deoxyribonucleic acid
CNS	central nervous system
CP	cortical plate
CR	Cajal-Retzius cells
CSF	cerebrospinal fluid
CT	C-terminal
CTF	carboxy-terminal fragment
Dab	disable homolog
DIV	day(s) in vitro
dKO	double knock-out
DMEM	Dulbecco's Modified Eagle Medium
DS	Down's syndrome
Dvl	disheveled
ECM	extracellular matrix
EGF	epidermal growth factor
EGFP	Enhanced Green Fluorescent Protein
EGFR	Epidermal growth factor
EPSCs	excitatory postsynaptic current
ER	endoplasmic reticulum
Erk	Extracellular signal-regulated kinase
ESCRT	endosomal sorting complexes required for transport

FAK	focal adhesion kinase
FGF	basic fibroblast growth factor
FoxO	Forkhead box O
GABA	gamma-Aminobutyric acid
GFLD	growth factor-like domain
GFP	Green Fluorescent Protein
GO	gene ontology
Grb2	Growth factor receptor-bound protein 2
GSK-3	Glycogen synthase kinase-3
HBD	heparin binding domain
Hrar	Retinoic acid nuclear receptors
IGF	insulin-like growth factor
ILK	integrin linked kinase
ILV	intraluminal vesicles
IP	immunoprecipitation
IZ	intermediate zone
Jip	Jun N-terminal kinase interaction protein
JMR	juxtamembrane region
JNK	c-Jun (N)-terminal kinase
KO	knock-out
KPI	Kunitz proteinase inhibitor
LAMP	Lysosome-associated membrane glycoprotein
LRP1	low density lipoprotein receptor-related protein-1
LTP	long-term potentiation
MAP	microtubule-associated protein
MAZ	multipolar cell accumulation zone
MEK	Dual specificity mitogen-activated protein kinase kinase 1/ ERK activator kinase 1
MEM	Minimum Essential Media
MP	multipolar
mRNA	messenger ribonucleic acid
MS	mass spectrometry
MT	microtubules
MVB	Multivesicular Bodies
MZ	marginal zone
NDf	Non-diferentiated Final
NDi	Non-differentiated Initial
NEC	neuroepithelial cells
NF-kB	Nuclear factor-kB
NGF	nerve growth factor
NMJ	neuromuscular junction
NTF	N-terminal fragments
O/N	overnight
PBS	Phosphate-Buffered Saline
PBS-T	Phosphate-Buffered Saline Tween

PCP	planar cell polarity
PD	Parkinson's disease
PFA	paraformaldehyde
PhC	phase contrast
PK	protein kinase
PM	plasma membrane
PNS	peripheral nervous system
PS	Presenilin
PSD	post-synaptic density
PSM	peptide spectrum matches
RA	all-trans retinoic acid
RAREs	Retinoic acid response elements
RBP	RNA binding protein
RE	recycling endosome
RGC	radial glial cells
RIPA	Radioimmunoprecipitation assay
RNA	ribonucleic acid
RT	room temperature
sAPP	soluble amyloid precursor protein ectodomain
SDS	Sodium Dodecylsulfate
SEM	Standard error of the mean
Shc	Src homology 2 domain-containing-transforming protein
Shh	Sonic hedgehog protein
SNARE	soluble NSF (Vesicle-fusing ATPase) attachment protein receptor
SP	signal peptide
SP	subplate
SVZ	subventricular zone
TAPI	TNF-α processing inhibitor
TBS-T	Tris-Buffered Saline Tween
TF	transcription factor
TGF	Tranforming growth factor
TGN	Trans-Golgi network
TKR	tyrosine Kinase receptor
TM	transmembrane domain
TNF	Tumor necrosis factor
Trk	Tyrosine kinases
VPS	vacuolar protein sorting
VZ	ventricular zone
WB	western blot
Wt	wild-type

A. General Introduction and Aims

1. Nervous system development

We all start as a single cell – the fertilized egg. After some rounds of cell division and rearrangements, the embryoblast (future embryo) forms two monolayers of cells: the top layer (dorsal position) on the side of the amniotic cavity is the ectoderm, and the bottom layer (ventral position) is the endoderm [1]. In the vertebrates, the nervous system is derived from the embryonic ectoderm (that also generates the skin). Around the embryonic day 14, specialized regions on the midline ectoderm (caudal end of the embryo) – the primitive streak and primitive node – originate a third layer of cells between the ectoderm and endoderm – the mesoderm. These new cells, migrate rostrally along the midline to form the notochordal process, later the notochord. The notochordal cells have the ability to secrete factors (like the sonic hedgehog protein, Shh) that diffuse dorsally to induce changes in the ectoderm. Namely, the ectoderm starts to differentiate into a central, thicker, spoon-shape neural ectoderm – the neural plate, and separates from a peripheral ectoderm that will form the skin [1].

During neurulation, the neural plate invaginates into the mesodermal layer to originate the neural tube [1]. Closure of the neural tube separates the ventricular system from the amniotic fluid [2]. After the completely closure of the neural tube (embryonic day 30 in humans), three vesicles can be distinguished: the primary forebrain vesicle (prosencephalon), the primary midbrain vesicle (mesencephalon), and the primary hindbrain vesicle (rhombencephalon). In the caudal half lies the presumptive spinal cord. Later, neural tube regions are further divided to form a five vesicles-stage neural tube. The primary hindbrain forms, rostrally, the secondary hindbrain (epenchephalon) and, caudally, the after brain (metencephalon). The primary forebrain gives rise to the endbrain (telencephalon) and the interbrain (diencephalon) [1].

Between the neural plate/neural tube and the somatic ectoderm there is a transition zone – the neural crest – that will form most of the ganglia of the peripheral nervous system. The neural crest migrates ventrally into the developing body to form sensory and motor neurons. Other sensory neurons are derived from “isolated” placodes (specially differentiated somatic ectoderm) [1].

At the point of the five vesicles-stage neural tube plus the spinal cord segment, the neuroepithelium is still a monolayer of stem cells. However, the neuroepithelium displays a layered appearance because the nuclei of neuroepithelial cells migrate up and down the apical–basal axis during the cell cycle (a phenomenon named interkinetic nuclear movement). Furthermore, neuroepithelial cells (NEC) are highly polarized along their apical-basal axis, presenting tight junctions and adherens junctions at the most apical end of the plasma membrane (PM) [3]. NEC undergo symmetric proliferative divisions increasing the pool of stem cells, and these proliferative cells form the ventricular zone (VZ) [3, 4].

1.1. Neurogenesis and development of the cerebral cortex

Neurogenesis begins soon after neural tube closure, and occurs throughout the entire neural tube following specific and spatial patterns and rates along the caudal-rostral, ventral-dorsal, and lateral-medial body axes, originating a series of longitudinal grooves in the inner surface of the wall of the neural tube [1, 5]. Neurogenesis specific events will be here described based on the example of the mammalian cerebral cortex development, in other words corticogenesis, and specifically cortical projection neurons development.

The mature cerebral neocortex is comprised of six layers along the radial axis, with areal and columnar subdivisions along the tangential axis [6]. Cortical neurons can be divided in two major types: excitatory projection neurons (pyramidal neurons) and inhibitory interneurons. All cortical pyramidal neurons are derived from neural progenitors in the dorsal telencephalon VZ and subventricular zone (SVZ, described below) [7]. Some evidences show that the VZ generates the projection neurons of the deeper layers of the neocortex whereas the SVZ produces those of the more superficial layers [4, 7]. Inhibitory interneurons derive from radial glial cells (RGC) in the medial and caudal ganglionic eminences of the ventral telencephalon and from dorsal telencephalon SVZ. These neurons migrate first tangentially to reach the dorsal telencephalon and then radially within the different cortical layers (not detailed here) [2, 7].

At the point of neurogenesis, many asymmetric, self-renewing division occur that originate a daughter stem cell and a more differentiated cell [3, 4]. The second cell can be a non-stem-cell progenitor (commonly named intermediate progenitor) or a neuron. In parallel, NEC lose some epithelial features (like tight junctions) and transform into RGC [3]. This seems to be induced by a set of genes that includes forkhead box G1 (*FOXG1*), LIM homeobox 2 (*LHX2*), paired box 6 (*PAX6*) and empty spiracles homologue 2 (*EMX2*) [4]. RGC possess both properties of neuroepithelial and astroglial cells. Like NEC, these cells express nestin, present an apical surface, important features of apical-basal polarity (like apical centrosomes and the transmembrane protein prominin-1), adherens junction, and establish contact with the basal lamina. They also show interkinetic nuclear migration, although with some small differences comparing to NEC. The characteristics that completely distinguishing RGC from NEC are the astroglial properties like the presence of glycogen granules, and astrocyte molecules (GLAST, S100Beta, GFAP, vimentin and BLBP) [3]. Furthermore, there is differentially expression of some genes from region to region [4].

The transitions from NEC to RGC correlates with the onset of neurogenesis in almost all regions of the developing CNS (around E10 and E12 in mice, ~E33 in Humans) [3, 4].

Symmetric proliferative divisions of NEC, and of apical RGC, cause the lateral (tangential) expansion of the VZ. At the same time, both type of cells can increase their basolateral-to-apical

plasma membrane ratio and thus become more elongated inducing growth in the radial dimension [5]. The existence of a distinct population of apical intermediate progenitors was described - short neural precursors - that generally divide just once to produce postmitotic neurons [4]. So, within the VZ at least three different classes of neural precursors seem to cohabit: NECs, (apical) RGCs, and the short neural precursors (see Figure A.1, top image). Additionally, bipolar RGC and unipolar progenitor cells can be found in the basal VZ (subapical progenitors) [4, 5].

With time, dividing cells generated from the asymmetrical division of RGC, namely the resulting non-RGC daughter, migrate away from the ventricle, round up, and start to accumulate at the basal border of the VZ in a new compartment – SVZ. These intermediate or "basal" progenitors are also neurogenic, but contrarily to NEC and RGC, are not attached to the ventricular surface and do not display interkinetic nuclear movement [4]. Intermediate precursors express the transcription factors TBR2, neurogenin 2 (NGN2), cut-like homeobox 1 (CUX1) and CUX2, and the non-coding RNA SVET1 [3, 4]. Basal progenitors contribute to neurogenesis by undergoing symmetric, neurogenic cell divisions that generate two neuronal daughter cells. Additional neural progenitors can be found within the SVZ, namely basal RGC (originated from the subapical bipolar RGC) and transit amplifying progenitors (see Figure 1, bottom image) [5].

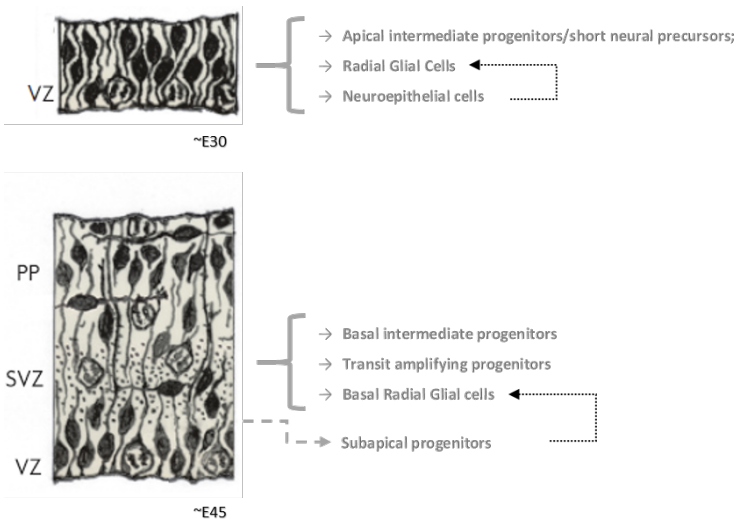

Figure A.1 - **Ventricular and Subventricular zone resident neural progenitor cells.** In the ventricular zone, during neurogenesis, neuroepithelial cells lose some epithelial features and transform into (apical) radial glial cells. When these cells perform asymmetric, self-renewing divisions they can originate a daughter stem cell and a more differentiated cell (upper image). The latter can be an intermediate progenitor or a neuron. In the basal ventricular zone bipolar radial glial cells and unipolar progenitors can also be found, collectively named subapical progenitors. With time, neural progenitors originated from basal radial glial divisions migrate away from the ventricle and accumulate in a new compartment – the subventricular zone (lower image). PP, preplate. Adapted from reference [4].

Asymmetric self-renewing divisions of NEC and apical RGC are the primary basis of neocortex expansion in the radial dimension. Animals with higher encephalization have more expanded SVZ,

with higher numbers and diversity of intermediate progenitors, which in turn correlates with increased number of neurons and thicker cortical layers [5, 8]. The mode of stem and progenitor cell division, cell fate choice, and programmed cell death plays a crucial role in establishing the correct number and organization (radial and tangential) of the cortex. Dysregulation of these processes might result in different development disorders, like microcephaly [9]. Several molecules, including transcription factors (TFs) regulate and coordinate cell fate and the appropriate mode of cell division. For instance, the anti-proliferative gene Tis21 is selectively expressed in essentially all NEC that are about to undergo a neurogenic division, but not in the proliferating ones. Also the TF factor PAX6 promotes asymmetric, neurogenic cell divisions, while the TF EMX2 appears to promote symmetric proliferative divisions [3, 10].

One aspect that seems fundamental in the determination of the proportion of symmetric, proliferative versus asymmetric, neurogenic divisions in NEC and RGC is the orientation of the mitotic spindle (and consequently the cleavage-plane orientation) that will establish, in turn, the symmetric versus asymmetric inheritance of specific subcellular components and molecules. Namely, it appears that the presence or absence of the apical PM (primarily defined by the position of the mitotic spindle), determines which daughter cell will be able to divide again and which will become a neuron, respectively. In order to follow a symmetric division there is to be fusion of the basal membrane with the apical membrane, which normally occurs via heterophilic fusion of the basal v-SNARE and the apical t-SNARE. This process allows that both cells keep portions of the apical PM. By the other hand, asymmetric/neurogenic division depends on hemophilic fusions between basal v-SNARE and lateral (tight-junction) t-SNARE. Such events suggest that there must be a signal(s) for proliferation that is transmitted through the apical membrane [3]. The apical membrane faces the ventricle which is filled with the cerebrospinal fluid (CSF). The CSF composition is dynamically regulated during development, and is rich in growth factors like the fibroblast growth factor (FGF), insulin-like growth factor (IGF), Shh, bone morphogenetic proteins (BMPs), and Wnts. Several receptors for these molecules were found in the apical PM, for example the glycoprotein megalin whose ligands include both BMPs and Shh; and the protein prominin-1 [5].

Furthermore, junctional components (cadherins and catenins, concentrated beneath the apical PM) have been reported to be asymmetrically partitioned during mitosis. For instance, β-catenin is an important downstream target of the Wnt pathway. Upon Wnt pathway activation there is accumulation of β-catenin (because its degradation complex GSK-3/APC/CK1 is inhibited) and its subsequent translocation to the nucleus, where it regulates proliferation and differentiation genes. During early developmental stages of the neocortex, active β-catenin might be necessary for cell cycle re-entry and increased progenitor proliferation. Nevertheless, activation of the Wnt signaling

has been implicated in NEC/apical RGC expansion, as well as in differentiation of basal progenitors [11]. The small GTPases RhoA, and Rac1 are associated with the tight-junctions, and link apical-basal polarity to cytoskeleton remodelling. These proteins were shown to affect progenitor proliferation (with region-specific differences) and cell fate [12]. In general, RhoA deletion leads to hyperproliferation of the progenitor pool, while Rac1 loss is associated with a decrease in proliferation and premature differentiation [13]. The atypical GTPase Rnd3 specifically controls the proliferation of basal progenitors, and is necessary for the maintenance of cleavage plain vertical orientation during RGC divisions [12, 13].

The differential inheritance of the primary cilium (including the centrosome and the ciliary membrane) also seems to correlate with cell fate and to have a specific role in neurogenesis, a fact stressed by the CNS defects observed in ciliopathies [5]. Inheritance of the basal process of NEC and RGC that extend towards the basal lamina is also considered important in determining daughter-cell fate. The cell that maintains the basal process normally maintains the proliferative abilities [3]. In early stages of development, the basal process is split between both daughter cells, but in mid- and late neurogenesis, the basal process is no longer split, resulting in its asymmetric inheritance. The basal endfoot may lead to alterations in the proliferative capacities of cortical stem/progenitor cells and gyrification via interaction with extracellular matrix components. In line with this, integrin manipulations affect neural stem and progenitor cell behaviour [14], and the basal process is the cell component that senses the Reelin gradients secreted by the Cajal-Retzius cells (discussed below) [5]. Other important neural progenitor cell-fate determining protein is Numb. Accordingly, Numb is segregated asymmetrically into the daughter cells, in a way that during mitosis the daughter cells with Numb will remain progenitors while the daughter cells without Numb assume a neuronal fate. Nevertheless, Numb is also required for neuronal survival and differentiation and its expression quickly rises in the neuronal daughter cells [5, 15].

Cell-cycle length also seems to have a role in the transition of NEC and RGC from proliferative to neurogenic divisions. In fact, neurogenic progenitors show a significantly longer cell cycle (mainly longer G1 phase) than the proliferating cells. The main hypothesis is that longer cell cycles give time for the cell to respond to cell cycle determinant molecules (ex: differentiation factor). In this view, if the cell cycle is long enough that the cell fate determinant is able to induce differentiation in both daughter cells, they will adopt a symmetric fate [3].

Of note, the existence of dividing neurogenic cells outside the classical proliferative VZ and SVZ was described in the rodent and human cortex [4].

The newly generated neurons will then migrate from the SVZ and VZ, and their postmitotic differentiation leads to the formation of new structures (some transient), until reaching their “final” destination – the cortical plate (CP) [2]. Shortly before the formation of the cortical plate, different

types of neurons (some of which migrating from extra-cortical sites) settle in a layer under the pial surface, forming the preplate (Figure A.2, second image from the left). The preplate is a dynamic and largely-transient structure that will further divide into two compartments. The compartment in the superficial sub-pial position is formed by the reelin-secreting Cajal-Retzius cells (CR). Reelin stops neuronal migration and will establish the upper boundary of the CP. The second compartment that extends to the SVZ has different types of cells, and will later originate the subplate (SP) [4]. The main role of SP cells is to guide thalamic axons to the CP [6]. In the boundary of the SP and above the SVZ another compartment seems to develop, the intermediate zone (IZ, very difficult to distinguish from the SP itself in early stages in humans) (Figure A.2, third and last image from the left). At later stages, after the invasion of large numbers of cortical fibres and the beginning of myelination this layer transforms into the white matter [4].

Additionally, after emergence of the CP, part of the preplate transforms in a cell-sparse layer formed by the subpial processes of ventricular cells and tangential migratory neurons – the marginal zone (MZ) (Figure A.2, third and last image from the left). Later this compartment becomes the layer 1 which contains few neurons and is largely filled with arborizations of apical dendrites and intrinsic tangential axons [4].

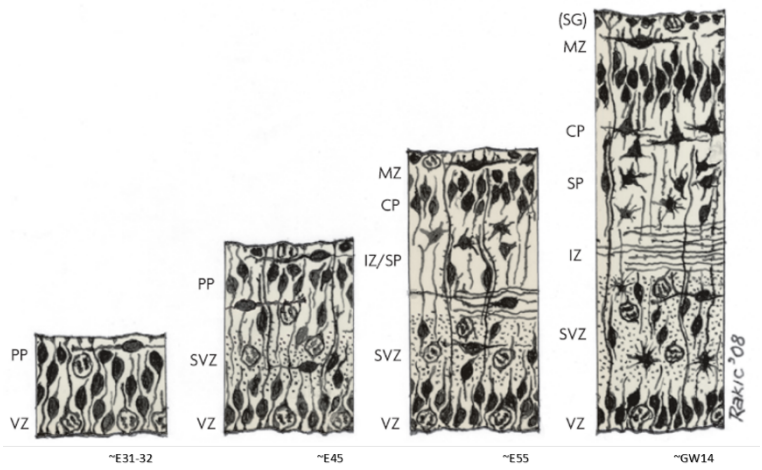

Figure A.2 - **Cortical layers during neurogenesis.** The preplate (PP) forms shortly before the formation of the cortical plate (CP), which will later divide into two compartments. One, in a sub-pial position, is formed by the reelin-secreting Cajal-Retzius cells, and the other extending to the subventricular zone (SVZ) that later originates the subplate (SP). In the boundary of the SP and above the SVZ another compartment seems to develop, the intermediate zone (IZ). After emergence of the CP, part of the PP, formed by the subpial processes of ventricular cells and tangential migratory neurons, transforms in the marginal zone (MZ). The subpial granular layer (SG), is a transient layer, part of the MZ, occupied by tangentially migrating small granular neurons (potential source of cortical interneurons and Cajal-Retzius cells). E, indicates embryonic day; GW, indicates gestational week. Adapted from [4].

Right after the formation of the preplate, RGCs begin to produce layer projection neurons [6]. The migration of newly born projection neurons to their final laminar position in the emerging CP occurs in a precise inside-first, outside-last gradient [2]. First neural progenitors shift their

"assembly line" from CR cell production to deep layer projection neurons production, and then a transition from deep layer projection neurons production to upper layer projection neurons production. In humans, CP appears first in the most lateral part of the rostral telencephalic wall, at E50. Peak migratory activity is thought to occur between the third and fifth months of gestation, and migration is completed during the third trimester [4]. Each layer of neurons arises from the VZ and SVZ progenitors and moves radially toward the pial surface via multi-step guided migration processes (Figure A.3). On the way, newborn neurons have to move along the SVZ, IZ, and the developing CP. The exact mechanism of migration adopted by a neuron and the molecules that induce or regulate such mechanism appear to depend on the subtype of neuron and migration distance. In the VZ, the proliferative cells resulting from asymmetric divisions of RGC adopt a long ascending process and rapidly migrate to the SVZ/IZ layers by somal translocation. On the other end, the RGC progeny resultant of a final division, migrate slowly and tend to accumulate in the lower part of the SVZ presenting a characteristic multipolar morphology (this zone is commonly named multipolar cell accumulation zone, MAZ). These cells extend and retract multiple processes while advancing slowly toward the cortical plate – multipolar migration (Figure A.3, step 2). Although the first type of cells mentioned enter the SVZ/IZ earlier, they still have to divide, and thus multipolar cells transform into locomotion cells and enter the CP earlier [16]. Very interestingly, after the acquisition of multipolar morphology it has been described a step of retrograde migration toward the ventricle. After contacting the ventricle this cells, similar to newborn neurons generated in the SVZ, assume bipolar morphology and travel by RGC-guided locomotion toward the cortical plate [17].

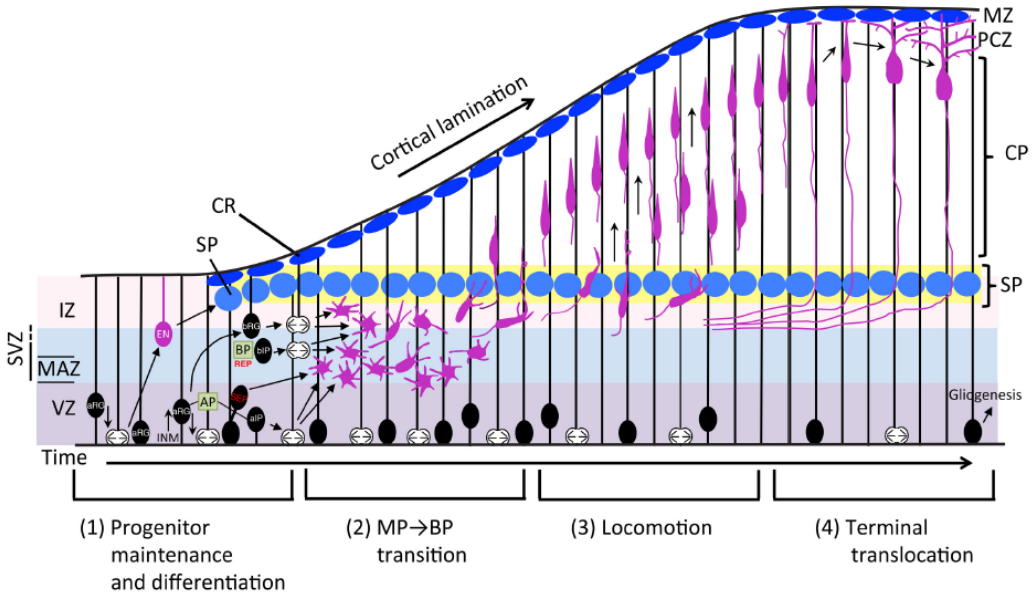

Figure A.3 - **Differentiation of layer projection neurons.** Each layer of neurons arises from ventricular zone (VZ) and subventricular zone (SVZ) progenitors that move radially toward the pial surface. In the VZ, the proliferative cells resulting from asymmetric divisions of apical radial glial cells (aRG), adopt a long ascending process and rapidly migrate to the SVZ/IZ layers by somal translocation. Non-dividing neural progenitors migrate slowly and tend to accumulate in the lower part of the SVZ - multipolar cell accumulation zone (MAZ) - presenting a characteristic multipolar morphology. Multipolar cells transform into bipolar locomotion cells and travel by RGC-guided locomotion toward the cortical plate. Neuronal polarization starts during this process, with the extension of the trailing process (ventricle oriented), and one selected neurite turning in a thick leading process (pia oriented). After reaching the CP, newborn neurons stop migrate, detach from the RG fibers, and anchor to the MZ for terminal translocation. Dendrites start to differentiate from the leading process branching out to generate an apical tuft. CR, Cajal-Retzius cell; EN, early born neuron; INM, interkinetic nuclear migration; PCZ, primitive cortical zone; SP, sub-plate neuron. Reproduced from reference [18].

The multipolar to bipolar (MP to BP) cell transition is crucial for radial migration, and appears to happen after delamination of cells from the apical surface of the VZ via suppression of E-cadherin [18]. Neuronal polarization starts during this process, with the extension of the trailing process (ventricle oriented), and one selected neurite turning into a thick leading process (pia oriented) [17, 18]. Thus, neuronal polarization/axon guidance events are coupled to neuronal migration, and both processes are commonly induced and regulated via the same cues and signals [19]. Axon extension is first detected in the lower IZ, and depends, at least in part, on homophilic interactions between surface TAG1 molecules present in the corticofugal axons that define the IZ and in the axons of newly-born projection neurons. Downstream signal events include Src family kinase Lyn and small GTPase Rac1 [20]. Neurotrophin receptors TrkB and TrkC and ligands brain-derived neurotrophic factor (BDNF) and neurotrophin (NT)-3 also regulate axon induction and radial migration in vivo [19]. Other crucial signalling, comprehends the Semaphorin protein family. Sema3A is secreted at the top of the CP originating a gradient through the cortex. This molecule, through its receptors Plexin and Neuropilin, is responsible for the growth of dendrites towards the pia (attractive cue), and axon growth towards the ventricle (repulsive cue). Downstream signalling might involve RhoA stimulation. In addition, Sema3A may provide a directional signal for radial migration [19, 21].

The kinase LKB1 (the mammalian ortholog of Par4) is activated via STRADalpha at the trailing process of newborn migrating neurons, which in turn activates SAD-A and SAD-B leading to tau phosphorylation and axon formation. LKB1 also regulates the transition from MP to BP and neuronal migration [22].

Migrating neurons express the Reelin receptors very low density lipoprotein receptor (VLDLR) and apolipoprotein E receptor type 2 (ApoER2), and the Reelin-Dab1 signalling pathway is critical for neuronal migration (glia-independent) and lamination [23]. Additional, MP exit and MP-BP transitions seems to require modulation of the activity of the Netrin receptor DCC by its co-receptor Unc5D [19]. ArfGEF2 and Filamin A gene mutations are associated with neuronal migration defects leading to human cortical malformations (for example, Periventricular heterotopia). By regulating vesicle trafficking and actin cytoskeleton, respectively, these proteins influence MP-BP transition [18]. Lissencephaly-1 (LIS1) gene mutations are also linked to human disorders resulting from incomplete and/or abnormal neuronal migration and abnormal cortical organization. It codes a MT- and MT organizing center-associated protein, and forms a protein complex with NDE1/NDEL1 and cytoplasmic dynein [9, 18]. LIS1 protein has been implicated in INM, axon extension, and MP-BP transition. Doublecortin (DCX) gene mutations produce similar phenotypes to LIS1 mutations. DCX is also an MT-associated protein, additional associated with vesicle trafficking, regulation of cell adhesion, and MT-actin crosstalk [9]. In line with the role of the centrosome position for MP-BP transition, it was found that the centrosomal protein SDCCAG8 regulates this transition step via interaction with PCM1.

After converting to a BP shape, neurons are able to migrate via RGC-guided locomotion (Figure A.3, step 3). This migratory mechanism involves nuclear translocation and forward movement of the cell body, and imply cytoskeleton coordination, endocytosis, and cell adhesion processes [18]. On the molecular level, RGC-guided locomotion depends on surface N-cadherin, regulated through Rab5-dependent endocytosis and Rab11-dependent recycling pathways and Reelin-Rap1-RalA signalling [24]. N-cadherin not only senses direction signals for radial migration but it is also involved in the earlier MP-BP transition. Recently, it was shown that N-cadherin mediates leading process formation at the RGC-neuron contact site via RhoA activation, and through Rac1 activation on the opposite site leads to axon formation [25]. The CDK5-Rap1-N-cadherin signalling is critical for exit from the MP phase. The Gap junction proteins Connexin 43 and Connexin 26 display cell adhesive properties and ensure the stabilization of the neurons' leading process along RGC and, consequently, neuronal migration [26].

Three distinct behaviours mark the end of migration once neurons reach their final destination: locomotion termination, detachment from the RG fibers, and anchoring to the MZ for terminal translocation (Figure A.3, step 4). Migrating neurons respond to a stop signal from the pia's

basement membrane. One of the most well described molecular mechanisms involves the GPCR GPR56. Collagen III binding to GPR56 leads to RhoA activation, a signal fundamental for pia basement integrity and to prevent neuronal over-migration. Interactions of this receptor with alpha3beta1 integrin produce a proper stop signal. The extracellular matrix with anti-adhesive properties, SC1, is involved in the detachment of neurons from the RGC, and Reelin-Dab1 signalling plays an essential role in terminal translocation [18]. Of note, in addition to migrate to their radial positions, projection neurons have to assume their correct cortical columnar areas by tangential dispersion, and their specific cortical area [21]. Neuron organization across tangential dimensions seems to be regulated, in general, by the Ephrin receptor and its ligands Ephrin A (stimulation) and Ephrin B1 (inhibition). However, other subtype-specific mechanism were already described, like translational regulation of NOS1 by FMRP for layer 5 neurons, and reelin signalling for Stab2-positive upper layer neurons [6, 19].

Upon arriving at the CP, neurons are instructed to stop migrating and continue to differentiate. Most differentiation processes, such as the extension and elaboration of dendrites and the formation of synaptic connections, take place mainly after neurons have assumed their final position in the CP [2]. The period after gestational week 22 is the most significant time for differentiation of the CP [4]. In pyramidal cortical neurons, the first dendrite derives from the leading process. This dendrite is oriented to the apical side and branches out generating an apical tuft. The guidance of axon and dendrite to opposite directions appears to be mediated, in part, by the same molecular gradient but different signalling pathways [27]. Later, basal dendrites and additional side branches from the apical shaft start to develop. Extensive (secondary and tertiary) branching events are necessary to efficiently cover the target field [28]. After this, there has to be growth restriction to define dendritic borders and avoid the overlap between dendrites of the same neuron type (a mechanism referred as self-avoidance), and coordination of the dendritic growth (defined as dendritic tiling). Neuronal maturation is marked by the (over-)development of dendritic spines, followed by dendrite pruning and post-synaptic differentiation. The final neuronal morphology will vary largely depending on which layer neurons are located [27, 28].

Distinct transcription factors may positively or negatively regulate dendrite arborization, and some transcription factors are further regulated by calcium signalling and neuronal activity. The bHLH transcription factor neurigenin 2, for instance, is involved in the specification of a unipolar apical dendrite in cortical pyramidal neurons. The mammalian Cut-like 1 and 2 (Cux1 and Cux2) appear to have specific functions in dendrite morphogenesis. In cortical pyramidal neurons, Cux1 appears to reduce dendritic complexity via RhoA modulation. The SYT-related nuclear protein calcium-responsive transactivator (CREST) responds to neuronal activity to elaborate dendrites. This molecule is part of a neuron-specific chromatin remodelling complex that controls the expression

of genes determinant for morphogenesis like GAP43, Stm2, Rap1a, Gprin1 and Ephexin1 [10, 28]. The small GTPase RhoA is associated with the restriction of dendrite growth, what might be important to define the correct innervation bondaries, whereas Rac1 and Cdc42 appear to drive dendrite elaboration [12, 28]. The Hippo family members and PI3K-mTor signalling play an important role in the correct definition of the target receptive fields and self-avoidance mechanisms [28].

Axon and dendrite outgrowth, and synaptogenesis are long events that extend into early childhood. The size of pyramidal neurons and length of dendrites increase greatly during the first postnatal year, and continue until the fifth postnatal year, although at a smaller extent. The first synapses in the CP appear around the 18th embryonic week, but the peak of neocortical synaptogenesis only occurs later in prenatal development and early postnatal development [2]. After this there is the refinement of synaptic connections and dendritic pruning, a process that can last until the 3rd decade of life [29, 30]. The latest transition in corticogenesis is the switch from upper layer neurons to gliogenesis, and the timing of this transition determines the overall number of neurons in the neocortex [6].

1.1.1. Experimental *in vitro* models of neuronal differentiation

In vitro dissociated neuronal cultures, either from CNS or PNS neurons, are a very useful experimental system to study the molecular and cell biology of neuronal differentiation.

Simpler model organism like *Drosophila melanogaster*, *Caenorhabditis elegans*, *Xenopus laevis*, *Danio rerio* are very attractive, but to study mammalian neuronal differentiation *Mus musculus* and *Rattus norvegicus* are most commonly used.

Dissociated rodent hippocampal neurons are a typical and well establish model system to study neuronal polarization and differentiation. Hippocampus is a widely adopted source for in vitro neuronal cultures because it has a relatively homogeneous population of neurons (80-95% are pyramidal neurons), and the hippocampal pyramidal neurons present a well-defined shape with a single axon and several dendrites (a single long apical dendrite and several shorter basilar dendrites). Furthermore, embryonic hippocampal neurons in culture acquire their characteristic polarized morphology during five well characterized distinct stages, as first described by [31] (Figure A.4). Most cortical neurons establish axon-dendrite polarization via events similar, to some extent, to that observed in cultured hippocampal neurons, for instance polarity formation primarily occurs in highly dynamic multipolar cells [32].

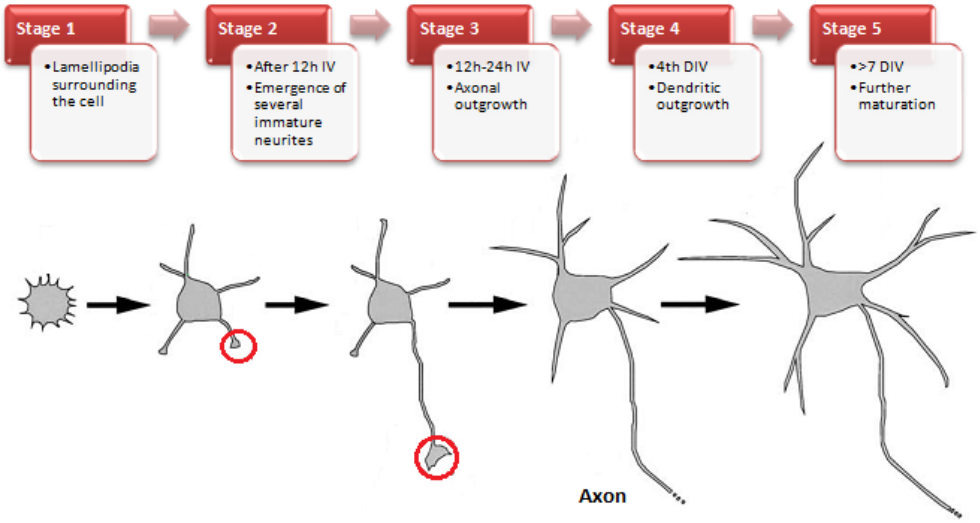

Figure A.4 - **Differentiation stages of hippocampal neurons *in vitro*.** Dissociated rodent hippocampal neurons are commonly used as models to study neuronal polarization and differentiation. In culture these neurons acquire their characteristic polarized morphology during five stages. The red circle indicates the growth cone. IV, in vitro; DIV, days in vitro. Adapted from reference [33].

The main event in stage 1 hippocampal neurons is the formation of lamellipodia, which develop around the periphery of the cell soon after the cells attach to the substrate. Changes in these structures were correlated to the formation of neurites, as lamellipodia break up into discrete motile patches that will become the neuritic growth cones. In stage 2 the lamellipodia are transformed into minor processes (typically 4 to 6) that extend to a length of 15-30 μm. Once they reach this length, there is no net elongation, but the processes still display a dynamic growth with cycles of extension and retraction. The cells maintain a symmetric appearance. The stage 3 is marked by the formation and growth of the axon. One of the minor processes begins to grow at a much more rapid rate (about 5-10 times greater than the other processes) and becomes the future axon, while the other neurites remain quiescent. As a result, stage 3 neurons have a single axon and several short neurites, which implies that the cell has become polarized [31, 33, 34]. Stage 4 comprehends the growth of dendrites that, similar to the axon, develop from the minor processes that appear during the first day in culture. Besides starting later than the axon growth, dendrites grow more slowly than axons. Additionally, unlike axons, several dendrites grow at the same time [31, 33, 34]. Eventually, after seven days in culture, dendritic arbors become more elaborated and branched. Neurons form large number of synaptic contacts, develop dendritic spines, and spontaneous electrical activity propagates throughout the neuronal network – stage 5 [31, 33, 34].

1.2. Cytoskeleton dynamics in neuronal polarization and axon/dendrite outgrowth

As explained above, in vivo, cortical projection neurons start to differentiate while migrating to their final location (Figure A.3). Specifically, these neurons acquire their polarity from the emergence of a leading process and a trailing process that will become the future dendrites and axon, respectively. The extensive stereotypical changes that neurons suffer from a round-shape stage right after division, to the intermediary multipolar stage and the bipolar stage during migration, until final dendrite morphogenesis and maturation, are extremely dependent on cytoskeleton dynamics and rearrangements.

The cytoskeleton both establishes and maintains polarity in neurons, and rearrangements of the actin cytoskeleton and microtubules are crucial for the initial establishment of polarity (see Figure A.5) [35]. Of central importance for neuronal polarity and neuritogenesis is the growth cone (schematic representation in Figure A.5) which is a highly motile cellular compartment at the tips of growing neurites that has the ability to sense extracellular cues and transducing those signals to the cytoskeleton. The growth cone is a broad flat expansion, with many long microspikes or filopodia that are protrusions of F-actin, and some veil-like sheets of branched actin, the lamellipodia [36, 37].

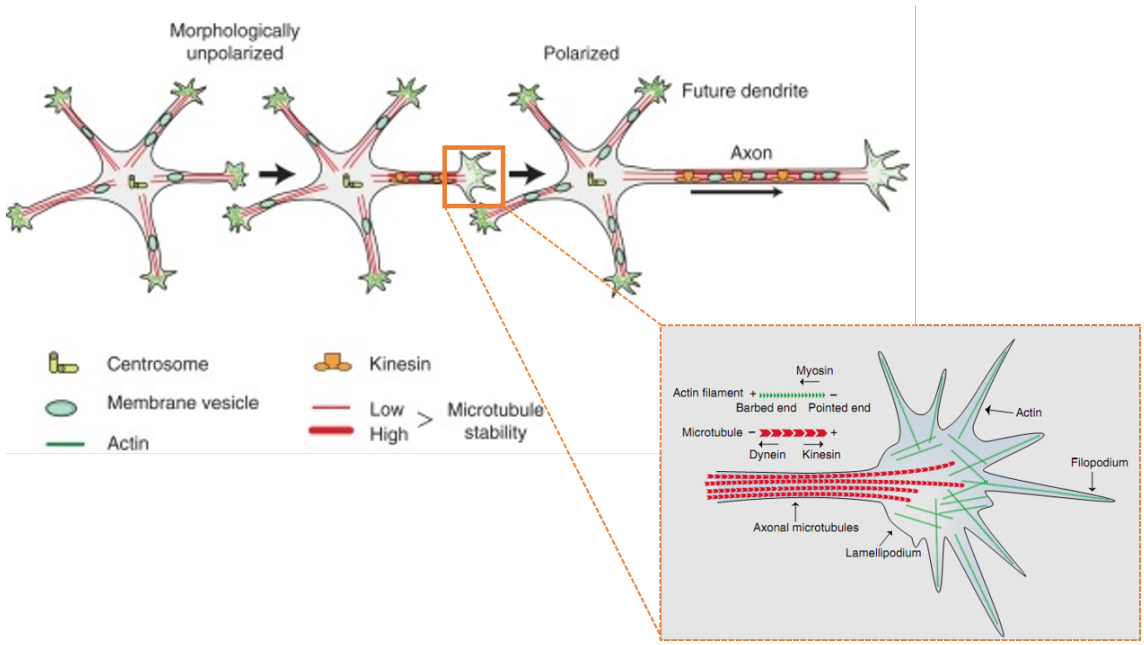

Figure A.5 - **Cytoskeleton dynamics during neuronal polarization.** Unpolarized neurons display several equal neurites. Axon polarization is marked by actin instability and increased microtubule stability. Kinesin motors induce unidirectional membrane trafficking towards the forming axon allowing its rapid elongation. Highlighted is a schematic representation of the growth-cone. Actin dominates the periphery of the growth-cone, forming filopodia and lamellipodia. Microtubules are distributed along the axonal shaft and protrude in the central region of the growth cone. Adapted from reference [35].

The basis of the actin cytoskeleton growth is the polymerization of ATP-bound globular actin (G-actin) into helical actin filaments (F-actin) [35, 36]. Barbed (plus)-ends of F-actin where actin monomers are continuously incorporated face the edges of the growth cone, while pointed (minus)-ends are oriented towards the base. The continuous F-actin disassembly at the pointed-ends and the F-actin assembly at the barbed-end is named F-actin treadmilling. F-actin treadmilling is responsible for the protrusion of lamelipodia and filopodia, and is an event essential for neurite outgrowth [38, 39]. The filopodia attach to the substrate and exert a force that pulls the rest of the cell forward, allowing it to move by elongation [38]. In stage 2 neurons (see previous section and Figure A.4), the future axon shows enhanced growth cone dynamics and, thereby, actin turnover, whereas the future dendrites, quiescent at that moment, have a static growth cone with a rigid actin cytoskeleton. Local actin instability, in the future axon, may cause reduced obstruction to the protrusion of microtubules (MT; mainly stable at this point) and, consequently, allows neurite outgrowth [36].

Current knowledge places actin-based processes as the central event in neuritogenesis, with a required balance between actin assembly and disassembly. Actin dynamics is regulated by several actin-binding proteins, like actin nucleator, severing, branching, and bundling proteins. Nucleation-promoting factors, such as WASP and WAVE, promote neurite growth by regulating actin polymerization via Arp 2/3 and profillin. The Arp2/3 complex initiates actin filaments branching in lamellipodia. Formins and fascin mediate bundling of actin filaments, and are involved in filopodia formation [38]. The alterations initiated by actin nucleators may be sufficient to induce neurite initiation once the correct dynamics is maintained after nucleation.

Cofilin has the ability to increase actin dynamics by filament severing and depolymerization, an event essential for neurite initiation. This protein promotes actin depolymerization by adding actin-ADP to the pointed (minus)-end of actin filaments, by promoting ATPase activity, and by increasing the rate of phosphate release and monomer loss. Its activity results in a general increase in the rate of actin treadmilling creating a pool of actin monomers free to bind actin filaments barbed (plus)-end. Cofilin is highly active in the growing axonal growth cones [36, 39]. Other actin severing protein is gelsolin, which binds actin barbed-ends and mediates calcium-dependent actin severing [37]. The released G-actin is sequestered, for example, by profillin. Profillin, in turn, will enhance the incorporation of ATP-actin monomers into actin barbed (plus)-ends. On the other end, beta-thymosin is a G-actin sequester protein that attenuates actin polymerization and delays neurite outgrowth. Nevertheless, its action seems crucial, for instance, during the response to extracellular cues. In this way, G-actin sequesters prevent spontaneous actin nucleation and control actin polymerization [36, 37]. Capping proteins such as CapZ prevent filament elongation. On the contrary, anti-capping proteins, as the proteins from the Ena/VASP family, prevent the binding of

capping proteins, allowing filament elongation. In addition, the Ena/VAPS proteins prevent actin branching and bundling [35, 36].

Axonal MT show increased stability with neuronal polarization. Stabilization of MT can be achieved by active stabilization of existing microtubules, increased polymerization, reduction of microtubule destabilization, and possibly by microtubule bundling.

Neuronal microtubule-associated proteins (MAPs: MAP2, tau, and MAP1B) are MT stabilizing proteins and are extensively involved in neurite formation [40]. By binding directly to MT, these proteins might also affect the binding of other proteins and might function as scaffolds. Plus-end tracking proteins (+TIPs) are MT-associated proteins that, as their name implies, bind MT plus-end and modify MT assembly and disassembly. This group includes the growth promoting factors, CLIPs (Cytoplasmic Linker Proteins); the stabilizing proteins, CLASPs (CLIP-associated proteins); core element proteins that regulate binding of other proteins, like the End-binding family members EB1-3; and the LIS1 and DCX proteins. These proteins mainly favor MT elongation [38]. MT destabilizing proteins such as Op18/Stathmin also have a role in neuronal polarity [36]. On the other hand, the MT stabilizing protein CRMP-2 binds to alpha/beta-tubulin dimers and promotes their binding to MT plus-ends. CRMP-2 is described to accumulate in the neurite that will originate the axon [41]. The inhibition of the microtubule destabilizer Stathmin via DOCK7 also increases microtubule stability [35]. The MT motors – kynesins and dynein - are equally important players in the events of neuronal differentiation, not only because of their function as long-range transporter and as the obvious link to the cell body, but also by their ability to modify the position and organization of MT, to contribute to MT stability, and to link MT to actin cytoskeleton.

Actin cytoskeleton and microtubules dynamics are not isolated events in neuritogenesis. Not only extracellular cues and intracellular signaling events will have the ability to induce rearrangements in both structures, but also these structures can physically interact and modulate each other. Kinesins and dynein link MT to the actin cytoskeleton and might promote MT movement and cell membrane protrusion using actin as scaffold [40]. The EB3 protein binds and forms a complex with the actin-binding protein drebrin. This complex seems to be involved in microtubule penetration into filopodia during neurite outgrowth [38]. MAP2 and MAP1B have the ability to bind F-actin and alter actin dynamics [40]. CRMP-2 regulates kinesin-mediated transport of the WAVE complex into the axon contributing to actin nucleation [41].

The progression through the different neuronal differentiation stages (from neuritogenesis to synaptogenesis) requires remodeling and a significant increase in cell size and plasma membrane surface area [34, 42]. Thus, regulated membrane trafficking events, including newly synthesized membrane from the exocytic secretory pathway (Tran-Golgi network-derived) and membrane recycling after endocytosis, will be tightly connected to the signaling pathways orchestrating

neuronal differentiation. The endocytic pathway (early endosome, the late endosome, recycling endosome, and the lysosome) will have a dual function during neuronal morphogenesis: to allow selective/polarized plasma membrane remodeling, as well as activation of intracellular signaling pathways that further enhance neuronal morphology. In this way, the structural constituents and regulators of membrane trafficking events will be crucial players during neuronal development and growth. Important examples include the SNARE complex proteins (vamp-2 and vamp-7, snap-25, -29, -47, and syntaxin and Sec22b) and their regulators (e.g. Munc18 family), the vesicle tethering proteins of the exocyst complex, the large family of Rab and ARF GTPases, and the motor proteins (e.g. Kynesin superfamily members) [42, 43].

1.3. Signaling events in neuronal differentiation

In vivo, neuronal polarity and differentiation derives from a complex interaction between extracellular cues and intrinsic properties. Gradients of physiological extracellular cues and cell-autonomous signaling cascades allow neurons to determine axon and dendrites. Maintenance of neuronal polarity depends on the maintenance of asymmetric distribution of signaling molecules what implies a precise spatial regulation of protein expression. Such regulation is accomplished through mechanisms of regulation of local protein synthesis, protein trafficking, and selective protein degradation. Of note, different neuron subtypes present differences in intrinsic signaling pathways what dictates different responses to a same extracellular cue.

1.3.1. Extracellular cues

Numerous extracellular ligands/cues act through distinct receptors existing in the plasma membrane of neurons and will promote localized changes in signaling pathways.

- **Netrin.** Bifunctional molecule, capable of attracting some axons and repelling others. By binding to DCC receptors netrin works as an attractive cue, while via UNC5 receptors netrin exerts repulsive effects [21]. This molecule is described to exert long-range and short-range effects [21].
- **Slits** bind receptors of the Robo family**.** It has been described as an axon repulsive cue, and as a branching factor for axons and dendrites [21, 27].
- **Semaphorins.** The semaphorins protein family includes secreted and transmembrane guidance cues. Binding to either semaphoring receptors Plexins or to co-receptors Neuropilin, induces active holoreceptor complexes and initiates intracellular signaling events. This extracellular cue has been implicated in several neuronal differentiation events including axon guidance, projection pruning, and synaptogenesis. In vivo, the best described member is **Sema3A.** Sema3A is present at high levels in the cortical plate and

mediates both the attraction of the pyramidal neurons' apical dendrites and the repulsion of the axon. This polarized response is a result of the presence of soluble guanylate cyclase (sGC) specifically in the dendrites [27, 44].

- **Ephrins family.** Comprehends two different classes of cell-surface molecules, which function in clusters as short-range cues. Bind the tyrosine kinase receptors Eph. These molecules have several roles in neuronal differentiation: attractive/repellent axon guidance properties, regulate axonal branching, regulate dendrite morphology and synaptogenesis [21].
- **Wnt** and respective frizzled family of seven transmembrane receptors [43]. Wnt comprehends a large family of secreted proteins (19 genes described in mice). Although initially described as an embryonic morphogen, Wnt and its highly conserved signaling components are now implicated in different aspects of neurite development (axon outgrowth, axon branching guidance and remodeling, dendritic arborization, and synaptogenesis). After binding to its receptor, there is activation of the adaptor protein disheveled (Dvl). Downstream Wnt signaling pathways include the canonical Wnt/β-catenin, and the planar cell polarity (PCP) pathways. The former induces the inhibition of GSK-3β (by disassembly of the complex formed by axin, adenomatous polyposis coli (APC), and GSK-3β), and consequently the promotion of the β-catenin-induced gene transactivation. The PCP pathway, by activation of the Rho GTPase and the c-Jun (N)-terminal kinase (JNK), generates signaling events that culminate in the reorganization of actin and microtubules [45].
- **Neurotrophins** belong to a family of extracellular molecules that has complex influences on neuronal development, and is composed by the nerve growth factor (NGF), the BDNF, the NT-3, and the NT-4. Neurotrophins mediate their effects by binding to two types of cell surface receptors, the tyrosine kinase receptors (Trk receptors: NGF binds to TrkA, BDNF and NT-4 bind to TrkB, and NT-3 binds to TrkC) and the p75 neurotrophin receptor (p75NTR). In general, Trk receptors transmit positive signals, while the p75NTR transmits both positive and negative signals. Neurotrophins are mainly associated with increases in the dendritic complexity of pyramidal neurons. BDNF was also shown to play an instructive role in axon specification, being this effect dependent on the activation of cAMP-dependent protein kinase (PKA) and phosphorylation of LKB1 by PKA [46, 47].
- Other growth factors: **Transforming growth factor beta** (TGFβ). Presents a graded expression in the developing cortex initiated at the VZ, and has a role in neuronal polarization. Downstream effectors include the Par6-Par3-aPKC complex – Rac1 activation [48, 49]; the **basic fibroblast growth factor** (bFGF), which accelerates the

outgrowth of both axons and dendrites in hippocampal neurons [50]; **insulin-like growth factor-1** (IGF-1) regulates neurite growth in developing brain and affects dendritic growth and branching of post-natal layer 2 cortical neurons [33].

- **Extracellular matrix and cell adhesion molecules –** Direct cell-cell or cell-matrix interactions mediated by membrane-associated receptors, ensure the coupling of extracellular signals to the cytoskeleton via distinct adaptor proteins. This allows site-directed cytoskeletal rearrangements and consequently proper growth cone motility. Adhesion receptors include the integrins (involved in cell-matrix interactions), the cadherins, and the immunoglobulin superfamily of cell adhesion molecules (IgCAMs). The two last receptors are mainly involved in cell-cell interactions [43]. In the nervous system examples of extracellular matrix molecules include laminins, tenascins, fibronectin, and chondroitin sulfate or heparin sulfate proteoglycans. These ECM molecules will present strategic and dynamic distributions during brain development (like the proliferative zone of the telencephalon or the preplate), and will bind transmembrane integrins and trigger integrin signaling pathways. Regulation of integrin activity is a recognized fundamental mechanism that controls neuritogenesis and neurite outgrowth, and integrin signaling pathways with roles in such processes include the focal adhesion kinase (FAK), the integrin linked kinase (ILK), and the adaptor paxillin [51]. Growth factors commonly cooperate with adhesion molecules to promote neuronal differentiation [43].

1.3.2. Intracellular signaling pathways

Intracellular signaling cascades, extracellular signal-induced and cell-autonomous ones, orchestrate the sequential events of neuronal differentiation. Several signaling networks operating in differentiation will culminate in the regulation of actin and/or microtubule dynamics, but also in the regulation of protein secretory, endocytic and degradation pathways. Of note, arrows bellow indicate activation of the molecules that follow.

- **LKB1 + Strad → SAD-A/B.** LKB1 is activated by its co-activator Strad and by phosphorylation at S431 (by PKA or p90RSK). This specific phosphorylation is induced by some extracellular cues, like Sema3A, neurotrophins and FGF. After activation, LKB1 phosphorylates and activates SAD-A/B and MARK kinases, which in turn target several MAPs (such as Tau and DCX) reducing their MT binding affinity [13, 52]. Clearly involved in the development of polarity of cortical neurons in vivo [36].
- **PI3K → PtdIns (3,4,5)$_3$ (PIP3).** The polarized activation of PI3K and the accumulation of PIP3 at the tip of a single minor neurite (future axon) are required for axon specification. It

is a well described event during axon formation in vitro, but there is sparse evidence for its role in vivo.

  - **PI3K → local increases in PIP3 → PKD** or **ILK → Akt → GSK3β.** Pathway described to be activated following neurotrophins-induced activation of Trk receptors. Its role in vivo is still questionable [41].
  - **PI3K → local increases in PIP3 → PKD** or **ILK → mTor.** Signaling event described to promote dendrite growth downstream of Reelin [41].
  - **(TrkA) → PI3K → RAP1B → Cdc42** and **Par complex.** Accumulation of RAP1B in the tips of the future axons precedes the accumulation of cdc42 and the PAR complex [41].

- **GSK3** (α and β) is a central molecule involved in the regulation of MT dynamics during neuronal differentiation, and appears to be a common link between several intracellular signaling pathways. This constitutively active kinase phosphorylates MAPs and contributes to MT instability. Its inactivation, following exposure to neurotrophins for instance, is necessary to MT stability. Described to be inactive at the growing axon and active at the dendrites, and to be one of the "control" signaling preventing dendrites to transform in axons [13]. However, its significance *in vivo* is still controversial. GSK3 main targets are:
  - **Tau,** and **MAP1B**.
  - **APC** phosphorylation, preventing APC binding to the MT plus end.
  - **CRMP2**, which in turn targets**: tubulin heterodimers** – to assist MT polymerization [41]; **Numb**-mediated endocytosis of neuronal cell-adhesion protein **L1** (an IgCAM) [41]; **Sra-1 – WAVE**, regulators of the actin cytoskeleton [41]. Furthermore, CRMP2 is a mediator of semaphorin-induced growth cone collapse.
- **Ras,** is activated downstream several growth factor receptors. This pathway seems to regulate axonal cytoskeleton via phosphorylation of several MAPS, and also regulates a broad range of transcription factors, including Serum Response Factor [53]. Downstream of Ras, two main signaling pathways can be activated [54]:
  - **PI3K** (described above);
  - **Raf → MEK → Erk1/2.** Haploinsufficiency of the MAPK1/ERK2 gene in humans results in microcephaly, neurodevelopmental deficits and learning disabilities. Furthermore, mutations in upstream or downstream signaling components of the ERK cascade are associated with a variety of neurodevelopment syndromes (characterized by developmental delay and mental retardation) [55]. For instance, in the developing cortex, ERK signalling is described to regulate the

proliferation of neural progenitors and, consequently, the progenitor pool size, by keeping the correct balance between proliferative and neurogenic divisions through downstream effectors p27Kip1 and cyclin D1 [56]. On the other hand, the conditional inactivation of ERK2 within neural progenitors at the beginning of the neurogenic period results in fewer neurons populating the cortex, and increased number of astrocytes. Indicating that ERK2 is responsible to suppress glial fate and promoting neurogenesis in the developing cortex. In addition this molecule plays critical roles in learning and memory [57].

- **Rho-family of small GTPases.** Growing evidence indicates that neurite initiation does not depend simply on constitutively activation or inactivation of small GTPases, but rather in a specific local and temporal cycling between activation and inactivation states [40]. Furthermore, different family members can be differentially activated by a particular signal. For instance, following neurotrophin treatment, local increases in PIP3 are associated with increases in the activation of cdc42 and Rac, but decreases in RhoA signaling [58].
    - **Cdc42** regulates actin dynamics, more specifically is involved in fillopodia formation and growth cone morphology [36]. In vivo studies strongly support its involvement in axon polarity initiation and growth. Major effectors: **Cdc42 → WASP**; **Cdc42 → PAK→ Cofilin → actin**; **Cdc42 → STEF/Tiam → Rac1** [12].
    - **Rac1 and Cdc42** might converge on a common signaling pathway to induce dendrite elaboration in immature cortical neurons: activation of the serine/threonine kinase Pak1. May also activate the Arp2/3 complex**.** During dendrite morphogenesis the activity of these proteins is regulated by neuronal depolarization by NMDA and glutamate receptors [28].
    - **Rac1** role in actin cytoskeleton dynamics is mainly associated to its role in lamellipodia formation [36]. Rac1 is a well described positive regulator of axon guidance in vivo [12]: **Rac1 → PAK; Rac1 → WAVE.** This small GTPase also controls MT dynamics via stathmin inactivation [58].
    - **RhoA → ROCK → profilin II** and **myosin II**: induces destabilization of actin cytoskeleton and neurite retraction. ROCK can also modulate MT. Contrarily to Rac and Cdc42, RhoA appears to associate with repulsive cues and growth-cone collapse, but there is a lack of *in vivo* studies [58].
- **Par complex** (Par3 and Par6) **→ atypical PKC.** Might be regulated downstream of PI3K. It is transported to the axon terminals by kinesin 2 motor.
    - **Cdc42 → STEF** or **TIAM1 GEFs → Rac1**

- **MARK2.** The Par complex via aPKC inhibits MARK2 and thus MAP phosphorylation at the axon tips. MARK2 overexpression inhibits axon formation, and its downregulation induces supernumerary neurons [59].

- Local **calcium a**nd **cAMP/cGMP** gradients can mediate filopodia formation and neurite growth. Calcium is key mediator of neurite outgrowth in almost all types of neurons. It can act directly, or through the activation of various calcium-binding proteins to modulate the state of polymerization of actin filaments and microtubules [50, 53]. For instance it activates the actin severing protein gelsolin.

2. The Amyloid Precursor Protein

Amyloid Precursor Protein (APP; also known as Amyloid beta A4 protein) is a ubiquitously expressed type 1 membrane glycoprotein that suffers proteolytic cleavages and, as its name implies, is the precursor protein of the amyloid β-peptide (Aβ). Aβ is the main component of the senile plaques present in the brain of patients with Alzheimer's disease (AD), the most common age-related neurodegenerative disorder, first described in 1906 by Alois Alzheimer. AD is a multifactorial illness of insidious onset and progressive decline in cognitive (including memory loss) and functional abilities, including as well, behavioral and psychiatric symptoms. Ultimately, it leads to a vegetative state and death [60, 61].

Although APP was initially mainly studied because of its association to AD, this protein is widely expressed on the cell surface, particularly in neurons, and has been implicated in physiological roles such as cell adherence, survival, migration and differentiation. Recently, it is being established as a neuromodulator of developing and mature nervous system.

2.1. APP characterization: gene family, isoforms and functional domains

In 1984, Aβ was isolated from deposits found in blood vessels of AD brains and Down's syndrome (DS) brains, which provided a partial sequence of this peptide [62, 63]. A year later, Aβ was identified as the main component of neuritic plaques in AD brain [64], and shortly thereafter, the gene encoding APP was identified, and found to be located on the DS region of the chromosome 21 (21q21.2-3) [65-67]. The human APP gene contains 19 exons (with more than 170 kb) and is expressed in many cell and tissue types including endothelial cells, glia and neurons of the brain [68]. APP is one of three members of a small gene family that, in humans, includes APLP1 and APLP2. APP and APLP1 are suggested to result from an earlier duplication event, and APLP2 from a later gene duplication event [69]. The redundancy of APP and APLPs is reflected in an analogous protein domain structure: all encode type 1 integral membrane glycoproteins with a large extracellular domain and a short cytoplasmic region, and undergo a similar proteolytic processing. These three related proteins are well conserved in evolution and share similar functions, but only APP contains the Aβ domain, encoded by parts of exons 16 and 17 [69, 70].

APP-like cDNAs were found in *Drosophila melanogaster* and *C. elegans*, the APPL and APL-1 respectively. Both species only have one member of the APP gene, and APL-1 is predicted to be the closest to the ancestral protein. Curiously, APLP1 and *D. melanogaster* APPL are only expressed in the nervous system, much like the APP695 isoform (see bellow) [69, 70].

APP gene mutations are reported to be associated with familial, early-onset AD, however these account for a very small portion of AD cases (~16%) [71]. In general, such mutations are localized

close to the beta-secretase or gamma-secretase cleavage sites. Examples include the V717I, V717F, V717G, and the Swedish double mutation K670N and M671L substitutions. In addition, APP mutations comprising amino acid substitutions within residues 21-34 of the Aβ domain are linked to cerebral amyloid arteriopathy (like the Dutch variant E693Q, the Flemish variant A692G, and the Artic variant E693G, among others). On the other hand, APP genetic variations in its core promoter and in its 5-prime upstream regulatory region might be correlated with late-onset AD [72, 73]. The importance of APP in the etiology of AD, namely the robust effect of the dose for *APP,* is also notorious by the fact that virtually all individuals with DS (who overexpress APP due to chromosome 21 trisomy) develop age-related cognitive decline and AD-related pathology, and duplications in the *APP* locus are described to be sufficient to cause early-onset AD. The APP-A673T coding mutation was shown to correlate with protection against AD and against cognitive decline in (Icelandic) elderly without AD [74].

APP gene transcripts suffer alternative splicing of exon 7, 8, and 15 to produce several protein isoforms. Main transcripts include the APP695 (exons 1-6, 9-18, not 13a) which is preferentially expressed in neuronal tissues; the APP751 (exons 1-7, 9-18, not 13a); and the APP770 (exons 1-18, not 13a). APP751 and APP770 contain the exon 7, which encodes a serine protease inhibitor (also called Kunitz proteinase inhibitor, KPI) domain, missing in APP655. APP770 contains, in addition, the exon 8 that encodes a domain with homology to the MRC OX-2 antigen found on the surface of neurons and certain immune cells such as thymocytes. The preceding isoforms are expressed mainly in non-neuronal cells. Other alternatively generated splice variants (the ‘L-‘ isoforms) lack exon 15 (encoding 18 amino acids), and are found in peripheral leukocytes and in microglia cells [75-77].

APP structure can be generally divided in a large extracellular amino-terminal domain, a single transmembrane spanning domain, and a small intracellular cytoplasmic domain. Structural data, suggests that the domains of a single APP molecule have a linear extended conformation without any strong interaction between them, so APP displays a conformation resembling "balls on a string" [78, 79]. In Figure A.6 is depicted the overall structure of APP and the relative position of its main functional domains.

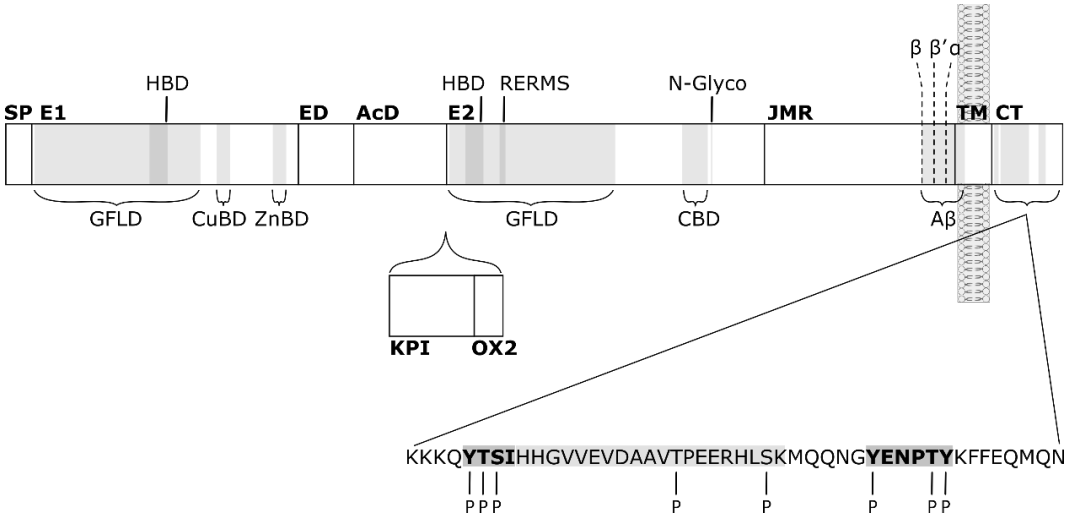

Figure A.6 - **APP functional domains**. APP has a large extracellular domain, a transmembrane domain (TM), and a small cytoplasmic domain comprising the protein C-Terminal (CT). The extracellular domain includes a 17 amino-acid signal peptide (SP), the E1 domain, the E2 domain, and a juxtamembrane region (JMR) that holds the Aβ sequence. The E1 domain contains a cysteine-rich growth factor-like domain (GFLD) with heparin binding properties (HBD), followed by zinc and copper binding domains (Zn/Cu-BD). The E2 domain includes an additional GFLD with an HBD and a RERMS, and a carbohydrate sub-domain containing the Collagen binding domain (CBD) and the N-glycosylation sites (N-Glyco) of the ectodomain. The KPI domain is only present in APP770 and APP751 isoforms, and the OX2 domain in APP770. On the bottom, the sequence of the CT is represented, and the sorting YTSI and YENPTY motifs are highlighted. In lighter grey is the binding site to the Gαo protein. 'P', indicate phosphorylation sites. The β-secretase (β and β') and α-secretase (α) cleavage sites are also represented.

The extracellular domain starts with a 17-residue signal peptide, and is organized in two N-terminal folded domains, the E1 and E2 domains, linked by a highly flexible and negatively charged subdomain – termed acidic domain (AcD). Before the AcD and uniquely present in APP, there is a small extension (sub)domain (ED) that holds at least two phosphorylation sites. In between E1 and E2 domains, APP770 and APP751 isoforms, display a KPI and an OX2 domains [75, 76].

The E1 domain contains a cysteine-rich growth factor-like domain (GFLD) with heparin binding properties (HBD), followed by zinc and copper binding domains (Zn/Cu-BD) [76]. The HBD is not present in APLP1, APPL or APL, the Cu-BD (142-151) is somehow less efficient in APLP2 and is not present in APLP1, while the Zn-BD (179-188 – BxxExxCC) is present in all elements of the APP superfamily. Binding of zinc II alters the ability of APP to bind heparin, when present the affinity for heparin increases [66, 67]. The E1 domain appears to provide APP family members the ability to form both homo- and hetero- dimers, cis- and trans- directed, promoting cell adhesion [76, 77].

The 56-amino acid long KPI, present in APP and APLP2, is suggested to influence the processing of APP770 and 751 isoforms, and is thought to affect cell adhesion by regulation of the time APP or sAPP is available to bind extracellular substrates before degradation. The OX-2 domain is a novel feature of APP, present in the APP770 isoform, and might affect the protease inhibitory aspects of the KPI domain [66, 75].

The E2 (mainly flexible alpha-helices) region includes an additional HBD/GFLD (370-393) present in all APP family, with the RERMS motif found only in APP. This main domain also includes the carbohydrate (sub)domain containing the N-glycosylation sites of the ectodomain, and the Collagen binding domain (CBD, 448-465) completely present in APP and APLP2. Furthermore, the E2 was recently found to bear a novel metal binding site (for Cu or Zn) [66, 75].

The Chondroitin sulphate attachment site is formed by alternative splice exclusion of exon 15 in human APP (a similar event occurs in APLP2 by alternative splice of exon 14) [66].

The juxtamembrane region (JMR) is the highly flexible region that connects the entire ectodomain to the sigle TM helix. The sites of β- and α-secretase cleavage are within or at the C-terminus of this segment, and the 16 amino acids that are contained in sAPPα, but not in sAPPβ, belong to the JMR [75, 76].

The Aβ domain comprises the 28 residues just outside the membrane plus the first 12-14 residues of the transmembrane domain (TM), and is a novel feature of APP conserved between species.

The TM contains three consecutive glycine-xxx-glycine (GxxxG) motifs, including one embedded within the Aβ sequence. In general, GxxxG motifs are involved in dimerization of transmembrane proteins. In fact, it has been shown that glycine to alanine substitutions within such motifs attenuate TM dimerization and reduce APP processing, including to toxic Aβ42 [77, 78].

The cytoplasmic region of APP contains a ^{682}YENPTY^{687} motif containing an NPXpY internalization signal for membrane proteins, and that is found in the entire APP superfamily [79, 80]. This motif mediates the interaction of APP with different binding partners via their phosphotyrosine interaction domains [81]. APP C-terminal also hold a ^{653}YTSI^{656} basolateral sorting domain described to bind PAT1 (or APPBP2), and AP-1, and AP-3. Besides function as basolateral sorting signals, canonical Yxxθ motifs have roles in endocytosis, lysosomal sorting, and retrograde sorting to the Golgi [80, 82, 83]. Near the YTSI motif, there is a Go binding site (H657-K676 of APP695) equally present in APP, APLP1 and APLP2 [66, 84].

2.2. APP cellular localization and intracellular trafficking

APP is an transmembrane protein that is dynamically sorted through the membranes of intracellular organelles and the plasma membrane (Figure A.7) [88]. In general, total cellular APP has a short-half life (30-60 min), but some results suggest the existence of a stable pool of membrane-tethered APP.

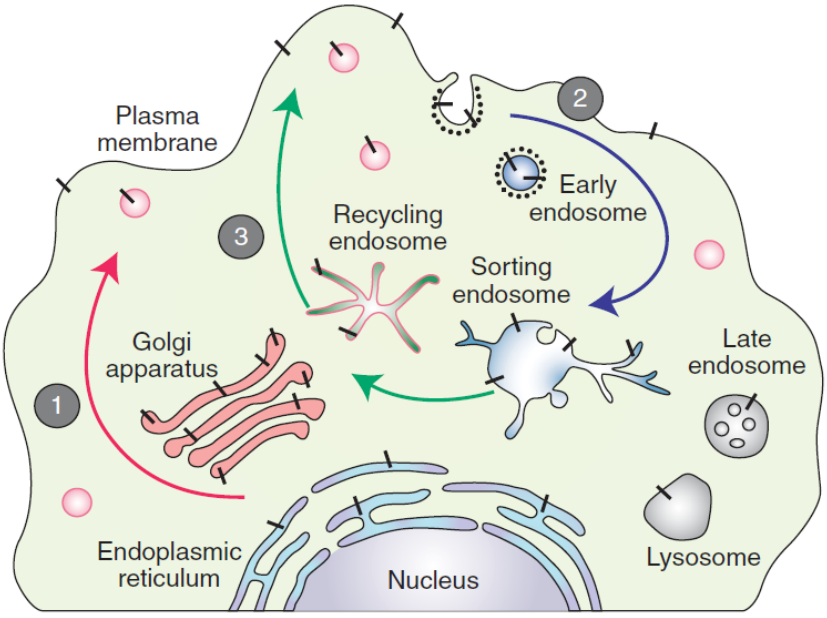

Figure A.7 - **Intracellular trafficking of APP.** After synthesis, APP is transported through the constitutive secretory pathway to the cell surface (1). After this, APP suffers internalization and is delivered to the endosomes - retrograde transport (2). From the endocytic pathway, APP is either recycled by transport vesicles to the trans-Golgi network and to the plasma membrane (3), or transported to lysosomes. Reproduced from reference [89].

APP is cotranslationally translocated into the endoplasmic reticulum (ER) via its signal peptide, and then post-translationally modified ("matured") through the secretory pathway. Acquisition of *N*- and *O*-linked sugars occurs rapidly after biosynthesis [60]. N-glycosylation localizes to the ER and early Golgi – immature APP, not cleaved by secretases – and O-glycosylation occurs during Golgi trafficking – mature APP that, from the TGN, enters into the late secretory pathway [84]. Only a small fraction of nascent APP molecules reach the PM (estimated to be ~10%), whereas the majority of APP at steady-state localizes to the Golgi apparatus and trans-Golgi network (TGN) [89]. After arrival at the cell surface, the APP that is not shed by alpha-secretase suffers internalization, via its YENPTY motif, being delivered to the endosomes - retrograde transport. From the late endosomes, APP is either transported to lysosomes, or recycled by transport vesicles to the TGN and to the cell surface [90]. In addition, APP is described to locate to the ER/nuclear envelop and to the ER-mitochondria [91]. Of note, during trafficking through the endocytic pathway, APP can undergo a variety of proteolytic cleavages, specified in the next topic.

In neurons, APP is subjected to the constitutive secretory pathway and undergoes fast axonal transport to presynaptic terminals. Some authors show evidences that the axonal transport of APP is mediated by the direct binding of APP to the kinesin light chain subunit of kinesin I [92], but such results are controversial [93]. APP is not only transported to axons, but also to dendrites, and axonal APP and dendritic APP can follow different fates [94] (discussed in the following topic).

The main coat complexes described to be involved in APP transport include the clathrin and the retromer. The clathrin coat complex is involved in two main sorting routes: the endocytic pathway, connecting the cell surface to the endosome, and the pathway connecting the TGN to the endosome. The targeting of APP to clathrin-coated vesicles is mediated by the NPXY amino acid motif. A number of clathrin adaptor proteins have been found to mediate the binding of the APP's NPXY motif to clathrin coats and therefore serve as regulators of APP endocytosis: autosomal-recessive hypercholesterolemia (ARH) protein, disable family member (Dab) 1, c-Jun N-terminal kinase interaction (Jip1b) protein, members of the Fe65, and members of the X11 families, in particular X11a [88]. The retromer is the second coat complex implicated in the rapid transport of APP (and of its β-secretase BACE) from the endosomes to the TGN. It is a coat complex composed of vacuolar protein sorting (VPS) 35, VPS26, VPS29, VSP5, and VPS17. VPS35 represents the core of the retromer complex and has been described to bind the cytoplasmic tail of the transmembrane protein cargo that is being sorted, including APP [95]. In addition, retromer binding to cargo proteins might also occur via its VPS10-containing sorting receptor proteins, such as SorLA and Sortilin. Both proteins were associated with APP trafficking and processing, and seem to mediate sAPP internalization. In hippocampal neurons SorLA, which binds to APP E2 domain, mainly colocalizes with APP in the soma, where it seems to protect APP from proteolytic processing, while Sortilin mainly interacts with APP in neurites and promotes its cleavage by the α-secretase. Sortilin mediated-sAPP internalization might facilitate lysosomal degradation of this fragment. SorLa colocalizes with sAPP in paranuclear regions [96].

In addition, to the already mentioned, multiple other signals and protein interactors can modulate APP trafficking. Estrogen (17-beta-estradiol) treatment is associated with accelerated APP trafficking through the TGN and reduced Aβ production [97]. The microtubule-interacting protein PAT1a (or APBP2) binds to the basolateral sorting domain of APP affecting APP surface levels and amyloidogenic metabolism [98, 99]. Clearance of Aβ from the brain across the blood brain barrier is mediated by the low density lipoprotein receptor-related protein-1 (LRP1), that binds Aβ directly, or via chaperone molecules like the proteinase inhibitor alpha-2-macroglobulin. LRP1 is also coupled to APP internalization and processing, with Fe65 and/or RanBP9 function as linkers [89]. In opposition to its clearance role, APP interaction with LRP1 accelerates APP endocytosis and is associated with increased processing to Aβ [100]. RanBP9 is described to increase APP localization to lipid rafts and enhances the association of LRP1, APP, and BACE1, to increase Aβ generation [101].

The fusion of transport vesicles to the membrane of the targeted organelle completes the process of transmembrane protein sorting. The fusion event is governed by three main families of proteins: SNAREs, Rabs, and Sec1/Munc18. The SNAREs expressed in the membrane of the transport

vesicle interact with a single SNARE protein in the membrane of the organelle, with Rab and Sec1/Munc18 mediating this interaction [88].

2.3. APP proteolytic processing

As described above, part of the newly synthesized APP undergoes anterograde transport and is targeted as a full-length protein to the plasma membrane, after which it may be cleaved to sAPP or reinternalized into the endocytic pathway. During this trafficking APP undergoes endoproteolytic cleavages by proteases, releasing biologically active peptides (Figure A.8).

Two main proteolytic cleavage sites have been identified close to the TM domain, and one site occurs within the TM domain. Starting from the amino terminus of the protein, these are termed β- (between residues Met596 and Asp597 of APP695), α- (between residues Lys612 and leu613 of APP695) and γ- (multiple sites, as described later) cleavage sites. Each cleavage is catalysed by separate enzymes: β-, α- and γ-secretases, respectively [102]. The α- and β-cleavages are mutually exclusive events, with APP undergoing two post-translational processing pathways. In the non-amyloidogenic pathway (Figure A.8 upper part, right side), APP is cleaved within the Aβ region by the α-secretase, liberating a large soluble extracellular N-terminal fragment - sAPPα. The carboxy-terminal fragment (CTF), named C83 or CTFα, remains tethered to the membrane, and is subsequently subjected to a transmembrane cleavage by γ-secretase, producing a non-pathogenic p3 peptide and the cytoplasmic APP intracellular C-terminal domain, AICD. In the alternative, amyloidogenic pathway (Figure A.8 upper part, left side), APP is first cleaved by β-secretase, generating the large soluble sAPPβ peptide and the CTFβ, C99. This is subsequently processed by γ-secretase, producing the Aβ peptide associated with Alzheimer's disease, and the intracellular AICD fragment. There is a second β-secretase cleavage site (β′, between Tyr606 and Glu697 of APP695) that is 10 amino acids towards the C-terminus from the β site, yielding CTF89 [61, 102].

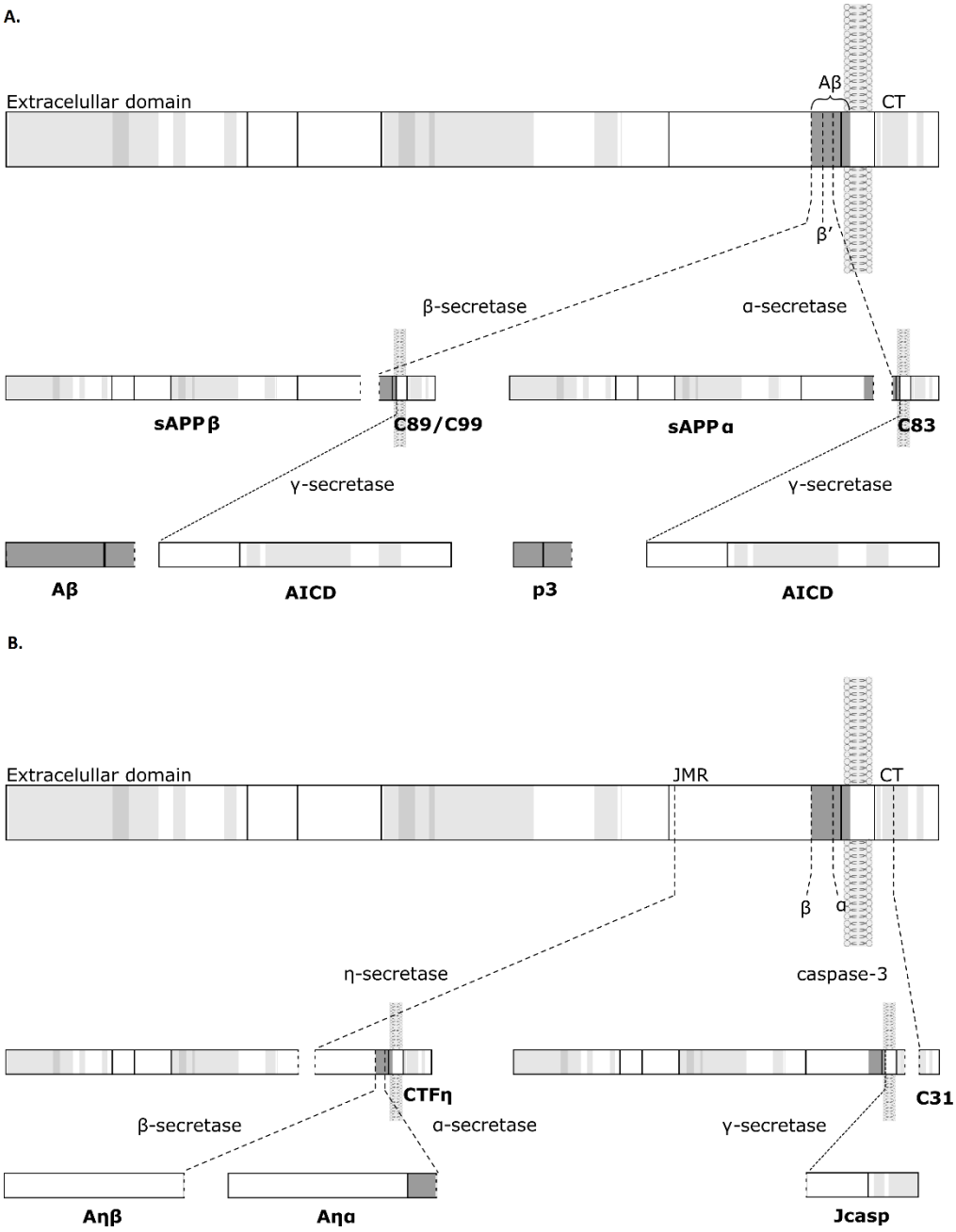

Figure A.8 - **APP proteolytic processing.** A. Main described cleavage pathways. In the non-amyloidogenic pathway, cleavage by α-secretase enables the secretion of the sAPPα and the preservation of the C83 fragment in the membrane. The C83 can undergo cleavage by γ-secretase to release the p3 and AICD (right side). Alternatively, in the amyloidogenic pathway, β-secretase cleavage results in the secretion of the slightly truncated sAPPβ and the membrane retention of a C99 or a C89 (depending on the cleavage site). The resulting C-terminal fragments can also undergo cleavage by γ-secretase to release the Aβ and AICD (on the left). B. Additional cleavage events. Caspase can also cleave APP to release C-terminal fragments: 'C31' when it cleaves APP full-length, or 'Jcasp' if there is also a cleavage event by γ-secretase (right side). During the η-secretase pathway, truncated soluble ectodomains and higher molecular mass C-terminal fragments (CTFη) are originated. CTFη can be further cleaved by the α-secretase or β-secretase to release Aηα or Aηβ (left side).

α-secretases: several membrane-bound disintregrin and zinc metalloproteinases including ADAM10, ADAM17 (or TACE), ADAM9 and MDC-9 have been identified has having α-secretase-like activity [103]. In neurons, the major functional (constitutively cleaving) α-secretase

activity is mediated by ADAM10. But α-secretase cleavage can be stimulated above its constitutive level - regulated α-secretase cleavage, which is thought to be mediated by ADAM17 [104]. Unregulated α-secretase cleavage of APP has been shown to occur at the cell surface [89]. However, α-secretase cleavage was shown to also occur intracellularly, in a late compartment of the default secretory pathway, and a large amount of sAPPα is already generated within the Golgi compartment long before it reaches the cell surface. The α-secretase proteins are synthesized as preproproteins, and to become active their prodomain is cleaved in the late Golgi by proprotein convertases (PPCs). Interestingly, these enzymes apparently can act at the same cell surface, or perform trans-cleavage of substrates located in neighbor cells [104]. The β-site APP-cleavage enzyme (BACE) 2 has also been identified as a α-secretase, as it can cleave APP in the middle of the Aβ domain (between Phe19 and Phe20). Importantly, PKC phosphorylation, either via treatment with phorbol esters or via activation of growth factor receptors, increases α-site cleavage of APP while decreases Aβ generation, an effect that can both depend on direct APP phosphorylation and on phosphorylation of APP-cleaving enzymes [105].

β-secretases: β-cleavage is attributed to the aspartyl protease BACE1. BACE1 is produced as a pro-enzyme in the ER and the in the nuclear envelop, and its prodomain is cleaved by furin or other PPCs just before trafficking through the Golgi [61, 102]. Mature BACE is mainly found in the endosome, but can also be found in lower levels in the Golgi, TGN, and at the cell surface. Nevertheless, "convenient" acidic environment for its optimal active form appears to be only found in the late Golgi, endosomes and lysosomes. Lipid rafts have also appeared as potential sites for BACE1 activity [89]. The zinc metalloprotease Meprinβ has been proposed as a candidate β-secretase acting at the cell surface [102].

γ-secretases: γ-secretase is a multimeric complex, made of four essential subunits: Presenilin-1 or -2 (PS1 and PS2), Nicastrin, APH-1, and PEN-2 [106]. Each subunit has been found to be necessary for the enzymatic activity of the complex, which is dramatically impaired when any of the components are deficient. Although still under debate, the work of many labs indicate that mature active γ-secretase is mainly localized at the PM and in the endosomal/lysosomal system, including phagosomes and autophagosomes (and not in ER, Golgi, or post-Golgi transport vesicles as previously thought) [89, 91]. The complex acts in multiple sites within the APP TM domain, cleaving the remaining APP CTFs inside the membrane. APP-CTFα (or CTF83) cleavage yields AICD and p3 fragment production, and βCTFs (CTF99 or 89) processing results in different Aβ forms and AICD. βCTFs are processed by γ-secretase first at the epsilon-site (Leu645-val646 bond, APP695 numbering), what releases AICD to the cytosol. Subsequent cleavage at the zeta-site of the membrane retained Aβ49 (between Val642 and Ile643) generates Aβ46 and, finally, cleavage at multiple γ-sites produces two main combinations of Aβ peptides: the predominantly Aβ49-Aβ46-

Aβ43-Aβ40-Aβ37 set from which Aβ40 is the principal end product, and the Aβ48-Aβ45-Aβ42-Aβ38 set that gives rise to the pathogenic Aβ42 and the Aβ38 in comparable amounts [104, 105].

Curiously, although most Aβ species were abolished in *PS1*/*PS2* -/- cells, the production of intracellular Aβ42 generated in the ER/intermediate compartment was unaffected by the absence of these proteins (either singly or in combination). Therefore, another γ-secretase activity must be responsible for APP cleavage within the early secretory compartments [107].

Recent work presented evidences that PS1 and PS2 take different paths in the cell. PS2 (by association with AP-1), but not PS1, resides in late endosomes and lysosomes. PS1 was spread across multiple cellular fractions, and nearly 10% of PS1 was detected in the plasma membrane, where PS2 is practically absent. In neurons, PS2-containing vesicles congregated in dendrites rather than axons or cell bodies, and cells expressing only PS2 contained higher amounts of intracellular Aβ (a higher ratio of Aβ42 to Aβ40) and secreted less Aβ than did cells expressing only PS1 [108, 109].

The γ-secretase complex acts through a mechanism known as regulated intramembrane proteolysis (RIP) that, besides a proteolytic process, comprises a transcriptional regulation event following AICD translocation to the nucleus [110]. This event has been reported (but still under discussion) to depend on AICD stabilization by Fe65 interaction, translocation of the protein complex to the nucleus, and association with Tip60. Such AICD-Fe65-Tip60 (AFT)-complexes were demonstrated to correspond to transcription factories [111]. On the contrary, association of RanBP9 with AICD recruits AICD to Tip60-enriched nuclear speckles, preventing AFT-complex formation and AICD-mediated nuclear signaling [112]. Very interestingly, it has been suggested that the origin of APP-CTFs, either from the β- or α-secretase processing, may determine the affinity of γ-secretase to the CTFs [110]. For example, it was demonstrated that the AICD produced following β-secretase cleavage is transported to the nucleus and binds to the neprilysin gene promoter, whereas that produced following α-secretase cleavage is rapidly degraded in the cytosol by insulin-degrading enzyme [102]. Nuclear signaling of AICD was also shown to occur predominantly through the neuronal 695 isoform [113].

Of note, recent evidence indicates that ADAM10 and γ-secretase physically interact and form a functional complex to sequentially cleave APP. This complex is further stabilized by members of the tetraspanin family of scaffold proteins (namely tetraspanin 12 and 17). There is also some data indicated a physical interaction between BACE1 and γ-secretase, and the existence of a distinct complex comprising these two secretases [114].

In addition to the aforementioned classic APP cleavage pathways, other proteolytic processing events have been described for APP, and several APP NTFs of unknown proteolytic origin have

also been reported in human and rodent tissues [91, 115]. The APP cytoplasmic domain can be directly cleaved by caspases, predominantly caspase-3 (cleaves APP695 between Asp664 and Ala665)**.** This event generates two fragments, C31 and Jcasp, which might be linked to neuronal apoptotic events **(**Figure A.8 lower part, right side**)** [116, 117]. Another physiologic APP processing pathway, mediated by membrane-bound matrix metalloproteinases (such as MT5-MMP), was termed η-secretase and generates proteolytic fragments capable of inhibiting neuronal activity within the hippocampus **(**Figure A.8 lower part, left side). This secretase activity (mainly at amino acids 504-505 of APP695) releases a truncated soluble ectodomain (~80-95 kDa) and generates higher molecular mass CTFs - CTFη. CTFη is further processed by ADAM10 and BACE1 to release long and short Aη peptides (termed Aηα and Aηβ). CTFs produced by η-secretase are enriched in dystrophic neurites in an AD mouse model and in human AD brains [118]. A δ-secretase event, mediated by an asparagine endopeptidase, cleaves APP at two different ectodomain sites (between N373-E374 and N585-I586) generating 3 soluble APP fragments (sAPP1-373, sAPP1-585, and sAPP374-585) and CTFs. The lysosomal cysteine protease Cathepsin B was associated with enhanced production of N-terminally truncated pyro-glutamate forms of Aβ which have highly propensity to aggregate and consequently might be more toxic [102].

Several efforts have been made to understand where the different APP fragments are generated, as well as their transport and final destination. As previously mentioned, axonal APP and dendritic APP can follow different fates. A study using primary hippocampal neurons transduced with APP chimeras selectively targeted to the axonal or the dendritic compartment, in combination with mutations that render the respective mutants secretase-resistant, showed interesting results regarding APP processing and APP fragments' origin in neurons. Surface APP is mainly APP full-length and is preferentially polarized to the axonal surface. Although β- and γ-secretases cleave APP either in the pre- or post-synaptic compartments, more Aβ peptides seem to be released from dendrites [94]. A subsequent study confirmed that the majority of APP is processed in the neuronal soma (as already suggested [119]), but local processing in axons/synapses can still occur, a mechanism that might be more significant in human neurons than in mouse neurons [120]. This is concordant with previously reports of endocytosis-dependent Aβ release following synaptic activity [121]. The authors report higher amounts of Aβ40 than Aβ42 in both the soma and axonal compartments of human brains, and higher amounts of sAPPα than sAPPβ. The transport of APP products generated in the soma depend on endocytosis, but at least APP full-length might enter the axons independently of endocytosis [120]. In fact, it was shown that APP can be transported independently of any sorting signal to the axonal and dendritic compartment [122]. Other studies add that the APP cleavage products are sorted into distinct vesicles before entering the axon. NTFs

display a perinuclear distribution and preferentially associate with acetylated microtubules and neurofilaments in neurons. CTFs are preferentially present in a compact region in the soma. A significant larger fraction of the CTFs is retained in the cell body, while NTFs appear to be massively exported from the soma into neurites and neurite terminals [119, 123].

Above it was described several factors that modulate APP trafficking and, consequently, APP proteolytic processing. In addition, γ-secretase is influenced by signal transduction pathways, namely by PDGF, Src, Rac1, and Ras. Activation of β2-adrenergic receptors and activation of the opioid receptor OPRD1 also stimulate γ -secretase activity and Aβ production. One important player in APP processing is its interaction partner PIN1, a peptidyl-prolyl cis/trans isomerase. PIN1 overexpression reduces Aβ secretion, and knockout of Pin1 increases its secretion. The mechanisms seems to involve PIN1 binding to the phosphorylated T(668)-P motif in APP and consequent prolyl isomerization [124].

2.4. Post-translational modifications – APP phosphorylation

As previously described, after biosynthesis APP suffers posttranslational glycosylation – termed as maturation – during its trafficking through the secretory pathway. This includes the acquisition of N- and O-linked sugars. APP N-glycosylation starts at the ER and further proceeds in the cis-Golgi. APP has two potential N-glycosylation sites, but only the one located at N467 was proved in vitro and in vivo. N-glycosylation was shown to affect the intracellular sorting and secretion of APP, including axonal sorting [125]. APP maturation by O-glycosylation occurs during trafficking through the TGN. APP has several O-glycosylation sites (for example T291, T292, T576 of APP695), and APP O-glycosylation is suggested to be necessary for the APP processing by secretases [125]. Secretory trafficking through the TGN also involves APP tyrosine sulfation [126]. In addition to glycosylation, APP might be modulated by phosphorylation events, acetylation, neddylation, sumoylation, and ubiquitination (as specified at PhosphoSite [127]).

Direct phosphorylation of the APP molecule is associated with important roles in the regulation of APP binding, traffic and processing. Indeed, APP is a phosphoprotein with several putative phosphorylation sites. Within the small ED domain (located between the E1 domain and the AcD domain) at least two phosphorylation sites were described, namely at Ser198, and Ser206 [126]. In addition, the APP cytoplasmic tail comprises at least three Tyr residues and five Ser/Thr putative phosphorylation sites: Tyr^{653}, Thr^{654}, Ser^{655}, Thr^{668}, Ser^{675}, Tyr^{682}, Thr^{686} and Tyr^{687}, most of which are located within three functional motifs: ^{653}YTSI^{656}, ^{667}VTPEER^{672}, and ^{682}YENPTY^{687}; and their phosphorylated forms were detected in post-mortem brain tissue of AD patients (except for the T654; See Figure A.6) [105, 128]. In spite of this, there is still some controversy concerning their functional value and in vivo validity. Of note, phosphorylation does not seem to be specific of the

APP full-length molecule, but some CTFs and AICD fragments are also detected as phosphorylated.

Threonine 668 is the APP phosphorylation residue most extensively studied, followed by Tyrosine 682. In fact, some level of interaction between these two phosphorylation residues was shown to exist and to modulate the APP interactome [129]. For example, the Shc and Grb2 protein adaptors only bind APP when this is phosphorylated at Y682, and the interaction is further increased by additional T688 phosphorylation. Nevertheless, the effect of APP phosphorylation at T668 in APP processing is still contradictory, but there is reports associating its phosphorylation to Aβ production [128], and to a decrease in APP cleavage by caspases. Importantly, APP phosphorylation at T668 appears to be important for APP binding to PIN1, and to Fe65 (or APBB1). Phosphorylation at T688 creates a recognition site for Pin1, but inhibits Fe65 binding.

Phosphorylation of S655, that has been observed to occur in mature APP molecules in vitro and in vivo, may be a pivotal regulatory process for APP trafficking and proteolysis, since this residue is located in the basolateral sorting motif, ^{653}YTSI^{656}, and it is the only APP Ser/Thr residue phosphorylated by PKC [128, 130, 131]. Additionally, NMR analysis showed that APP phosphorylation at S655 induces significant local conformational changes in the APP C-terminus at and downstream the ^{653}YTSI^{656} motif [132]. Besides PKC, S655 may be phosphorylated by calmodulin-dependent protein kinase II (CaMKII) [130], and by APP kinase I [131]. APP phosphorylated at S655 is an active molecule, crucial in the regulation of the APP subcellular trafficking. Through the use of APP S655 phosphomutants - serine 655 to alanine (S655A), and serine 655 to glutamate (S655E), mimicking dephosphorylated and phosphorylated APP, respectively – evidence was gather that S655 phosphorylation of mature APP molecules is a signal for APP traffic via the secretory pathway, facilitating its incorporation into TGN vesicles and Golgi exit**.** S655A is thus highly retained at the Golgi, exhibiting delayed incorporation into secretory post-TGN vesicles and delayed sAPPα medium secretion. In contrast, S655E appears to have facilitated Golgi exit, enhanced traffic between the Golgi and the PM, as well as a higher rate of sAPPα secretion. In addition, the APP S655 phosphomimetic mutant displayed enhanced half-life and recycling via increased binding to the retromer complex and consequent facilitated retromer-mediated retrieval to the TGN [95, 133]. More recently, the S655 phosphomimetic mutant was associated to a decrease in APP trafficking to lysosomes and decreased Aβ42 production, potentially via disruption of the APP interaction with AP-3 [134]. This raises the hypothesis that part of the mature APP population is phosphorylated at S655 when it is necessary to target APP for a more dynamic TGN-to-PM trafficking, and sAPPα generation, what may occur through the catalytic action of PKC [133].

3. APP interactors – evidence for an APP role in nervous system development and function

The complexity of APP derives not only from its elaborate intracellular trafficking, posttranslational modifications and proteolytic cleavage, but also from the existence of multiple protein interactors. A search in the expert curated human protein-protein interaction database 'HIPPIE' retrieved more than 2000 protein partners for APP (accessed on June 27, 2016) [135]. APP protein interactions will depend on APP intracellular localization, posttranslational modifications and proteolytic cleavage. On the other hand, different APP partners will modulate the protein cellular "behavior" and will guide APP to specific functions (and dysfunction). Previously, some APP interactors that could modulate APP intracellular trafficking and proteolytic cleavage were mentioned, namely Fe65, SorLA, Sortilin, RanBP9, PAT1a, and PIN1. It was also mentioned that the phosphorylation status of the APP YENPTY motif modulates different APP protein-protein interactions. This C-terminal motif has been associated to several other important APP partners, as X11α/mint1, JIP, Dab1, and Numb, which have also been described to modulate the APP "life-cycle".

X11α/Mint1 binds to APP, independently of the APP phosphorylation status, and this interaction appears to modulate several aspects of APP trafficking and metabolism, including reduction of Aβ levels [136, 137]. In addition, Mint proteins are critical players in regulating activity-dependent APP endocytosis and insertion, which, in turn, affects Aβ generation. Upon synaptic activity, Mint mediates the convergence of APP/PS1 co-localization [138].

JIP scaffold proteins, JIP1 and JIP2, are structurally related proteins proposed to assembly functional JNK modules (binding MLK3, MKK7, and JNK) supporting the activation of the JNK signaling pathway. Both proteins are described to bind APP, which is suggested to mediate the APP binding to JNK, and in turn APP T688 phosphorylation. JIP1b seems to modulate the processing of APP (decreases intracellular CTFα, and sAPPα and Aβ secretion), while JIP-2 apparently has no effect on APP processing [139, 140]. Furthermore, the JIP1 and JIP2 proteins, similar to APP, can bind the light chain of Kinesin-1 and are transported via MT to growth cones in cultured neurons [141]. The binding of JIP proteins to Kinesin-1 might be involved in the activation of Kinesin-1 and cargo release [142], and JIP1 (and to some extent JIP2) is reported to modulate the transport of T668-phosphorylated APP into neurites by Kinesin-1 [143, 144].

Dab1 is an adaptor protein involved in the Reelin signaling pathway, whose binding to APP is associated with increased levels of surface APP and α-secretase cleavage. In addition, Dab1 overexpression seems to increase APP/CTFβ levels as well as Aβ secretion [145, 146]. Numb is a negative regulator of Notch, and has four alternatively spliced variants, described in mammals, that

differ in the length of their PTB and proline-rich region. Neural cells expressing short Numb isoforms (that lack inserts in the PTB domain) exhibited marked accumulation of APP in early endosomes and recycling compartments, and increased levels of APP-CTFs. On the other hand, cells expressing long Numb isoforms (with the insertion in the PTB domain) exhibited reduced amounts of cellular APP and its fragments. The expression of short Numb isoforms, and consequently increased amyloidogenic processing of APP, appear to be favored during trophic factor deprivation in primary cortical neurons [147].

Since the majority of the mentioned APP interactors bind to the same C-terminal motif in APP, some of which have opposing effects on APP cell fate, it is feasible that APP interactors have to compete for APP binding and that this competition will determine different APP fates in different cellular physiologic and pathologic contexts. Competition for APP binding has been described, for instance, for Dab1 and X11 [145], for Dab1 and Fe65 [148], and for X11 (β isoform) and Fe65 [149]. Complementarily, the phosphorylation status of APP and APP proteolytic processing might dictate the identity of APP binding partners in the different contexts. Some interactions will depend on the phosphorylation status of specific residues, as already mentioned through the text, and some interactions might depend on the cleavage status of APP (full length protein versus APP cleavage products). For example, RanBP9 has been shown to interact more strongly with AICD than with the APP full-length protein, and ShcA preferentially interacts with C99 [112, 150].

The extracellular domain of APP also mediates several APP protein interactions, a fraction of which are secreted proteins that could function as APP ligands and place APP as a potential receptor. Reported potential APP ligands include: TAG-1 [151], F-spondin [152], contactins [153], Reelin [146, 154], and pancortins [155]. Curiously, the described ligands and their relation to APP are commonly associated with neurodevelopment. APP interaction with Reelin has effects on both proteins. On one hand, APP interaction with Reelin may be important to maintain normal Reelin levels in the brain. On the other hand, Reelin increases surface APP by decreasing APP internalization, increases APP α-cleavage, and decreases Aβ production. Importantly, APP and Reelin functionally interact to promote dendritic complexity and length, in vitro and in vivo, and apparently this effect might further involve β1-integrin [154]. Previous studies, had already shown that in rat hippocampal neurons, cell surface APP co-localized selectively with α1β1 and α5β1 integrin heterodimers at characteristic segmental locations in the axonal membrane [156]. The role of pancortins in the regulation of neural precursors' migration into the cortical plate might depend, at least in part, on their action as extracellular ligands of APP [155]. In addition, the extracellular region of membrane bound APP has been shown to interact with various extracellular matrix components (like heparin, collagen type I, and laminin), and other cell adhesion molecules (NCAM and NgCAM) suggesting a role for APP in cell-matrix and cell-cell adhesion [157].

If we look at the known APP protein interactors retrieved by the HIPPIE database, select the interactors with the higher confidence scores (Supplementary Table A.1), and perform the Panther overrepresentation test [158], we can appreciate which functions might be enriched in this APP interactome and know which APP partners might be involved in each function. In the Panther overrepresentation test, analysis results are sorted accordingly to the hierarchy system established by the Gene Ontology Consortium[159] based on the interrelatedness of enriched functional terms - parent-child method. Focusing on gene ontology terms related to nervous system function, we can organize the APP known protein interactors into four functional groups of specific interest (Table A.1; for the complete list of selected gene ontology terms see Supplementary Table A.2).

Table A.1 - **APP known protein interactors are implicated in functions related to nervous system development and synapse function**. In the panther overrepresentation test, here used, analysis results are sorted accordingly to a hierarchy system based on the interrelatedness of enriched functional terms (parent-child method). "Parent terms" were used to organize the APP known protein interactors into three functional groups of specific interest: Nervous system development group, Synapse function group, and Neuron death group. A fourth group includes additional gene ontology terms corresponding to functions tightly associated with brain development, function and organization. GO Biological process, indicates significantly enriched biological processes corresponding to more specific (child) terms. F. Enrichment, the fold enrichment of the genes observed in the APP protein interactors list over the expected based on the reference list (the human genome). A number greater than 1, indicates that the category is overrepresented. pvalue, calculated pvalue with Bonferroni correction. Only pvalues higher than 0.05 were considered.

	GO Biological process	F. Enrichment	pvalue
Nervous system development	cerebral cortex development	11.64	1.76E-04
	glial cell differentiation	9.07	1.74E-03
	limbic system development	9.76	1.71E-02
	negative regulation of neuron projection development	8.99	7.62E-03
	regulation of axonogenesis	8.36	9.50E-04
	axonogenesis	7.56	1.08E-07
	positive regulation of neuron projection development	5.89	2.79E-02
Synapse Function	regulation of synaptic vesicle transport	24.56	1.77E-03
	regulation of neuronal synaptic plasticity	18.13	1.30E-03
	neuron-neuron synaptic transmission	15.86	3.15E-03
	chemical synaptic transmission, postsynaptic	13.88	7.62E-03
	presynaptic process involved in synaptic transmission	10.88	1.59E-03
	synapse organization	10.43	2.23E-05
	positive regulation of synaptic transmission	10.38	2.34E-03
	regulation of neurotransmitter levels	8.41	2.32E-04
Neuron death	Neuron apoptotic process	24.68	1.63E-04
	positive regulation of neuron apoptotic process	24.30	1.69E-06
	negative regulation of neuron apoptotic process	11.20	1.02E-05
others	Learning or memory	8.04	2.77E-05
	Extracellular matrix organization	8.27	6.09E-09
	Regulation of cell adhesion	4.38	6.54E-05
	Cell migration	4.18	1.41E-05
	Cytoskeleton organization	4.09	4.56E-06

The two major functional groups obtained, presenting more gene ontology terms and higher number of proteins associated were Nervous system development with 31 terms associated, and Synapse function (including synaptic signaling and synapse organization) with 15 terms, see Table A.1 and Table A.2. Analysis of such APP protein interactors can give us more clues about APP physiological function in the nervous system.

Table A.2 - APP protein interactors associated with Nervous system development, Synapse function, Neuron death, and other related functions. The proteins are here represented by the gene symbol. ECM, extracellular matrix.

	APP protein interactors (by gene name)
Nervous system development	UCHL1; NUMB; RANBP9; NOTCH1; SHC1; YWHAG; GSN; SORL1; NEFL; RAB3A; CALR; CFL1; NF1; GSK3B; HSP90AA1; KLK6; DLG4; ITM2A; CASP3; GFAP; STXBP1; MAPT; TNFRSF21; ACTB; LRP1; CAV1; TGFB2; RNF2; UBB; COL25A1; TGFB1; APBB2; APOE; GSK3A; APBA1; AKT2; ACHE; CLU; ABL1; PIN1; CDK5; GNAO1; APOA1; MBP; APBB1; DAB1; FLOT1; PARK2; PSEN1; SPTAN1; SHC3; MAPK8IP2; NGFR; CUL7; FOS; EGFR; APBA2; TMEM30A; APLP1
Synapse function	RAB3A; NF1; GSK3B; DLG4; SNCA; STXBP1; CHRNA7; SNCB; APBA3; HSPA8; DNM1; APOE; GSK3A; APBA1; ACHE; CDK5; KIF1B; MBP; PARK2; PSEN1; SHC3; MAPK8IP2; APBA2; YWHAG; GFAP; CLSTN1; FLOT1; NGFR; PIN1
Neuron death	KLK6; CASP3; TNFRSF21; GAPDH; CDK5; PSEN1; NAE1; SORL1; NEFL; SNCA; STXBP1; SNCB; LRP1; SET; NGFR; NF1; GSK3B; MAP3K5; UBE2M; TGFB2; CLU; ABL1.
Learning and memory	NF1; DLG4; CASP3; CHRNA7; PRNP; CDK5; PARK2; PSEN1; SHC3; MAPK8IP2; FOS; EGFR
ECM organization	A2M; GSN; NF1; FBLN1; SNCA; GFAP; HSPG2; TGFB2; COL4A6; TGFB1; APBB2; TTR; FLOT1; BGN; NOTCH1; HSPA8; ABL1
Regulation of cell adhesion	NOTCH1; GSN; CALR; NF1; GSK3B; HSPD1; FBLN1; CASP3; TNFRSF21; CAV1; TGM2; TGFB2; PRNP; TGFB1; ABL1; APOA1; DAB1; FLOT1
Cell migration	NUMB; MAPRE1; NOTCH1; GSN; SORL1; CALR; NF1; GSK3B; FBLN1; LRP1; TGFB2; TGFB1; APOE; AKT2; TIRAP; CDK5; DAB2; EGFR; ADAM17
Cytoskeleton organization	RANBP9; SHC1; MYH9; GSN; QRICH1; NEFL; CALR; EPB41; CFL1; CRYAB; NF1; GFAP; MAPT; DNAH1; CAV1; GAPDH; APOE; MAST1; ABL1; CDK5; SPTAN1; CUL7; TUBB; ARRB1

Interestingly, the APP protein interactors in the three main functional groups shown in Table A.1 and table A.2 (‘Nervous system development’, ‘Synapse function’, and ‘Neuron death’) seem to be highly interconnected, has demonstrated in Figure A.9. Some of the interactors here represented were already mentioned due to their effect on APP, namely APBB1 (or Fe65), APBA1 (or X11α, or Mint1), MAPK8IP2 (or JIP2), Dab1, Sorl1 (or SorLA), RanBP9, LRP1, Shc, Numb, Pin1.

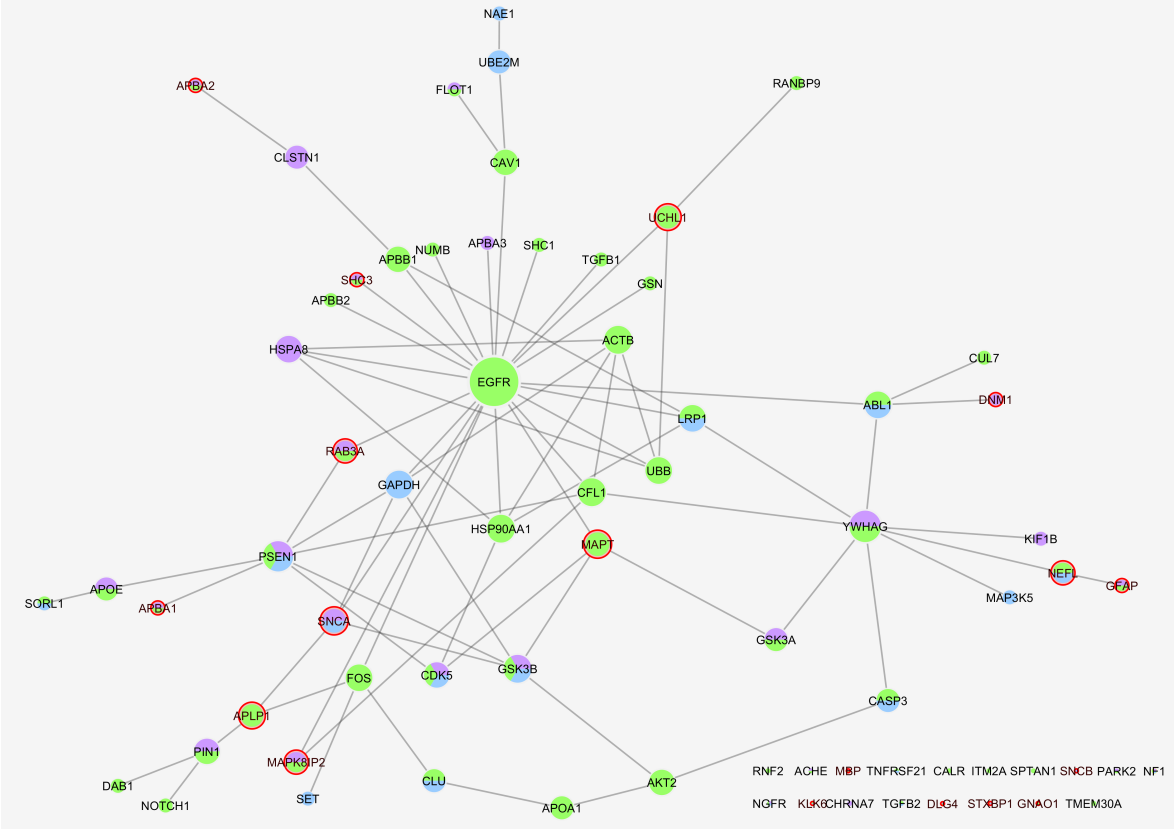

Figure A.9 - Protein-protein interaction network of the APP interactors attributed to the Nervous system development, Synapse function, and Neuron death functional groups. The network was constructed using the Cytoscape software (version 3.4.0). Information about how the APP partners interact between each other was retrieved from the International Molecular Exchange (IMEx) consortium partners only. Red outlined circles represent proteins that are brain specific/enriched as indicated in the Human Protein Atlas database. Network nodes are configured by size accordingly to node degree (low values to small sizes) and by color accordingly to the functional group ('Nervous system development', green; 'Synapse function', purple; and 'Neuron death', blue)

Based on simple topological parameters like node degree (number of interactors) and betweenness centrality (a measure of node's centrality, that is, how frequent a node represents the shortest-path between other nodes), one of the highlighted nodes is EGFR (Figure A.9). APP interaction with EGFR was detected in a screen of integral membrane protein-protein interactions using a variation of a membrane yeast two-hybrid assay. In the study, the interaction seems to be stronger with a constitutive kinase active EGFR mutant [160]. The EGFR (and its ligands) are expressed in various regions of the CNS, and their expression pattern is suggestive of a role in neurodevelopment. In addition, EGFR signaling has been implicated in several neurological disorders including in Alzheimer's disease. Interestingly, a study using single-cell RNA-seq to characterize DCX-expressing immature neurons during neurogenesis in the hippocampus of adult mammals, showed that the progression from early, stem-like stage, to the more mature neuronal stage is marked by an up-regulation of genes enriched for interactions with EGFR along with synapse and dendrite localization, cellular transport, nitric oxide signaling and long-term potentiation [161].

APP and Fe65 (APBB1) colocalize and interact at two type of mobile membranes namely, integrin-based focal complexes characteristic of extending lamellipodia [162] and growth cones of developing neurons [163]. The interaction between APP and Fe65 accelerates cell migration during a wound-healing assay, an effect that is thought to also involve the Fe65 protein interactor Mena, an actin-binding cytoskeletal protein that regulates lamellipodia dynamics [162]. Additional studies, showed that disruption of APP and Fe65 interaction in cultured hippocampal neurons results in aberrant axonal branching, again with indications of the involvement of a third protein that binds to the WW domain of FE65 [164]. The phenotypes displayed by *Fe65* KO mice (either single or *Fe65/Fe65l1* double KO), which have several similarities to APP family members triple KO mice, further implicate Fe65 in cortical development [165], and in central and peripheral synapses modulation [166]. Curiously, Fe65 (and Fe65L/APBB2) also binds EGFR (see Figure A.9).

In Figure A.9, we can see that APP shares another interesting protein interactor with EGFR, the protein Numb. Numb inhibition of Notch1 signaling pathways, an important signaling in cell fate decisions during central nervous system development and maturation [167], is thought to depend on its function as an endocytic adapter protein that mediates the internalization of receptors. Conditional mouse mutants with deletion of numb in developing sensory ganglia show reduced endocytosis, a significant increase in nuclear Notch1, and a severe reduction in axonal arborization in afferent fibers. Contrarily, overexpression of Numb induces accumulation of Notch1 in markedly enlarged endocytic-lysosomal vesicles, reduced nuclear Notch1, and aberrant axonal arborization [168]. Other studies also implicated Numb in neuronal differentiation and neurite outgrowth [169, 170]. Curiously, enhanced EGFR signaling has been described to reduce Notch1 expression through Numb, mediating the expansion of the neural progenitor cells pool and decreasing neural stem cells number and self-renewal in the subventricular zone [171]. Apparently, binding of APP to Numb prevents Numb from inhibiting Notch, and increases Notch activity [172]. Ectopic expression of human APP-family members induced Notch gain-of-function phenotypes in the mechano-sensory organs (MSOs) of Drosophila, and expression of high levels of APP (and APLP2) suppresses the abnormal phenotypes in drosophila development induced by Numb overexpression [173]. Noteworthy, in the mentioned work, Dab was also shown to play a role in the fly phenotypes induced by APP, as Dab also binds Notch, authors propose it could be also mediating the interaction between APP and Notch [173]. Dab1 is an important mediator of Reelin signaling crucial not only for neuronal migration and positioning, but also for dendritogenesis during neocortex development [174]. In utero electroporation of Dab1 RNA interference in a subset of migrating neurons at E16, resulted in simplified leading processes that are less likely to contact the marginal zone at E20 (even in the presence of Reelin) comparing to non-electroporated

cells. At postnatal day 2, electroporated cells show simplified dendrites also less likely to contact the MZ. This shows that Reelin-Dab1 signaling has an important function in the establishment or elaboration of neurites in the stage between neuronal precursor and postmigratory neuron [174]. Interestingly, the APP role in the regulation of neural precursor cells entry in the cortical plate appears to depend on binding to Dab1 (and downstream Dab1, on DISC) [175, 176].

The X11α (or Mint1, or APBA1 in the network) presents brain specific expression and also comes up as an APP protein interactor with potential function in neuronal development and synapse function. Although not mapped in the Figure A.9 network, X11α interacts with the synaptic fusion protein, and APP interactor, Munc 18-1 (or STXBP1) [177]. In addition, X11α is described to be part of a tricomplex, formed by pre-synaptic protein CASK (which binds β-neurexin) and Veli proteins, proposed to couple membrane traffic and synaptic vesicle exocytosis to neuronal cell adhesion [178, 179]. *X11* KO mice confirm the role of this protein in presynaptic function and neurotransmitter release, what might be dependent on a functional interaction with Munc 18-1 [180]. The X11 family of adaptor proteins also interacts with ApoEr2 (a Reelin receptor), and might contribute, together with Reelin, to the regulation of ApoEr2-mediated cell motility (in this study, neither X11 nor Reelin had an effect in APP-mediated cell motility) [181]. X11α is also described to interact with Kalirin-7, a Rho-GEF that regulates dendritic morphogenesis [177]. In aged *X11α/App* double transgenic mice that produce high levels of brain Aβ and develop age-related memory defects, X11α is able to decrease brain Aβ levels and to rescue the memory defects [182]. Munc 18-1 (or STXBP1; an isolated protein in the protein-protein interaction network in Figure A.9) is a neuronal protein required for synaptic vesicle exocytosis that interacts with syntaxin 1 and X11α, as mentioned. *Stxbp1* KO mice develop neurodegeneration and present abnormal synaptic transmission and complete loss of neurotransmitter secretion from synaptic vesicles during development [183]. Mutations in the human *STXBP1* gene cause epileptic encephalopathies associated with intellectual disability, and neuronal cultures from human iPSCs of *STXBP1* haploinsufficiency show impaired neurite outgrowth [184].

JIP2 (or MAPK8IP2, or islet brain-2 protein) is a brain enriched protein that seems to be an attractive APP protein interactor (high-confidence APP interactor) concerning its implication in nervous system development, synaptic transmission, and learning and memory. Within the network it binds to EGFR and Cofilin-1, an actin-severing protein (Figure A.9). JIP-2 is an integral constituent of postsynaptic densities in cerebellar and cerebral cortices, and JIP-2 null-mice display motor and cognitive (social interaction, exploratory, and learning) deficits [185]. Such defects might be due to the described alterations in Purkinje cell morphology associated with abnormal glutamatergic transmission in the cerebellum [185, 186], or might reflect synaptic transmission deficits throughout the brain, an aspect still not evaluated. This protein has also been linked to

human neurodevelopment syndromes [187]. The proline-rich domain in the cytoplasmic tail of ApoER2 interacts with JIP-2 and JIP-1 proteins. The expression of proline-rich domain-containing splice variants of ApoER2 and the expression of JIP-2 coincide with murine brain stem cells differentiation into neurons. Binding of ApoER2 to JIPs links the Reelin signal to the JNK pathway, a parallel signal event to the well described Dab1 [188].

One fascinating aspect, at this point, is that not only does Reelin interacts with APP, and APP is able to interact and signal via Dab1, but also the Reelin receptor ApoER2 seems to share several interactors with APP (JIP proteins, X11α, and even Fe65 [189]). Furthermore, APP seems to be tightly involved in lipoprotein metabolism, and vice-versa, via interactions with LDL receptor related proteins (LPR; APP is described to bind LRP1, LRP1b, ApoeR2 and LRP2/megalin, and the related family member SorLA). This is an important aspect since neurons in the adult brain depend on cholesterol derived from internalized lipoproteins via lipoprotein receptors. Cholesterol is, for example, required for membrane reorganization during synaptogenesis [190]. For instance, selective deletion of LRP1 (here highlighted as an APP protein interactor functioning in 'Nervous system development' and 'Neuron death', see Table A.2 and Figure A.9), in mice forebrain neurons, leads to decreased brain levels of cholesterol and results in age-dependent dendritic spine degeneration, synapse loss and memory decline [191]. LRP1 was also involved in a signaling pathway with major implications in neuronal function, through the activation of Src family kinases and transactivaton of Trk receptors. By this way, different LRP1 ligands were shown to be able to activate Akt and ERK1/2 and promote neurite outgrowth in PC12 cells and rat cerebellar granular neurons [192].

In Figure A.9, we can also notice another brain-enriched APP interactor, the ubiquitin C-terminal hydrolase (UCH)-L1, also binding to EGFR, RanBP9, and polyubiquitin-B (UBB). Although mainly described for its role in the recycling of ubiquitin, deletion of the *Uchl1* gene (and *Uchl1* mutant mice) causes a specific type of axonal degeneration, suggesting that this protein has a crucial role in the maintenance of axonal integrity [193]. During embryonic brain development, UCH-L1 expression changes showing increased levels in the cortical plate at the time of neuritogenesis and neuronal maturation. UCH-L1 is expressed in neural precursor cells and seems to regulate their morphology [194]. In addition, this enzyme is downregulated in sporadic AD brains, and impaired activity has been reported in many neurodegenerative diseases. UCH-L1 inactivation leads to the inhibition of hippocampal LTP and impairs contextual learning. In APP/PS1 mice, transduction of UCH-L1 protein restores Aβ-induced synaptic dysfunction and also re-establishes synaptic plasticity and improves associative memory [195]. Such effect depends on the ability of UCHL1 to interact with APP and to mediate APP ubiquitination followed by trafficking to lysosome for degradation [196].

Within the constructed protein-protein interaction network, UCH-L1 binds RanBP9. This APP protein interactor is also of interest when referring to neuronal development. RanBP9 (or RanBPM) is an evolutionarily conserved small GTPase located in cytoplasm and nucleus. Functionally, it was first described as having a role in nuclear import and export and spindle formation [197]. It has also been described to function as an adapter protein coupling membrane receptors to intracellular signalling pathways; namely, it was proposed to stimulate Ras-Erk-SRE pathway activation by recruiting Sos [198]. However, recently, RanBP9 was reported to function as an inhibitor of the ERK pathway by binding the c-Raf complex and regulating c-Raf stability. In this way, RanBP9 loss of expression results in constitutive activation of the ERK pathway and promotes cell proliferation and cell migration [199]. Concordantly, RanBP9 is shown to physically interact with Plexin-A1, and when overexpressed cooperates with PlexinA1 to reduce cell spreading and to strongly inhibit axonal outgrowth and branching in vitro and in vivo [200]. Noteworthy, Sema3A is reported to promote dendritogenesis (in contrast to inhibition of axonal outgrowth), and RanBP9 could also contribute (positively) to such process. Interestingly, it has been shown that RanBP9 colocalizes with APP and Fe65 at lamellipodia, and in *Ranbp9*-transgenic mice, reduced levels of surface β1-integrin, LRP, and APP correlated with inhibition of neurite arborization in primary hippocampal neurons. In this way, the RanBP9 modulatory effects on the endocytosis and cell surface levels of β1-integrin, LRP, and APP appear to be correlated with its roles in cell attachment, spreading, focal adhesion signalling and assembly, and neurite arborisation [201]. A recent report showed that the endogenous levels of RanBP9 are required for Aβ-induced collapse of growth cones in immature neurons and depletion of synaptic proteins in mature neurons. RanBP9 reductions protected against cofilin–actin pathology, synaptic damage, gliosis, and Aβ accumulation associated with AD mice models [202].

As already mentioned, residues 657–676 of APP cytoplasmic domain possess affinity for Gαo (one of the isolated proteins in the Figure A.9). Although, the interaction between APP and Gαo is confirmed, it remains to be clarified whether it promotes Gαo activation [87] or inhibition [203]. Analysis of this interaction in human brain samples from AD patients revealed that the interaction is decreased with disease progression, which further correlates with increases in the levels of membrane Aβ and Gαo activity [204]. In *Manduca sexta* nervous system, endogenously expressed full-length APPL (which retains the Gαo binding site) interacts with Gαo and both proteins colocalize in regions of active motility, including the leading processes of migrating neurons and the growth cones of elongating neurites. Furthermore, either interference with APPL expression or inhibition of Gαo leads to a similar phenotype characterized by inappropriate migration and outgrowth [205].

The significance of APP and its protein-protein interactions can be further supported by their involvement in human diseases. The DisGeNET database (consulted on June 26, 2016) integrates human gene-disease associations from various expert curated databases and text-mining derived associations [206]. By exporting all the genes sharing diseases with APP, and filtering the exported list by MeSH Disease Class including Nervous System Diseases and/or Mental Disorders, we can see with which genes APP is commonly associated in these classes of diseases. By crossing the resulting list with the APP protein-interactors involved in nervous system development, synaptic function, and neuron death presented on Table A.2, we can see that APP and these specific protein interactors are annotated to 45 different nervous system or mental disorders (see Figure A.10).

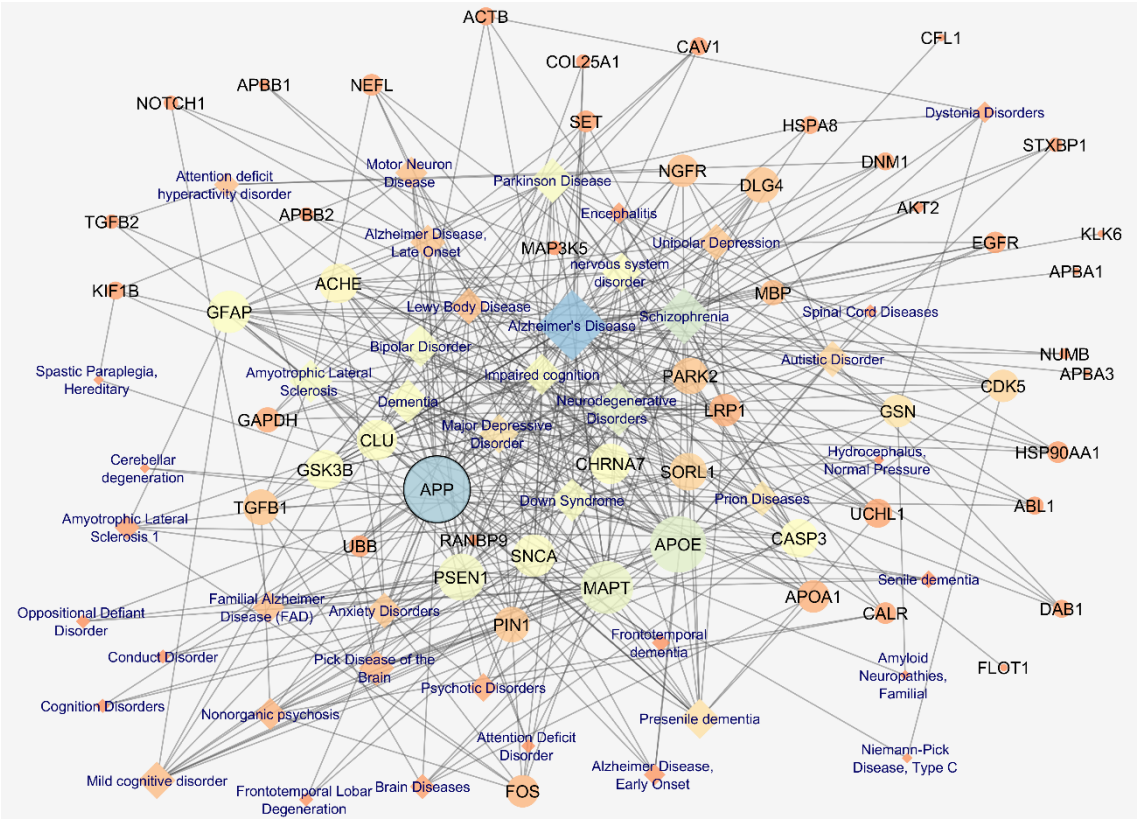

Figure A.10 - **Nervous system diseases network shared by APP and its binding partners.** The complete list of diseases shared by APP and other human genes was retrieved from the DisGeNET database. This list was filtered for Nervous system diseases and mental disorders only. The APP protein interactors previously implicated in Nervous system development, Synapse function, and neuron death were searched in the obtained list, to create a network of diseases shared between all these human genes. Of note, SNCB, CLSTN1, NAE1, UBE2M, SHC1, YWHAG, RAB3A, NF1, ITM2A, TNFRSF21, RNF2, GSK3A, GNAO1, SPTAN1, SHC3, MAPK8IP2, CUL7, APBA2, TMEM30A, and APLP1 were not attributed to any APP associated Nervous System Diseases or Mental Disorders. Diseases are represented in diamond shape nodes and names are in blue. Gene name are represented by their symbol in circular nodes and dark color letters. Network nodes are configured by size accordingly to node degree (low values to small sizes) and by color accordingly to betweenness centrality (low values to bright colors). Network edges are configured by size accordingly to edge betweenness (low values to small sizes).

The diseases associated with the highest number of APP protein-interactors included Alzheimer's Disease (linked to 45 APP interactors), Schizophrenia (30), Parkinson Disease (20), Down Syndrome (16), Amyotrophic Lateral Sclerosis (16), and Bipolar Disorder (15). On the other hand, APP protein-interactors sharing more diseases associations with APP include APOE (31), MAPT (27), PSEN1 (21), GFAP (16), SNCA (16), CLU (14), and CHRNA7 (14).

Concerning the above highlighted APP interactors all their coding genes seem to be associated, together with APP, with Alzheimer's Disease. In addition, UCHL1 seems to be involved with APP in other specific diseases like Parkinson Disease, Lewy Body Disease, and Presenile dementia; SORL1 is involved in Bipolar Disorder, Mild cognitive disorder, Schizophrenia, Presenile dementia, and Down Syndrome; LRP1 is involved in Schizophrenia, Unipolar Depression, Major Depressive Disorder, and Presenile dementia; EGFR is involved in Major Depressive Disorder, Unipolar Depression, and Amyotrophic Lateral Sclerosis; DAB1 in Autistic Disorder, Schizophrenia, and Prion Diseases; STXBP1 is involved in Autistic Disorder, and Schizophrenia; NUMB is involved in Bipolar Disorder; RANBP9 is involved in Schizophrenia. APBB1 (or Fe65) and APBA1 (X11) are only annotated for Alzheimer's disease. Again, Schizophrenia is the second most common disease associated with APP and these specific APP protein interactors. This is a very interesting aspect, since alterations in neuritogenesis have been recognized as an etiological factor for this development disease, and Schizophrenia's neuroanatomical findings include reduced intraneural space (the space occupied by dendrites and axons), decreased dendritic markers and reduced dendritic length [207]. Furthermore, a study of abnormally expressed genes in postmortem prefrontal cortex samples of schizophrenia, bipolar disorder, and major depression patients highlighted APP as an essential gene. Namely, APP was defined as a tissue-specific gene, highly abundant in all disease and control samples, with the highest ranks in the centrality analysis of the constructed protein-protein interaction networks, where it emerged as a critical node interacting with marker genes of the specific diseases [208].

The simple analysis presented here demonstrates how APP, through its numerous bind partners, can be related to nervous system development and function, and disease.

4. APP physiological role in brain development and maturation – specific role in neurite outgrowth

In the previous sections, details about the complexity of APP biology were shown, namely the intricate relationships between its intercellular trafficking, proteolytic processing, phosphorylation events, and protein-protein interactions. It was also demonstrated how the APP interactome could relate with APP function in nervous system development and disease.

Early in brain development, APP mRNA is expressed by all neuroepithelial cells in the ventricular zone, with the APP protein specifically localized within the apical cellular compartment. APP mRNA is also found in the cortical plate [70, 209]. During development, APP is present in growing neurites of neonatal rat brain [210], and developing neurons undergo increased APP expression, with this protein being preferentially localized in the neuritic growth cones [156, 211]. APP levels peak in the second postnatal week, the time of brain maturation and completion of synaptic connections, and the APP expression pattern correlates well with this protein having a role in brain development [212].

Although *App* knock-out (KO) mice do not show severe brain phenotypes, analysis of *App* KO phenotypes further implicated APP in brain development and brain function processes like neuritogenesis, axon guidance, dendritic organization and integrity, axonal transport, synaptogenesis and (pre- and post-) synaptic function, synaptic plasticity and adaptive spine remodeling associated events, and experience-dependent axonal pruning (See Table A.3).

Table A.3 - APP knock-out (KO) mice studies. Ref, study reference.

APP suggested function	KO mice described Phenotypes (vs control wild-type mice)	Ref
Neuritogenesis and axon guidance	Retarded somatic growth; Severely impaired spatial learning and exploratory behavior; Reduced locomotor activity and grip strength; Alterations in sensorimotor development; Agenesis of the corpus callosum.	[213]
Neuro-muscular function	Reduced body weight (decreased food and water intake); Decreased locomotor activity and forelimb grip strength; Age-dependent reactive gliosis in the hippocampus and various parts of the neocortex; Histopathological evaluation showed no signs of abnormal brain structures; No compensatory up-regulation of Aplp1 and Aplp2 mRNA.	[214]
Neuronal excitation/inhibition balance	Hypersensitivity to kainate-induced seizures (Seizures started earlier, were more severe, and led to enhanced mortality); Enhanced expression of c-fos in the cortex and cingulate gyrus (but not in hippocampus); No differences in the amount of morphological damage, synaptodendritic damage and extent of TUNEL labeling.	[215]
(Postnatal) brain development (maturation); Neuritogenesis and axon guidance	Retarded gain of body weight during postnatal development (no consistent reduction of body weight as adults); ~10% reduction of adult brain weight (no difference when littermates); Size reduction of the anterior commissure; Increased frequency of callosal dysgenesis and agenesis in specific strains sometimes associated with smaller ventral hippocampal commissure.	[216]

APP suggested function	KO mice described Phenotypes (vs control wild-type mice)	Ref
Modulation of copper homeostasis	Increased copper levels in cerebral cortex (no difference in the levels of iron or zinc; no difference in the levels of metals in cerebella); Increased copper levels in the liver (no difference in the spleen); Tendency to decrease copper levels in sera.	[217]
Maintenance of neuronal homeostasis and synaptic function during ageing – potential role in spatial learning	Decrease in the efficiency of LTP within the CA1 region of the hippocampus (impaired LTP after high-frequency stimuli, reduction in the EPSP slope immediately after the burst stimulus); Reactive gliosis; Younger mice show decreased body weight, are less active, and have lower forelimp grip strength; No differences in the levels of presynaptic markers, synapsin and synaptophysin, and MAP-2 either in younger or older mice; but a subgroup of mice showing weight loss and hypolocomotor activity revealed severe morphological abnormalities in the cortex and hippocampus (namely decreased levels of presynaptic and dendritic markers, and reduced branching of dendrites); No motor or sensory deficit; Older mice show impaired performance in the conditioned avoidance test; Inferior performance in the water maze test of spatial learning (for both younger and older mice).	[218]
Pre-synaptic and post-synaptic function within the hippocampus of mature animals	Reactive gliosis throughout the hippocampus of 8–12-month-old mice; Morphological alterations: disrupted immunostaining for MAP-2 and synaptophysin within the stratum radiatum of the CA1 region of the hippocampus; Greater proportion of atypical neurons with smaller mean overall length; Reduction in the projections of CA1 neurons into the stratum radiatum; Reductions in overall dendritic length and loss of smaller branching fibers; Similar biophysical properties of post-synaptic neurons; Intrinsically lower capacity for LTP: impaired amplitude of action potentials; reduced paired-pulse depression of GABA-mediated synaptic currents (no difference in facilitation of glutamate-mediated EPSPs and no change in paired-pulse facilitation).	[219]
Lipid homeostasis	Increased brain levels of cholesterol and sphingomyelin. Particular involvement of Aβ.	[220]
Control of cell cycle progression during cortical development	Increased proportion of cells in G2/mitosis and in the duration of G2 (no alteration in the proportion of neurons and cell death; no gross morphological differences; no alteration in the expression of APLP1 or APLP2) in the developing cortex of the E15 mouse embryo.	[209]
Synapse formation and transmission (early development changes)	No differences in the resting membrane potential in autaptic hippocampal neurons at 18–20 days in culture; Enhanced strength of excitatory synaptic transmission (AMPA-mediated EPSCs and NMDA-receptor-mediated EPSCs); Higher frequency of spontaneous mEPSCs (but mean amplitude unaffected); Enhanced readily releasable vesicle pool size per cell; Increased evoked EPSCs amplitude; Increased dendritic length and synapse number; Higher staining intensity of synaptophysin-positive presynaptic terminals in the stratum radiatum.	[221]
Spatial learning	Decreased body weight and a strong reduction of wet brain (age: 10–12 months of age); No apparent abnormalities shown by histopathological analysis; Grip strength deficit; Altered circadian locomotor activity Reduced exploratory activity under aversive conditions; Spatial navigation deficit and delayed learning (increased thigmotaxis, less efficient orientation toward the platform, and increased swim path length in the water maze place navigation task) associated with motor impairment (reduced swim speed); Defect in the rate of induction and maintenance of LTP in the CA3/CA1 pathway on acute hippocampal slices (but unaltered basal synaptic transmission and presynapse functionality).	[222]

APP suggested function	KO mice described Phenotypes (vs control wild-type mice)	Ref
Modulation of dendritic spine density	Two fold increase in the number of dendritic spines in apical dendrites of layer III/V cortical neurons of 4-6 months age mice (by in vivo transcranial two photon); Increased level of thin-, stubby-, and mushroom-shaped spines (especially of stubby- and mushroom-shaped persistent and functional spines).	[223]
Modulation of synaptic properties of GABAergic neurons by regulation of Cav1.2. subunit of L-type calcium channels	Increased levels of Cav1.2 in GABAergic inhibitory neurons in striatum and hippocampus; Increased peak calcium current density and selective increase in Ca2+ influx; Normal GABA-mediated inhibition under baseline conditions; Reduced paired-pulse inhibition of GABAergic inhibitory postsynaptic currents; Increased GABAergic post-tetanic potentiation; Increases in GABAergic calcium currents.	[224]
Spine formation and development	Fewer and shorter dendritic spines in cortical layers II/III and hippocampal CA1 pyramidal neurons of 1 year-old mice (by Golgi staining); Decreased in apical oblique and basal dendrites of cortical pyramidal neuron; Decreased glutamate levels and increased GABA levels (by NMR analysis of brain extracts).	[225]
Axonal transport	Reduced (in vivo) axonal transport at 2–4 months of age and 12-17 months of age mice (by Manganese Enhanced MRI).	[226]
Dendritic integrity and synaptic structure and function in the hippocampus	Decreased spine density and dendritic complexity in cultured hippocampal neurons from P0-P1 neonatal pups; Decreased apical arbors complexity of CA1 neurons (brain slices of 13 months old mice), shorter apical dendritic length, no alteration in basal dendritic length; Reduction of spine numbers confirmed in vivo with no difference in mean spine volume for all spines and subtypes (younger mice showed a non-significant trend in reduction in spine density); Reduction in long-term potentiation after tetanic stimulation, but no changes in basal synaptic transmission.	[227]
Axonal transport	Reduced transport from the hippocampus to the septal nuclei and amygdala after 7 hours of Mn2+ administration, and reduced transport to the contralateral hippocampus after 25 hours (by MEMRI); Reduced Mn2+ transport in the visual pathway from eye to midbrain and superior colliculus.	[228]
Axon guidance of commissural neurons	No major defect in the number of bundles or in the overall pathway of commissural extension in E11.5 spinal cord sections; Change in the distribution of axon bundles with significantly thicker bundles.	[229]
Dendritic architecture and spine density	Reduced dendritic complexity in mid-apical dendrites and an increased number of primary and secondary basal dendrites, without overall differences in total dendritic length in organotypic hippocampal cultures (prepared at postnatal day 0 and analysed at day in vitro 17); Decreased spine density and reduced number of mushroom spines (but increased number of stubby spines) in both apical and basal dendrites; No difference in basal synaptic transmission and no significant differences in paired-pulse facilitation.	[230]
Glial cell activation and innate immune cell response to inflammatory injury	Reduced Iba-1-positive microglia cell number, with smaller cell body size, shorter microglia processes and less ramifications in both 3 and 9 months old mice (in response to intracranial LPS injection); Reduced astrocyte cell number, which were smaller and presented shorter processes only in 3 months old mice; Reduced expression of glia markers Iba1, CX3CR1, P2ry12 and Hexb mRNA, and increased expression of CD11b and Trem2 in 3 months old mice; Reduced expression of glia markers P2ry12 and Hexb, and increased expression of DAP12 in 9 months old mice; Reduced expression of innate immune cytokine TNF-α, IL-1β, Il-10 and TGFβ mRNA in the hippocampus in 3 months old mice; more drastically reductions in the levels of TNFα, IL-1β and IL-10; Altered expression of Synaptophysin, PSD-95, and BNDF mRNA levels in response to injury.	[231]

APP suggested function	KO mice described Phenotypes (vs control wild-type mice)	Ref
Dendritic spine dynamics and adaptive spine remodeling in the adult brain associated with maintenance of D-serine homeostasis	No difference in spine densities in apical tufts of layer V pyramidal neurons in the somatosensory cortex of 4-5-month-old mice (by long-term in vivo two-photon microscopy); Reduced turnover rate (elimination and formation) of dendritic spines; Failed increase in spine density after: environmental enrichment due to abnormal rate of spine elimination; Reduced fraction of thin spines (more dynamic and responsive to external stimulation) and enhancement in relative number of mushroom spines; Decreased extracellular concentration of endogenous D-serine (increase of total D-serine and L-serine); Memory deficits showed in the novel objective recognition test (similar time to explore novel and already familiar objects).	[232]
Axonal pruning (in the adult somatosensory cortex after sensory loss)	Block of axonal pruning 1, 2, and 7 days after whisker plucking; Increased length of axon collaterals 2 days after (no difference 7 days after); Impaired axonal pruning confirmed in the APPflox/flox conditional KO mice; Alteration on gross overall structure (e.g.: more branch points at baseline); Increased bouton density on stable axons 1 day after whisker plucking, pruned back by day 2; More bouton elimination 2 days after whisker plucking.	[233]

App KO mice are viable and fertile, but present reduced body weight and brain weight. Reactive gliosis, loss of grip strength and reduced locomotor activity appear to be consistent phenotypes, together with spatial learning and exploratory behavior deficits, sometimes correlated with long-term potentiation (LTP) alterations. In general, it appears to exist a positive correlation between APP expression levels and spine density, but there are some contradictory results (see Table A.3), further complicated by results of transgenic mouse models of AD [234]. The APP role on dendritic spine formation and synaptic transmission is, therefore, very complex and most probably dependent on age, neuron type, and cognitive process.

The mild phenotypes observed in *App* KO mice, and the phenotypes of combined KO of APP family members suggest the existence of functional complementation within the APP gene family, but also reveal key physiological roles for APLP2 and APP (see Table A.4).

Table A.4 - APP family members combined knock-out (KO) mice and APP knock-ins. Ref, study reference.

Type of KO or KI	Main phenotypes described	Ref
App$^{-/-}$Aplp1$^{-/-}$	Viable and fertile; body weight deficit similar to single KO; No apparent abnormalities, and no upregulation of APLP2 protein in brain homogenates.	[235]
Aplp1$^{-/-}$Aplp2$^{-/-}$	Lethality (24h after birth)	[235]
App$^{-/-}$Aplp2$^{-/-}$	Lethality (during development or 24h after birth) Reduced vesicle density in the presynaptic active zone, excessive nerve terminal sprouting and reduced apposition of presynaptic and postsynaptic markers at NMJ, and impaired synaptic transmission; No obvious histopathological abnormalities in the brain.	[235], [236], [230].
Conditional App$^{-/-}$ Aplp2$^{-/-}$ in excitatory forebrain neurons (results vs APLP2KO)	Normal grip strength, basal locomotor activity, and locomotor activity and exploratory behavior in a novel environment; Water maze place navigation task: reduced learning, goal orientation, and spatial reference memory; Impaired spatial working memory, and impaired nested behavior; No gross brain abnormalities, no necrotic or apoptotic cell death, no overt disruptions of the cortical laminar cytoarchitecture or ectopias, absence of	[237]

Type of KO or KI	Main phenotypes described	Ref
	gliosis; but small reduction in hippocampal volume; Reductions in dendritic length and complexity in proximal and distal apical dendrites, and reductions in basal dendritic length and branching in CA1 hippocampal neurons brain slices from adult mice; Reduced spine density in both apical and basal dendrites, fewer mushroom-type spines and increased stubby spines, and smaller spine head diameters (adult brain in vivo); Deficit in early LTP and late LTP, impaired paired pulse facilitation, reduction of PSD95 expression in both cortical and hippocampal brain extracts (no differences in patch clamp recordings of CA1 pyramidal cells in acute slices).	
Triple KO	Perinatal lethality; Ectopic clusters of neuroblasts within the marginal zone and pial membrane (fronto-parietal cortex) originated ~E12-14 (incomplete penetrance); Disruption of the cortical architecture underneath the clusters (normal inside-out generation of cortical layers); Reduced survival of Cajal Retzius cells; Disruption of the basal membrane, defective interactions of basal lamina and radial glia, and defects in neuronal markers in the region of the clusters.	[238]
App$^{-/-}$APPsαki (constitutively production of sAPPα)	Rescues the decreases in body weight; Completely corrects the reduction of brain mass; Partial rescues the deficit of grip strength; Rescues alterations in circadian locomotor activity; Rescues reduced exploratory activity under aversive conditions, spatial navigation deficit, delayed learning, and the LTP deficits.	[222]
App$^{-/-}$APPΔCT15ki (lacks the last 15 CT residues)	Rescues the decreases in body weight; Attenuated the reduction of brain mass; Rescues the deficit of grip strength; Rescues alterations in circadian locomotor activity; Reduced exploratory activity under aversive conditions, spatial navigation deficit, and delayed learning; Rescues the LTP deficits.	[222]
App$^{-/-}$Aplp2$^{-/-}$ sAPPβki/ki	The secreted APPsβ protein is stable in vivo (and no further proteolytic cleavage in vitro); No rescue of the lethality of the App/Aplp2 dKO mice; APPsβ is inactive in APP-mediated survival and neuromuscular synapse function.	[239]
App$^{-/-}$Aplp2$^{-/-}$ sAPPαki/ki	Partial rescue of the lethality of the App/Aplp2 dKO (still presented widened end plate, excessive nerve growth, impaired neuromuscular transmitter release, and structural abnormalities at the neuromuscular synapses); Rescues the defects in spine density and in dendritic branching of distal apical segments (but shows impaired LTP and impaired spatial memory).	[230]
App$^{-/-}$Aplp2$^{-/-}$ APPΔCT15ki	Partially viable (partially rescues the lethality of dKO mutants); Reduced Aβ40, Aβ42, and βCTF in cortical brain lysates, and reduced sAPPβ (no difference in sAPPα); NMJ morphology is aberrant (similar to dKO mice), nerve terminal sprouting, reduced pre- and post-synaptic contacts, and fragmented endplates; NMJ defective transmitter release and muscular weakness: reduction in the number of presynaptic release sites and grip strength deficit (but normal spontaneous transmitter release, normal paired-pulse facilitation, and normal basal locomotion); Impairments of synaptic plasticity in the CNS: postsynaptic, (but no presynaptic) defect, with defects in LTP induction and maintenance; Reduced performance in spatial working memory tests (different dry mazes) and hippocampus-dependent behavior tests (nesting behavior and burrowing behavior).	[240]
APPY682G/Y682G mice in Aplp2 KO	Ssimilar to App/Aplp2 dko mice; Increase in sAPPα production and decrease in sAPPβ.	[241], [242]
APPT668A/T668A mice in Aplp2 KO	Viable; No neuromuscular defects.	[242]

Aplp1 KO and *Aplp2* KO revealed somatic growth deficit, but presented normal locomotor activity and unchanged forelimb strength [230, 235]. Only the triple (all App family members) KO mice or the mice haploinsufficient for *Aplp2* are lethal, and die 24h after birth. These mice have no gross abnormality in the brain, and the likely cause of dead relates to impaired neuromuscular transmission [238]. The main phenotypes described include ectopic clusters of neuroblasts within the marginal zone and pial membrane, similarly to type 2 lissencephaly, and decreased number of Cajal Retzius cells. Interestingly, as mentioned before, Fe65 and Fe65L1 double KO mice showed a strikingly similar phenotype to APP family triple KO [165], and the interaction between APP and Fe65 has been implicated in cell migration and axonal branching. Intriguingly, there is a report that embryonic stem cells derived from APP triple KO mice still form neuronal precursors, and apparently behave normally either in vitro or in vivo (normal neuronal migration, are able to extend long neurites, without differences in neuronal polarity, and can form active synapses) [243].

Since the Aplp2 KO is viable without any significant abnormal phenotype, APP and APLP1 must be compensating for the apparent indispensable function(s) of APLP2. For instance, in the peripheral nervous system, APP and APLP2 play a redundant and essential role for the correct organization and function of neuromuscular synapse formation. However, contrarily to *App* KO, analysis of dendritic spines of *Aplp2* null mutant neurons did not reveal alterations in spine density of apical and basal hippocampal dendrites or LTP defects [230]. The $App^{-/-}Aplp2^{-/-}$ double (d)KO also did not induced further alterations (only an additional branching defect in proximal apical dendrites). Organotypic hippocampal slices of $App^{-/-}Aplp2^{-/-}$ dKO revealed defects in basal glutamatergic synaptic transmission in comparison to $Aplp2^{-/-}$ mice, probably due to reduced levels of vesicular glutamate transporter 2 expression [244]. Recently, conditional *App* and *Aplp2* dKO in excitatory forebrain neurons, which overcomes the dKO lethality, indicates that both proteins might be required for normal neuronal morphology and complexity in vivo. Conditional dKO presented reduced total neurite length, dendritic branching, spine density and spine head volume in adult hippocampal CA1 neurons, and pronounced deficits in the induction and maintenance of hippocampal LTP and impairments in paired pulse facilitation, together with impairments in nesting behavior and hippocampus-dependent learning and memory tasks [237]. A transcriptional profile of prefrontal cortex of adult *App* and *Aplp2* single KO mice showed different sets of genes for the two conditions. From the 1242 genes that are up or down regulated after deletion of *Aplp2*, only 181 are also found altered in *App* mutant mice. Genes only significantly down regulated in *App* mutant mice (359 genes were differentially regulated: 274 up-regulated, and 85 down-regulated) strength the evidence for APP function in synaptic plasticity. Interestingly, the expression of genes involved in neurogenesis is altered in *Aplp2* KO brains [245]. Despite their redundant role, APP and APLPs may regulate distinct processes in different regions of the

developing cortex. Accordingly, while App mRNA is found in all neuroepithelial cells in the ventricular zone and in the cortical plate, Aplp2 exists in the ventricular zone and subventricular zone, and Aplp1 in the cortical plate only. In addition, some authors propose that while APP is functional in both progenitors and post-mitotic migrating neurons, APLP2 is playing a specific role in regulating progenitor proliferation and differentiation [70].

Besides the increasing evidences for a role in synaptic formation and function, other results point to the involvement of APP in axonal outgrowth and dendritogenesis. Concordantly, several analyses of *App* KO revealed dendritic and axonal defects either in young and/or older mice (Table A.3). Such processes will have implications not only during brain development and maturation, but will also be indispensable for neuronal regeneration after brain injury or disease. In fact, alterations in APP levels, trafficking and proteolytic processing might contribute to the altered synaptic plasticity and pathology of several neurological disorders in addition to Alzheimer's disease, namely to fragile X syndrome, Down's syndrome, autism, epilepsy and Parkinson's disease, and brain injury (see Figure 10; and for a review see reference [246]).

The first evidences that APP was involved in neurite outgrowth came from the findings that antibodies against APP specifically diminished the effects of the nerve growth factor on neurite length and branching in pheochromocytoma PC12 cells, indicating that APP mediates neurite outgrowth promotion by NGF [247]. The expression of APP695, the major APP neuronal isoform, is developmentally regulated during the differentiation of hippocampal neurons and neuronal-like cell lines in vitro. Interestingly, despite fetal neuronal cells express high levels of APP, they show little secretory processing into its soluble derivative, suggesting that the principal functional role in central nervous system development is responsibility of APP membrane-bound full-length protein [248]. In the same line of evidence, by the use of a system in which developing neurons were grown on transfected non-neuronal cells expressing various isoforms of APP, Qui et al (1995) showed that neurite outgrowth from hippocampal neurons was promoted by increased surface-expressed APP but not by increased sAPP or other secreted derivatives in the medium [249]. In addition, they showed that surface-expressed, KPI-positive APP770 and APP751 isoforms promote neurite outgrowth more vigorously than APP695, most probably due to their higher roles in cell adhesion [249]. In this same year, Allinquant et al. reported that a 6, 18, and 24h block of APP expression using antisense oligonucleotides was sufficient to produce significant inhibitory effects on neurite growth (both axon and dendrite) of primary cortical neurons, without changes in the size or pattern of cell bodies spreading on the substratum [250]. A previous study had demonstrated that the binding of APP to specific proteoglycan species of heparan sulfate proteoglycans (HSPGs), a component of the extracellular matrix, is an important step in the regulation of neurite outgrowth. Moreover, the study established that APP must be substrate-bound in vitro to exert its physiological

effects, since when added to the cultures in its soluble form, APP did no stimulate neurite outgrowth as efficiently [251]. Recent studies also showed that although APP is highly enriched in growth cones, where it forms complexes with integrin α3β1 and the tetraspanin CD81 to mediate growth cones adhesion, APP-mediated adhesion does not require integrin β1 (Itgβ1) participation and, by itself, can sustain neurite outgrowth [252].

A couple years later, an experience was performed exploiting the differences in neuron survival and development between hippocampal neurons deriving from wild-type (Wt) or *App* KO mice, co-cultured with astrocytes from Wt or *App* KO mice. The *App* KO neurons showed markedly shorter axons at 1 day in vitro (DIV), but the *App* KO neurons grown with Wt astrocytes would end up to developed axons equal in length to those of Wt neurons. Moreover, Wt neurons had more branched neurites and ultimately had more minor processes than did *App* KO hippocampal neurons. At 3 DIV, Wt and *App* KO neurons co-cultured with Wt astrocytes had significantly shorter axons than neurons co-cultured with *App* KO astrocytes, while the number of minor processes and the number of branch points were significantly greater. Data indicated that both cell-associated APP and secreted APP products appear to be important for normal neuronal development, but might affect specific events: cell-associated APP enhanced neuron survival, and contributed to the onset of axon formation and axon arborisation, whereas APP secreted products from astrocytes appeared to modulate neuronal polarization limiting the growth of axons and enhancing dendritic growth [253].

So the first hypothesis pointed out that full-length APP could act in a cell autonomous manner to promote neurite outgrowth, both in vitro and in vivo. But, apparently sAPP addition to neurons also stimulated neurite outgrowth. Later, a study showed that sAPPα competes with full-length APP for binding to Itgβ1. On one hand, sAPPα is able to inhibit the ability of APP to regulate Itgβ1-induced neurite outgrowth, and on the other hand sAPPα is not able to stimulate neurite outgrowth in the absence of cell surface APP. Noteworthy, in this study APP-deficient neurons, either from *App* KO hippocampal primary cultures or from in utero electroporation of APP shRNA, are reported to present longer longest neurites (axon) [254]. It is also important to mention that inhibition of sAPP generation, specifically sAPPα, can promote APP mediated trans-cellular adhesion via the protein E1 domain. Thus, shedding of APP can significantly impact the cell adhesion-dependent functions, like the demonstrated synaptogenic actitivity of APP [255].

In Drosophila mutants displaying an age-dependent degeneration of the central nervous system, either expression of APPL (the Drosophila orthologue of APP) or expression of human APP695 protect against progressive neurodegeneration. Importantly, the study presents evidence that this protection is mediated by the extracellular ectodomain, more specifically by the α-cleaved form, and only in the presence of full-length APP protein [256]. Previous studies had already shown that flies lacking APPL exhibited neurological phenotypes (especially in the peripheral nervous system)

that could be partially rescued by expression of human APP695 [257]. APPL is approximately 30% identical to human APP695, with significantly higher homology in specific extracellular domains and in the AICD, and can be processed by secretases resembling α-, β-, and γ-secretases. APPL is expressed in all neurons, and during embryogenesis it is, like mammalian APP, especially abundant in growing axons and in areas of synaptogenesis [70].

In Drosophila models, both APPL and the human homologue APP can promote post-developmental neurite arborization. APP or APPL expression resulted in increased axonal extension and more extensive arborization in postmitotic Drosophila brain neurons (small lateral neurons ventral), in a dose-dependent manner. Such effect seems to depend on the presence of the C-terminal, specifically, on the presence of the YENPTY motif harboring intact tyrosines 682 or 687 (susceptible to phosphorylation). APP downstream signal is transduced through the Abelson tyrosine kinase (Abl) pathway to profillin-induced actin cytoskeleton modifications, and in parallel through JNK pathway [258]. Furthermore, the study links APPL signals to brain injury and mortality after trauma [258], concordantly with previous results showing APP upregulation after brain injury in humans and mammalian models [259]. Loss of APPL was also shown to induce a developmental defect in axonal outgrowth in mushroom bodies (the D. melanogaster center for learning and memory). The molecular mechanism involved the interaction of APP with core components of the PCP-Wnt signaling, namely with Frizzled receptor and Van Gogh protein, and stabilization of the interaction between Abl with Disheveled, the cytoplasmic transducer component that is activated upon phosphorylation by Abl [260]. In flies and mice, JNK is the final effector of PCP in axon outgrowth and JNK was shown to be required for the effect of APP overexpression in the fly by the same group, as explained above [258]. In this way, APP could function, in a cell-autonomous manner, as neuronal-specific modulator of the PCP signaling efficiency at the developing growth cone to promote axonal outgrowth [260]. Interestingly, the authors also report a physiological role of the APPL soluble form in a different group of neurons of the Drosophila mushroom bodies (αlobe neurons) [260].

Differentiation of human induced pluripotent stem cells into fully mature neurons show a distinct, cell-stage dependent, pattern of APP expression and proteolytic processing. APP mRNA and protein expression are detected since day 0 until the end, and the first stage (stem cells) is characterized by expression of APP but no proteolytic processing. Around day 10 of differentiation, when cells start to express the marker Pax-6, sAPPα starts to be detected together with short Aβ peptides (1-16 and 1-19). This indicates a preference for non-amyloidogenic processing of APP and low rate of γ-secretase in this second-stage, when neuronal progenitors are being developed. Around day 45-50, while post-mitotic neurons form, sAPPβ is detected and longer Aβ peptides are favored. This last and third phase is, thus, characterized by an increase in

the activity of β- and γ-secretase coinciding with neuronal maturation [261]. However, the proteolytic biology of APP appears far more complex, with APP cleavage depending on additional cell state specifications. In other words, there will be groups of cells secreting high levels of sAPPα and distinct groups of cells (of the same type) secreting high levels of Aβ. Moreover, apparently different types of brain cells, including not only glutamatergic neurons but also GABAergic neurons and astrocytes, are capable of secreting high levels of sAPPα and Aβ [262].

Several studies strengthen that the APP proteolytic processing is highly regulated during brain development and neuronal maturation, and that most probable, each of resulting APP fragments will have specific roles. Furthermore, it has been proposed that not only the accumulation of Aβ but also reductions in the level or activity of the different APP fragments play a critical role in the cognitive dysfunction characteristics of AD, and potentially of other neurodegenerative and neurodevelopment disorders. Three APP products have received particular attention in regard to the here discussed APP role in neuronal development and function, namely the Aβ, the sAPPα, and the AICD.

Aβ is uniquely present in APP, and is mainly referred as a cytotoxic fragment exerting opposite effects to sAPPα [263]. Soluble Aβ oligomers (overexpressed in e.g. transgenic AD model mice) are associated with severe disruption of the dendritic cytoskeleton as well as the axonal cytoskeleton (reviewed in reference [264]) and are reported to reduce spine density and impair synaptic plasticity in the cortex and hippocampus (see reference [265]). However, low concentration of Aβ (pM to nM) have been shown to have protective effects on neurons and synapses (reviewed in reference [266]).

Secreted APPα is described to be neuroprotective and neurotrophic, and to regulate cell excitability, calcium homeostasis, and synaptic plasticity, therefore potentially regulating learning and memory [263]. The APP N-terminal domain display structural similarities with cysteine-rich growth factors, and most of the growth-promoting properties of sAPP in vivo are related to this attribute [267]. Importantly, this secreted fragment of APP is reported to function as a proliferation factor for adult neural progenitor cells [268, 269]. In adult mouse brain, total sAPP is produced in high levels and appear to have a superior half-life comparing to full-length APP [270]. Several lines of work report the rescue effects of sAPPα on the anatomical, behavioural and electrophysiological abnormalities of *App* KO mice and dKO (see Table A.4), and above we already discuss some of the reported sAPPα functions in neurite outgrowth in "coordination" with APP full-length. Infusion of sAPPα into the ventricle or an indirect increase in sAPPα levels due to α-secretase overexpression have been shown to increase synaptic density [271], but the opposite effects were also reported [255]. Nevertheless, reduced CSF levels of sAPPα, ADAM10 protein

level, and activity are prominent features of sporadic AD cases, and sAPPα is reported to decrease sAPPβ and Aβ production [272].

The neuroprotective and neurotrophic roles are mainly attributed to sAPPα, and the introduction of sAPPβ knock-in alleles does not rescue the lethality of App/Aplp2 double KO. Nevertheless, both sAPPα and sAPPβ can interact with the p75 neurotrophin receptor to stimulate neurite outgrowth [273]. Additionally, both fragments are reported to stimulate axon outgrowth via Egr1 signaling pathway [274]. Interestingly, N-APP, derived from sAPPβ, may act as a ligand for DR6 to induce axon pruning of peripheral sensory neurons and apoptosis during growth-factor dependent axonal outgrowth [275].

Intracellular CTFs of APP also deserve attention due to their ability to bind several proteins, as already mentioned. Particularly, AICD has been described to possess transcriptional regulatory activity when in complexes with other proteins, such as the ternary complex composed by AICD, Fe65 and TIP60. However, there is little consensus and several conflicting findings regarding the AICD-dependent regulated genes, with candidate target genes being: APP itself, KAI1, a tumor suppressor and antimetastasis gene; neprilysin, a neutral endopeptidase with Aβ-degrading activity; LRP1; the EGFR; GSK-3β, a kinase involved in tau phosphorylation; Transgelin, an actin cross-linking protein; and α2-actin [276]. Furthermore, AICD has been shown to contribute to apoptosis, development, synaptic plasticity and cytoskeletal dynamics [110]. Independently of its transcriptional activity, AICD has also been related to neuronal differentiation with reports of both negative and positive effects. One study correlated increased AICD levels with suppression of NGF-induced PC12 differentiation [277]. It appears that AICD interferes with the TrkA signalling, and that elevated AICDs signalling to the nucleus downregulates p53 and cyclinD and suppresses STAT3 phosphorylation (an activator of transcription), potentially enhancing cell proliferation and inhibiting neuronal differentiation [277]. Such results corroborate previous studies in an *in vivo* mouse model using TAG1, as a functional ligand of APP that increases AICD production and simultaneously leads to low neurogenesis [151]. Mouse knock-ins lacking the last 15 aminoacids of APP C-terminal (APPΔCT15ki; see Table A.4) fail to completely rescue the *App* or *App/Aplp2* KO phenotypes, indicating (especially in the *App/Aplp2* dKO rescue experiments) that this domain has essential functions for PNS and CNS physiology.

Recently, by the modulation of γ-secretase-dependent processing of APP-CTF (through pharmacological inhibition or loss-of-function PS1 mutations) and by the use of a membrane-tethered APP intracellular domain construct, it was shown that the accumulation of membrane APP-CTF stimulates neurite outgrowth in mouse N2a neuroblastoma cells, rat H19-7 immortalized hippocampal cells, and mouse cortical primary neurons. The molecular mechanism involves the interaction between APP intracellular domain and the heterotrimeric G-protein subunit Gαs, which

stimulates adenylate cyclase and leads to steady-state increase of phosphorylated protein kinase A (PKA) substrates such as CREB and GSK3β (which is inhibited) [278]. A following up study confirmed that alterations of γ-secretase activity, including via expression of FAD-linked PS1 variants, result in APP-CTF accumulation and that the subsequent signaling enhances neurite outgrowth. Importantly, the authors confirmed that APP is the major contributing substrate in FAD-linked PS1 mutation induced neurite outgrowth [279].

APP is thus a very complex molecule that suffers alternative splicing and posttranslational modifications, undergoes tightly regulated trafficking and processing, and participates in protein interactions with multiple partners. Various studies currently address the physiological roles of APP, but there are many contradictory results and missing pieces that deserve further attention and work. This means that the detailed dynamics of APP biology underlying each APP physiological function is still unknown. For example, regarding its role in neurite outgrowth, it is still unclear if APP (or one of its processing products) affects axon and dendritic outgrowth differentially, or if APP is particularly involved in the arising of new processes, in processes' elongation or branching. In addition, although it is already described that APP phosphorylation at S655 can alter APP trafficking and processing (e.g.: promoting the generation of neurotrophic sAPPα), the effect of this phosphorylation on neuronal differentiation events is yet to be addressed.

Supplementary Data

Supplementary Table A.1 – **APP protein interactors.** Known APP protein interactors were extracted from the HIPPIE database (http://cbdm-01.zdv.uni-mainz.de/~mschaefer/hippie/index.php, downloaded on June 27, 2016). The protein interactors list is ordered accordingly to the given score, and only the protein interactors with a minimum score of 0.59 were considered here. Scores ≥ 0.73 can be considered high-confidence interactors. Gene, indicates the gene symbol; Uniprot nr, indicates the uniprot accession number; Score, refers to the HIPPIE confidence score that ranges from 0 to 1; experimental evidence, identifies the experimental techniques used in the detection of the interaction; # pub, the number of scientific publications describing the existence of the interaction. Together with the reproducibility in model organisms, the experimental evidence (number and quality) and the number of publication, define subscores used to compute the final confidence score. NMR, nuclear magnetic resonance; coIP, coimmunoprecipitation; ELISA, enzyme linked immunosorbent assay; Reconstituted complex, Rcomplex; AC, affinity chromatography; PCA, protein complementation assay; FRET, fluorescent resonance energy transfer; TAP, tandem affinity purification.

Gene	Uniprot nr	Score	Experimental evidence	# pub
APBB1	O00213	0.99	Rcomplex; NMR; anti tag coIP; AC technology; PCA; Two-hybrid; anti-bait coIP; Affinity Capture-Western; pull down; in vitro; in vivo.	21
APBB3	O95704	0.99	Rcomplex; PCA; two-hybrid; pull down; in vitro; in vivo	5
APBA2	Q99767	0.99	Rcomplex; AC technology; Affinity Capture-Western; two-hybrid; pull down; in vitro; in vivo	3
SHC1	P29353	0.97	Rcomplex; AC technology; Affinity Capture-Western; two-hybrid; coIP. pull down; in vitro; in vivo	4
MAPK8IP1	Q9UQF2	0.97	FRET; anti tag coIP; coIP; AC technology; Two-hybrid; pull down; colocalization/visualisation technologies; in vitro; enzymatic study; imaging technique; in vivo.	6
APBA1	Q02410	0.96	Rcomplex; anti bait coIP; Affinity Capture-Western; anti tag coIP; AC technology; pull down; in vitro; fluorescence microscopy; in vivo	3
APBB2	Q92870	0.96	AC technology; Affinity Capture-Western; two-hybrid; anti-tag coIP; in vitro; in vivo	4
KLC1	Q07866	0.95	Rcomplex; AC technology; pull down; in vitro; in vivo	3
APBA3	O96018	0.95	Rcomplex; AC technology; Affinity Capture-Western; two-hybrid; pull down; in vitro; in vivo	2
DAB1	O75553	0.93	Rcomplex; pull down; in vitro	3
HSD17B10	Q99714	0.90	Rcomplex; ELISA; AC technology; Affinity Capture-Western; cross-linking study; two-hybrid; pull down; in vivo	4
KAT5	Q92993	0.89	FRET; Two-hybrid; AC technology; pull down; in vivo	6
FBLN1	P23142	0.89	Rcomplex; AC technology; Affinity Capture-Western; two-hybrid; pull down; in vitro	2
SNCA	P37840	0.89	Rcomplex; AC technology; pull down; in vitro; imaging technique	5
BLMH	Q13867	0.89	Rcomplex; two-hybrid; pull down; in vitro; co-fractionation	3
APPBP2	Q92624	0.89	Rcomplex; AC technology; two-hybrid; pull down; in vitro	3
PRNP	P04156	0.89	surface plasmon resonance; ELISA; anti bait coIP; pull down	4
PSEN1	P49768	0.88	AC technology; anti bait coIP; Two-hybrid; in vitro	6
NAE1	Q13564	0.88	Rcomplex; AC technology; Affinity Capture-Western; pull down; in vitro; in vivo	2
APOA1	P02647	0.88	Two-hybrid; far western blotting; anti tag coIP; ELISA; pull down	2
ACHE	P22303	0.87	Rcomplex; electron microscopy; pull down; in vitro;	2
BACE1	P56817	0.87	protease assay; AC technology; in vitro; fluorescence microscopy	3
TGFB2	P61812	0.87	anti bait coIP; competition binding; protein cross-linking with a bifunctional reagent; imaging technique; in vivo; chromatography technology	2
CALR	P27797	0.87	Affinity Capture-Western; AC technology; comigration in non denaturing gel electrophoresis; in vivo; imaging technique	4
COL25A1	Q9BXS0	0.87	Rcomplex; pull down; in vitro; imaging technique; in vivo; Co-localization	2
UBQLN1	Q9UMX0	0.86	FRET; AC technology; Two-hybrid	2
TGFB1	P01137	0.86	protein cross-linking with a bifunctional reagent; competition binding; in vitro; imaging technique; in vivo	4

Gene	Uniprot nr	Score	Experimental evidence	# pub
EGFR	P00533	0.86	Two-hybrd; PCA; ubiquitin reconstruction	2
BGN	P21810	0.85	Rcomplex; pull down; in vitro	2
PSEN2	P49810	0.84	Two-hybrid; anti bait coIP; in vivo	3
HGS	O14964	0.84	Rcomplex; pull down	3
HOMER3	Q9NSC5	0.84	anti bait coIP; anti tag coIP; pull down	2
NGFR	P08138	0.84	ELISA; anti bait coIP; pull down	2
MAPK8IP2	Q13387	0.82	Two-hybrid; AC technology	2
CTSD	P07339	0.82	protease assay; in vitro; in vivo	6
GSK3B	P49841	0.82	AC technology; pull down; in vivo; in vitro	5
CLSTN1	O94985	0.82	AC technology; Affinity Capture-Western	2
HSP90AA1	P07900	0.82	AC technology; anti bait coIP	2
HSPA8	P11142	0.82	AC technology; anti bait coIP	2
A2M	P01023	0.82	coIP; Two-hybrid	2
SLC40A1	Q9NP59	0.82	anti tag coIP; anti bait coIP	2
NUMB	P49757	0.82	pull down; in vivo; imaging technique; in vitro	4
UCHL1	P09936	0.82	AC technology; anti bait coIP	2
CRYAB	P02511	0.81	anti bait coIP; pull down; in vitro	4
LRP1	Q07954	0.81	AC technology; pull down; in vivo	4
GSN	P06396	0.79	Rcomplex; Affinity Capture-Western; AC technology; pull down; in vivo; in vitro	1
MAPT	P10636	0.79	surface plasmon resonance; protein kinase assay; peptide array; ELISA; pull down; confocal microscopy	1
RNF32	Q9H0A6	0.79	Two-hybrid; pull down	3
STXBP1	P61764	0.78	anti bait coIP; pull down	2
TUBB	P07437	0.78	anti bait coIP; pull down	2
GFAP	P14136	0.78	anti bait coIP; pull down	2
PPIA	P62937	0.78	anti bait coIP; pull down	2
YWHAZ	P63104	0.78	anti bait coIP; pull down	2
HOMER2	Q9NSB8	0.78	anti tag coIP; pull down	2
CAT	P04040	0.78	ELISA; pull down	2
AKT2	P31751	0.78	Two-hybrid; pull down	2
TMCC2	O75069	0.78	anti bait coIP; pull down	2
HSPD1	P10809	0.78	AC technology; pull down	2
MAPRE1	Q15691	0.78	Two-hybrid; pull down	2
COPS5	Q92905	0.78	AC technology; pull down	2
APOE	P02649	0.78	anti tag coIP; experimental interaction detection; in vitro	4
BCAP31	P51572	0.77	Two-hybrid; PCA; AC technology; imaging technique; in vivo; Co-fractionation	1
TNFRSF21	O75509	0.76	saturation binding; ELISA; pull down	1
IFIT3	O14879	0.76	AC technology; anti bait coIP; Two-hybrid	1
FLOT1	O75955	0.75	Two-hybrid; anti bait coIP; pull down; in vitro	1
HMOX2	P30519	0.75	Two-hybrid; in vivo	2
SNCB	Q16143	0.75	Rcomplex; pull down; in vitro	1
TP53BP2	Q13625	0.75	Two-hybrid; ELISA; pull down; pull down	1

Gene	Uniprot nr	Score	Experimental evidence	# pub
DAB2	P98082	0.75	Rcomplex; pull down	1
PCBD1	P61457	0.75	AC technology; TAP; pull down	1
FOS	P01100	0.75	AC technology; TAP; pull down	1
PARK2	O60260	0.75	AC technology; imaging technique	2
NEFL	P07196	0.75	anti bait coIP; imaging technique	2
MAP3K5	Q99683	0.75	anti bait coIP; imaging technique	2
PDIA3	P30101	0.74	comigration in non-denaturing gel electrophoresis; pull down	2
CLU	P10909	0.73	pull down; in vivo; in vitro	3
NF1	P21359	0.73	anti bait coIP; Two-hybrid; in vivo	1
CDK5	Q00535	0.73	pull down; in vivo; in vitro	4
NCSTN	Q92542	0.73	Affinity Capture-Western; AC technology; in vivo	1
TM2D1	Q9BX74	0.73	Two-hybrid; AC technology; in vitro	1
ND3	P03897	0.73	phage display; ELISA	1
SET	Q01105	0.73	AC technology	1
ITM2A	O43736	0.72	anti tag coIP; anti bait coIP	1
YWHAG	P61981	0.72	Two-hybrid; AC technology	1
NOS3	P29474	0.72	AC technology; Two-hybrid	1
GPR3	P46089	0.72	anti tag coIP; anti bait coIP	1
PCOLCE	Q15113	0.72	surface plasmon resonance	1
QRICH1	Q2TAL8	0.72	Two-hybrid; AC technology	1
GAPDH	P04406	0.70	pull down; in vitro	5
COL4A6	Q14031	0.70	pull down; in vitro	3
GNAO1	P09471	0.70	anti bait coIP	1
NECAB3	Q96P71	0.69	pull down; in vitro	2
PPID	Q08752	0.69	pull down; in vitro	2
CHRNA7	P36544	0.69	anti bait coIP; in vitro; in vivo; imaging technique	1
CASP4	P49662	0.69	pull down; in vitro	2
UBE2M	P61081	0.69	pull down; enzymatic study	2
MAPK8	P45983	0.69	pull down; enzymatic study	2
CASP3	P42574	0.69	in vivo; in vitro; imaging technique	3
SHC3	Q92529	0.68	pull down; in vivo; in vitro	1
GSK3A	P49840	0.68	protein kinase assay	1
ADAM17	P78536	0.68	protease assay	1
KLK6	Q92876	0.68	protease assay	1
PITRM1	Q5JRX3	0.68	protease assay	1
GGA1	Q9UJY5	0.68	AC technology; pull down	1
LDLRAP1	Q5SW96	0.67	Two-hybrid; in vivo; in vitro	1
DLG4	P78352	0.67	anti bait coIP; cosedimentation in solution	1
ABL1	P00519	0.66	pull down; in vivo	1
BACE2	Q9Y5Z0	0.66	in vivo; in vitro	5
TGM2	P21980	0.66	pull down	2
GRB2	P62993	0.65	anti bait coIP; in vivo	1

Gene	Uniprot nr	Score	Experimental evidence	# pub
CAV1	Q03135	0.65	Co-fractionation; in vitro; Protein-RNA	2
SYVN1	Q86TM6	0.65	AC technology; enzymatic study	1
NEDD8	Q15843	0.65	AC technology; enzymatic study	1
FBXL2	Q9UKC9	0.65	AC technology; enzymatic study	1
PION	A4D1B5	0.65	AC technology; enzymatic study	1
CASP6	P55212	0.65	imaging technique; in vitro	2
EPB41	P11171	0.63	Two-hybrid	1
SERPINA3	P01011	0.63	in vivo	3
DNM1	Q05193	0.63	anti bait coIP	1
NSF	P46459	0.63	anti bait coIP	1
SPTAN1	Q13813	0.63	anti bait coIP	1
ACTB	P60709	0.63	anti bait coIP	1
MBP	P02686	0.63	anti bait coIP	1
MYH9	P35579	0.63	anti bait coIP	1
DNAH1	Q9P2D7	0.63	anti bait coIP	1
PGAM1	P18669	0.63	anti bait coIP	1
APLP1	P51693	0.63	anti tag coIP	1
APLP2	Q06481	0.63	anti tag coIP	1
TTR	P02766	0.63	coIP	1
UGP2	Q16851	0.63	Two-hybrid	1
PHLPP1	O60346	0.63	Two-hybrid	1
PRAM1	Q96QH2	0.63	Two-hybrid	1
MAST1	Q9Y2H9	0.63	Two-hybrid	1
CDC37	Q16543	0.63	Two-hybrid	1
AP1M2	Q9Y6Q5	0.63	Two-hybrid	1
EXOC6	Q8TAG9	0.63	Two-hybrid	1
MED4	Q9NPJ6	0.63	anti bait coIP	1
TIRAP	P58753	0.63	Two-hybrid	1
TPD52L2	O43399	0.63	Two-hybrid	1
HSPA4	P34932	0.63	AC technology	1
NOTCH1	P46531	0.63	AC technology	1
STUB1	Q9UNE7	0.63	AC technology	1
NAPG	Q99747	0.63	PCA	1
UBB	P0CG47	0.63	PCA	1
YWHAB	P31946	0.63	pull down	1
ECSIT	Q9BQ95	0.63	Two-hybrid	1
KIF1B	O60333	0.63	AC technology	1
CFL1	P23528	0.63	Two-hybrid	1
PAXIP1	Q6ZW49	0.63	Two-hybrid	1
PI4K2A	Q9BTU6	0.63	Two-hybrid	1
RAB3A	P20336	0.63	Two-hybrid	1
PTGER2	P43116	0.63	anti tag coIP	1

Gene	Uniprot nr	Score	Experimental evidence	# pub
ARRB1	P49407	0.63	anti tag coIP	1
RANBP9	Q96S59	0.63	AC technology	1
RNF2	Q99496	0.63	AC technology	1
TMEM30A	Q9NV96	0.63	AC technology	1
USP25	Q9UHP3	0.63	AC technology	1
SORL1	Q92673	0.63	AC technology	1
CUL7	Q14999	0.63	AC technology	1
PIN1	Q13526	0.62	pull down; light microscopy; in vivo	1
HSPG2	P98160	0.62	in vitro	2
HADHB	P55084	0.62	in vitro	2
F12	P00748	0.62	in vivo	2
SPON1	Q9HCB6	0.59	pull down; in vitro	2

Supplementary Table A.2 - **Complete list of biological process gene ontology terms related to nervous system function and development and significantly enriched in the APP interactome.** F. Enrichment, the fold enrichment of the genes observed in the APP protein interactors list over the expected based on the reference list (the human genome). A number greater than 1, indicates that the category is overrepresented. pvalue, calculated pvalue with Bonferroni correction. Only pvalues higher than 0.05 were considered.

	GO Biological process	# proteins	F. enrichment	pvalue
Nervous system development	cerebral cortex development	10	11.64	1.76E-04
	pallium development	13	10.38	5.08E-06
	telencephalon development	16	8.68	6.69E-07
	forebrain development	21	7.30	1.60E-08
	brain development	28	5.21	8.18E-09
	central nervous system development	38	5.42	9.28E-14
	nervous system development	71	4.28	3.66E-24
	glial cell differentiation	10	9.07	1.74E-03
	gliogenesis	12	8.51	2.06E-04
	neurogenesis	55	4.91	5.96E-20
	limbic system development	8	9.76	1.71E-02
	negative regulation of neuron projection development	9	8.99	7.62E-03
	regulation of neuron projection development	19	5.82	8.10E-06
	regulation of neuron differentiation	25	5.66	2.71E-08
	regulation of neurogenesis	31	5.84	2.07E-11
	regulation of nervous system development	32	5.34	7.77E-11
	generation of neurons	53	5.03	1.61E-19
	negative regulation of neuron differentiation	14	9.11	5.72E-06
	negative regulation of neurogenesis	17	8.77	1.42E-07
	negative regulation of nervous system development	18	8.56	5.23E-08
	regulation of axonogenesis	11	8.36	9.50E-04
	axonogenesis	19	7.56	1.08E-07
	axon development	21	7.66	6.58E-09
	neuron projection development	32	7.49	6.16E-15

	GO Biological process	# proteins	F. enrichment	pvalue
	neuron development	33	6.03	8.84E-13
	neuron differentiation	37	5.32	5.05E-13
	neuron projection morphogenesis	25	7.99	1.39E-11
	cell morphogenesis involved in neuron differentiation	22	7.65	1.85E-09
	positive regulation of neuron projection development	11	5.89	2.79E-02
	positive regulation of neurogenesis	16	5.27	6.98E-04
	positive regulation of nervous system development	17	4.87	8.33E-04
Synapse function	regulation of synaptic vesicle transport	6	24.56	1.77E-03
	regulation of neuronal synaptic plasticity	7	18.13	1.30E-03
	regulation of synaptic plasticity	12	10.80	1.52E-05
	regulation of synapse structure or activity	15	8.21	5.67E-06
	modulation of synaptic transmission	19	7.98	4.27E-08
	neuron-neuron synaptic transmission	7	15.86	3.15E-03
	synaptic transmission	25	7.89	1.84E-11
	anterograde trans-synaptic signaling	25	7.89	1.84E-11
	trans-synaptic signaling	25	7.89	1.84E-11
	synaptic signaling	25	7.70	3.19E-11
	chemical synaptic transmission, postsynaptic	7	13.88	7.62E-03
	presynaptic process involved in synaptic transmission	9	10.88	1.59E-03
	synapse organization	12	10.43	2.23E-05
	positive regulation of synaptic transmission	9	10.38	2.34E-03
	regulation of neurotransmitter levels	12	8.41	2.32E-04
Neuron Death	neuron apoptotic process	7	24.68	1.63E-04
	neuron death	8	21.15	5.10E-05
	positive regulation of neuron apoptotic process	9	24.30	1.69E-06
	positive regulation of neuron death	15	28.41	1.40E-13
	regulation of neuron death	26	12.99	3.29E-17
	regulation of neuron apoptotic process	20	13.15	1.21E-12
	negative regulation of neuron apoptotic process	12	11.20	1.02E-05
	negative regulation of neuron death	14	10.27	1.24E-06
Cell migration	negative regulation of cell migration	11	6.81	7.01E-03
	negative regulation of cell motility	13	7.64	1.86E-04
	regulation of cell motility	28	4.96	2.56E-08
	regulation of cell migration	26	4.94	1.85E-07
	positive regulation of cell migration	15	4.88	4.73E-03
	positive regulation of cell motility	15	4.74	6.87E-03
	cell migration	25	4.18	1.41E-05
	cell motility	26	3.95	2.10E-05
ECM	regulation of extracellular matrix organization	6	26.26	1.20E-03
	extracellular matrix organization	20	8.27	6.09E-09
Cell adhesion	negative regulation of cell adhesion	12	6.86	2.04E-03
	regulation of cell adhesion	22	4.38	6.54E-05

	GO Biological process	# proteins	F. enrichment	pvalue
-	**cytoskeleton organization**	27	4.09	4.56E-06
-	**Learning or memory**	14	8.04	2.77E-05

References

1. Swanson, L.W., *Brain architecture: understanding the basic plan*. 2nd ed. 2012: Oxford University Press.
2. Silbereis, John C., et al., *The Cellular and Molecular Landscapes of the Developing Human Central Nervous System.* Neuron. **89**(2): p. 248-268.
3. Gotz, M. and W.B. Huttner, *The cell biology of neurogenesis.* Nat Rev Mol Cell Biol, 2005. **6**(10): p. 777-88.
4. Bystron, I., C. Blakemore, and P. Rakic, *Development of the human cerebral cortex: Boulder Committee revisited.* Nat Rev Neurosci, 2008. **9**(2): p. 110-22.
5. Taverna, E., M. Gotz, and W.B. Huttner, *The cell biology of neurogenesis: toward an understanding of the development and evolution of the neocortex.* Annu Rev Cell Dev Biol, 2014. **30**: p. 465-502.
6. Toma, K. and C. Hanashima, *Switching modes in corticogenesis: mechanisms of neuronal subtype transitions and integration in the cerebral cortex.* Front Neurosci, 2015. **9**: p. 274.
7. Guérout, N., X. Li, and F. Barnabé-Heider, *Cell fate control in the developing central nervous system.* Experimental Cell Research, 2014. **321**(1): p. 77-83.
8. Workman, A.D., et al., *Modeling transformations of neurodevelopmental sequences across mammalian species.* J Neurosci, 2013. **33**(17): p. 7368-83.
9. Francis, F., et al., *Human disorders of cortical development: from past to present.* Eur J Neurosci, 2006. **23**(4): p. 877-93.
10. Guillemot, F., *Spatial and temporal specification of neural fates by transcription factor codes.* Development, 2007. **134**(21): p. 3771-3780.
11. Chenn, A., *Wnt/β-catenin signaling in cerebral cortical development.* Organogenesis, 2008. **4**(2): p. 76-80.
12. Azzarelli, R., T. Kerloch, and E. Pacary, *Regulation of cerebral cortex development by Rho GTPases: insights from in vivo studies.* Front Cell Neurosci, 2014. **8**: p. 445.
13. Barnes, A.P. and F. Polleux, *Establishment of Axon-Dendrite Polarity in Developing Neurons.* Annual Review of Neuroscience, 2009. **32**(1): p. 347-381.
14. Loulier, K., et al., *beta1 integrin maintains integrity of the embryonic neocortical stem cell niche.* PLoS Biol, 2009. **7**(8): p. e1000176.
15. Zhou, Y., et al., *The Mammalian Golgi Regulates Numb Signaling in Asymmetric Cell Division by Releasing ACBD3 during Mitosis.* Cell. **129**(1): p. 163-178.
16. Tabata, H., S. Kanatani, and K. Nakajima, *Differences of Migratory Behavior between Direct Progeny of Apical Progenitors and Basal Progenitors in the Developing Cerebral Cortex.* Cerebral Cortex, 2009. **19**(9): p. 2092-2105.
17. Noctor, S.C., et al., *Cortical neurons arise in symmetric and asymmetric division zones and migrate through specific phases.* Nat Neurosci, 2004. **7**(2): p. 136-44.
18. Ohtaka-Maruyama, C. and H. Okado, *Molecular Pathways Underlying Projection Neuron Production and Migration during Cerebral Cortical Development.* Front Neurosci, 2015. **9**: p. 447.
19. Cooper, J.A., *Molecules and mechanisms that regulate multipolar migration in the intermediate zone.* Front Cell Neurosci, 2014. **8**: p. 386.
20. Namba, T., et al., *Pioneering axons regulate neuronal polarization in the developing cerebral cortex.* Neuron, 2014. **81**(4): p. 814-29.
21. Kolodkin, A.L. and M. Tessier-Lavigne, *Mechanisms and Molecules of Neuronal Wiring: A Primer.* Cold Spring Harbor Perspectives in Biology, 2011. **3**(6): p. a001727.
22. Shelly, M. and M.M. Poo, *Role of LKB1-SAD/MARK pathway in neuronal polarization.* Dev Neurobiol, 2011. **71**(6): p. 508-27.
23. Franco, S.J., et al., *Reelin regulates cadherin function via Dab1/Rap1 to control neuronal migration and lamination in the neocortex.* Neuron, 2011. **69**(3): p. 482-97.
24. Jossin, Y. and J.A. Cooper, *Reelin, Rap1 and N-cadherin orient the migration of multipolar neurons in the developing neocortex.* Nat Neurosci, 2011. **14**(6): p. 697-703.
25. Xu, C., et al., *Radial Glial Cell–Neuron Interaction Directs Axon Formation at the Opposite Side of the Neuron from the Contact Site.* The Journal of Neuroscience, 2015. **35**(43): p. 14517-14532.
26. Elias, L.A., D.D. Wang, and A.R. Kriegstein, *Gap junction adhesion is necessary for radial migration in the neocortex.* Nature, 2007. **448**(7156): p. 901-7.
27. Dong, X., K. Shen, and H.E. Bulow, *Intrinsic and extrinsic mechanisms of dendritic morphogenesis.* Annu Rev Physiol, 2015. **77**: p. 271-300.

28. Puram, S.V. and A. Bonni, *Cell-intrinsic drivers of dendrite morphogenesis.* Development (Cambridge, England), 2013. **140**(23): p. 4657-4671.
29. Petanjek, Z., et al., *Extraordinary neoteny of synaptic spines in the human prefrontal cortex.* Proceedings of the National Academy of Sciences, 2011. **108**(32): p. 13281-13286.
30. Low, L.K. and H.-J. Cheng, *Axon pruning: an essential step underlying the developmental plasticity of neuronal connections.* Philosophical Transactions of the Royal Society B: Biological Sciences, 2006. **361**(1473): p. 1531-1544.
31. Dotti, C., C. Sullivan, and G. Banker, *The establishment of polarity by hippocampal neurons in culture.* J. Neurosci., 1988. **8**(4): p. 1454-1468.
32. Sakakibara, A. and Y. Hatanaka, *Neuronal polarization in the developing cerebral cortex.* Frontiers in Neuroscience, 2015. **9**: p. 116.
33. Fukata, Y., T. Kimura, and K. Kaibuchi, *Axon specification in hippocampal neurons.* Neuroscience Research, 2002. **43**(4): p. 305-315.
34. Bradke, F. and C.G. Dotti, *Changes in membrane trafficking and actin dynamics during axon formation in cultured hippocampal neurons.* Microscopy Research and Technique, 2000. **48**(1): p. 3-11.
35. Witte, H. and F. Bradke, *The role of the cytoskeleton during neuronal polarization.* Current Opinion in Neurobiology, 2008. **18**(5): p. 479-487.
36. Tahirovic, S. and F. Bradke, *Neuronal Polarity.* Cold Spring Harbor Perspectives in Biology, 2009. **1**(3).
37. Ishikawa, R. and K. Kohama, *Actin-Binding Proteins in Nerve Cell Growth Cones.* Journal of Pharmacological Sciences, 2007. **105**(1): p. 6-11.
38. Flynn, K.C., *The cytoskeleton and neurite initiation.* BioArchitecture, 2013. **3**(4): p. 86-109.
39. Igarashi, M., *Proteomic identification of the molecular basis of mammalian CNS growth cones.* Neurosci Res, 2014. **88**: p. 1-15.
40. Sainath, R. and G. Gallo, *Cytoskeletal and signaling mechanisms of neurite formation.* Cell Tissue Res, 2015. **359**(1): p. 267-78.
41. Arimura, N., et al., *Role of CRMP-2 in neuronal polarity.* J Neurobiol, 2004. **58**(1): p. 34-47.
42. Winkle, C.C. and S.L. Gupton, *Membrane Trafficking in Neuronal Development: Ins and Outs of Neural Connectivity.* Int Rev Cell Mol Biol, 2016. **322**: p. 247-80.
43. Decurtis, I., *Intracellular Mechanisms for Neuritogenesis*. 2007: Springer US.
44. Whitford, K.L., et al., *Molecular control of cortical dendrite development.* Annu Rev Neurosci, 2002. **25**: p. 127-49.
45. Rosso, S.B. and N.C. Inestrosa, *WNT signaling in neuronal maturation and synaptogenesis.* Frontiers in Cellular Neuroscience, 2013. **7**: p. 103.
46. Yuen, E.C., et al., *Neurotrophins and the Neurotrophic Factor Hypothesis.* Neural Notes, 1996. **1**(4): p. 3-7.
47. Kaplan, D.R. and F.D. Miller, *Neurotrophin signal transduction in the nervous system.* Current Opinion in Neurobiology, 2000. **10**(3): p. 381-391.
48. Takano, T., et al., *Neuronal polarization.* Development, 2015. **142**(12): p. 2088-93.
49. Yi, J.J., et al., *TGF-beta signaling specifies axons during brain development.* Cell, 2010. **142**(1): p. 144-57.
50. Mattson, M.P., *Establishment and plasticity of neuronal polarity.* Journal of Neuroscience Research, 1999. **57**(5): p. 577-589.
51. Clegg, D.O., et al., *Integrins in the development, function and dysfunction of the nervous system.* Front Biosci, 2003. **8**: p. d723-50.
52. Barnes, A.P., et al., *LKB1 and SAD Kinases Define a Pathway Required for the Polarization of Cortical Neurons.* Cell, 2007. **129**(3): p. 549-563.
53. Polleux, F. and W. Snider, *Initiating and Growing an axon.* Cold Spring Harbor Perspectives in Biology, 2010. **2**: p. 1-15.
54. Zhong, J., *RAS and downstream RAF-MEK and PI3K-AKT signaling in neuronal development, function and dysfunction.* Biol Chem, 2016. **397**(3): p. 215-22.
55. Samuels, I.S., S.C. Saitta, and G.E. Landreth, *MAP'ing CNS Development and Cognition: an ERKsome process.* Neuron, 2009. **61**(2): p. 160-167.
56. Pucilowska, J., et al., *Disrupted ERK Signaling during Cortical Development Leads to Abnormal Progenitor Proliferation, Neuronal and Network Excitability and Behavior, Modeling Human Neuro-Cardio-Facial-Cutaneous and Related Syndromes.* The Journal of Neuroscience, 2012. **32**(25): p. 8663-8677.

57. Samuels, I.S., et al., *Deletion of ERK2 mitogen-activated protein kinase identifies its key roles in cortical neurogenesis and cognitive function.* J Neurosci, 2008. **28**(27): p. 6983-95.
58. Hall, A. and G. Lalli, *Rho and Ras GTPases in Axon Growth, Guidance, and Branching.* Cold Spring Harbor Perspectives in Biology, 2010. **2**(2).
59. Chen, Y.M., et al., *Microtubule affinity-regulating kinase 2 functions downstream of the PAR-3/PAR-6/atypical PKC complex in regulating hippocampal neuronal polarity.* Proceedings of the National Academy of Sciences, 2006. **103**(22): p. 8534-8539.
60. Selkoe, D.J., *Alzheimer's Disease: Genes, Proteins, and Therapy.* Physiological Reviews, 2001. **81**(2): p. 741-766.
61. Ling, Y., K. Morgan, and N. Kalsheker, *Amyloid precursor protein (APP) and the biology of proteolytic processing: relevance to Alzheimer's disease.* The International Journal of Biochemistry & Cell Biology, 2003. **35**(11): p. 1505-1535.
62. Glenner, G.G. and C.W. Wong, *Alzheimer's disease: initial report of the purification and characterization of a novel cerebrovascular amyloid protein.* Biochem Biophys Res Commun, 1984. **120**(3): p. 885-90.
63. Glenner, G.G. and C.W. Wong, *Alzheimer's disease and Down's syndrome: sharing of a unique cerebrovascular amyloid fibril protein.* Biochem Biophys Res Commun, 1984. **122**(3): p. 1131-5.
64. Masters, C.L., et al., *Amyloid plaque core protein in Alzheimer disease and Down syndrome.* Proc Natl Acad Sci U S A, 1985. **82**(12): p. 4245-9.
65. Tanzi, R., et al., *Amyloid beta protein gene: cDNA, mRNA distribution, and genetic linkage near the Alzheimer locus.* Science, 1987. **235**(4791): p. 880-884.
66. Goldgaber, D., et al., *Characterization and chromosomal localization of a cDNA encoding brain amyloid of Alzheimer's disease.* Science, 1987. **235**(4791): p. 877-880.
67. Robakis, N., et al., *Chromosome 21q21 sublocalisation of gene encoding beta-amyloid peptide in cerebral vessels and neuritic (senile) plaques of people with Alzheimer disease and Down syndrome.* Lancet., 1987. **14**(1): p. 384-5.
68. Schmechel, D., et al., *Cellular localization of messenger RNA encoding amyloid-beta-protein in normal tissue and in Alzheimer disease.* Alzheimer Dis Assoc Disord., 1988. **2**(2): p. 96-111.
69. Coulson, E.J., et al., *What the evolution of the amyloid protein precursor supergene family tells us about its function.* Neurochemistry International, 2000. **36**(3): p. 175-184.
70. Shariati, S.A.M. and B. De Strooper, *Redundancy and divergence in the amyloid precursor protein family.* FEBS Letters, 2013. **587**(13): p. 2036-2045.
71. Raux, G., et al., *Molecular diagnosis of autosomal dominant early onset Alzheimer's disease: an update.* J Med Genet, 2005. **42**(10): p. 793-5.
72. Theuns, J., et al., *Promoter mutations that increase amyloid precursor-protein expression are associated with Alzheimer disease.* Am J Hum Genet, 2006. **78**(6): p. 936-46.
73. Guyant-Marechal, L., et al., *Variations in the APP gene promoter region and risk of Alzheimer disease.* Neurology, 2007. **68**(9): p. 684-7.
74. Jonsson, T., et al., *A mutation in APP protects against Alzheimer's disease and age-related cognitive decline.* Nature, 2012. **488**(7409): p. 96-9.
75. Sandbrink, R., C.L. Masters, and K. Beyreuther, *APP gene family: unique age-associated changes in splicing of Alzheimer's betaA4-amyloid protein precursor.* Neurobiol Dis, 1994. **1**(1-2): p. 13-24.
76. Sandbrink, R., et al., *Expression of the APP gene family in brain cells, brain development and aging.* Gerontology, 1997. **43**(1-2): p. 119-31.
77. Tanaka, S., et al., *Tissue-specific expression of three types of [beta]-protein precursor mRNA: Enhancement of protease inhibitor-harboring types in Alzheimer's disease brain.* Biochemical and Biophysical Research Communications, 1989. **165**(3): p. 1406-1414.
78. Coburger, I., et al., *Analysis of the Overall Structure of the Multi-Domain Amyloid Precursor Protein (APP).* PLoS ONE, 2013. **8**(12): p. e81926.
79. Coburger, I., S. Hoefgen, and M.E. Than, *The structural biology of the amyloid precursor protein APP - a complex puzzle reveals its multi-domain architecture.* Biol Chem, 2014. **395**(5): p. 485-98.
80. Ben Khalifa, N., et al., *What is the role of amyloid precursor protein dimerization?* Cell Adhesion & Migration, 2010. **4**(2): p. 268-272.
81. Munter, L.-M., et al., *GxxxG motifs within the amyloid precursor protein transmembrane sequence are critical for the etiology of Aβ42.* The EMBO Journal, 2007. **26**(6): p. 1702-1712.
82. Chen, W.J., J.L. Goldstein, and M.S. Brown, *NPXY, a sequence often found in cytoplasmic tails, is required for coated pit-mediated internalization of the low density lipoprotein receptor.* Journal of Biological Chemistry, 1990. **265**(6): p. 3116-23.

83. Lai, A., S.S. Sisodia, and I.S. Trowbridge, *Characterization of sorting signals in the beta-amyloid precursor protein cytoplasmic domain.* J Biol Chem, 1995. **270**(8): p. 3565-73.
84. Suzuki, T. and T. Nakaya, *Regulation of Amyloid β-Protein Precursor by Phosphorylation and Protein Interactions.* Journal of Biological Chemistry, 2008. **283**(44): p. 29633-29637.
85. Haass, C., et al., *Polarized sorting of beta-amyloid precursor protein and its proteolytic products in MDCK cells is regulated by two independent signals.* J Cell Biol, 1995. **128**(4): p. 537-47.
86. Zheng, P., et al., *PAT1, a microtubule-interacting protein, recognizes the basolateral sorting signal of amyloid precursor protein.* Proc Natl Acad Sci U S A, 1998. **95**(25): p. 14745-50.
87. Nishimoto, I., et al., *Alzheimer amyloid protein precursor complexes with brain GTP-binding protein G(o).* Nature, 1993. **362**(6415): p. 75-9.
88. Small, S.A. and S. Gandy, *Sorting through the Cell Biology of Alzheimer's Disease: Intracellular Pathways to Pathogenesis.* 2006. **52**(1): p. 15-31.
89. Haass, C., et al., *Trafficking and proteolytic processing of APP.* Cold Spring Harb Perspect Med, 2012. **2**(5): p. a006270.
90. Bayer, T.A., et al., *Key Factors in Alzheimer's Disease: β-amyloid Precursos Protein Processing, Metabolism and Intraneuronal Transport.* Brain Pathology, 2001. **11**: p. 1-11.
91. Muresan, V. and Z. Ladescu Muresan, *Amyloid-β precursor protein: Multiple fragments, numerous transport routes and mechanisms.* Experimental Cell Research, 2015. **334**(1): p. 45-53.
92. Kamal, A., et al., *Axonal transport of amyloid precursor protein is mediated by direct binding to the kinesin light chain subunit of kinesin-I.* Neuron, 2000. **28**(2): p. 449-59.
93. Lazarov, O., et al., *Axonal transport, amyloid precursor protein, kinesin-1, and the processing apparatus: revisited.* J Neurosci, 2005. **25**(9): p. 2386-95.
94. DeBoer, S.R., et al., *Differential release of beta-amyloid from dendrite- versus axon-targeted APP.* J Neurosci, 2014. **34**(37): p. 12313-27.
95. Vieira, S., et al., *Retrieval of the Alzheimer's amyloid precursor protein from the endosome to the TGN is S655 phosphorylation state-dependent and retromer-mediated.* Molecular Neurodegeneration, 2010. **5**(1): p. 40.
96. Gustafsen, C., et al., *Sortilin and SorLA Display Distinct Roles in Processing and Trafficking of Amyloid Precursor Protein.* The Journal of Neuroscience, 2013. **33**(1): p. 64-71.
97. Greenfield, J.P., et al., *Estrogen lowers Alzheimer beta-amyloid generation by stimulating trans-Golgi network vesicle biogenesis.* J Biol Chem, 2002. **277**(14): p. 12128-36.
98. Kuan, Y.H., et al., *PAT1a modulates intracellular transport and processing of amyloid precursor protein (APP), APLP1, and APLP2.* J Biol Chem, 2006. **281**(52): p. 40114-23.
99. Dilsizoglu Senol, A., et al., *PAT1 inversely regulates the surface Amyloid Precursor Protein level in mouse primary neurons.* BMC Neuroscience, 2015. **16**: p. 10.
100. Cam, J.A., et al., *Rapid endocytosis of the low density lipoprotein receptor-related protein modulates cell surface distribution and processing of the beta-amyloid precursor protein.* J Biol Chem, 2005. **280**(15): p. 15464-70.
101. Lakshmana, M.K., et al., *Novel role of RanBP9 in BACE1 processing of amyloid precursor protein and amyloid beta peptide generation.* J Biol Chem, 2009. **284**(18): p. 11863-72.
102. Andrew, R.J., et al., *A Greek Tragedy: The Growing Complexity of Alzheimer Amyloid Precursor Protein Proteolysis.* Journal of Biological Chemistry, 2016. **291**(37): p. 19235-19244.
103. Decourt, B., et al., *Recent Perspectives on APP, Secretases, Endosomal Pathways and How they Influence Alzheimer's Related Pathological Changes in Down Syndrome.* J Alzheimers Dis Parkinsonism, 2013. **Suppl 7**: p. 002.
104. Lichtenthaler, S.F., C. Haass, and H. Steiner, *Regulated intramembrane proteolysis--lessons from amyloid precursor protein processing.* J Neurochem, 2011. **117**(5): p. 779-96.
105. Jacobsen, K.T. and K. Iverfeldt, *Amyloid precursor protein and its homologues: a family of proteolysis-dependent receptors.* Cell Mol Life Sci, 2009. **66**(14): p. 2299-318.
106. Iwatsubo, T., *The [gamma]-secretase complex: machinery for intramembrane proteolysis.* Current Opinion in Neurobiology, 2004. **14**(3): p. 379-383.
107. Wilson, C.A., et al., *Presenilins are not required for A beta 42 production in the early secretory pathway.* Nat Neurosci, 2002. **5**(9): p. 849-55.
108. Sannerud, R., et al., *Restricted Location of PSEN2/gamma-Secretase Determines Substrate Specificity and Generates an Intracellular Abeta Pool.* Cell, 2016. **166**(1): p. 193-208.
109. Meckler, X. and F. Checler, *Presenilin 1 and Presenilin 2 Target gamma-Secretase Complexes to Distinct Cellular Compartments.* J Biol Chem, 2016. **291**(24): p. 12821-37.

110. Müller, T., et al., *The amyloid precursor protein intracellular domain (AICD) as modulator of gene expression, apoptosis, and cytoskeletal dynamics--Relevance for Alzheimer's disease.* Progress in Neurobiology, 2008. **85**(4): p. 393-406.
111. Konietzko, U., et al., *Co-localization of the amyloid precursor protein and the Notch intracellular domains in nuclear transcription factories.* Neurobiology of aging, 2010. **31**(1): p. 58-73.
112. Domingues, S.C., et al., *RanBP9 modulates AICD localization and transcriptional activity via direct interaction with Tip60.* J Alzheimers Dis, 2014. **42**(4): p. 1415-33.
113. Konietzko, U., *AICD nuclear signaling and its possible contribution to Alzheimer's disease.* Curr Alzheimer Res, 2012. **9**(2): p. 200-16.
114. Chen, A.C., et al., *Physical and functional interaction between the alpha- and gamma-secretases: A new model of regulated intramembrane proteolysis.* J Cell Biol, 2015. **211**(6): p. 1157-76.
115. Vella, L.J. and R. Cappai, *Identification of a novel amyloid precursor protein processing pathway that generates secreted N-terminal fragments.* FASEB J, 2012. **26**(7): p. 2930-40.
116. Gervais, F.G., et al., *Involvement of caspases in proteolytic cleavage of Alzheimer's amyloid-beta precursor protein and amyloidogenic A beta peptide formation.* Cell, 1999. **97**(3): p. 395-406.
117. Soriano, S., et al., *The Amyloidogenic Pathway of Amyloid Precursor Protein (APP) Is Independent of Its Cleavage by Caspases.* Journal of Biological Chemistry, 2001. **276**(31): p. 29045-29050.
118. Willem, M., et al., *eta-Secretase processing of APP inhibits neuronal activity in the hippocampus.* Nature, 2015. **526**(7573): p. 443-7.
119. Muresan, V., et al., *The cleavage products of amyloid-beta precursor protein are sorted to distinct carrier vesicles that are independently transported within neurites.* J Neurosci, 2009. **29**(11): p. 3565-78.
120. Niederst, E.D., S.M. Reyna, and L.S.B. Goldstein, *Axonal amyloid precursor protein and its fragments undergo somatodendritic endocytosis and processing.* Molecular Biology of the Cell, 2015. **26**(2): p. 205-217.
121. Cirrito, J.R., et al., *Endocytosis is required for synaptic activity-dependent release of amyloid-beta in vivo.* Neuron, 2008. **58**(1): p. 42-51.
122. Back, S., et al., *beta-amyloid precursor protein can be transported independent of any sorting signal to the axonal and dendritic compartment.* J Neurosci Res, 2007. **85**(12): p. 2580-90.
123. Villegas, C., V. Muresan, and Z. Ladescu Muresan, *Dual-tagged amyloid-beta precursor protein reveals distinct transport pathways of its N- and C-terminal fragments.* Hum Mol Genet, 2014. **23**(6): p. 1631-43.
124. Pastorino, L., et al., *The prolyl isomerase Pin1 regulates amyloid precursor protein processing and amyloid-beta production.* Nature, 2006. **440**(7083): p. 528-34.
125. Schedin-Weiss, S., B. Winblad, and L.O. Tjernberg, *The role of protein glycosylation in Alzheimer disease.* FEBS J, 2014. **281**(1): p. 46-62.
126. Walter, J. and C. Haass, *Posttranslational modifications of amyloid precursor protein : ectodomain phosphorylation and sulfation.* Methods Mol Med, 2000. **32**: p. 149-68.
127. Hornbeck, P.V., et al., *PhosphoSitePlus, 2014: mutations, PTMs and recalibrations.* Nucleic Acids Res, 2015. **43**(Database issue): p. D512-20.
128. Lee, M.-S., et al., *APP processing is regulated by cytoplasmic phosphorylation.* The Journal of Cell Biology, 2003. **163**(1): p. 83-95.
129. Tamayev, R., D. Zhou, and L. D'Adamio, *The interactome of the amyloid beta precursor protein family members is shaped by phosphorylation of their intracellular domains.* Mol Neurodegener, 2009. **4**: p. 28.
130. Gandy, S., A.J. Czernik, and P. Greengard, *Phosphorylation of Alzheimer disease amyloid precursor peptide by protein kinase C and Ca2+/calmodulin-dependent protein kinase II.* Proc Natl Acad Sci U S A, 1988. **85**(16): p. 6218-21.
131. Isohara, T., et al., *Phosphorylation of the Cytoplasmic Domain of Alzheimer's [beta]-Amyloid Precursor Protein at Ser655 by a Novel Protein Kinase.* Biochemical and Biophysical Research Communications, 1999. **258**(2): p. 300-305.
132. Ramelot, T.A. and L.K. Nicholson, *Phosphorylation-induced structural changes in the amyloid precursor protein cytoplasmic tail detected by NMR.* Journal of Molecular Biology, 2001. **307**(3): p. 871-884.
133. Vieira, S., et al., *S655 phosphorylation enhances APP secretory traffic.* Molecular and Cellular Biochemistry, 2009. **328**(1): p. 145-154.

134. Tam, J.H., et al., *Tyrosine Binding Protein Sites Regulate the Intracellular Trafficking and Processing of Amyloid Precursor Protein through a Novel Lysosome-Directed Pathway.* PLoS One, 2016. **11**(10): p. e0161445.
135. Schaefer, M.H., et al., *HIPPIE: Integrating Protein Interaction Networks with Experiment Based Quality Scores.* PLOS ONE, 2012. **7**(2): p. e31826.
136. Borg, J.P., et al., *The X11alpha protein slows cellular amyloid precursor protein processing and reduces Abeta40 and Abeta42 secretion.* J Biol Chem, 1998. **273**(24): p. 14761-6.
137. Mueller, H.T., et al., *Modulation of amyloid precursor protein metabolism by X11alpha /Mint-1. A deletion analysis of protein-protein interaction domains.* J Biol Chem, 2000. **275**(50): p. 39302-6.
138. Sullivan, S.E., et al., *Mint Proteins Are Required for Synaptic Activity-dependent Amyloid Precursor Protein (APP) Trafficking and Amyloid β Generation.* The Journal of Biological Chemistry, 2014. **289**(22): p. 15374-15383.
139. Taru, H., et al., *Interaction of Alzheimer's beta -amyloid precursor family proteins with scaffold proteins of the JNK signaling cascade.* J Biol Chem, 2002. **277**(22): p. 20070-8.
140. Taru, H., Y. Kirino, and T. Suzuki, *Differential roles of JIP scaffold proteins in the modulation of amyloid precursor protein metabolism.* J Biol Chem, 2002. **277**(30): p. 27567-74.
141. Verhey, K.J., et al., *Cargo of kinesin identified as JIP scaffolding proteins and associated signaling molecules.* J Cell Biol, 2001. **152**(5): p. 959-70.
142. Koushika, S.P., *"JIP"ing along the axon: the complex roles of JIPs in axonal transport.* Bioessays, 2008. **30**(1): p. 10-4.
143. Inomata, H., et al., *A scaffold protein JIP-1b enhances amyloid precursor protein phosphorylation by JNK and its association with kinesin light chain 1.* J Biol Chem, 2003. **278**(25): p. 22946-55.
144. Muresan, Z. and V. Muresan, *Coordinated transport of phosphorylated amyloid-β precursor protein and c-Jun NH(2)-terminal kinase–interacting protein-1.* The Journal of Cell Biology, 2005. **171**(4): p. 615-625.
145. Parisiadou, L. and S. Efthimiopoulos, *Expression of mDab1 promotes the stability and processing of amyloid precursor protein and this effect is counteracted by X11α.* Neurobiology of Aging, 2007. **28**(3): p. 377-388.
146. Hoe, H.S., et al., *DAB1 and Reelin effects on amyloid precursor protein and ApoE receptor 2 trafficking and processing.* J Biol Chem, 2006. **281**(46): p. 35176-85.
147. Kyriazis, G.A., et al., *Numb endocytic adapter proteins regulate the transport and processing of the amyloid precursor protein in an isoform-dependent manner: implications for Alzheimer disease pathogenesis.* J Biol Chem, 2008. **283**(37): p. 25492-502.
148. Kwon, O.Y., et al., *Dab1 binds to Fe65 and diminishes the effect of Fe65 or LRP1 on APP processing.* J Cell Biochem, 2010. **111**(2): p. 508-19.
149. Lau, K.F., et al., *Fe65 and X11beta co-localize with and compete for binding to the amyloid precursor protein.* Neuroreport, 2000. **11**(16): p. 3607-10.
150. Russo, C., et al., *Signal transduction through tyrosine-phosphorylated C-terminal fragments of amyloid precursor protein via an enhanced interaction with Shc/Grb2 adaptor proteins in reactive astrocytes of Alzheimer's disease brain.* J Biol Chem, 2002. **277**(38): p. 35282-8.
151. Ma, Q.H., et al., *A TAG1-APP signalling pathway through Fe65 negatively modulates neurogenesis.* Nat Cell Biol, 2008. **10**(3): p. 283-94.
152. Ho, A. and T.C. Sudhof, *Binding of F-spondin to amyloid-beta precursor protein: a candidate amyloid-beta precursor protein ligand that modulates amyloid-beta precursor protein cleavage.* Proc Natl Acad Sci U S A, 2004. **101**(8): p. 2548-53.
153. Osterfield, M., et al., *Interaction of amyloid precursor protein with contactins and NgCAM in the retinotectal system.* Development, 2008. **135**(6): p. 1189-99.
154. Hoe, H.S., et al., *Interaction of reelin with amyloid precursor protein promotes neurite outgrowth.* J Neurosci, 2009. **29**(23): p. 7459-73.
155. Rice, H.C., et al., *Pancortins interact with amyloid precursor protein and modulate cortical cell migration.* Development, 2012. **139**(21): p. 3986-96.
156. Yamazaki, T., E.H. Koo, and D.J. Selkoe, *Cell Surface Amyloid β-Protein Precursor Colocalizes with β1 Integrins at Substrate Contact Sites in Neural Cells.* The Journal of Neuroscience, 1997. **17**(3): p. 1004-1010.
157. Muller, U.C. and H. Zheng, *Physiological functions of APP family proteins.* Cold Spring Harb Perspect Med, 2012. **2**(2): p. a006288.
158. Mi, H., et al., *Large-scale gene function analysis with the PANTHER classification system.* Nat. Protocols, 2013. **8**(8): p. 1551-1566.

159. Ashburner, M., et al., *Gene Ontology: tool for the unification of biology.* Nat Genet, 2000. **25**(1): p. 25-29.
160. Petschnigg, J., et al., *The mammalian-membrane two-hybrid assay (MaMTH) for probing membrane-protein interactions in human cells.* Nat Meth, 2014. **11**(5): p. 585-592.
161. Gao, Y., et al., *Integrative Single-Cell Transcriptomics Reveals Molecular Networks Defining Neuronal Maturation During Postnatal Neurogenesis.* Cereb Cortex, 2016.
162. Sabo, S.L., et al., *The Alzheimer Amyloid Precursor Protein (APP) and Fe65, an APP-Binding Protein, Regulate Cell Movement.* The Journal of Cell Biology, 2001. **153**(7): p. 1403-1414.
163. Sabo, S.L., et al., *The Amyloid Precursor Protein and Its Regulatory Protein, FE65, in Growth Cones and Synapses In Vitro and In Vivo.* The Journal of Neuroscience, 2003. **23**(13): p. 5407-5415.
164. Ikin, A.F., et al., *A macromolecular complex involving the amyloid precursor protein (APP) and the cytosolic adapter FE65 is a negative regulator of axon branching.* Molecular and cellular neurosciences, 2007. **35**(1): p. 57-63.
165. Guenette, S., et al., *Essential roles for the FE65 amyloid precursor protein-interacting proteins in brain development.* EMBO J, 2006. **25**(2): p. 420-31.
166. Strecker, P., et al., *FE65 and FE65L1 share common synaptic functions and genetically interact with the APP family in neuromuscular junction formation.* Sci Rep, 2016. **6**: p. 25652.
167. Guo, M., L.Y. Jan, and Y.N. Jan, *Control of daughter cell fates during asymmetric division: interaction of Numb and Notch.* Neuron, 1996. **17**(1): p. 27-41.
168. Huang, E.J., et al., *Targeted deletion of numb and numblike in sensory neurons reveals their essential functions in axon arborization.* Genes Dev, 2005. **19**(1): p. 138-51.
169. Lu, C.B., et al., *Numb-mediated neurite outgrowth is isoform-dependent, and requires activation of voltage-dependent calcium channels.* Neuroscience, 2009. **161**(2): p. 403-12.
170. Tarn, W.Y., et al., *RBM4 promotes neuronal differentiation and neurite outgrowth by modulating Numb isoform expression.* Mol Biol Cell, 2016. **27**(10): p. 1676-83.
171. Aguirre, A., M.E. Rubio, and V. Gallo, *Notch and EGFR pathway interaction regulates neural stem cell number and self-renewal.* Nature, 2010. **467**(7313): p. 323-7.
172. Roncarati, R., et al., *The gamma-secretase-generated intracellular domain of beta-amyloid precursor protein binds Numb and inhibits Notch signaling.* Proc Natl Acad Sci U S A, 2002. **99**(10): p. 7102-7.
173. Merdes, G., et al., *Interference of human and Drosophila APP and APP-like proteins with PNS development in Drosophila.* EMBO J, 2004. **23**(20): p. 4082-95.
174. Olson, E.C., S. Kim, and C.A. Walsh, *Impaired Neuronal Positioning and Dendritogenesis in the Neocortex after Cell-Autonomous Dab1 Suppression.* The Journal of Neuroscience, 2006. **26**(6): p. 1767-1775.
175. Young-Pearse, T.L., et al., *A critical function for beta-amyloid precursor protein in neuronal migration revealed by in utero RNA interference.* J Neurosci, 2007. **27**(52): p. 14459-69.
176. Young-Pearse, T.L., et al., *Biochemical and functional interaction of disrupted-in-schizophrenia 1 and amyloid precursor protein regulates neuronal migration during mammalian cortical development.* J Neurosci, 2010. **30**(31): p. 10431-40.
177. Okamoto, M. and T.C. Südhof, *Mints, Munc18-interacting Proteins in Synaptic Vesicle Exocytosis.* Journal of Biological Chemistry, 1997. **272**(50): p. 31459-31464.
178. Borg, J.-P., et al., *Identification of an Evolutionarily Conserved Heterotrimeric Protein Complex Involved in Protein Targeting.* Journal of Biological Chemistry, 1998. **273**(48): p. 31633-31636.
179. Butz, S., M. Okamoto, and T.C. Sudhof, *A tripartite protein complex with the potential to couple synaptic vesicle exocytosis to cell adhesion in brain.* Cell, 1998. **94**(6): p. 773-82.
180. Ho, A., et al., *Genetic analysis of Mint/X11 proteins: essential presynaptic functions of a neuronal adaptor protein family.* J Neurosci, 2006. **26**(50): p. 13089-101.
181. Minami, S.S., et al., *The cytoplasmic adaptor protein X11α and extracellular matrix protein Reelin regulate ApoE receptor 2 trafficking and cell movement.* The FASEB Journal, 2010. **24**(1): p. 58-69.
182. Mitchell, J.C., et al., *Expression of the neuronal adaptor protein X11alpha protects against memory dysfunction in a transgenic mouse model of Alzheimer's disease.* J Alzheimers Dis, 2010. **20**(1): p. 31-6.
183. Verhage, M., et al., *Synaptic assembly of the brain in the absence of neurotransmitter secretion.* Science, 2000. **287**(5454): p. 864-9.
184. Yamashita, S., et al., *Mislocalization of syntaxin-1 and impaired neurite growth observed in a human iPSC model for STXBP1-related epileptic encephalopathy.* Epilepsia, 2016. **57**(4): p. e81-6.

185. Giza, J., et al., *Behavioral and cerebellar transmission deficits in mice lacking the autism-linked gene islet brain-2.* J Neurosci, 2010. **30**(44): p. 14805-16.
186. Kennedy, N.J., et al., *Requirement of JIP scaffold proteins for NMDA-mediated signal transduction.* Genes Dev, 2007. **21**(18): p. 2336-46.
187. Aldinger, K.A., et al., *Cerebellar and posterior fossa malformations in patients with autism-associated chromosome 22q13 terminal deletion.* American journal of medical genetics. Part A, 2013. **0**(1): p. 131-136.
188. Stockinger, W., et al., *The reelin receptor ApoER2 recruits JNK-interacting proteins-1 and -2.* J Biol Chem, 2000. **275**(33): p. 25625-32.
189. Hoe, H.S., et al., *FE65 interaction with the ApoE receptor ApoEr2.* J Biol Chem, 2006. **281**(34): p. 24521-30.
190. Lane-Donovan, C., G.T. Philips, and J. Herz, *More than cholesterol transporters: lipoprotein receptors in CNS function and neurodegeneration.* Neuron, 2014. **83**(4): p. 771-87.
191. Liu, Q., et al., *Neuronal LRP1 knockout in adult mice leads to impaired brain lipid metabolism and progressive, age-dependent synapse loss and neurodegeneration.* J Neurosci, 2010. **30**(50): p. 17068-78.
192. Shi, Y., et al., *Ligand binding to LRP1 transactivates Trk receptors by a Src family kinase-dependent pathway.* Sci Signal, 2009. **2**(68): p. ra18.
193. Bishop, P., D. Rocca, and Jeremy M. Henley, *Ubiquitin C-terminal hydrolase L1 (UCH-L1): structure, distribution and roles in brain function and dysfunction.* Biochemical Journal, 2016. **473**(16): p. 2453-2462.
194. Sakurai, M., et al., *Ubiquitin C-terminal hydrolase L1 regulates the morphology of neural progenitor cells and modulates their differentiation.* J Cell Sci, 2006. **119**(Pt 1): p. 162-71.
195. Gong, B., et al., *Ubiquitin hydrolase Uch-L1 rescues beta-amyloid-induced decreases in synaptic function and contextual memory.* Cell, 2006. **126**(4): p. 775-88.
196. Zhang, M., et al., *Overexpression of ubiquitin carboxyl-terminal hydrolase L1 (UCHL1) delays Alzheimer's progression in vivo.* Sci Rep, 2014. **4**: p. 7298.
197. Nakamura, M., et al., *When overexpressed, a novel centrosomal protein, RanBPM, causes ectopic microtubule nucleation similar to gamma-tubulin.* J Cell Biol, 1998. **143**(4): p. 1041-52.
198. Wang, D., et al., *Activation of Ras/Erk pathway by a novel MET-interacting protein RanBPM.* J Biol Chem, 2002. **277**(39): p. 36216-22.
199. Atabakhsh, E. and C. Schild-Poulter, *RanBPM is an inhibitor of ERK signaling.* PLoS One, 2012. **7**(10): p. e47803.
200. Togashi, H., E.F. Schmidt, and S.M. Strittmatter, *RanBPM contributes to Semaphorin3A signaling through plexin-A receptors.* J Neurosci, 2006. **26**(18): p. 4961-9.
201. Woo, J.A., et al., *Pivotal role of RanBP9 in integrin-dependent focal adhesion signaling and assembly.* FASEB J, 2012. **26**(4): p. 1672-81.
202. Woo, J.A., et al., *RanBP9 at the intersection between cofilin and A[beta] pathologies: rescue of neurodegenerative changes by RanBP9 reduction.* Cell Death Dis, 2015. **6**: p. 1676.
203. Brouillet, E., et al., *The amyloid precursor protein interacts with Go heterotrimeric protein within a cell compartment specialized in signal transduction.* J Neurosci, 1999. **19**(5): p. 1717-27.
204. Shaked, G.M., et al., *Interactions between the amyloid precursor protein C-terminal domain and G proteins mediate calcium dysregulation and amyloid beta toxicity in Alzheimer's disease.* FEBS J, 2009. **276**(10): p. 2736-51.
205. Ramaker, J.M., T.L. Swanson, and P.F. Copenhaver, *Amyloid Precursor Proteins Interact with the Heterotrimeric G Protein Go in the Control of Neuronal Migration.* The Journal of Neuroscience, 2013. **33**(24): p. 10165-10181.
206. Piñero, J., et al., *DisGeNET: a comprehensive platform integrating information on human disease-associated genes and variants.* Nucleic Acids Research, 2016. **45**(D1): p. D833-D839.
207. Bellon, A., *New genes associated with schizophrenia in neurite formation: a review of cell culture experiments.* Mol Psychiatry, 2007. **12**(7): p. 620-9.
208. Lee, S.-A., et al., *Construction and analysis of the protein-protein interaction networks for schizophrenia, bipolar disorder, and major depression.* BMC Bioinformatics, 2011. **12**(13): p. S20.
209. Lopez-Sanchez, N., U. Muller, and J.M. Frade, *Lengthening of G2/mitosis in cortical precursors from mice lacking beta-amyloid precursor protein.* Neuroscience, 2005. **130**(1): p. 51-60.
210. Masliah, E., et al., *Amyloid precursor protein is localized in growing neurites of neonatal rat brain.* Brain Research, 1992. **593**(2): p. 323-328.

211. Ferreira, A., A. Caceres, and K. Kosik, *Intraneuronal compartments of the amyloid precursor protein.* J. Neurosci., 1993. **13**(7): p. 3112-3123.
212. van der Kant, R. and Lawrence S.B. Goldstein, *Cellular Functions of the Amyloid Precursor Protein from Development to Dementia.* Developmental Cell. **32**(4): p. 502-515.
213. Muller, U., et al., *Behavioral and anatomical deficits in mice homozygous for a modified beta-amyloid precursor protein gene.* Cell, 1994. **79**(5): p. 755-65.
214. Zheng, H., et al., *beta-Amyloid precursor protein-deficient mice show reactive gliosis and decreased locomotor activity.* Cell, 1995. **81**(4): p. 525-31.
215. Steinbach, J.P., et al., *Hypersensitivity to seizures in beta-amyloid precursor protein deficient mice.* Cell Death Differ, 1998. **5**(10): p. 858-66.
216. Magara, F., et al., *Genetic background changes the pattern of forebrain commissure defects in transgenic mice underexpressing the β-amyloid-precursor protein.* Proceedings of the National Academy of Sciences of the United States of America, 1999. **96**(8): p. 4656-4661.
217. White, A.R., et al., *Copper levels are increased in the cerebral cortex and liver of APP and APLP2 knockout mice.* Brain Res, 1999. **842**(2): p. 439-44.
218. Dawson, G.R., et al., *Age-related cognitive deficits, impaired long-term potentiation and reduction in synaptic marker density in mice lacking the beta-amyloid precursor protein.* Neuroscience, 1999. **90**(1): p. 1-13.
219. Seabrook, G.R., et al., *Mechanisms contributing to the deficits in hippocampal synaptic plasticity in mice lacking amyloid precursor protein.* Neuropharmacology, 1999. **38**(3): p. 349-59.
220. Grimm, M.O., et al., *Regulation of cholesterol and sphingomyelin metabolism by amyloid-beta and presenilin.* Nat Cell Biol, 2005. **7**(11): p. 1118-23.
221. Priller, C., et al., *Synapse formation and function is modulated by the amyloid precursor protein.* J Neurosci, 2006. **26**(27): p. 7212-21.
222. Ring, S., et al., *The secreted beta-amyloid precursor protein ectodomain APPs alpha is sufficient to rescue the anatomical, behavioral, and electrophysiological abnormalities of APP-deficient mice.* J Neurosci, 2007. **27**(29): p. 7817-26.
223. Bittner, T., et al., *Gamma-secretase inhibition reduces spine density in vivo via an amyloid precursor protein-dependent pathway.* J Neurosci, 2009. **29**(33): p. 10405-9.
224. Yang, L., et al., *Amyloid precursor protein regulates Cav1.2 L-type calcium channel levels and function to influence GABAergic short-term plasticity.* J Neurosci, 2009. **29**(50): p. 15660-8.
225. Lee, K.J., et al., *Beta amyloid-independent role of amyloid precursor protein in generation and maintenance of dendritic spines.* Neuroscience, 2010. **169**(1): p. 344-56.
226. Smith, K.D., et al., *Increased Human Wildtype Tau Attenuates Axonal Transport Deficits Caused by Loss of APP in Mouse Models.* Magn Reson Insights, 2010. **4**: p. 11-18.
227. Tyan, S.H., et al., *Amyloid precursor protein (APP) regulates synaptic structure and function.* Mol Cell Neurosci, 2012. **51**(1-2): p. 43-52.
228. Gallagher, J.J., et al., *Deficits in axonal transport in hippocampal-based circuitry and the visual pathway in APP knock-out animals witnessed by manganese enhanced MRI.* Neuroimage, 2012. **60**(3): p. 1856-1866.
229. Rama, N., et al., *Amyloid precursor protein regulates netrin-1-mediated commissural axon outgrowth.* J Biol Chem, 2012. **287**(35): p. 30014-23.
230. Weyer, S.W., et al., *Comparative analysis of single and combined APP/APLP knockouts reveals reduced spine density in APP-KO mice that is prevented by APPsalpha expression.* Acta Neuropathol Commun, 2014. **2**: p. 36.
231. Carrano, A. and P. Das, *Altered Innate Immune and Glial Cell Responses to Inflammatory Stimuli in Amyloid Precursor Protein Knockout Mice.* PLoS One, 2015. **10**(10): p. e0140210.
232. Zou, C., et al., *Amyloid precursor protein maintains constitutive and adaptive plasticity of dendritic spines in adult brain by regulating D-serine homeostasis.* EMBO J, 2016. **35**(20): p. 2213-2222.
233. Marik, S.A., et al., *Physiological role for amyloid precursor protein in adult experience-dependent plasticity.* Proc Natl Acad Sci U S A, 2016. **113**(28): p. 7912-7.
234. Hoe, H.S., H.K. Lee, and D.T. Pak, *The upside of APP at synapses.* CNS Neurosci Ther, 2012. **18**(1): p. 47-56.
235. Heber, S., et al., *Mice with combined gene knock-outs reveal essential and partially redundant functions of amyloid precursor protein family members.* J Neurosci, 2000. **20**(21): p. 7951-63.
236. Wang, P., et al., *Defective neuromuscular synapses in mice lacking amyloid precursor protein (APP) and APP-Like protein 2.* J Neurosci, 2005. **25**(5): p. 1219-25.

237. Hick, M., et al., *Acute function of secreted amyloid precursor protein fragment APPsalpha in synaptic plasticity.* Acta Neuropathol, 2015. **129**(1): p. 21-37.
238. Herms, J., et al., *Cortical dysplasia resembling human type 2 lissencephaly in mice lacking all three APP family members.* The EMBO Journal, 2004. **23**(20): p. 4106-4115.
239. Li, H., et al., *Soluble amyloid precursor protein (APP) regulates transthyretin and Klotho gene expression without rescuing the essential function of APP.* Proc Natl Acad Sci U S A, 2010. **107**(40): p. 17362-7.
240. Klevanski, M., et al., *The APP Intracellular Domain Is Required for Normal Synaptic Morphology, Synaptic Plasticity, and Hippocampus-Dependent Behavior.* J Neurosci, 2015. **35**(49): p. 16018-33.
241. Barbagallo, A.P., et al., *Tyr(682) in the intracellular domain of APP regulates amyloidogenic APP processing in vivo.* PLoS One, 2010. **5**(11): p. e15503.
242. Barbagallo, A.P., et al., *The intracellular threonine of amyloid precursor protein that is essential for docking of Pin1 is dispensable for developmental function.* PLoS One, 2011. **6**(3): p. e18006.
243. Bergmans, B.A., et al., *Neurons generated from APP/APLP1/APLP2 triple knockout embryonic stem cells behave normally in vitro and in vivo: lack of evidence for a cell autonomous role of the amyloid precursor protein in neuronal differentiation.* Stem Cells, 2010. **28**(3): p. 399-406.
244. Schrenk-Siemens, K., et al., *Embryonic stem cell-derived neurons as a cellular system to study gene function: lack of amyloid precursor proteins APP and APLP2 leads to defective synaptic transmission.* Stem Cells, 2008. **26**(8): p. 2153-63.
245. Aydin, D., et al., *Comparative transcriptome profiling of amyloid precursor protein family members in the adult cortex.* BMC Genomics, 2011. **12**: p. 160-160.
246. Westmark, C.J., *What/'s hAPPening at synapses[quest] The role of amyloid [beta]-protein precursor and [beta]-amyloid in neurological disorders.* Mol Psychiatry, 2013. **18**(4): p. 425-434.
247. Milward, E.A., et al., *The amyloid protein precursor of Alzheimer's disease is a mediator of the effects of nerve growth factor on neurite outgrowth.* Neuron, 1992. **9**(1): p. 129-137.
248. Hung, A.Y., et al., *Increased expression of beta-amyloid precursor protein during neuronal differentiation is not accompanied by secretory cleavage.* Proceedings of the National Academy of Sciences of the United States of America, 1992. **89**(20): p. 9439-9443.
249. Qiu, W., et al., *Cell-surface beta-amyloid precursor protein stimulates neurite outgrowth of hippocampal neurons in an isoform-dependent manner.* J. Neurosci., 1995. **15**(3): p. 2157-2167.
250. Allinquant, B., et al., *Downregulation of amyloid precursor protein inhibits neurite outgrowth in vitro.* The Journal of Cell Biology, 1995. **128**(5): p. 919-927.
251. Small, D., et al., *A heparin-binding domain in the amyloid protein precursor of Alzheimer's disease is involved in the regulation of neurite outgrowth.* J. Neurosci., 1994. **14**(4): p. 2117-2127.
252. Sosa, L.J., et al., *Amyloid precursor protein is an autonomous growth cone adhesion molecule engaged in contact guidance.* PLoS One, 2013. **8**(5): p. e64521.
253. Perez, R.G., et al., *The beta -Amyloid Precursor Protein of Alzheimer's Disease Enhances Neuron Viability and Modulates Neuronal Polarity.* J. Neurosci., 1997. **17**(24): p. 9407-9414.
254. Young-Pearse, T., et al., *Secreted APP regulates the function of full-length APP in neurite outgrowth through interaction with integrin beta1.* Neural Development, 2008. **3**(1): p. 15.
255. Stahl, R., et al., *Shedding of APP limits its synaptogenic activity and cell adhesion properties.* Front Cell Neurosci, 2014. **8**: p. 410.
256. Wentzell, J.S., et al., *Amyloid precursor proteins are protective in Drosophila models of progressive neurodegeneration.* Neurobiol Dis, 2012. **46**(1): p. 78-87.
257. Luo, L., T. Tully, and K. White, *Human amyloid precursor protein ameliorates behavioral deficit of flies deleted for Appl gene.* Neuron, 1992. **9**(4): p. 595-605.
258. Leyssen, M., et al., *Amyloid precursor protein promotes post-developmental neurite arborization in the Drosophila brain.* EMBO J, 2005. **24**(16): p. 2944-55.
259. Plummer, S., et al., *The Neuroprotective Properties of the Amyloid Precursor Protein Following Traumatic Brain Injury.* Aging Dis, 2016. **7**(2): p. 163-79.
260. Soldano, A., et al., *The Drosophila homologue of the amyloid precursor protein is a conserved modulator of Wnt PCP signaling.* PLoS Biol, 2013. **11**(5): p. e1001562.
261. Bergstrom, P., et al., *Amyloid precursor protein expression and processing are differentially regulated during cortical neuron differentiation.* Sci Rep, 2016. **6**: p. 29200.
262. Liao, M.C., et al., *Single-Cell Detection of Secreted Abeta and sAPPalpha from Human IPSC-Derived Neurons and Astrocytes.* J Neurosci, 2016. **36**(5): p. 1730-46.
263. Turner, P.R., et al., *Roles of amyloid precursor protein and its fragments in regulating neural activity, plasticity and memory.* Progress in Neurobiology, 2003. **70**(1): p. 1-32.

264. Henriques, A.G., et al., *Abeta Influences Cytoskeletal Signaling Cascades with Consequences to Alzheimer's Disease.* Mol Neurobiol, 2014.
265. Selkoe, D.J., *Soluble oligomers of the amyloid beta-protein impair synaptic plasticity and behavior.* Behav Brain Res, 2008. **192**(1): p. 106-13.
266. Bishop, G.M. and S.R. Robinson, *Physiological roles of amyloid-beta and implications for its removal in Alzheimer's disease.* Drugs Aging, 2004. **21**(10): p. 621-30.
267. Rossjohn, J., et al., *Crystal structure of the N-terminal, growth factor-like domain of Alzheimer amyloid precursor protein.* Nat Struct Biol, 1999. **6**(4): p. 327-31.
268. Demars, M.P., et al., *Soluble amyloid precursor protein: a novel proliferation factor of adult progenitor cells of ectodermal and mesodermal origin.* Stem Cell Res Ther, 2011. **2**(4): p. 36.
269. Caille, I., et al., *Soluble form of amyloid precursor protein regulates proliferation of progenitors in the adult subventricular zone.* Development, 2004. **131**(9): p. 2173-81.
270. Morales-Corraliza, J., et al., *In vivo turnover of tau and APP metabolites in the brains of wild-type and Tg2576 mice: greater stability of sAPP in the beta-amyloid depositing mice.* PLoS One, 2009. **4**(9): p. e7134.
271. Bell, K.F., et al., *ADAM-10 over-expression increases cortical synaptogenesis.* Neurobiol Aging, 2008. **29**(4): p. 554-65.
272. Obregon, D., et al., *Soluble amyloid precursor protein-alpha modulates beta-secretase activity and amyloid-beta generation.* Nat Commun, 2012. **3**: p. 777.
273. Hasebe, N., et al., *Soluble beta-amyloid Precursor Protein Alpha binds to p75 neurotrophin receptor to promote neurite outgrowth.* PLoS One, 2013. **8**(12): p. e82321.
274. Chasseigneaux, S., et al., *Secreted amyloid precursor protein beta and secreted amyloid precursor protein alpha induce axon outgrowth in vitro through Egr1 signaling pathway.* PLoS One, 2011. **6**(1): p. e16301.
275. Nikolaev, A., et al., *APP binds DR6 to trigger axon pruning and neuron death via distinct caspases.* Nature, 2009. **457**(7232): p. 981-9.
276. Muller, T., et al., *Modulation of Gene Expression and Cytoskeletal Dynamics by the Amyloid Precursor Protein Intracellular Domain (AICD).* Mol. Biol. Cell, 2007. **18**(1): p. 201-210.
277. Sim, P.-L. and K. Heese, *Ligand-Dependent Activation of the Chimeric Tumor Necrosis Factor Receptor-Amyloid Precursor Protein (APP) Reveals Increased APP processing and Suppressed Neuronal Differentiation.* Neurosignals, 2010. **18**: p. 9-23.
278. Deyts, C., et al., *Novel GalphaS-protein signaling associated with membrane-tethered amyloid precursor protein intracellular domain.* J Neurosci, 2012. **32**(5): p. 1714-29.
279. Deyts, C., et al., *Loss of presenilin function is associated with a selective gain of APP function.* Elife, 2016. **5**.

Aims

The major goal of the work here presented was to characterize the physiological role of APP in the morphological alterations underlying neuronal differentiation, especially in neurite outgrowth and elongation.

We were particularly dedicated in unravelling signaling mechanisms mediated by APP and its proteolytic fragment sAPP relevant for neuronal differentiation, and how APP phosphorylation at serine 655 modulates such mechanisms.

To this end we delineated the following specific aims:

1. Establishment and characterization of a cell model system to study neuronal-like differentiation, which allowed to evaluate time-dependent protein profiles of APP and its cleavage to sAPP with differentiation (Chapter 5).
2. To unravel the functional interplay between APP and the Epidermal Growth Factor and downstream neurotrophic/neuritogenic signaling pathways, and their dependence on APP S655 phosphorylation (Chapter 6).
3. Identification of specific protein binding partners of S655 phosphoAPP involved in neurotrophic functions, to better characterize the molecular mechanisms triggered by this phosphorylation, and to find novel APP protein effectors and regulators (Chapter 7).

B. RESULTS

5. Analysis of the amyloid precursor protein role in neuritogenesis reveals a biphasic SH-SY5Y neuronal cell differentiation model

Joana F. da Rocha[1,2], Odete A. B. da Cruz e Silva[2], Sandra I. Vieira[*1,2]

[1] Cell Differentiation and Regeneration group, Institute of Biomedicine (iBiMED), Department of Medical Sciences, Universidade de Aveiro, Campus de Santiago, 3810-193 Aveiro, Portugal;

[2]Neurosciences and Signalling group, Institute of Biomedicine (iBiMED), Department of Medical Sciences, Universidade de Aveiro, Campus de Santiago, 3810-193 Aveiro, Portugal.

[*]Corresponding author: Sandra Isabel Vieira; e-mail: sivieira@ua.pt.

DOI: 10.1111/jnc.13133

5.1. Abstract

The existence of an intrinsic program controlling neuritogenesis and activated during early neuronal differentiation and regeneration stages, is well established. However, the identity and role of each molecular player and event, as well as how such a program is modified by environmental signals, remain a focus of research. The Amyloid Precursor Protein (APP) is a neuromodulator of the developing and mature nervous system, although in a highly complex manner, far from clear. To study APP-induced neuritogenesis, the Retinoic Acid (RA)-induced SH-SY5Y cell differentiation model was first detailed characterized in terms of RA dose, morphological outputs and relevant biochemical markers. The findings here reported unveiled two differentiation phases for the 10 μM RA dose: 1-4 (4 days excluded) and 4-8 days, clearly defined by the ratio between APP and acetylated Tubulin fold increases. Moreover, we describe for the first time a unique peak of secreted APP (sAPP)/APP ratio at the first phase. Subsequent APP and sAPP modulations confirmed that a high sAPP/APP ratio potentiates the elongation of smaller processes at the earlier neuritogenic phase. This ratio drops in the second phase, as holoAPP levels increases to assist the maintenance of the longer neurites, potentially via their stabilization.

5.2. Introduction

The Amyloid Precursor Protein (APP) is an ubiquitously expressed type I transmembrane glycoprotein, dynamically sorted through the membranes of intracellular organelles and the plasma membrane. Intracellularly, it undergoes two mutually exclusive post-translational cleavage pathways. Briefly, proteolytic cleavage by an α-secretase enables the production and secretion of sAPPα into the extracellular medium or the lumen of the vesicles, and leaves the remaining C83 fragment in the membrane. C83 can be cleaved by the γ-secretase complex to release two peptides, p3 and the APP intracellular C-terminal domain (AICD). Alternatively, cleavage by β-secretase results in the secretion of the slightly truncated sAPPβ molecule, and the retention of the C99 fragment. This appears to be the major substrate of γ-secretase cleavage, leading to the production of AICD and Aβ, a potentially toxic peptide [1-3].

While mainly studied for its association with the Alzheimer's disease (AD), this complex APP molecule is determinant for neuronal function, including neurite outgrowth and neuronal differentiation. In fact, APP is upregulated in the developing nervous system, where it is preferentially enriched in growing neurites and neuritic growth cones [4-6]. Furthermore, APP was observed to mediate the in vitro neuritic outgrowth promoted by neurotrophic molecules such as the Nerve Growth Factor (NGF) [7], and an association of Retinoic Acid (RA) plus Brain Derived Neurotrophic Factor (BDNF) [8, 9].

Although the neuritogenic activity was formerly attributed solely to the membrane-bound APP holoprotein (holoAPP) [10-13] and further on to its sAPPα product [14, 15], there is now evidence that both sAPPα and cell-associated holoAPP intervene in neuritogenesis, since sAPP is not able to stimulate neurite outgrowth in the absence of cell surface holoAPP [16, 17]. Several studies focusing the APP role in neuronal differentiation have been performed in RA-differentiated SH-SY5Y cells, a well-documented neuronal-like model [18, 19]. The treatment of SH-SY5Y cells with RA induces a shift towards the α-secretase pathway, leading to increased sAPPα [8]. Additionally, different RA concentrations (mainly 1 and 10 μM) were shown to increase total APP gene expression. However, the time period indicated for this up regulation onset is contradictory [8, 9, 20, 21]. On the other hand, it was suggested that it is the specific increase in the levels of the APP695 mRNA transcript, and not of total APP mRNA, that supports a neuronal phenotype in RA-treated SH-SY5Y cells [22]. Besides this non-uniformity in APP-related data, the literature lacked a more detailed characterization of the RA-induced SH-SY5Y differentiation process. Thus, the first goal of the work here described was to establish a comprehensive and reproducible cellular differentiation model, by characterizing in detail the neuritogenic-related alterations of RA-mediated SH-SY5Y neuronal-like differentiation. The time-dependent APP expression, sAPP/APP ratio, and a correlation between APP and acetylated tubulin were monitored using this model.

Based on the findings here presented, we propose a biphasic temporal response induced by 10 μM RA SH-SY5Y differentiation, where a sAPP/APP peak assists the initial phase marked by neuritic elongation, and increased holoAPP protein levels portrays the second phase, when it is necessary to sustain neuritic elongation and circumvent neuritic retraction.

5.3. Material and Methods

5.3.1. SH-SY5Y cell culture and differentiation

The SH-SY5Y human neuroblastoma cell line was maintained in MEM/F12 medium [23] and was previously enriched in the neuroblastic N-type of cells (immature nerve cells that are RA-differentiated into neuronal-like cells), on the basis of their lower substrate adherence than S-type cells [24]. N-type enriched $1.0x10^4$ cells/cm^2 SH-SY5Y cells were plated onto six-wells plates and differentiated with 1 or 10 μM all-trans RA in 10% FBS medium for 2, 4, 6 and 8 days (D2-D8). Optimal cell densities to be plated and FBS % were previously optimized by us. RA was added every other day, and cell medium replaced at that time.

5.3.2. Microscopy and morphological analyses

Cell counts and morphometric analysis of SH-SY5Y differentiated cells were performed on phase contrast (PhC) images of live cells (Olympus IX-81 inverted microscope; 350 cells/condition), analyzed using the AnalySIS (Olympus) and ImageJ software.

Cell counts were expressed as a percentage relative to the number of cells initially plated. Cellular projections ('processes') were categorized as indicated. "Total": all processes arising from a cell. "≥20 μm": processes longer than 20 μm; "20-35 μm": processes longer than 20 μm but shorter than 35 μm (pre-neurites); "≥35 μm": processes longer than 35 μm (neurites). When specified, neurites were further divided into shorter (<50 μm) and longer neurites (≥50 μm). Data was expressed as the number of processes per cell, or their percentage out of the 'Total' number of processes.

For immunocytochemistry analysis, cells grown on coverslips were fixed with 4% paraformaldehyde and permeabilized with 0,2% TRITON [25]. Primary and secondary antibodies used (1-2h incubation): anti-APP C-terminal (CT695 antibody, Invitrogen), monoclonal anti-acetylated α-tubulin (Sigma-Aldrich); Alexa 488- and 405-conjugated IgGs (Molecular Probes). To stain F-actin, AlexaFluor Phalloidin in 1% BSA PBS was added for 30 min in the dark. Preparations were mounted with Vectashield® media (Vector Labs) and visualized either by epifluorescence microscopy [Olympus IX-81 microscope; 20x/0.40 objective [25]], or by confocal microscopy [LSM 510 META confocal microscope (Zeiss); 63x oil objective [26]].

5.3.3. Modulation of APP/sAPP levels

SH-SY5Y cells were co-incubated for 48h with 10 μM of RA and 10 μM TAPI-1 (Santa Cruz Biotechnology) either at the onset of RA exposure (from D0 to D2) or at the 2nd day (D2 to D4). TAPI-1 is a metalloproteases' inhibitor that hinders APP cleavage into sAPPα by the α-secretase TACE. For sAPP overexposure, cells were incubated from D0 to D2 with 10 nM recombinant

human sAPPα (Sigma-Aldrich; [27, 28]). Cells were fixed and morphometric analyses performed on PhC microphotographs; differentiated cells at D4 were further subjected to immunocytochemistry analyses (as above described). The role of holoAPP was assayed by transfecting 10 μM RA differentiated cells at D6 with an APP_{695}-GFP cDNA or the respective N1-eGFP vector [29]. Cells were fixed at D8, and about 100 fluorescing cells/experiment were monitored for their neuritic number and length (n=3).

5.3.4. Western blot assays

Cells and media were collected into 1% boiling SDS, cell lysates sonicated for 30 sec, and the total protein content measured (Pierce's BCA kit; Thermo Scientific). Mass-normalized aliquots were resolved on 5-20% gradient SDS-PAGE and electrotransferred onto nitrocellulose membranes. These were initially processed for Ponceau S staining to assess gel loading [30], since beta-actin and other cytoskeleton markers are not suitable loading controls in cell differentiation assays [31-33]. Primary antibodies used (2h-O/N incubation): anti-APP N-terminus (22C11, Chemicon), anti-actin N-terminal (Sigma-Aldrich), anti-acetylated tubulin, and anti-MAP-2 clone HM2 (Sigma-Aldrich). Horseradish peroxidase-linked secondary antibodies were from GE Healthcare. Membranes were washed (1X TBS-T or PBS-T) and submitted to ECL detection (see [34].

5.3.5. Data analysis and Statistics

Ponceau-S stained membranes and autoradiograms were scanned (GS-800 imaging densitometer, Bio-Rad) and protein bands quantified (Quantity One densitometry software, Bio-Rad). All data was corrected to the relative loading control (Ponceau-S) and expressed as mean±SEM (standard error) of at least three independent experiments. When appropriated, data were analysed using two-way ANOVA followed by the Bonferroni test (GraphPad Prism5 software); the RA dose and the differentiation day were the independent variables as follows: 0, 1 and 10 μM RA at days 2 and 8; 1 and 10 μM RA at days 2-to-8. Step-down one-way ANOVAs were additionally performed within each RA dose, followed by the Dunnett's test (for comparison of data with control values) or the Tukey-Kramer multicomparisons test (to compare between indicated conditions). For clarification purposes, not all these statistical differences are shown (e.g. some differences to control NDf were left out of the graphs). Otherwise, the statistical analysis was conducted by one-way ANOVA or by the unpaired Student's t-test.

5.4. Results

5.4.1. A biphasic differentiation model emerges for 10 μM RA-treated SH-SY5Y cells

The differentiation output of neuronal-like cells is time- and morphogen dose-dependent. To characterize SH-SY5Y differentiation in respect to these factors, two concentrations (1 and 10 μM) of the RA morphogen were used, and differentiation was characterized at various time points: 2 (D2), 4 (D4), 6 (D6) and 8 (D8) days. Non-differentiated (ND) cells, cultured for 2 (NDi, initial) and 8 days (NDf, final) in the absence of RA (0 μM RA), were used as controls.

Morphological differences are readily evident from the PhC microphotographs representative of each differentiation day (Figure B.1). While ND cells maintain a more cuboid/polygonal shape, RA-differentiated cells are more plastic or elongated, and present elongated cellular projections ('processes') (Figure B.1 A versus B). Relatively to cell growth (Figure B.1 C), the number of non-differentiated cells increases by 30% after two days in culture, and further duplicates from days 2 to 8. This duplication in cell number already occurs at day 2 for 1 μM RA ($p<0.05$ against control 0 μM RA), and the cell number remains unaltered thereafter. Contrarily, a dose of 10 μM RA decreases the cell number at D2 ($p=0.053$ against control 0 μM RA). This number only marginally increases thereafter, and cell number at day 8 is 130% lower than control values ($p<0.001$). Indeed, the higher 10 μM RA dose always decreases the cell number when compared to 1 μM RA ($p<0.001$ and $p<0.05$, by two-way ANOVA). Retinoic acid also modifies the cellular morphology, shifting the usual cuboid morphology of non-differentiated cells to a more plastic or elongated one (Supplementary Figure B.1). The majority (~70%) of SH-SY5Y non-differentiated cells (NDi and NDf) are cuboid in shape, and both 1 and 10 μM RA doses significantly lower this percentage to 30-40% already at D2 (Supplementary Figure B.1, 'cuboids'). The percentage of elongated cells is RA dose-dependent, and 10 μM RA treatment immediately significantly increases its number at D2 (to ~50%), while for 1 μM RA this only occurs later on and at lower percentages (D8, ~40%) (Supplementary Figure B.1 B, 'elongated'). Interestingly, 1 μM RA is the dose that significantly increases the percentage of plastic cells when compared to non-differentiated controls (Supplementary Figure B.1 A vs B, 'plastic'). The plastic phenotype appears thus to be an intermediate phenotype, before the acquisition of an elongated morphology by cells when fully committed to differentiate.

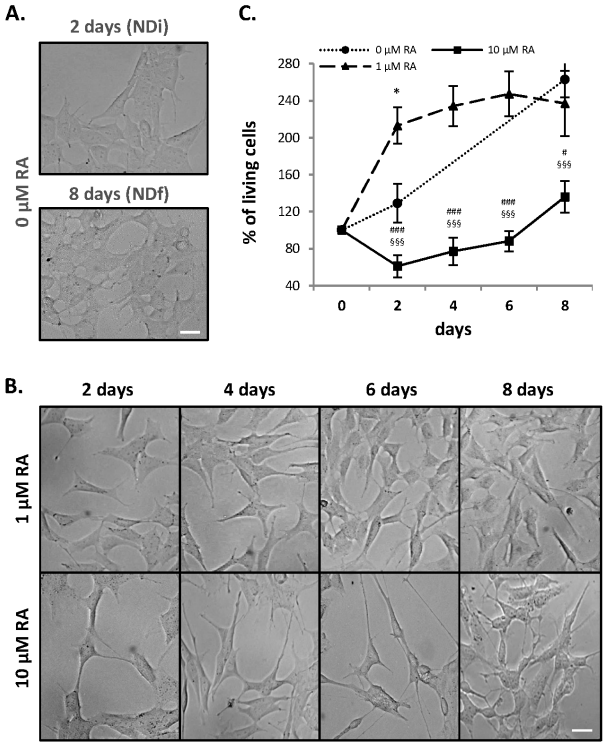

Figure B.1 - **SH-SY5Y cells differentiated for 8 days with 1 and 10 µM RA.** PhC microphotographs of SH-SY5Y undifferentiated (**A.**) and RA-differentiated (**B.**) cells. NDi: initial non-differentiated cells (day 2); NDf: final non-differentiated cells (day 8). Bar, 30 µm. **C.** Effects of RA concentration on cell number, expressed as percentages of the initial number of plated cells (100%). n=4. Statistic symbols: (*)(§), for comparison of 1 and 10 µM data with 0 µM RA controls (NDi and NDf, respectively), using one-way ANOVA followed by the Dunnett's test. ($^{\#}$), for differences between 1 µM and 10 µM RA data, using two-way ANOVA. This analysis revealed extremely significant effects of the RA dose and differentiation time on cells number, but no significant interaction between these two variables. */$^{\#}$p<0.05; §§§/$^{\#\#\#}$p<0.001.

Neuritogenesis was also evaluated, by scoring the number and length of the cellular processes (Figure B.2). RA significantly increases the number of processes per cell at D2 (Figure B.2 A, D2 vs NDi), but in a RA dose-independent manner (no significant differences between doses were detected with two-way ANOVA). Nevertheless, while the 10 µM dose does not increase the final number of total processes (Figure B.2 A, NDf vs D8 10 µM), 1 µM RA is capable to induce the emergence of new processes. Indeed, 8 days of 1 µM RA exposure increases the number of processes above NDf (Figure B.2 A) and above the 10 µM dose ($p<0.05$ by the unpaired Student's t-test).

When the longer processes were divided by length (20-35 µm and >35 µm), another RA neuritogenic effect was revealed (Figure B.2 B). Incubation with 10 µM RA for only 2 days significantly decreases the 20-35 µm processes (also here termed as 'pre-neurites') to half of their percentage (Figure B.2 B, D2 10 µM vs NDi), while it simultaneously increases the percentage of >35 µm ones (neurites, as longer than two body lengths [35]. A second phase of increase in the number of these neurites is visible between D2 and D4, from which it stabilizes (no differences

being found in-between D4, D6 and D8). The lower 1 µM RA dose also significantly increases the number of neurites, but only at D6. Further, the 10 µM RA-induced increases in neurites and decreases in pre-neurites at D2 and D4 are significantly different from the 1 µM RA effects (D2 $p<0.05$; D4 $p<0.01$ and $p<0.05$, by two-way ANOVA).

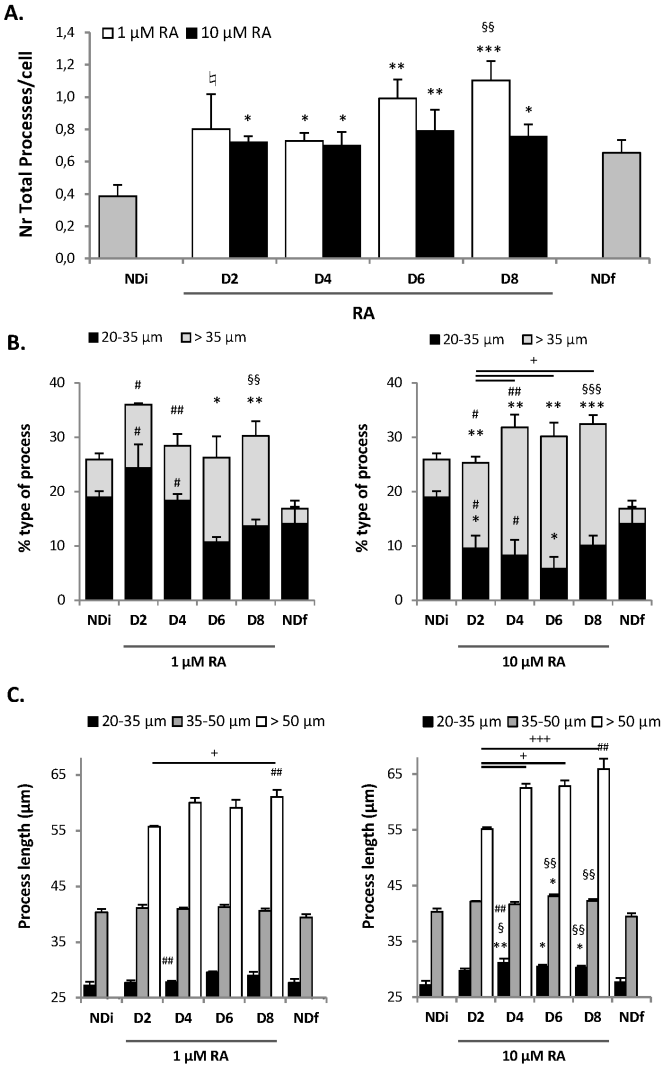

Figure B.2 - **Morphometric analysis of the cellular processes in 1 and 10 µM RA differentiated SH-SY5Y cells.** A. Total number of processes per cell (all processes protruding from a cell, of all sizes, were scored). B. Percentage of each type of process. Processes were categorized according to their lengths, and the percentages of pre-neurites (20-35 µm) and neurites (≥35 µm) calculated out of the total number of processes ('Total'). C. The mean lengths of pre-neurites (20-35 µm), and neurites (35-50 and ≥50 µm processes) were determined; noticeably, control cells do not present >50 µm neurites. NDi: initial non-differentiated cells (day 2); NDf: final non-differentiated cells (day 8). D2-D8: days 2, 4, 6 and 8 of differentiation. n=4. */§/+/#/♮p<0.05, **/§§/##/++p<0.01, ***/§§§/+++p<0.001. Statistic symbols: (*) (§), for comparisons to control NDi and NDf data, respectively; (+), for comparisons between indicated conditions, by using one-way ANOVA followed by the Dunnett's or the Tukey-Kramer tests. (♮) for comparisons to NDi data; (#) for differences between 1 µM and 10 µM RA data, by two-way ANOVA. Two-way ANOVA further revealed: significant RA dose effect and interaction between RA dose and differentiation time on the % of type of processes; a very significant RA dose effect on the 20-35 µm processes length; extremely significant RA dose effect and interaction between RA dose and differentiation time on the length of >50 µm neurites.

The mean length of the processes was also evaluated, with neurites being further divided into shorter (35-50 μm) and longer (>50 μm) neurites in this assessment (Figure B.2 C). 10 μM RA significantly increases the pre-neurites mean length (20-35 μm) from D4 on, when compared to both ND controls. For both RA doses, the shorter neurites length (35-50 μm) generally remains unchanged throughout time (exception for the 10 μM RA D6 and D8 increases). Differences in the length of the longer neurites (>50 μm) are however very notorious given their absence in both non-differentiated controls. Moreover, this length is affected by the RA dose, the day of differentiation, and by the interaction of these two factors ($p<0.0001$, by two-way ANOVA). From D4 on, the 10 μM RA dose tends to be more able to elongate and maintain neurites than 1 μM RA, inducing significantly lengthier >50 μm neurites at D8. In summary, again the 10 μM RA induced two specific neuritogenic phases, this time related to the elongation of longer neurites: a first increase at D2, and a second period from D4 on (where D4, D6 and D8 are equal in-between and all significantly different from D2).

5.4.2. APP and sAPP/APP time-dependent profiles follow the 10 μM RA biphasic model

The time-dependent protein expression profiles of APP and its sAPP cleavage product were further monitored (Figure B.3) and related to the differentiation outputs.

Interestingly, neither 1 nor 10 μM RA are able to immediately (D2) increase holoAPP expression. At D4 however, 10 μM RA-treated cells significantly express more APP than control NDi and 1 μM RA cells, and these levels are maintained thereafter. 1 μM RA also up-regulates APP expression, but later in time (at D6) and less efficiently (Figure B.3 A vs B, 'holoAPP': 2.4-fold increase against 3.2 for 10 μM RA, $p<0.05$ by the Student's t-test). Consistently, the 10 μM RA data again significantly separates D2 from the following time points (D4 to D8).

Significantly, 1 μM RA induces similar time-dependent variation profiles in both holoAPP expression (Figure B.3 A) and in the percentage of neurites (Figure B.2 B '1 μM RA'). Likewise, 10 μM RA also induces similar time-dependent behaviours of the following parameters: holoAPP expression, percentage of neurites (>35 μm), and mean length of longer neurites (>50 μm) (Figure B.3 A, Figure B.2 B and C '10 μM').

APP shedding to sAPP is also affected by RA, and shows a major difference in-between RA doses at D2. The 10 μM RA dose induces a 2-fold increase in sAPP levels already at D2, from which it stabilizes (Figure B.3 B 'sAPP'; compare to non-differentiated controls), while 1 μM RA only produces significant differences at D6 (Figure B.3 A 'sAPP'). Both doses reach equal final sAPP fold increases.

Since sAPP was reported to support neuritogenesis by competing with membranar APP [17], the time-dependent profiles of sAPP/APP ratio were calculated. The sAPP/APP ratio has a downward trend with time in culture: from NDi vs NDf, and from D2 to D6 (Figure B.3 C for 10 μM; data not shown for 1 μM). For 1 μM RA, the increase in holoAPP is accompanied by a similar increase in sAPP secretion (Figure B.3 A), and thus no significant alterations in the sAPP/APP ratio occur (data not shown). The 10 μM RA dose, however, induces a significant increase in this ratio at D2 (compared to both NDi and 1 μM RA), reflecting an increased APP cleavage into sAPP. At D4 the sAPP/APP ratio decreases to control NDi values, and tends to further decrease unto NDf values (D4 vs D6 only significantly different when using the Student's t-test), revealing a tendency for APP to be less cleaved with the differentiation time. Two-way ANOVA did not identify significant differences in-between D4, D6 and D8, and again two groups emerge: D2 and D4-D8.

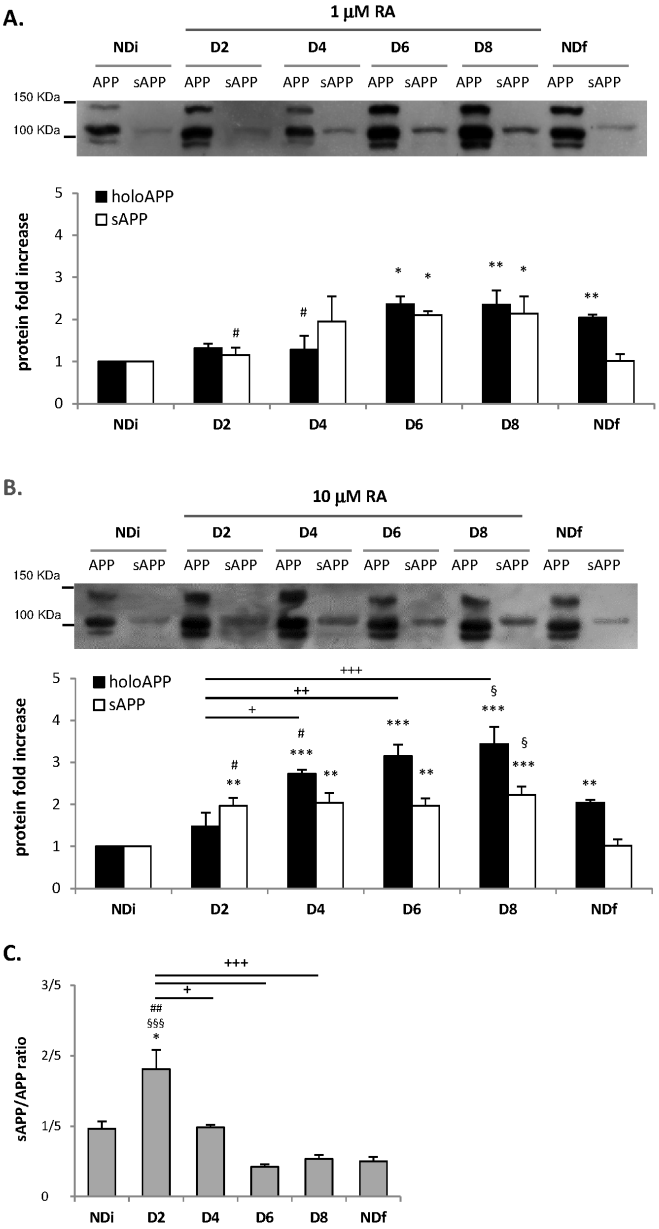

Figure B.3 - Time-dependent holoAPP and sAPP protein profiles in SH-SY5Y cells differentiated with 1 (A.) or 10 µM RA (B.). Cellular APP and medium sAPP were probed with the 22C11 antibody. C. The sAPP/APP ratios in 10 µM RA-differentiated cells were directly calculated from the optical densities values. NDi: initial non-differentiated cells (day 2); NDf: final non-differentiated cells (day 8); D2-D8: day 2, 4, 6 and 8 of differentiation. n=3-5. */§/+/#p<0.05, **/§§/++/##p<0.01, ***/§§§/+++p<0.001 for data against control NDi (*), NDf (§), or D2 values (+), using one-way ANOVA followed by the Dunnett's or the Tukey-Kramer tests. Two-way ANOVA (#, for differences between 1 µM and 10 µM RA data) further revealed extremely significant effects of RA dose and time of differentiation on holoAPP protein levels, but no significant interaction in-between these variables.

Given the morphological alterations associated with differentiation, cytoskeleton alterations were also essayed (Figure B.4). Acetylated α-tubulin levels are an indirect measure of microtubules (MT) stabilization and neuronal differentiation [36], and morphogenic alterations in neuritogenesis

also rely on actin remodelling [37]. This type of cytoskeleton response, with time of SH-SY5Y cellular differentiation, is surprisingly not well documented in the literature.

Levels of acetylated tubulin are markedly affected by the RA dose applied ($p<0.0001$, by two-way ANOVA). While 1 μM RA treatment only significantly alters tubulin acetylation at D6 (Figure B.4 A 1 μM RA graph), 10 μM RA induces an extremely significant decrease in tubulin acetylation at D2, potentially reflecting its higher need for MTs instability. Two distinct periods emerge again for this dose: until D2 acetylated tubulin levels decrease; from D2 to D4 these levels significantly increase, remaining overall stable from D4 on (D4-D8). Noteworthy, at D8 α-tubulin acetylation levels are equal in-between RA doses and significantly lower than NDf (Figure B.4 A, D8 vs NDf). This is most relevant to any future study using tubulin acetylation as a differentiation biochemical marker, as one could expect the opposite to occur. Actin levels also tend to increase with RA but also with time in culture; the highest increase appears to occur from D2 to D4 for both RA doses, and no decrease is visible from NDi to D2 (Figure B.4, actin immunoblots).

Interestingly, when plotting the ratio between APP and acetylated tubulin fold increases for the 10 μM RA (Figure B.4 B 'APP/ATub ratio'), one can observe that APP induction correlates with tubulin acetylation in a very clear biphasic manner (Figure B.4 B). Again the differentiation process presents two distinct phases: from D0 until D4 (D4 excluded), and from D4 onward (D4 included). In the first phase, APP/ATub ratio linearly increases with a slope of 1.5; in the second phase this ratio is maintained at its highest values (~4). Therefore, during the first period APP is much more induced than tubulin is acetylated; in the second period, the rate of APP increase equals the rate of increase in tubulin acetylation.

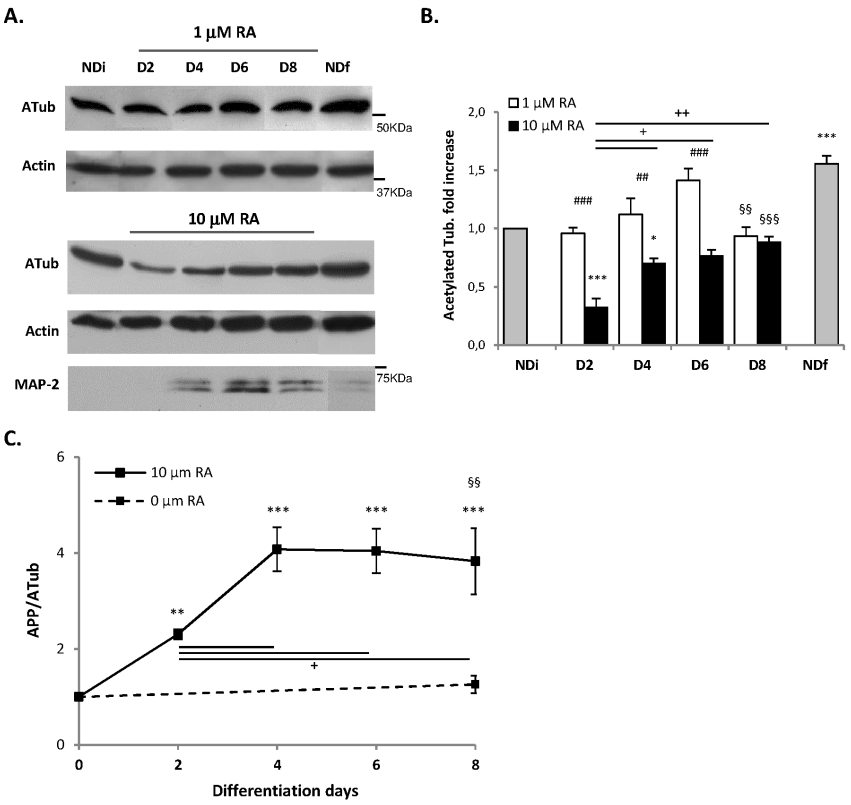

Figure B.4 - **Differentiation time-dependent profiles of acetylated α-tubulin levels and APP/acetylated α-tubulin ratio. A.** Immunoblot analyses of acetylated α-tubulin (Atub) and actin in 1 and 10 µM RA-exposed SH-SY5Y cells. MAP-2 was probed as a differentiation marker. Acetylated tubulin levels were plotted as fold increases of NDi values. Of note, all the lanes are from the same blot, being rearranged into the presented order. **B.** The ratio between APP and Atub fold increases was plotted against days of differentiation with 10 µM RA. NDi: initial non-differentiated cells (day 2); NDf: final non-differentiated cells (day 8); D2-D8: day 2, 4, 6 and 8 of differentiation. n=3-5. */+p<0.05, **/§§/++/##p<0.01, ***/§§§/###p<0.001 for data against control NDi (*), NDf (§) values, or D2 values (+), determined by one-way ANOVA followed by the Dunnett's or the Tukey-Kramer tests; or for 1 µM versus 10 µM RA data (#) using two-way ANOVA. This later revealed extremely significant RA dose and differentiation time effects on acetylated α-tubulin levels, and a very significant interaction in-between these variables.

The subcellular distribution of APP and acetylated α-tubulin were further analysed by immunostaining (Figure B.5). Non-differentiated and 10 µM RA differentiated cells were probed for APP (green), acetylated α-tubulin (blue) and F-actin (red) at D2 and D8. In NDi and NDf non-differentiated cells, APP and acetylated tubulin are more abundant in a Golgi-like region [26], and are uniformly distributed throughout the fewer cellular processes. As expected from the immunoblots data, 2 days of RA incubation do not alter the holoAPP intensity but decrease α-tubulin acetylation staining (Figure B.5, D2 vs NDi). In D2 differentiated cells, APP and acetylated α-tubulin stain less the proximal and/or middle parts of the cellular processes, and part of the APP pool is enriched in their tips (as F-actin positive growth cones, Figure B.5 arrowheads). Completion of differentiation (D8) is accompanied by an increase in APP and acetylated α-tubulin signals. At D8, the cellular processes have elongated and APP and acetylated α-tubulin stain these processes along all their length. Comparatively, the 8 days control NDf cells are characterized by cellular

overconfluence, a cuboid cellular shape with fewer and smaller processes, decreased APP and increased acetylated α-tubulin staining (Figure B.5 NDf).

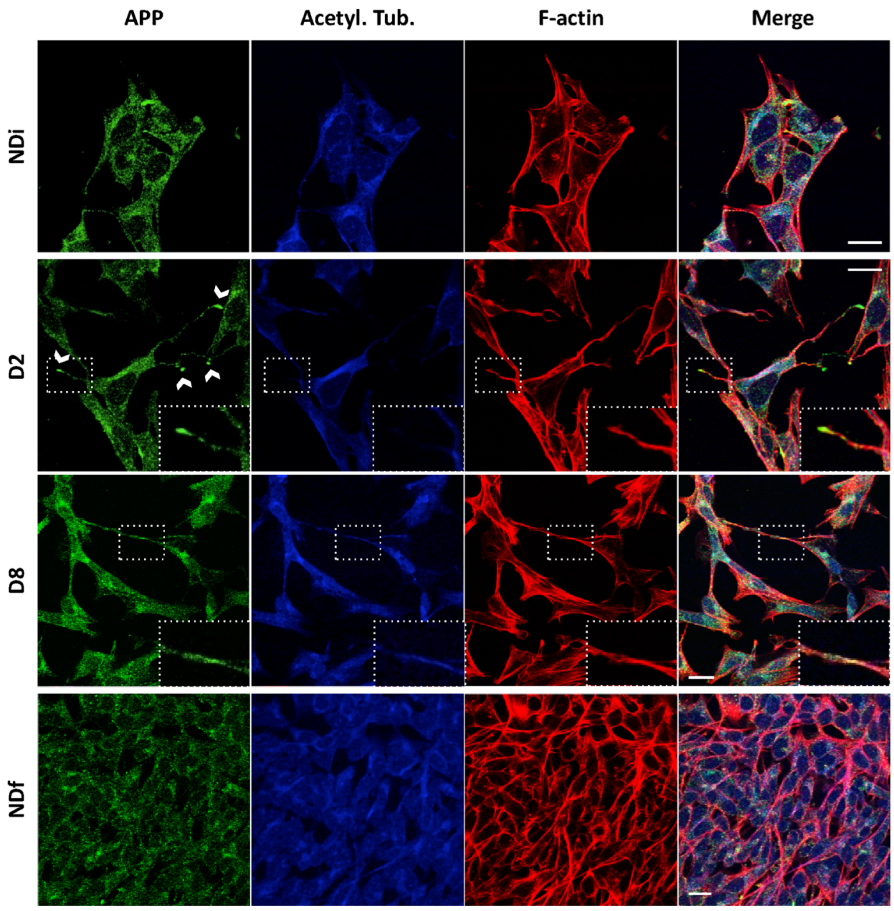

Figure B.5 - **Cellular localization of APP and acetylated α-tubulin in non-differentiated and 10 µM RA-differentiated SH-SY5Y cells.** APP (green) and acetylated α-tubulin (blue) were monitored by immunocytochemistry means using the anti-APP c-terminus and the anti-acetylated α-tubulin antibodies. F-actin was probed with red fluorescent-labelled phalloidin. Arrowheads indicate APP-enriched growth cones. ROIs of neurites are shown (2x zoom). NDi: initial non-differentiated cells (day 2); D2 and D8: day 2 and 8 of differentiation; NDf: final non-differentiated cells (day 8). Bar, 20 µm.

5.4.3. APP and sAPP neuritogenic functions in the biphasic model

Since a unique peak of sAPP/APP ratio was observed at D2 (Figure B.3) for 10 µM RA, the RA dose with higher differentiation triggering abilities, further evidence for the involvement of sAPP in early neurite elongation was sought.

The effects of sAPP were first assessed in the absence of RA. Non-differentiated SH-SY5Y cells expressing GFP were incubated with sAPP-enriched medium for 24h, and while sAPP enrichment does not significantly alter the number of processes (Supplementary Figure B.3 A), it tends to elongate pre-existing ones. Indeed, cells exposed to sAPP-enriched medium tend towards higher percentages of >20 µm and >35 µm processes, and exhibited significantly longer >35 µm processes

(neurites) (Figure B.3 B and Supplementary Figure B.3 C, respectively). sAPP medium-enrichment also led to an elongation of the cell body (Supplementary Figure B.3 D).

Subsequently, sAPPα levels were modulated in 10 μM RA-treated cells by co-exposure to specific drugs for 48h, from D0 to D2 and from D2 to D4 (Figure B.6). sAPPα was increased by addition of 10 nM recombinant sAPPα, or decreased by inhibiting APP α-cleavage with 10 μM TAPI; both types of sAPP modulations increased holoAPP levels (Figure B.6 A). Morphometric analyses of the D0-D2 modulations revealed that these tend to primarily affect >20 μm processes and >35 μm ones (neurites) (Figure B.6 B, D0-D2 TAPI and D0-D2 sAPP). Decreasing sAPP levels from D0 to D2 resulted in a general reduction of neuritogenesis (Figure B.6 B, 'D0-D2 TAPI'), whilst the opposite occurred in cells exposed to recombinant sAPPα (Figure B.6 B, 'D0-D2 sAPP'). Although both treatments are not statistically different from D2, they are significantly different from each other, particularly for the >20 and >35 μm processes.

Regarding the second time interval, TAPI exposure from D2 to D4 mainly affected 35 and >50 μm processes (shorter and longer neurites) (Figure B.6 B 'D2-D4 TAPI'). The decrease in the neuritic network mainly resulted from a significant retraction of the >50 μm neurites (Figure B.6 B and C). The number of these longer neurites also decreased to half, with the smaller 20-35 μm pre-neurites proportionally doubling in number (data not shown). Neuritic retraction induced by D2-D4 TAPI is accompanied by a considerable increase in acetylated tubulin (1.66±0.32 versus 0.69±0.06 for control D4; data not shown) resulting in a decrease in the APP/ATub ratio to c.a. D2 levels (Figure B.6 D). This reversion on processes' elongation is also visible in Figure B.6 E microphotographs, accompanied by a reversion of the cellular body elongation, rendering more plastic and cuboid cells. TAPI also induces visible APP and acetylated tubulin increases at the Golgi-like region, distributions more similar to the ones of D4 non-differentiated cells (Figure B.6 E, ND4).

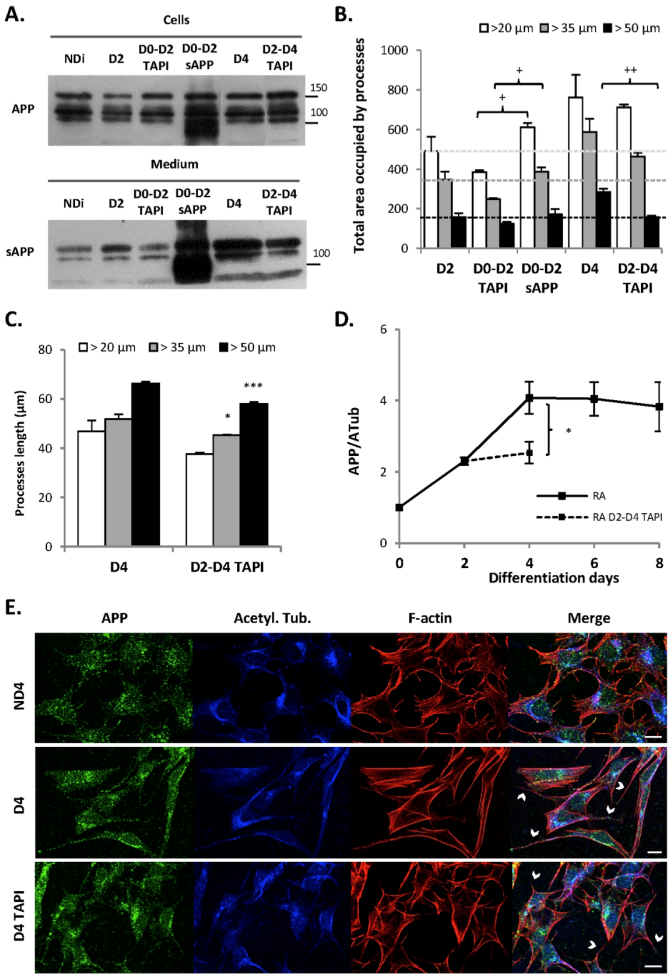

Figure B.6 - **Modulation of sAPPα levels during the first phase of 10 µM RA-induced SH-SY5Y differentiation. A.** Immunoblot determination of APP and sAPP levels (22C11 antibody) upon modulation of sAPP production. D2-D4: days 2 and 4 of RA differentiation; D2 TAPI: 2 days of incubation with RA and 10 µM TAPI; D2 sAPP: 2 days of incubation with RA and 10 nM recombinant human sAPP; D4 TAPI: day 4 of RA differentiation with addition of 10 µM TAPI at D2. Of note, all the lanes are from the same blot, being rearranged into the presented order. **B.** The mean lengths of >20, >35 or >50 µm processes were summed up and expressed as µm per mm^2 of occupied area ('Total area occupied by processes'). **C.** The average lengths of the >20, >35 and >50 µm processes were determined for the D4 and D4 TAPI conditions. n=3. **D.** The APP/Acetylated α-Tubulin ratio (dashed line in graph) was determined for the D4 TAPI condition (based on immunoblots). **E.** Representative confocal microphotographs of D4 and D4 TAPI differentiating cells; ND4, control non-differentiated cells at D4. Staining: APP in green (C-terminal antibody), acetylated α-tubulin in blue, and F-actin in red (phalloidin). Bar, 10 µm. $*/^{+}p<0.05$, $**/^{++}p<0.01$, $**p<0.001$, for data against control conditions (*), and for comparisons between indicated conditions ($^{+}$), by unpaired two-tailed Student's t-test.

Finally, as significant APP fold increases are concomitant with the second differentiation period, the relevance of holoAPP at this phase was also investigated. SH-SY5Y differentiated cells were transfected with an APP-GFP cDNA from D6 until D8, and their neuritogenic output compared to the one of vector GFP transfected cells (Figure B.7). Microphotographs and morphometric analyses of Figure B.7 show that APP overexpression from D6 to D8 did not produce significant alterations in the final average length of 20-35 µm pre-neurites, and 35-50 µm neurites, but resulted in a tendency for lengthier >50 µm neurites (Figure B.7 B, 'x>50'). More significantly, the number of

these longer neurites per cell significantly doubled in APP-GFP fluorescing cells, from 0.17±0.03 to 0.34±0.02 (Figure B.7 C; $p<0.01$), at the apparent expense of the smaller pre-neurites (longer than 20 µm but shorter than 35 µm), as denoted in the 'type of processes' Figure B.7 D graph. These results indicate that APP potentiates neuritic elongation in this later differentiation phase, potentially via increasing neuritic stabilization.

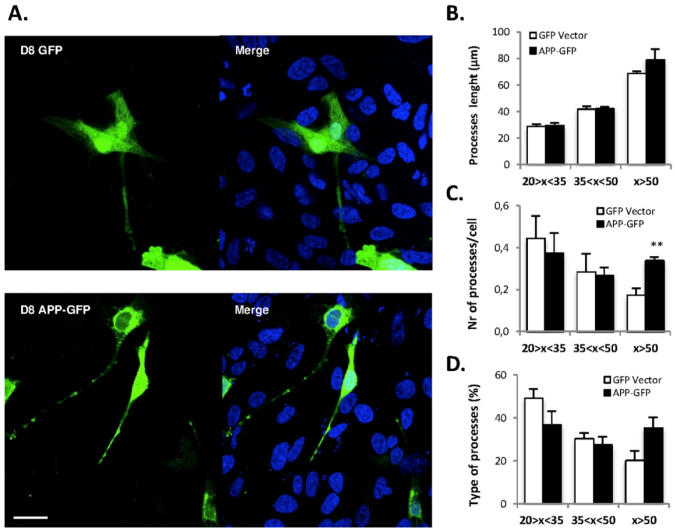

Figure B.7 - **Full-length APP potentiates neuritic elongation in the second 10 µM RA SH-SY5Y differentiation phase.** SH-SY5Y cells differentiated for 6 days with 10 µM RA were transfected for 48h (from D6 to D8) with APP-GFP or the GFP vector alone. **A.** Representative confocal microphotographs of D8 GFP and APP-GFP differentiating cells; the DAPI nuclear marker was used as a counterstaining. Bar, 20 µm. The average lengths of processes (**B.**), the number of processes per cell (**C.**), and the percentage of processes (**D.**) with 20-35, 35-50 µm, and >50 µm of length were determined in GFP and APP-GFP expressing cells. n=3. **$p<0.01$, by unpaired two-tailed Student's t-test. A statistical trend for an increase % of the >50 µm processes occurs in APP-GFP cells ($p=0.08$ when compared to GFP cells).

5.5. Discussion

APP is reported to be neuritogenic, but the underlying mechanisms are still focus of ongoing research. RA-induced SH-SY5Y differentiation, a widely used neuronal differentiation model, was adopted to address the APP neuritogenic role. A search on the time-dependent characterization of this model revealed that morphologic and some biochemical parameters have not been characterized in full detail. We thus first addressed neuritogenic-related morphologic alterations and specific protein shifts occurring at key differentiation periods.

Concerning cell number, SH-SY5Y cells are reported to synchronously arrest in the G1-phase of the cycle as soon as 2 days after RA treatment [18]. In our model, while 1 μM RA increased cell proliferation at an early time point, 10 μM RA arrested it, as expected (Figure B.1). The later observed slight increase in cell number for 10 μM RA (from D6 to D8) may reflect a higher degree of transdifferentiation from N- to S-type cells, the two main cellular phenotypes in neuroblastomas-derived cell lines. Although our SH-SY5Y population was previously enriched in N-type cells, a percentage of S-type cells is expected to still coexist and to increase due to transdifferentiation events [24]. A way to surpass this and to have fully differentiated cells for longer periods may rely in the concomitant administration of BDNF from D6 onward [38]. Regarding the 1 μM RA dose, contrary to the strong decrease observed at D4 by [9] (the only data found in the literature), our results suggest that SH-SY5Y cellular division is allowed during the first 48h, and cell number maintained from this point on (Figure B.1 C).

Regarding cellular morphology, RA appears to first induce cell plasticity (Figure B.1 A/B and Supplementary Figure B.1) that progresses to cellular elongation with time and at higher RA doses (as 10 μM). RA-induced neuronal like phenotypes (plastic and elongated) were not acquired homogeneously by the population, but only by about two thirds of it (Supplementary Figure B.1), possibly reflecting the presence of S-type cells. Unfortunately, the reported literature normally solely addresses the elongated phenotype [20-22, 38].

Acquisition of a neuronal-like phenotype also involves the generation and elongation of cellular processes into neurites. Exposure of SH-SY5Y cells to RA readily increased the number and length of processes in a time- and morphogen dose-dependent manner. As expected, the longest neurites (>50 μm) were inexistent in non-differentiated cells, described as possessing ‘truncated’ processes [19]. Both RA doses significantly and equally increased the total number of processes per cell at D2 Figure B.2 A), an early time point greatly characterized by the emergence of new processes. The following D4-D8 time points are more related to the elongation of pre-neurites and neurites, especially efficient when using 10 μM RA. This dose highly increased the percentage of neurites (Figure B.2 B, ‘>35μm’), and significantly increased the length of pre-neurites (at D4) and longer neurites (at D8) (Figure B.2 C, ’20-35 μm’’ and ‘>50 μm’).

Neuronal differentiation depends on cytoskeleton-based cell body and neuritic remodelling, and is linked to increased tubulin acetylation, a dynamic process generally restricted to stable MTs [36, 39]. However, our results stress that although tubulin acetylation may increase during the time of differentiation, it is never increased over control non-differentiated cells. Indeed, cells exposed to 10 μM RA had significantly less acetylated tubulin than control NDi and 1 μM RA cells (Figure B.4 A graph), and both RA doses reduced tubulin acetylation at D8 (Figure B.4 A, D8 vs NDf). These decreases may reflect a need for higher initial MT instability in cells suffering more dramatic differentiation-related alterations. Indeed, the higher decreases in tubulin acetylation occur in 10 μM RA treated cells, consistent with their higher number of neurites and their increased length. In agreement, sAPP D2-D4 inhibition highly induced tubulin acetylation, resulting in an abnormally low APP/ATub ratio (Figure B.6 D) and in inhibited neuritogenesis (Figure B.6 B/C/E). Solinger et al.reported that in the neurons of *C. elegans* mutant for α-tubulin acetyltransferase, the α-tubulin is hyperacetylated and the MTs are too short or prone to depolymerize, resulting in shorter neurites [40]. However, α-tubulin acetyltransferase silencing also results in impaired differentiation and branching defects in mouse cortical neurons [41]. This is in agreement with our data, which indicate that α-tubulin acetylation has to be tightly controlled during neuronal differentiation.

The 10 μM RA-induced SH-SY5Y differentiation was, at this point, established as a more comprehensive model. Data collected already outlined frontiers of two specific time phases: a first early phase (D0-D4, D4 excluded) more associated with the emergence of new and the elongation of smaller processes and pre-neurites into neurites, and a second phase (D4-D8), more involved in neuritic elongation and stabilization. The first phase presents the lowest level (and highest fold increase) of the cytoskeleton-related acetylated tubulin, whilst in the second phase its levels are the highest and tend to stabilize. Distinct expression patterns of other cytoskeleton-related transcripts occur between early time points (as D3) and later time points (D5 and D8) of RA incubation, as unravelled by unsupervised hierarchical cluster analysis. These molecules have important role in neuronal-like differentiation, and include integrin α1, integrin β1 and RAC1 [42].

The effects of RA in APP cell fate [9] were further addressed taking these key differentiation periods into account. Comparison of our RA time-dependent APP expression with previous reports revealed several matches and reinforces our data. The 10 μM RA dose greatly increased holoAPP protein levels at D4, almost up to its highest final level, in agreement with the D4 APP mRNA peak observed by König et al [20]. At D6, a 3-fold increase in holoAPP was observed by us, similar to the 3-fold increase reported by Holback et al [8]. The high levels of holoAPP expression during the D4-D8 period (10 μM RA) are concomitant with the second phase, supporting its particular involvement in the neuritic elongation mechanism. Also, APP values are higher for 10 μM RA, the dose that induces more efficient neuritic elongation. Regarding 1 μM RA, our results

agree with increases in APP mRNA and sAPP levels reported for this RA dose to occur between D4 and D6 [9].

A significant increase in sAPP levels in response to both RA doses was also observed (Figure B.3 A D6, and B D2), most probably via α-secretase modulation [8, 9]. Distinct α-secretases can mediate APP α-cleavage into sAPPα in a cell-specific fashion, with TACE more related to regulated sAPPα release, and ADAM 10 to its constitutive production [43]. RA treatment of SH-SY5Y cells increases both α-secretase activities, by inducing ADAM10 mRNA and protein levels [44, 45], TACE protein levels, and the activities of both α-secretases [46]. However, sAPPα levels do not only depend on α-secretase activity but also on APP availability, a balance reflected in the sAPP/APP ratio. Our findings showed, for the first time, that 10 μM RA induces an early and unique peak in the sAPP/APP ratio at D2. From this time point on the ratio progressively decreases to non-differentiation control values. This sAPP/APP D2 peak suggested a strong involvement of sAPP in the first differentiation phase, potentially on the onset of elongation. sAPPα medium enrichment potentiates the elongation of pre-neurites and smaller neurites (20-35 and 35-50 μm, respectively) in early differentiated cells (Figure B.6 B, D0-D2 sAPP), and even in cells non-exposed to RA (Supplementary Figure B.3 C, '>35 μm'). Contrastingly, the lengths of these processes are tendentiously shorter in TAPI-exposed cells (Figure B.6 B, D0-D2 TAPI), which have decreased sAPP levels and sAPP/APP ratio (0,44±0,05 at 'D2'; 0,33±0,04 at 'D0-D2 TAPI'). If we decrease the sAPP/APP ratio later on (from 0,16±0,03 at 'D4' to 0,12±0,01 in 'D2-D4 TAPI') a significant neuritic retraction is again observed (Figure B.6 B, C). Noteworthy, neither TAPI treatment nor recombinant sAPP addition produced significant alterations in the number of processes (data not shown).

In essence, the data strengthens a role for the singular D2 sAPP/APP peak in the elongation of all processes at the first differentiation phase. The sAPP/APP ratio is not only important to the early elongation of processes, but also to the maintenance of an elongated bipolar differentiated phenotype of the cell body, highly reverted by TAPI at D4 (Figure B.6 E). Noteworthy, by inhibiting TACE we only slightly decreased APP shedding to sAPPα, and the consequences of more robust sAPPα modulations (such as complete abolition) to processes' elongation would probably be more dramatic.

Finally, the high and stable holoAPP levels observed at the second phase (D4-D8) suggested a key role for membranar holoAPP during this period. This phase is characterized by neuritic elongation and concomitant neuritic stabilization, related to increased tubulin acetylation. Through APP overexpression means we have confirmed that APP has a positive effect on neurites at this second differentiation phase (Figure B.7). The increased number of longer neurites with no real alteration in their average length strengthens our working hypothesis where holoAPP is not an inducer but a

positive modulator of neuritogenic mechanisms, such as the stabilization of longer neurites. Overall, our data agrees with the Young-Pearse et al.view, in which the sAPP/holoAPP balance is of most importance in establishing regional stability or motility in a cellular process, thus modulating neuritic elongation [17].

Importantly, the data here presented reveal specific phases of SH-SY5Y neuronal-like differentiation, well defined for the 10 μM RA dose. A first phase, from D0 to D4 (D4 excluded) is characterized by a 2 fold-increase in the number of processes, and by consecutive increases (D0-D2, and D2-D4) in the percentage of neurites and in the length of > 50 μm neurites. A linear increase in the APP/ATub fold increases ratio also characterizes this phase, to which sAPP is crucial. In this phase, APP is cleaved to sAPP and only later it is transcriptionally activated at the same rate, resulting in an early unique sAPP/APP peak that correlates with processes' elongation. Of note, we did not find a direct correlation between APP and tubulin acetylation levels in APP-GFP transfected versus non-transfected RA-differentiated SH-SY5Y cells [47] or in assays of increased transfected APP doses (data not shown).

In the second phase, from D4 to D8 (D4 included), 10 μM RA-differentiated SH-SY5Y cells display more neurites. These become stable with time, in accordance with the concomitant higher levels of acetylated α-tubulin. The steady holoAPP (and APP/ATub ratio) values also indicate that APP has a role in this stabilization, securing that retraction will not occur, a hypothesis strengthened by our findings that APP does not increase the mean length but mainly the number of longer neurites.

In conclusion, profiling neuritogenesis permits the establishment of new neurochemical marker(s) reflecting the status of neuronal differentiation, and allows studying how specific molecules such as APP affect that status, with clear benefits to neuroscientists.

5.6. References

1. Haass, C., et al., *Trafficking and proteolytic processing of APP.* Cold Spring Harb Perspect Med, 2012. **2**(5): p. a006270.
2. da Cruz e Silva, E.F. and O.A. da Cruz e Silva, *Protein phosphorylation and APP metabolism.* Neurochem Res, 2003. **28**(10): p. 1553-61.
3. Goodger, Z.V., et al., *Nuclear signaling by the APP intracellular domain occurs predominantly through the amyloidogenic processing pathway.* J Cell Sci, 2009. **122**(Pt 20): p. 3703-14.
4. Ferreira, A., A. Caceres, and K. Kosik, *Intraneuronal compartments of the amyloid precursor protein.* J. Neurosci., 1993. **13**(7): p. 3112-3123.
5. Masliah, E., et al., *Amyloid precursor protein is localized in growing neurites of neonatal rat brain.* Brain Research, 1992. **593**(2): p. 323-328.
6. Schubert, W., et al., *Localization of Alzheimer [beta]A4 amyloid precursor protein at central and peripheral synaptic sites.* Brain Research, 1991. **563**(1-2): p. 184-194.
7. Milward, E.A., et al., *The amyloid protein precursor of Alzheimer's disease is a mediator of the effects of nerve growth factor on neurite outgrowth.* Neuron, 1992. **9**(1): p. 129-137.
8. Holback, S., L. Adlerz, and K. Iverfeldt, *Increased processing of APLP2 and APP with concomitant formation of APP intracellular domains in BDNF and retinoic acid-differentiated human neuroblastoma cells.* Journal of Neurochemistry, 2005. **95**(4): p. 1059-1068.
9. Ruiz-León, Y. and A. Pascual, *Induction of tyrosine kinase receptor b by retinoic acid allows brain-derived neurotrophic factor-induced amyloid precursor protein gene expression in human sh-sy5y neuroblastoma cells.* Neuroscience, 2003. **120**(4): p. 1019-1026.
10. Allinquant, B., et al., *Downregulation of amyloid precursor protein inhibits neurite outgrowth in vitro.* The Journal of Cell Biology, 1995. **128**(5): p. 919-927.
11. Hung, A.Y., et al., *Increased expression of beta-amyloid precursor protein during neuronal differentiation is not accompanied by secretory cleavage.* Proceedings of the National Academy of Sciences of the United States of America, 1992. **89**(20): p. 9439-9443.
12. Qiu, W., et al., *Cell-surface beta-amyloid precursor protein stimulates neurite outgrowth of hippocampal neurons in an isoform-dependent manner.* J. Neurosci., 1995. **15**(3): p. 2157-2167.
13. Small, D., et al., *A heparin-binding domain in the amyloid protein precursor of Alzheimer's disease is involved in the regulation of neurite outgrowth.* J. Neurosci., 1994. **14**(4): p. 2117-2127.
14. Mattson, M.P., *Establishment and plasticity of neuronal polarity.* Journal of Neuroscience Research, 1999. **57**(5): p. 577-589.
15. Taylor, C.J., et al., *Endogenous secreted amyloid precursor protein-alpha regulates hippocampal NMDA receptor function, long-term potentiation and spatial memory.* Neurobiol Dis, 2008. **31**(2): p. 250-60.
16. Perez, R.G., et al., *The beta -Amyloid Precursor Protein of Alzheimer's Disease Enhances Neuron Viability and Modulates Neuronal Polarity.* J. Neurosci., 1997. **17**(24): p. 9407-9414.
17. Young-Pearse, T., et al., *Secreted APP regulates the function of full-length APP in neurite outgrowth through interaction with integrin beta1.* Neural Development, 2008. **3**(1): p. 15.
18. Constantinescu, R., et al., *Neuronal differentiation and long-term culture of the human neuroblastoma line SH-SY5Y.* J Neural Transm Suppl, 2007(72): p. 17-28.
19. Kovalevich, J. and D. Langford, *Considerations for the use of SH-SY5Y neuroblastoma cells in neurobiology.* Methods Mol Biol, 2013. **1078**: p. 9-21.
20. König, G., C.L. Masters, and K. Beyreuther, *Retinoic acid induced differentiated neuroblastoma cells show increased expression of the [beta]A4 amyloid gene of Alzheimer's disease and an altered splicing pattern.* FEBS Letters, 1990. **269**(2): p. 305-310.
21. Beckman, M. and K. Iverfeldt, *Increased gene expression of [beta]-amyloid precursor protein and its homologues APLP1 and APLP2 in human neuroblastoma cells in response to retinoic acid.* Neuroscience Letters, 1997. **221**(2-3): p. 73-76.
22. Murray, J.N. and O.J. Igwe, *Regulation of [beta]-amyloid precursor protein and inositol 1,4,5-trisphosphate receptor gene expression during differentiation of a human neuronal cell line.* Progress in Neuro-Psychopharmacology and Biological Psychiatry, 2003. **27**(3): p. 351-363.
23. Santos, M., et al., *The nuclear envelope protein, LAP1B, is a novel protein phosphatase 1 substrate.*

PLoS One, 2013. **8**(10): p. e76788.
24. Bell, N., et al., *Store-operated Ca(2+) entry in proliferating and retinoic acid-differentiated N- and S-type neuroblastoma cells.* Biochim Biophys Acta, 2013. **1833**(3): p. 643-51.
25. Vieira, S.I., et al., *S655 phosphorylation enhances APP secretory traffic.* Mol Cell Biochem, 2009. **328**(1-2): p. 145-54.
26. Vieira, S., et al., *Retrieval of the Alzheimer's amyloid precursor protein from the endosome to the TGN is S655 phosphorylation state-dependent and retromer-mediated.* Molecular Neurodegeneration, 2010. **5**(1): p. 40.
27. Demars, M.P., et al., *Soluble amyloid precursor protein: a novel proliferation factor of adult progenitor cells of ectodermal and mesodermal origin.* Stem Cell Res Ther, 2011. **2**(4): p. 36.
28. Vrotsos, E.G., P.E. Kolattukudy, and K. Sugaya, *MCP-1 involvement in glial differentiation of neuroprogenitor cells through APP signaling.* Brain Res Bull, 2009. **79**(2): p. 97-103.
29. Rebelo, S., et al., *Tyr687 dependent APP endocytosis and Abeta production.* J Mol Neurosci, 2007. **32**(1): p. 1-8.
30. Romero-Calvo, I., et al., *Reversible Ponceau staining as a loading control alternative to actin in Western blots.* Anal Biochem, 2010. **401**(2): p. 318-20.
31. Dittmer, A. and J. Dittmer, *Beta-actin is not a reliable loading control in Western blot analysis.* Electrophoresis, 2006. **27**(14): p. 2844-5.
32. Farmer, S.R., et al., *Regulation of actin mRNA levels and translation responds to changes in cell configuration.* Mol Cell Biol, 1983. **3**(2): p. 182-9.
33. Castaño, Z. and R.M. Kypta, *Housekeeping Proteins: Limitations as References During Neuronal Differentiation* The Open Neuroscience Journal, 2008. **2**: p. 36-40.
34. Henriques, A.G., et al., *Intracellular sAPP retention in response to Abeta is mapped to cytoskeleton-associated structures.* J Neurosci Res, 2009. **87**(6): p. 1449-61.
35. Dehmelt, L. and S. Halpain, *Actin and microtubules in neurite initiation: Are MAPs the missing link?* Journal of Neurobiology, 2004. **58**(1): p. 18-33.
36. Perdiz, D., et al., *The ins and outs of tubulin acetylation: more than just a post-translational modification?* Cell Signal, 2011. **23**(5): p. 763-71.
37. da Silva, J.S. and C.G. Dotti, *Breaking the neuronal sphere: regulation of the actin cytoskeleton in neuritogenesis.* Nat Rev Neurosci, 2002. **3**(9): p. 694-704.
38. Encinas, M., et al., *Sequential treatment of SH-SY5Y cells with retinoic acid and brain-derived neurotrophic factor gives rise to fully differentiated, neurotrophic factor-dependent, human neuron-like cells.* J Neurochem, 2000. **75**(3): p. 991-1003.
39. Henriques, A.G., et al., *Abeta Influences Cytoskeletal Signaling Cascades with Consequences to Alzheimer's Disease.* Mol Neurobiol, 2014.
40. Solinger, J.A., et al., *The <italic>Caenorhabditis elegans</italic> Elongator Complex Regulates Neuronal α-tubulin Acetylation.* PLoS Genet, 2010. **6**(1): p. e1000820.
41. Creppe, C., et al., *Elongator Controls the Migration and Differentiation of Cortical Neurons through Acetylation of α-Tubulin.* Cell, 2009. **136**(3): p. 551-564.
42. Korecka, J.A., et al., *Phenotypic characterization of retinoic acid differentiated SH-SY5Y cells by transcriptional profiling.* PLoS One, 2013. **8**(5): p. e63862.
43. Slack, B.E., L.K. Ma, and C.C. Seah, *Constitutive shedding of the amyloid precursor protein ectodomain is up-regulated by tumour necrosis factor-alpha converting enzyme.* Biochem J, 2001. **357**(Pt 3): p. 787-94.
44. Endres, K., et al., *Shedding of the amyloid precursor protein-like protein APLP2 by disintegrin-metalloproteinases.* FEBS J, 2005. **272**(22): p. 5808-20.
45. Prinzen, C., et al., *Genomic structure and functional characterization of the human ADAM10 promoter.* FASEB J, 2005. **19**(11): p. 1522-4.
46. Holback, S., et al., *PI3-K- and PKC-dependent up-regulation of APP processing enzymes by retinoic acid.* Biochem Biophys Res Commun, 2008. **365**(2): p. 298-303.
47. Rocha, J.F., S.I. Vieira, and O.A.B.d.C.e. Silva, *APP Phosphorylation at S655 Correlates with F-actin Cytoskeleton Dynamics—Relevance in Neuronal Differentiation.* Microscopy and Microanalysis, 2012. **18**(SupplementS5): p. 57-58.

5.7. Supplementary Data

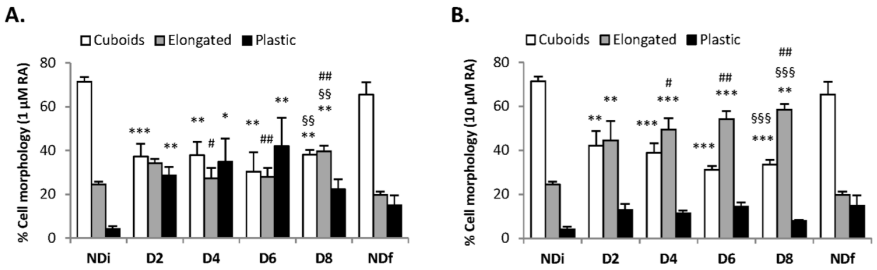

Supplementary Figure B.1 - **Effects of RA concentration on cell morphology.** SH-SY5Y cells, differentiated with 1 or 10 µM RA, were grouped into three different phenotypic categories, namely: "Cuboids" - polygonal cells with practically no cell processes; "Elongated" - longer cells with a slender cell body and normally with one or two extended processes; and "Plastic" - cells presenting an irregular morphology (normally derived from the other two morphologies), with numerous emerging processes, lamellipodia and/or fillopodia. Data are expressed as percentages of the total number of cells. Ndi: initial non-differentiated cells (day 2); NDf: final non-differentiated cells (day 8); D2-D8: day 2, 4, 6 and 8 of differentiation. n=4. $*/^{\#}p<0.05$, $**/^{\S\S}/^{\#\#}p<0.01$, $***/^{\S\S\S}p<0.001$ for data against NDi (*) or NDf (§) controls, using one-way ANOVA followed by the Dunnett's or the Tukey-Kramer tests. Two-way ANOVA analysis revealed an extremely significant RA dose effect for the % of cuboid cells (only between RA absence and presence, but not between 1 and 10 µM RA) and elongated cells, and a very significant RA dose effect for the percentage of plastic cells (§ symbol for differences between 1 and 10 µM RA).

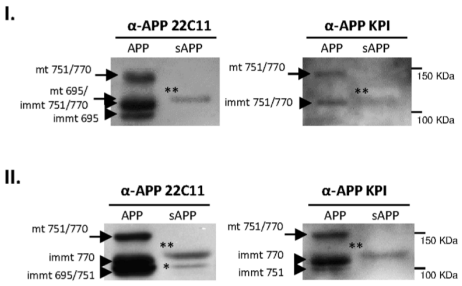

Supplementary Figure B.2 - **Identification of APP and sAPP bands in SH-SY5Y cellular and media lysates.** SH-SY5Y cells and media were collected into 1% SDS lysates and resolved in 5-20% homemade gradient SDS-PAGE gels. Immunoblot analysis was conducted using either the anti-APP N-terminus antibody, which detects all APP (and APLP) isoforms and their derived sAPP fragments, or the anti-APP KPI antibody, which detects the KPI-containing APP (and APLP) isoforms such as the highly abundant 751 and 770, and their derived sAPP fragments. I and II. represent different resolutions of equivalent samples, where the immature 751 APP isoform either co-migrates with the 770 isoform (I.) or with the 695 APP isoform (II.). 'Immt' - immature isoforms (arrowheads); 'mt'- mature isoforms (arrows). '**'KPI-negative sAPP.

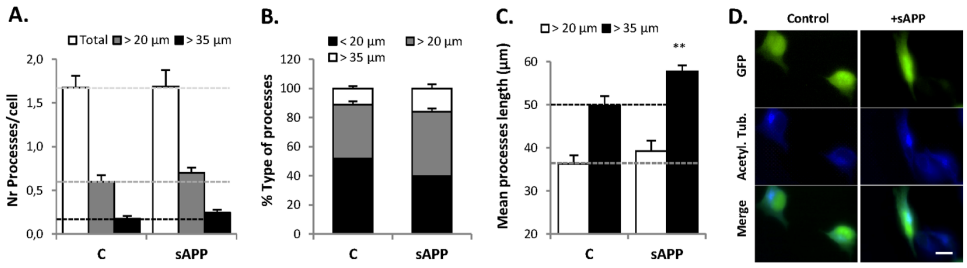

Supplementary Figure B.3 - **Effects of sAPP medium enrichment on non-differentiated SH-SY5Y cells.** Non-differentiated SH-SY5Y GFP-transfected cells were incubated for 24h with sAPP-enriched conditioned medium, previously obtained by transfecting SH-SY5Y cells for 24h with an APP_{695}-GFP cDNA. Fluorescence microphotographs were obtained, and an average of 60 GFP-expressing cells per condition analysed. Morphometric analyses of sAPP effects included: **A.** Number of processes per cell [all processes protruding from a cell ('Total'), processes >20 and 35 µm were scored, and the scores divided by the total cell number]; **B.** Percentage of Types of processes (the percentage of processes < and >20 µm, and >35 µm, were calculated out of the total number of processes); **C.** Mean neuritic length (the mean neuritic lengths of all processes >20 and 35 µm were calculated); n=4. **p<0.01, between control and plus sAPP conditions, as determined by unpaired two-tailed Student's t-test; of note, the number of >20 and >35 processes per cell and their % of type of processes, showed a statistical tendency (not quite significant, p<0.1, for C vs sAPP values). **D.** Representative epifluorescence microphotographs are shown. Immunocytochemistry of acetylated α-tubulin (blue) is shown, exhibiting no major differences between control and sAPP conditions. Bar, 10 µm.

6. PhosphoS655 APP promotes neuritogenesis via modulation of EGFR trafficking and enhanced ERK activation

Joana F. da Rocha[1,2], Patrícia Correia[1], Roberto A. Dias[1,2], Luísa Bastos[1,2], Uwe Konietzko[3], Odete A. B. da Cruz e Silva[2], Sandra I. Vieira[*1,2]

[1]Cell Differentiation and Regeneration group, Institute of Biomedicine (iBiMED), Department of Medical Sciences, Universidade de Aveiro, Campus de Santiago, 3810-193 Aveiro, Portugal;

[2]Neurosciences and Signalling group, Institute of Biomedicine (iBiMED), Department of Medical Sciences, Universidade de Aveiro, Campus de Santiago, 3810-193 Aveiro, Portugal.

[3]Division of Psychiatry Research, University of Zurich, Zurich, Switzerland.

[*]Corresponding author: Sandra Isabel Vieira; e-mail: sivieira@ua.pt.

6.1. Abstract

The amyloid precursor protein (APP) and the epidermal growth factor/receptor (EGF/EGFR) are implicated in common neurological diseases and aging. Both are widely expressed in the central nervous system and have a role in brain development.

In the present work we show the existence of a functional interplay between APP and EGF-EGFR signaling in neuronal differentiation. APP is able to interact with both proEGF and EGFR, and combined APP overexpression and EGF stimulation have a synergistic effect on neuronal-like differentiation. Such effect seems to relate well with promotion of ERK1/2 activation, and APP ability to modulate both EGFR expression levels and trafficking. In addition, we show that APP S655 phosphorylation is able to positively modulate EGFR and ERK1/2 activation, while the constitutively dephosphorylated mutant seems to target EGFR to LAMP2-positive lysosomes and is associated with lower levels of ERK1/2 phosphorylation. Finally, we show that APP S655 seems to play a role in dendritogenesis in mice cortical neurons.

6.2. Introduction

The amyloid precursor protein (APP) is a type 1 integral membrane glycoprotein with a large extracellular domain and a short cytoplasmic region. During its dynamic intracellular trafficking, APP undergoes proteolytic cleavages to release biologically active peptides [1]. Close to the membrane domain APP can be cleaved by β-secretase or α-secretase, releasing soluble N-terminal fragments. The resulting membrane tethered C-terminal fragments are subsequently cleavage by the γ-secretase complex to release two peptides: Abeta and the APP intracellular domain, AICD (after β-secretase), or p3 and AICD (after α-secretase) [2]. In addition, direct phosphorylation of the APP has important roles in the regulation of APP traffic and sorting [3-6], processing [5-8], and binding to protein interactors [9].

APP is a central protein in the most prevalent neurodegenerative disorder, the Alzheimer's disease (AD) [10], and has been further implicated in several other neurological disorders and brain injury [11]. Highly enriched in neurons, APP appears to be critical for normal brain development and adult brain plasticity [12]. Specific roles in neurogenesis [13], neuronal migration [14], neurite outgrowth [15] and guidance [16], synaptogenesis [17], and synaptic plasticity [18] have been described.

Similar to APP, the epidermal growth factor precursor (proEGF) is a type I transmembrane glycoprotein cleaved by cell surface proteases to release the mature epidermal growth factor (EGF). The human precursor has a large extracellular domain with 9 EGF-like domains, a helical transmembrane domain, and a shorter cytoplasmic domain [19, 20]. Solubilized forms of the precursor have been described as biological active, competing with EGF for EGF Receptor (EGFR) binding [21].

EGF is a well described mitogen for multiple cell lines, ranging from epithelial cells and fibroblasts to neural stem and progenitor cells of different origins in the central nervous system (CNS) [22]. Moreover, it is also a neurotrophic and neuromodulator actor in postmitotic neurons, promoting differentiation, maturation, survival and synaptic plasticity [23-25]. Both EGF and EGFR (also known as ErbB1) are expressed in various regions of the CNS, and their expression pattern is suggestive of a role in neurodevelopment, i.e., in the telencephalon EGFR expression is precisely increased from early embryonic stages to mid-late embryonic stages, where higher levels of EGFR mRNA and protein are expressed by different cell populations, namely astrocytes, neurons and multipotent stem cells [26]. Additionally, both EGF and EGFR have been implicated in neurological disorders like Schizophrenia, Parkinson's and Alzheimer's diseases, and in neurometabolic aging [27].

EGF binding to EGFR induces receptor dimerization and auto-phosphorylation of receptor tyrosine residues, which in turn recruits phosphotyrosine binding proteins and initiates different signaling events. The major pathways activated by EGFR include Ras stimulation of RAF-MEK-ERK1/2 cascade, PI3K stimulation of Akt and PLCgamma, and JAK stimulation of STAT pathway [28]. Activated receptors are internalized (potential via CBL recruitment) in early endosomes, where it is now known that tyrosine kinase receptors' signal continues [29]. After activation, the receptor follows two possible fates: 1) recycling to the cell surface; or 2) sorting onto intraluminal vesicles of maturating endosomes and targeting to lysosomal degradation. Modulation of this EGFR trafficking has major consequences for signaling outcomes [30, 31].

EGF stimulation has been implicated in the regulation of APP expression and processing [32, 33]. On the other hand, the AD-related APP Swedish mutation has been shown to alter EGFR degradation after EGF stimulation [34], and AICD seems to regulate EGFR gene expression [35].

The aim of the present work was to investigate the interplay between APP and EGF-EGFR signaling in neuronal differentiation. We here show that combined APP and EGF have a synergistic effect on neuronal-like differentiation that relates to ERK1/2 activation. This might be in part due to the APP ability to modulate both EGFR expression levels and trafficking. Furthermore, we show that APP phosphorylation at S655 positively modulates such events.

6.3. Material and Methods

6.3.1. Antibodies and Reagents

The following primary antibodies were used: rabbit anti-EGF (antibodies-online), rabbit anti-proEGF (against aa 700-800; Novus Biologicals), rabbit anti-EGFR (Abcam), rabbit anti-APP C-Terminal (clone CT695; Invitrogen), mouse anti-APP N-terminal (clone 22C11; Chemicon), mouse anti-APP residues 1-16 of Abeta (clone 6E10), rabbit anti-phosphorylated ERK1/2 (Thr202/Tyr204 and Thr185/Tyr187 for Erk1 and Erk2, respectively; Millipore), rabbit anti-ERK1/2 (Millipore), mouse anti-Grb2 (BD Bioscience), rabbit anti-Shc (BD Bioscience), mouse anti-BIII Tubulin (Sigma-Aldrich), mouse anti-MAP2 (Sigma-Aldrich), mouse anti-Rab5, and mouse anti-Rab4 (Sicgen), mouse anti-LAMP2 (Abcam ab25631). HRP-conjugated secondary antibodies, anti-mouse and anti-rabbit, were from GE-Healthcare. Secondary antibodies Alexa Fluor 405 goat anti-mouse or goat anti-rabbit, and Alexa Fluor 594 goat anti-rabbit or goat anti-mouse were from Life Technologies. Donkey anti-mouse Cy3 was also used.

Human recombinant EGF was from Cell Signaling and was diluted to a final concentration of 100ng/mL. Human recombinant sAPPalpha (diluted to 5 nM) and the EGFR inhibitor drug PD 168393 (diluted to 10 μM) were from Sigma-Aldrich. Texas Red-conjugated Transferrin was from Molecular Probes.

6.3.2. Cell culture

Cell cultures cells were kept in a humidified, 37^{o}C, 5% CO_2 incubator. The HeLa cell line was maintained in 10% FBS DMEM, and cells were plated onto 60 mm plates in order to reach 60-80% confluency next day. The SH-SY5Y human neuroblastoma cell line was maintained in 10% FBS MEM/F12 medium. For morphometric and immunocytochemistry studies initial cell density plated was $2.0x10^4$ cells/cm^2 onto six-wells plates containing sterile coverslips, and cells were allowed to grow for 24h. For biochemical studies cells were plated onto six or twelve-wells plates in order to reach 60-80% confluency next day.

6.3.3. Expression vectors and DNA constructs

Human APP isoform 695 (APPWt) cDNA, and the respective S655 phosphomutants, Serine 655 to Alanine (S655A, APPSA) or to Glutamate (S655E, APPSE) are fused in frame with GFP in the pEGFP-N1 mammalian expression vector, and were previously produced and described by our lab [36]. These cDNAs were used as template to generate an additional Tyrosine 682 to Phenylalanine (Y682F, APPYF) point mutation using the QuikChange Site-Directed Mutagenesis Kit (Stratagene). The following primers were used: FW-

GATGCAGCAGAACGGCTTCGAAAATCCAACCTAC; RV-GTAGGTTGGATTTTCGAAGCCGTTCTGCTGCATC (NZYTech). Resulting constructs and mutations were confirmed by DNA sequencing (ABI PRISM 310 Genetic Analyzer, Applied Biosystems). Empty pEGFP-N1 expression vector (here named 'V) was used as control in experiments involving transfection.

6.3.4. Cellular Transfection and incubation with EGF

Mammalian cell lines transfections were carried out with the TurboFect^{TM} reagent according to the manufacturer's instructions (Fermentas Life Sciences). Briefly, for each monolayer of cells grown in 6-well plates, 2 µg of cDNAs (GFP empty vector or APPs-GFP cDNA) were diluted in 100 µL of serum-free growth medium. After being briefly vortex, 4 µL of TurboFect^{TM} were added to the diluted DNA. The mixture was vortexed and incubated for 15-20 min at room temperature (RT), after what the mixture was added dropwise, to each well, with gently rocking. Cells were further incubated for 6h at 37^{o}C in a CO_2 incubator, after which medium was changed. For cell morphology/morphometric assays, EGF treatment included a brief pulse of 3-5 minutes before transfection medium change; when indicated the PD 168393 inhibitor was added 1h before the EGF stimulation. For immunoblot analysis of protein levels, EGF was added to the cells 1h before cells' harvesting.

Mouse cortical primary neurons were transfected using Lipofectamine® 2000 (ThermoFisher Scientific). To sum up, for each well of a 24-well plate, 2 µL of Lipofectamine were diluted in 50µL Neurobasal medium, and incubated for 5 min at RT. cDNAs were diluted in 50µL Neurobasal medium in a separate microtube. Both solutions were mixed, and the mixture incubated for 20 min, RT. During this time, neurons conditioned medium was collected and new pre-warmed Neurobasal medium (without supplements) was added to the neurons. Lipofectamine-cDNA precipitates were added to the neurons for 3h, after which medium was replaced by the previous conditioned medium. At this time, the PD 168393 inhibitor was included in the respective conditions, and after 3h EGF was added. Transfection was let to occur for 24h at 37^{o}C in a CO_2 incubator.

6.3.5. GFP-Trap co-precipitation assay

GFP tagged-APP protein overexpressed by HeLa cells, were precipitated by pulling-down the GFP moiety with GFP-Trap® (Chromotek), according to the manufacturer's instructions. Briefly, after transfection, cells were washed in phosphate buffer saline (PBS), and collected with a scrapper in 1 ml ice-cold PMSF-containing PBS, on ice. After a centrifugation step, cell pellet was lysed for 30 min on ice with non-denaturant lysis buffer 1 (10 mM Tris-HCl pH 7.5, 0.5 mM EDTA, 0.5%

Gepac-ca-630, 150 mM NaCl, 1 mM PMSF) supplemented with protease inhibitors cocktail (Sigma-Aldrich), 1 mM NaF, and 10 mM sodium orthovanadate. Following centrifugation (5 min at 20000 g, 4°C), the supernatant was collected, an aliquot of 25 µL was taken ('cells lysates' fraction), and total protein quantified (Pierce's BCA kit; Thermo Scientific). Mass normalized lysates were pull-downed with GFP-Trap for 3h with orbital shaking at 4°C. The beads were magnetically separated until supernatant was clear, and ressuspended in wash buffer (10 mM Tris-HCl pH 7.5; 150 mM NaCl; 0.5 mM EDTA; 10 min incubation with agitation at 4°C). Magnetic separation and washing step were repeated 4 times, after what the proteins were eluted in Laemmli sample buffer.

6.3.6. Cortex dissection and Co-Immunoprecipitation

Wistar Hannover rats (9–12 weeks) were obtained from Harlan Interfaune Ibérica, SL. Animal suffering and the number of animals were minimized, and all the experiments met the European legislation for animal experimentation (2010/63/EU; European Council Directive 86/609/EEC). The experiment was approved and supervised by our Institutional Animal Care and Use Committee (IACUC): Comissão Responsável pela Experimentação e Bem-Estar Animal (CREBEA). Briefly, animals were sacrificed by cervical stretching followed by decapitation and, cortex was dissected out on ice. Tissues were further weighed and homogenized on ice with a Potter-Elvehjem tissue homogenizer (10–15 pulses at 650–750 rpm) in non-denaturating lysis buffer 2 (50 mM Tris–HCl pH 8.0, 120 mM NaCL and 4% CHAPS) containing protease inhibitors [37]. The tissue extracts were used for immunoprecipitation analysis as described below.

Mice cortex dissection was performed as described above for rat, but tissue was homogenized in non-denaturating lysis buffer 1, containing protease inhibitors.

For immunoprecipitation of rodent cortices, dynabeads Protein G (Dynal, Invitrogen) were washed in 3% bovine serum albumin (BSA) in PBS, and primary antibodies (rabbit anti-proEGF or mouse anti-APP 22C11) were incubated with Dynabeads according to the manufacturer's instructions. Cortex lysates were precleared with 0.6 mg Dynabeads for 1 h at 4°C with agitation and incubated with antibody-Dynabeads overnight (O/N) at 4°C with agitation. The immunoprecipitates were washed in PBS and proteins denatured by boiling in Laemmli loading buffer followed by SDS-PAGE and immunoblotting.

6.3.7. Neuronal primary cultures

Pregnant mouse (E14-15; in-house breed) was anaesthetized with Isoflurane (Piramal Healthcare India, 99.9% purity) followed by cervical stretching and decapitation. The mouse embryos were then decapitated and used for the isolation of cortex to prepare cortical primary cultures. Briefly,

after dissociation with TrypLE™ Express Enzyme (Thermo Scientific), cells were plated onto poly-D-lysine-coated dishes at a density of 100000 cells/cm^2 in 10% horse serum DMEM (Invitrogen). After 12h DMEM medium was removed and replaced by serum-free, B27-supplemented Neurobasal A (Thermo Scientific), plus Glutamax (Invitrogen) and sodium pyruvate (Sigma-Aldrich). Cultures were maintained in an atmosphere of 5% CO2 at 37°C, and every 2 days half of medium was replaced by fresh medium.

6.3.8. SH-SY5Y cells proliferation assay

Immediately before changing the medium of cell transfection, 100 ng/mL of EGF were added to the culture medium in the defined conditions for 3-5 min [38]. Transfection medium was changed to cell medium without FBS. Immediately after changing the medium, the 10 μM of 5-ethynyl-2'-deoxyuridine (EdU) was added to the cell medium to perform the proliferation assay. Cells were maintained for further 12h, in a total of 18h of transfection.

Cell proliferation was determined using the Click-iT® EdU Alexa Fluor® imaging kit (Invitrogen) according to the manufacturer's protocol. This kit uses the EdU as a nucleoside analogue of thymidine to directly measure DNA synthesis. Coverslips containing the cells monolayer were fixed with 4 % paraformaldehyde in PBS (PFA) for 15 min. After washing twice with 3% bovine serum albumin (BSA) in PBS the cells were permeabilized with 0.5% Triton X-100 in PBS for 20 min, and again twice washed with 3% BSA in PBS. EdU detection is performed by incubating the coverslips with a Click-iT® reaction cocktail (Click-iT® reaction buffer, $CuSO_4$, Alexa Fluor® 594 Azide, and reaction buffer additive) for 30 min while protected from light, followed by a wash with 3% BSA in PBS. For subsequent DNA staining, coverslips were first washed 1x with PBS, and incubated with 5 μg/mL Hoechst 33342 in PBS for 30 min. Finally, coverslips were directly mounted on microscope slides with Vectashield® mounting media (Vector Labs).

EdU and Hoechst double labelled SH-SY5Y cells were imaged with the Olympus IX81 inverted epifluorescence microscope. For each condition random images of 20 fields were taken in triplicate, in which EdU positive and Hoechst positive nuclei were manually scored using the Fiji software. The total number of positive cells in the well was estimated based on the area covered by the objective, and the percentage of cell proliferation was determined by calculating the number of EdU positive cells against the number of Hoechst positive cells.

6.3.9. Endocytic trafficking assays

Endocytosis of Texas Red-conjugated Transferrin (Molecular Probes) was monitored in SH-SY5Y 24h transfected with the GFP vector ('V'), and APPWt. In order to eliminate endogenous transferrin, cells were further incubated for 30 min at 37^{o}C with DMEM medium supplemented

with 20 mM HEPES. Medium was exchanged for 500 µL fresh medium of equal composition but containing 1mg/ml BSA and 100 nM Texas Red-conjugated transferrin, and cells incubated for a further 15 min at 37^{o}C. In the last 5 min, EGF was include in a subset of cells [4]. The plates were immediately cooled to 4^{o}C, washed twice with ice-cold PBS, and cells fixed and processed for immunocytochemistry.

To compare the ability of the different APP-GFP proteins (Wt, SA, SE) to regulate EGFR endocytic trafficking, SH-SY5Y cells were plated and transfected for 24h with the GFP vector ('V'), APPWt, APPS655A and APPS655E as described above. Cells were washed with ice-cold PBS and fixed with 4% PFA. Immunocytochemistry with rabbit anti-EGFR and mouse anti-Rab5, mouse anti-Rab4, or mouse-LAMP2 were subsequently performed [31].

6.3.10. Immunocytochemistry assays

SH-SY5Y cells grown on coverslips were fixed with a 4% PFA for 20 min and, upon three washes with PBS, permeabilized with a 0.2% TRITON PBS solution for subsequent immunocytochemistry analysis. Briefly, cells were first blocked for 30 min-1h with 5% BSA in PBS, then incubated with specific primary antibodies, and finally incubated with fluorophore conjugated-secondary antibodies. Preparations were washed with PBS, mounted with Vectashield® mounting media, with or without DAPI (Vector Labs).

Mouse cortical primary neurons, grown on coverslips, were pre-fixed for 10 min by adding equal amounts of warm 4% PFA to the culture medium, followed by a fixation step as described above. Permeabilization was performed by washing coverslips 3 times, 10 min each, with 1X TBS with 0.05% Triton, and unspecific sites were blocked by 1h incubation at RT with fresh 1X TBT with 0.2% Triton, 5% goat serum and 5% horse serum. Primary antibodies were incubated O/N at 4^{o}C, and after washing cells were blocked again for 30 min, and secondary antibodies were incubated for 2h. Before mounting with Mowiol, coverslips were washed 3 times with 1X TBS with 0.05% Triton.

Cells visualization was performed by epifluorescence microscopy under an Olympus IX-81 motorized inverted microscope equipped with a LCPlanFl 20x/0.40 objective lens [5], or by confocal microscopy using a LSM 510 META confocal microscope (Zeiss) and a 63x oil objective [4].

For colocalization studies related to EGFR trafficking, stack images of delimited single cells (APP-GFP or control GFP vector transfected cells) were analysed using the Fiji plugin JaCoP [39]. The percentage of colocalization of one protein with another (for example of EGFR with the endosomal protein markers Rab5 or Rab4; specified in each graph) was obtained by applying the Manders' method.

6.3.11. Morphometric analyses of cell neuritogenesis

For the experiments including cells treatment with EGFR inhibitor PD 168393, morphometric analysis of cells was performed on ~30 random digitized images per sample, with an average of 140 transfected cells per biological replica of each condition being analyzed. Transfected cells were identified by GFP expression, measurements were performed on matching acetylated-tubulin fluorescent microphotographs (similar to using PhC microphotographs). All the measurements were performed as previously described [40], using Fiji. Process scoring was divided as follows: 1) "Total", all processes arising from a cell; 2) ">20 μm", processes longer than 20 μm; and 3) "35 μm", processes longer than two times the cell body length (≥ 35 μm). Data was expressed as a quotient of the total number of processes per cell.

For quantitative morphometric analysis of cortical primary neurons, GFP-positive and MAP2/BIII-Tubulin-positive neurons were randomly imaged. Neurons extensively entangled, or the exceptional cases when neurites extended outside the visualization field were excluded. Neurites were quantified using NeuronJ [41], a Fiji Plug-in. Several parameters were analyzed for each cell, chosen accordingly to previous reports [42, 43] (see Supplementary Table 1), with a total of ~50 cells being analyzed for each condition.

6.3.12. Western blot assays

For western blot (WB) purposes, cells were washed and harvested with either 1% boiling SDS, or RIPA buffer (Sigma-Aldrich-Aldrich) containing 1% protease inhibitors cocktail (Sigma-Aldrich-Aldrich), 1 mM NaF, and 10 mM sodium orthovanadate. SDS harvested cell lysates were further boiled for 10 min, cells with RIPA buffer are incubated for 5 min at 4^{o}C. Cell lysates were sonicated for 30 sec, and total protein content was measured as above described. When required, conditioned medium was collected, cleared by centrifugation, and harvested into final 1% SDS samples. Aliquots for WB were mass-normalized to the respective lysates total protein content.

Mass-normalized aliquots were subjected to electrophoresis on 5-20% gradient SDS-PAGE, being subsequently electrotransferred into nitrocellulose membranes. These were initially processed for Ponceau-S staining in order to assess gel loading (according to [44]), since in cell differentiation studies beta-actin and other cytoskeleton markers are not suitable loading controls [40, 45-47]. Following, primary antibodies were incubated as specified by the manufacturer's instructions (from 2h to O/N) and secondary antibodies for 2h. Membranes were further washed 3x with TBS-T or PBS-T for 10 min, and submitted to the ECL^{TM} (enhanced chemiluminescence; GE Healthcare) detection method, using x-ray films (GE Healthcare), or directed imaged by ChemiDoc^{TM} touch Imaging System (BioRad).

Ponceau-S stained membranes and ECL x-ray films were scanned (GS-800 imaging densitometer, BioRad) and protein immunoreactive bands quantified (Quantity One densitometry software or Image Lab software from BioRad). All data is presented as fold-increase of a control condition (stated in figure caption), corrected to Ponceau-S used as loading control, and expressed as mean ± SEM (standard error of the mean). The number of independent experiments is specified in the figure caption.

6.3.13. Protein phosphorylation analysis by Phos-tag SDS-PAGE

SH-SY5Y cells 24h transfected with the APP-GFPs proteins and stimulated or not with EGF for 5 min, were directly harvested in Laemmli buffer. Samples were then subjected to phos-tag SDS-PAGE performed with 5% polyacrylamide gels containing 25 µM phos-tag™ (AAL-107, Wako Pure Chemicals Industries, Ltd) and 100 µM MnCl2. After electrophoresis, phos-tag acrylamide gels were washed with transfer buffer (25 mM Tris, 192 mM glycine and 20% methanol) containing 10 mM EDTA, for 10 min with agitation and then with transfer buffer without EDTA for 10 min according to the manufacturer´s protocol. Proteins were transferred onto nitrocellulose membranes followed by immunoblotting detection as indicated above.

6.3.14. Statistical analysis

All statistical analysis was performed using the GraphPad Prism5 software. The test applied to infer statistical significance is stated in each figure caption. In general, to compare 3 or more groups one-way ANOVA followed by the Dunnett's post-test or the Tukey-Kramer multicomparision post-test were performed; to compare two groups the unpaired Student's t-test was applied. Cortical neurons morphometric data and the specified colocalization data included non-normally distributed samples were analyzed by the Kruskal-Wallis test with Dunn´s multiple comparison post-test (comparison of 3 or more groups) or by the by the Mann Whitney test (comparison of two groups). Colocalization data following normal distribution were analyzed by the unpaired t-test or by the one-way ANOVA followed by the Tukey-Kramer multicomparision post-test.

6.4. Results

6.4.1. APP interacts with precursor form of the epidermal growth factor

APP and proEGF are both type 1 transmembrane glycoproteins. Due to the display of overlapping cell and tissue expression and functions, we tested the hypothesis of a physical interaction between both proteins. Human HeLa cells transiently overexpressing APPWt were used to pull down the APP-GFP protein and its interactors, using the GFP-trap technique (Figure B.8 A, upper panel). The anti-EGF antibody detects 3 protein forms of proEGF in HeLa cells' lysates (between ~95 and 120 kDa, possibly indicating different glycosylated forms), with the band of lowest molecular weight (~95 kDa) co-immunoprecipitating with APP-GFP (Figure B.8 A, lower panel).

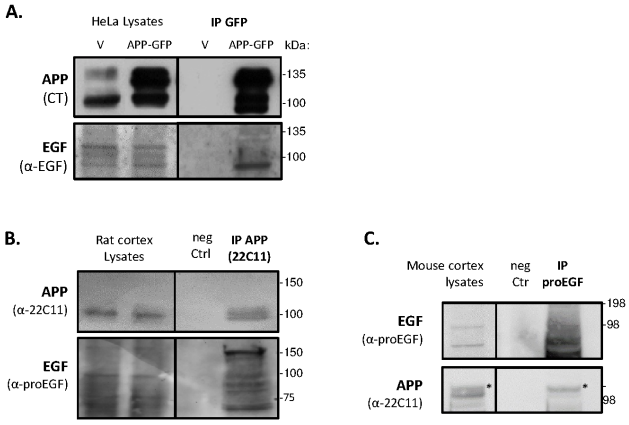

Figure B.8 - **APP interacts with the precursor form of EGF. A.** HeLa cell lysates from cells transiently overexpressing the GFP empty vector (V) or the wild-type APP_{695}-GFP cDNA (APP) were immunoprecipitated using GFP-Trap® magnetic beads. No APP is pull down in the control condition. The anti-EGF antibody reveals that a precursor form of EGF is precipitated bound to APP-GFP. n=3. **B.** Rat cortices were lysated with CHAPS buffer and immunoprecipitated by anti-APP antibody (22C11, against APP N-terminal) bound to Protein G Dynabeads. Immunobloting with anti-proEGF (specific antibody for the precursor form of the EGF protein) revels several immunoreactive bands in cortex lysates and confirms that pro-EGF is co-precipitated with APP. Negative control: absence of the 22C11 primary antibody. n=2. **C.** Rat cortices were lysated with NP-40 based buffer and immunoprecipitated by anti-proEGF antibody. Immunobloting with anti-APP 22C11 proved that APP is co-precipitated with pro-EGF. Negative control ('Ctr neg' - cortex extracts incubated with protein G Dynabeads but no primary antibody). Cortex lysate from APP knock-out animals (APPKO) was included to show the specificity of the APP antibody. n=1.

Next, we tested the physical interaction between APP and proEGF in rat and mouse cortex lysates. Rat cortex lysates homogenised and lysed with non-denaturant CHAPS buffer were immunoprecipitated with anti-APP N-terminal antibody 22C11. Figure B.8 B shows that the majority of the proEGF immunoreactive bands found in rat cortex lysates co-precipitate with APP. Mouse cortex lysed with non-denaturant NP-40 based lysis buffer was immunoprecipitated with the anti-proEGF antibody. In mouse cortex lysates, proEGF appears mainly as 3 immunoreactive bands (Figure B.8 C, upper blot): one around 98 kDa, and other two below this marker. An additional higher molecular weight band (above 198 kDa) can also be detected with longer exposure time. Concordantly with these results from HeLa cells and rat cortex, proEGF also co-

immunoprecipitates full-length APP. The APP form of higher molecular weight, most probably corresponding to its mature glycosylated form, is particularly more efficiently co-precipitated with proEGF (Figure B.8 C, * in lower panel). In mouse cortex proEGF could also be co-precipitated with an anti-APP antibody (data not shown).

6.4.2. APP potentiates EGF-mediated neuritogenesis in SH-SY5Y cells

Following the evidence on the physical interaction between APP and proEGF, the role of such interaction was pursued. Since EGF is a known strong mitogen, we combined APP overexpression and EGF stimulation to study a potential functional interaction in cellular proliferation (Supplementary Figure B.4). An Edu incorporation assay was performed in SH-SY5Y cells transiently transfected with the GFP empty vector ('V') or with APPWt for 18h, and exposed or not to a 3 min EGF pulse right before transfection medium exchange (Supplementary Figure B.4 A). After the EGF pulse, the DNA of SH-SY5Y cells undergoing mitosis was labelled by incubation with the fluorescing nucleotide Alexa594-Edu for 12h (Supplementary Figure B.4 B). In these conditions, no differences in the percentage of proliferating cells (Edu-positive/Hoescht-positive nuclei ratio) are observed in all the conditions (Supplementary Figure B.4 C). Although EGF does potentiate proliferation over basal values, at the assay's end point there is a higher number of EGF-stimulated cells than non-stimulated cells, indicating a pro-survival effect. APP has no influence in this EGF pro-survival effect, as no differences are observed between APP transfected cells and vector transfected cells (Supplementary Figure B.4 D).

A closer look on the morphology of the SH-SY5Y cells of the proliferation assay suggested that an APP-proEGF functional interaction may reside on neuronal-like differentiation (Figure B.9). Morphometric analyses included scoring the total number of neurite-like processes arising from each cell ('Total', all processes of all sizes), and measuring and categorizing these processes by length: processes higher than 20 µm, and processes higher than 35 µm (pre-neurites and neurites, respectively) [40]. Relatively to the number of processes longer than 20 µm, EGF alone-stimulated cells tend to increase this number (Figure B.9 B, 2C, 'V+EGF') while APP overexpression alone significantly increases it (Figure B.9 C, 'APP'). The concomitant overexpression of APP with EGF stimulation ('APP+EGF') further increases the number of longer processes. Particularly, combined APP overexpression and EGF treatment increases the number of processes longer than 35 µm per cell when compared to any of the other conditions (Figure B.9 C), and is the only condition able to significantly increase neuritic length (Figure B.9 D).

Since EGFR activation mediates EGF neuritogenic effects, its involvement in the APP+EGF co-induced neuronal-like differentiation was pursued. SH-SY5Y cells were transfected with APPWt and, in addition to EGF stimulation, cells were also exposed to the EGFR inhibitor PD168393

(Figure B.9 B scheme). Cells concomitantly treated with EGF and the EGFR inhibitor ('INIB') show significantly lower number of processes per cell than EGF only treated cells (Figure B.9 B and C, Total and >20 μm processes). The number of total processes per cell is only slightly decreased in APP+EGF cells tretated with the EGFR inhibitor, and the number is very similar to APP alone (Figure B.9 B, 'APP+INIB+EGF' vs 'APP'). However, EGFR inhibition has a more drastic effect on neurite elongation, significantly decreasing the number of >20 μm processes and the number of processes > 35 μm when compared to both 'APP' and 'APP+EGF' conditions (Figure B.9 C; $p=0.0399$ for > 35 μm processes in 'APP' vs 'APP+INIB+EGF' conditions by the two-tailed unpaired t test). These results suggest that the EGFR receptor has a role in APP-induced processes elongation, besides mediating EGF-induced elongation. Further confirmation was obtained from the significant decrease in the mean processes' length when APP overexpressing cells are exposed to EGF in the presence of the EGFR inhibitor (Figure B.9 D, 'APP+INIB+EGF' vs 'APP+EGF'). This also resulted in a decrease in the neuronal BIII-tubulin protein levels comparing to the EGF+APP condition (data not shown).

ERK1/2 activation is a well-known signalling event downstream EGF-EGFR that has been implicated in neuronal differentiation events. To confirm that ERK was also a mediator of this APP/EGF neuritogenic effect, ERK1/2 activation was monitored via western blot analysis of phosphorylated ERK1/2 levels (pERK1/2, Figure B.9 E and F). The immunoblots clearly show that EGF-stimulated cells presented high levels of pERK and, more interestingly, that APP overexpression appears to promote this ERK activation state. The presence of the EGFR inhibitor hindered this EGF- and APP+EGF-induced pERK1/2 activation bellow control ('V ctr') levels.

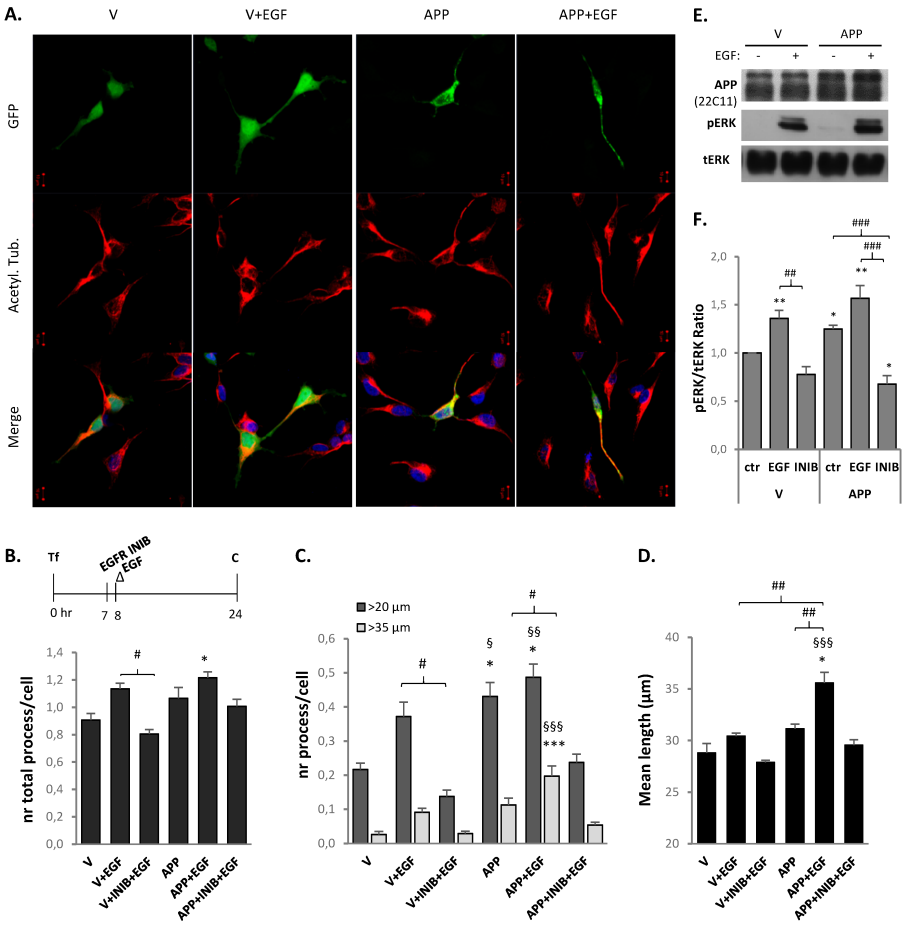

Figure B.9 - **APP increases EGF-mediated neuronal-like differentiation.** SH-SY5Y cells were either transfected with the GFP empty vector ('V') or wild-type APP-GFP cDNA ('APP') and exposed or not for 3 min to 100 ng/mL human recombinant EGF ('V+EGF' and 'APP+EGF'). When indicated, EGF stimulation was performed under EGFR inhibition by PD168393 ('INIB'). **A.** Representative epifluorescence microphotographs of vector GFP or APP-GFP expressing cells labeled for acetylated α-tubulin ('Acetyl Tub', in red) and nuclear stained with DAPI (blue). Bar, 10 µm. **B.** Total number of processes per cell (all processes protruding from a cell, independently of the size, were scored). **C.** Number of processes longer than 20 µm ('>20 µm') and longer than 35 µm ('>35 µm') per cell were scored. **D.** Processes mean length, determined based on all processes longer than 20 µm. n=4-6 independent assays. On average, 30 microphotographs (>100 cells) were analyzed per independent assay. */#/§ $p < 0.05$, **/##/§§ $p < 0.01$, ***/###/§§§ $p < 0.001$ by one-way ANOVA followed by the Tukey's post-test against control empty vector ('V'), between indicated conditions or against condition 'APP+INIB+EGF', respectively. Statistical differences not fundamental for result interpretation are omitted. **E.** Immunoblots of cell lysates probed with the 22C11 antibody for the APP N-terminal, phospho-ERK1/2 ('pERK'), and total ERK 1/2 ('ERK'), suggested a synergy of APP and EGF on ERK1/2 activation. **F.** pERK/ERK ratio was calculated based on immunoblots of cell lysates probed with the antibody for phospho-ERK1/2 and total ERK 1/2, and plotted as fold increases of control ("ctr") empty vector ("V").

6.4.3. APP binds to and modulates EGFR protein levels

The mechanisms by which APP could influence EGFR and ERK activation were subsequently studied. EGF stimulation has been observed to regulate APP expression and processing. This was confirmed to occur under our experimental conditions (Figure B.10 A). Immunoblots of cell lysates exposed to the previous conditions of Figure B.9 B show that EGF stimulation significantly increases APP protein levels (both endogenous APP and exogenous APP-GFP upper bands);

concomitant EGFR inhibition blocks this effect (Figure B.10 A, upper blot and left graph). Furthermore, EGF also significantly stimulates total sAPP secretion, either in control cells ('V sAPPtotal') or APPWt expressing cells ('APP sAPPtotal') (Figure B.10 A middle blot, and right graph). In APP overexpressing cells we were able to confirm that EGF stimulates sAPPalpha release by using the anti-APP 6E10 antibody (Figure B.10 A lower blot, and 'APP sAPPalpha' in right graph). As seen for cellular APP protein levels, EGFR inhibition blocks this EGF-induced sAPP production/medium secretion. Noteworthy, EGFR treatment in APP overexpressing cells significantly decreases all sAPP levels below control cells (untreated APPWt overexpressing cells, established as 1.0).

These results indicate that neuritogenesis mediated by APP+EGF might involve EGF-induced APP cleavage into sAPPalpha, the most neuritogenic sAPP fragment [48], in a EGFR activation-dependent manner. Further analyses indicate that it may also involve APP-induced EGFR protein levels. As shown in Figure B.10 B, APP overexpression increases EGFR protein levels, in a dose-dependent manner (at least until 1.25μg of APPWt cDNA). Although APP overexpression is accompanied by increased production of medium sAPP, incubation with recombinant sAPPalpha does not increase EGFR protein levels per se (Figure B.10 C).

This co-increased APP and EGFR half-life may occur via APP-proEGF-EGFR co-endocytosis. Indeed, we found evidence that endogenous APP and EGFR also physically interact, by efficient co-immunoprecipitation of EGFR after immunoprecipitation of APP using an anti-APP 22C11 antibody in rat cortex (Figure B.10 D). Additionally, transfected APP-GFP and endogenous EGFR were observed to highly co-localize in cytoplasmic vesicles in APPWt transfected SH-SY5Y cells (Figure B.10 E).

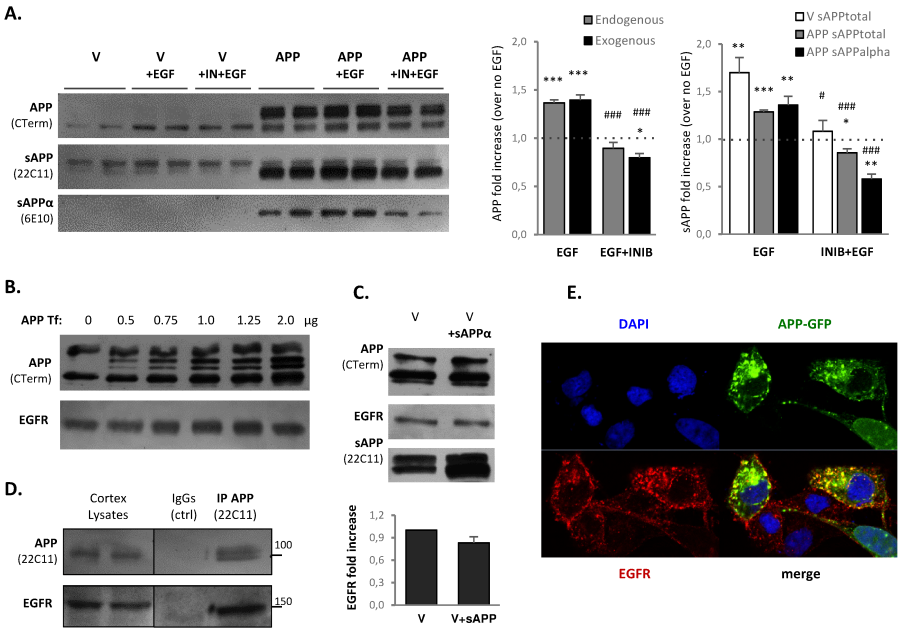

Figure B.10 - **EGF increases APP and sAPP levels via EGFR activation.** SH-SY5Y cells either transfected for with the GFP empty vector ('V') or wild-type APP-GFP cDNA ('APP'), stimulated or not for 3 min with 100 ng/mL human recombinant EGF ('V+EGF' and 'APP+EGF') in the presence ('V+IN+EGF' and 'APP+IN+EGF') or not of 10 µM EGFR inhibitor PD168393. **A.** Immunoblots of cell lysates and medium were probed with: anti-APP C-terminal antibody ('APP CT', to detect APP in cell lysates), and the anti-APP N-terminal antibodies 22C11 (detecting all sAPP forms in the medium, 'sAPP') and 6E10 (only recognizing 'sAPPalpha'). The effects of EGF on endogenous and exogenous full-length APP protein levels were plotted as fold increases of EGF treated conditions over their corresponding controls (left graph). n=8 independent assays. *p < 0.05, ***p < 0.001 against control condition (established as 1.0) by one-way ANOVA followed by the Dunnet's post-test. ###p < 0.001 against EGF stimulated cells by unpaired two-tailed t-test. The effects of EGF on all sAPP forms (endogenous: 'V sAPP total'; and after APPWt transfection: 'APP sAPP total') or specifically on sAPP alpha ('APP sAPPalpha', after APPWt transfection) were also plotted (right graph). n=4-6. *p < 0.05, **p < 0.01, ***p < 0.001 against control condition (established as 1.0) by one-way ANOVA followed by the Dunnet's post-test. #p < 0.05, ### p < 0.001 against EGF-stimulated cells by unpaired two-tailed t-test. **B.** SH-SY5Y cells transfected with increasing concentrations of APPWt cDNA (final concentration of transfected cDNA was normalized to 2.0 µg/µL of cDNA with empty vector cDNA). The immunoblots of cell lysates were probed with the anti-APP C-terminal ('APP CT') and anti-EGFR antibodies. **C.** SH-SY5Y cells transfected with vector GFP plasmid and treated with 5 nM human recombinant sAPP for 18h. Immunoblots of cell lysates were probed with anti-APP C-terminal ('APP CT') and anti-EGFR antibodies. Cell medium was collected and the 22C11 immunoblot shows a sAPP enrichment in treated cells. EGFR protein fold increase was calculated relative to control (non-treated vector-transfected cells, 'V'). n=4. **D.** Rat cortices were lysed with CHAPS buffer and immunoprecipitated with anti-APP 22C11 antibody. Immunobloting with anti-EGFR antibody shows that EGFR co-precipitates with APP. No reactive bands appear in the negative control ('Ctr neg'): cortex extracts incubated with protein G Dynabeads in the absence of the 22C11 antibody. n=2. **E.** Representative microphotographs of APP-GFP (green) expressing cells immunolabeled for EGFR (in red), and nuclear stained with DAPI (blue).

6.4.4. APP S655 phosphorylation modulates EGFR trafficking

One fundamental aspect of EGF signal is the availability and activation of its receptor, modulated in turn by receptor expression levels, endocytosis and degradation [49].

Based on the results from APP overexpression on EGFR protein levels, their binding, and their high cytoplasmic colocalization, we predicted that APP might be modulating EGFR endocytosis and degradation. We tested this possibility by first monitoring the co-localization of EGFR with three proteins that are associated with the endocytic route - endocytosed Texas red-conjugated transferrin molecules; the early/sorting endosomal marker Rab5 and Rab4 (both stained by

immunocytochemistry means). Besides colocalizing with EGFR (Figure B.10 D), APP-GFP is observed to colocalize with intracellular EGF/proEGF in basal conditions, although at lesser extent than with EGFR (Figure B.11 A microphotographs). Importantly, the percentages of colocalization between endocytosed fluorescent transferrin and EGF or EGFR increase in conditions of APPWt overexpression, when compared to vector GFP expressing cells (Figure B.11 A graph). An increase of the EGFR endocytic population in APPwt overexpressing cells was also observed when using the Rab5 marker for early endosomes (by the Unpaired t test p=0,0182) (Figure B.11 B microphotographs and 4D graph). Since APP S655 phosphorylation regulates APP endocytic route and fate [4, 5], the effect of mimicking APP S655 constitutive dephosphorylation (S655A, 'SA') and phosphorylation (S655E, 'SE') on endocytic EGFR was analyzed. From Fig. 4B and 4D we can observe that all APP-GFP species (Wt, SA, SE) increased the EGFR population in Rab5-positive endosomes, although APPSE shown the highest increases (statistically different from control empty vector cells and from APPWt or APPSA cells). When at the Rab5 early/sorting endosome, EGFR is thought to follow three possible fates – fast recycle to the surface via Rab4-positive vesicles; mature to late endosomes (also termed Multivesicular Bodies, MVB) and to LAMP2-lysosomes for degradation; and slowly recycle to the surface via Rab11-positive recycling endosomes. We investigated directly the first two, and observed that although all APP species tend to decrease the amount of EGFR rapidly recycled to the surface, assessed via EGFR/Rab4 colocalization (Figure B.11 E graph), only APPSA significantly lowers the percentage of colocalization comparing to control empty vector. Relatively to EGFR degradation pathway, only APPSA increases the presence of EGFR in LAMP2-positive lysosomes (Figure B.11 C microphotographs and 4F graph).

We have subsequently examined the percentage of EGFR colocalization with the different APP-GFP species. Results show that APPSE presents significantly higher percentage of colocalization comparing to APPSA (Figure B.12 A). Following, we determined the effects of the APPS655 phosphomutants on the endogenous EGFR protein levels, either in basal conditions or following EGF treatment (Figure B.12 B). All APP species increase EGFR protein levels in basal non-stimulated conditions. As expected, EGF-stimulated control cells (V+EGF) show a high decrease in EGFR levels. This is a well described mechanism of signal regulation in which, following EGF stimulation, the levels of the EGFR protein are downregulated due to receptor increased degradation [30]. In cells transfected with any of the APP species, EGF stimulation is not able to induce EGFR downregulation as efficiently (Figure B.12 B, '+EGF' conditions).

In order to understand if the APPWt and the phosphomutants activated EGFR, we performed a phostag assay that allows to separate proteins accordingly to their level of phosphorylation (Figure B.12 C '+Phostag'). Results suggest that, under basal conditions, the EGFR receptor is slightly

more phosphorylated in cells expressing APPWt and APPSE (red asterisks) than in vector GFP expressing cells. This delayed migration of EGFR bands due to higher phosphorylation does not occur in cells expressing APPSA (blue asterisks) (Figure B.12 C, '-EGF' '+Phostag').

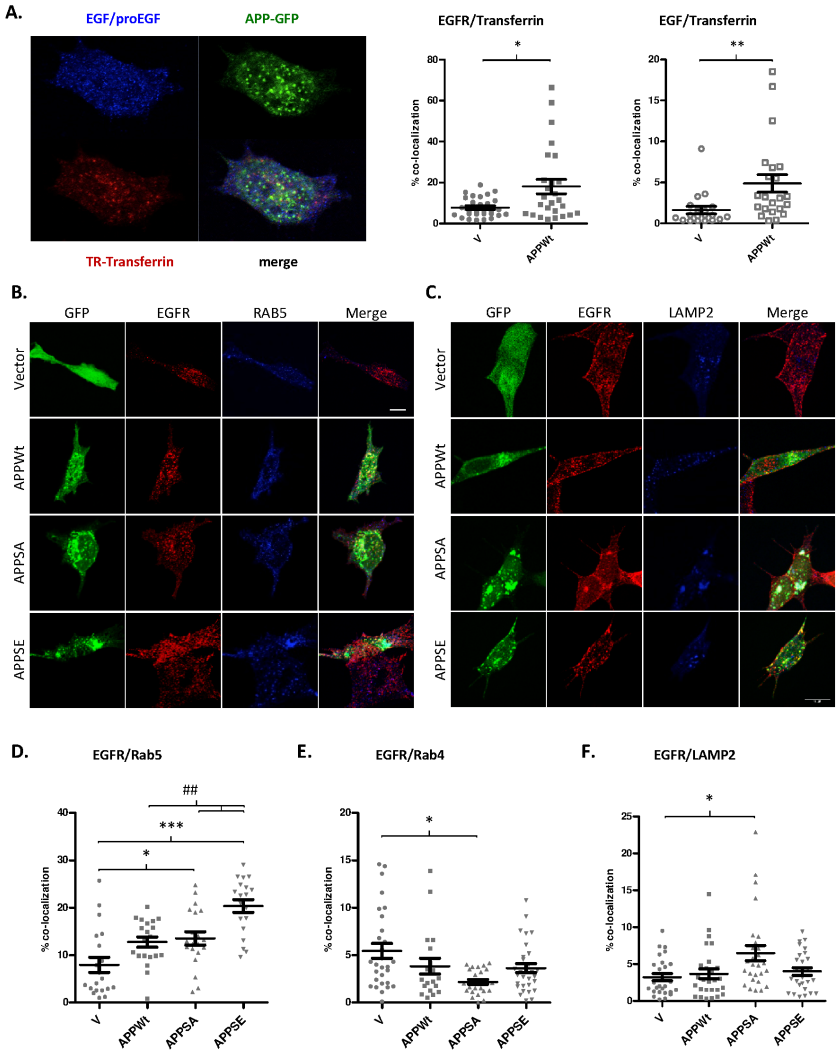

Figure B.11 - **APP modulates EGFR intracellular trafficking in a phosphoS655-APP dependent manner.** SH-SY5Y cells were transfected for 24h with the GFP empty vector ('V'), or different APP-GFP cDNAs: wild-type ('APP-Wt'), S655A mutant ('APP-SA'), S655E mutant ('APP-SE'). **A.** Co-localization of EGFR or EGF with Texas-Red (TR)-conjugated Transferrin following 15 min of TR-Transferrin incubation, when TR-Transferrin and its receptor are expected to be on the early endocytic route. n=30 and n=20 cells analyzed for each condition ('V' and 'APP-Wt') for the EGFR and the EGF groups, respectively. *p<0.05, ** p<0.01 by the Mann Whitney test (failed normality test). **B**. Representative microphotographs showing the co-localization of EGFR with the early endocytic marker Rab5 in APP-GFP transfected cells. **C.** Representative microphotographs showing the co-localization of EGFR with the lysosome marker LAMP2 in APP-GFP transfected cells. Represented images are maximum projections of the stack images used to calculate the percentage of colocalization between proteins. Scale bar, 10 µm. **D.** Percentage of EGFR colocalization with Rab5. n=20 cells analyzed per condition. * p<0.05 by one-way ANOVA followed by the Tukey's Multiple Comparison Test (data followed normal distribution). **E.** Percentage of EGFR colocalization with Rab4. n=20-30 cells analyzed per condition. * p<0.05 by Kruskal-Wallis test followed by the Dunn's Multiple Comparison Test (data failed normality test). **F**. Percentage of EGFR colocalization with LAMP2. n=30 cells analyzed per condition. * p<0.05 by Kruskal-Wallis test followed by the Dunn's Multiple Comparison Test (data failed normality test).

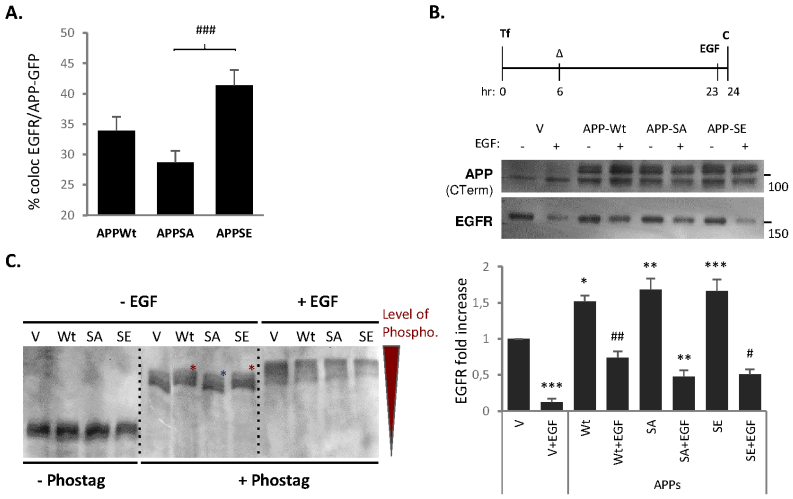

Figure B.12 - **APP overexpression reduces EGFR degradation induced by EGF stimulation.** SH-SY5Y cells were either transfected with the GFP empty vector ('V'), or the three APP-GFP cDNAs: wild-type ('APP-Wt'), S655A mutant ('APP-SA'), S655E mutant ('APP-SE'), for 24h. **A.** Co-localization of EGFR with the different APP-GFP proteins. n=80-90 cells analyzed per condition, from 3 independent assays. $^{###}$ $p < 0.001$ by Kruskal-Wallis test followed by the Dunn's Multiple Comparison Test. **B.** SH-SY5Y transfected cells were exposed to 100 ng/mL of hEGF for 1h in the indicated conditions, and immunoblots of cell lysates were probed with the anti-EGFR and the anti-APP C-terminal ('APP CT') antibodies. EGFR protein fold increase relative to control empty-vector ('V') was calculated. n=3-8. *$p < 0.05$, **$p < 0.01$, ***$p < 0.001$ against control condition 'V' (established as 1.0) by one-way ANOVA followed by the Dunnet's post-test. #$p < 0.05$, ## $p < 0.01$ against APP-Wt by one-way ANOVA followed by the Tukey's post-test. **C.** Analysis of the phosphorylation state of EGFR by the phos-tag SDS-PAGE assay, in the SH-SY5Y cells transfected with the APP-GFP cDNAs. Cell samples were loaded onto a normal SDS-PAGE gel ('- Phostag') or onto a phos-tag SDS-PAGE gel ('+ Phostag') gels. Phostag gels delay the migration of phosphorylated proteins, which appear in apparently higher molecular weight bands. In unstimulated cells, EGFR bands of APPWt and APPSE transfected cells (red asterisks) presented slightly delayed migrations, while in APPSA cells the EGFR bands did not (blue asterisks). n=3.

Together these data suggest that 1) All the APP-GFP species are able to retain EGFR molecules in Rab5-positive endosomes, retarding EGFR degradation, and thus increasing their levels; 2) APPSA increases EGFR targeting to LAMP2 vesicles destined to the degradation route, while APPWt and APPSE do not; 3) thus APPWt and APPSE might perpetuate more EGFR signalling in the sorting endosomes.

6.4.5. APP activates ERK1/2 in a S655 phosphorylation-dependent manner

Based on the previous trafficking results, and as APPWt overexpression enhanced EGF-induced ERK1/2 activation (Figure B.9), the levels of phosphorylated ERK (pERK) were quantified in SH-SY5Y cells overexpressing APPWt or its S655 phosphorylation mutants. The assay was performed in the presence (EGF stimulation) or absence (basal conditions) of EGF (Figure B.13).

In basal conditions, and as shown in Figure B.13 A and B, APPWt again increased pERK levels above vector transfected cells. Comparing to APPWt, the APP S655 dephosphomimimetic mutant ('APPSA') presents a significantly decreased pERK/total ERK ratio (Figure B.13 B right graph, APPSA vs APPWt). The phosphomimetic mutant ('APPSE'), however, is able to significantly increase pERK levels above the Wt species (Figure B.13 B, APPSE vs APPWt right graph).

Upon cells stimulation with EGF (Figure B.13 C, 'EGF stimulation' condition), APPWt overexpressing cells ('APPWt+EGF') significantly increases pERK activation when compared to vector transfected cells ('V+EGF'), confirming the previous Figure B.9F observations. This increased pERK stimulation above control V cells is not observed in cells overexpressing the APP S655A mutant ('APPSA+EGF'), while the phosphomimetic mutant ('APPSE+EGF') is able to further increase pERK levels. The same pattern is seen for the ratio between pERK and total ERK 1/2 protein levels (Figure B.13 C, 'pERK/ERK ratio').

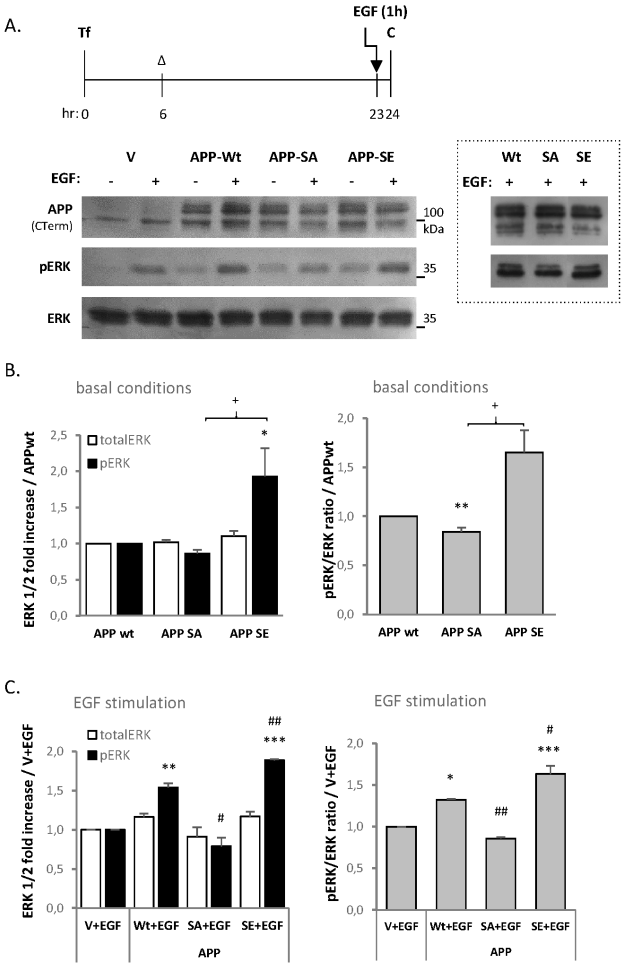

Figure B.13 - **APP increases ERK 1/2 activation in basal and EGF-stimulated conditions in a S655 phosphorylation- dependent manner. A.** SH-SY5Y cells were either transfected either with the GFP empty vector ('V'), the Wt or the S655 mutants APP-GFP cDNAs ('APP-Wt', 'APP-SA', 'APP-SE'). Before cell harvesting stimulated cells were exposed to 100 ng/mL of hEGF for 1 hr. Immunoblots of cell lysates were probed with the antibody for the APP C-terminal ('APP CTerm'), phospho-ERK1/2 ('pERK'), and total ERK 1/2 ('ERK'). Dashed square at the right: a blot corresponding to a different biological replicate of the blot in the left but with more similar levels of APP-SA and APP-SE transfection confirms an increased ERK1/2 activation for APP-SE. **B.** pERK and total ERK were plotted as fold increases of APP-Wt samples for the basal condition, since in some biological replicates their band could not be detected in empty-vector transfected cells. pERK/ERK ratio is shown on the right. n=9 independent assays. * $p<0.05$, ** $p<0.01$ against control condition 'APP-Wt' (established as 1.0) by one-way ANOVA followed by the Dunnet's post-test. + $p<0.05$ unpaired t-test (with Welch correction) to compare indicated conditions. **C.** pERK and total ERK were plotted as fold increases of empty vector samples for EGF-stimulated cells. pERK/ERK ratio is shown on the right. n=3 independent assays. * $p<0.05$, ** $p<0.01$, *** $p<0.001$ against control condition 'V+EGF' (established as 1.0) by one-way ANOVA followed by the Dunnet's post-test. # $p<0.05$, ## $p<0.01$ against APP-Wt by one-way ANOVA followed by the Tukey's post-test. Note that APP-SA is also significantly different from APP-SE ($p<0.001$).

Noteworthy, the induction of pERK1/2 signalling by APP overexpression was found to be equally sensitive to the EGFR inhibitor as vector transfected cells (~40% less pERK in the presence of the EGFR inhibitor) in this experimental design. The S655 phosphomimetic mutants were also sensitive to cells treatment with the EGFR inhibitor as the APPWt (Supplementary Figure B.5).

6.4.6. pS655 APP-induced ERK1/2 activation does not depend on pY682 APP

APP has been reported to interact with the adaptor proteins Grb2 and Shc, involved in linking tyrosine kinases receptors as EGFR to downstream Ras-MEK-ERK1/2 signalling [9]. The APP binding to Grb2 and Shc is dependent on APP Y682 phosphorylation. In order to understand the involvement of Grb2 and Shc binding in the APP-induced ERK activation, an (additional) point mutation - Tyrosine 682 to Phenylalanine (Y682F) - was introduced in the APP-GFP Wt, SA and SE cDNAs. In the case of the APPWt protein, the Y682F mutation indeed significantly reduces pERK levels (Figure B.14, 'YF' vs 'Wt' left graph), although it does not significantly change the pERK/ERK ratio (right graph). The combination of S655A and Y682F showed the lowest levels of both pERK and pERK/ERK ratio (Figure B.14, 'SAYF'), indicating this to be the APP species more dependent on pY682 phosphorylation. Surprisingly, the combination of S655E and Y682F does not decrease the levels of pERK, and also shows a tendency to slightly increase the pERK/ERK ratio (Figure B.14 right graph, 'SEYF' vs 'SE' and other conditions). These results suggest that APP phosphorylated at S655 (mimicked by the SE mutant) can bind by itself to the adaptor protein(s) or is using an alternative mechanism to induce ERK1/2 activation, other than via direct binding to Grb2 and Shc. We have also attempted to directly access the interaction of S655 phosphomutants with Grb2 and Shc, via pull-down of the GFP-moiety, but unfortunately we were not successful. However, we could observe in the immunoblots of the lysates that Grb2 and Shc levels are differently altered by the different APP S655 mutants (Supplementary Figure B.6). Further quantification showed that APPSA overexpression is associated with increased protein levels of Grb2 and Shc, while the APPSE does not affect the levels of both adaptor proteins (Supplementary Figure B.6).

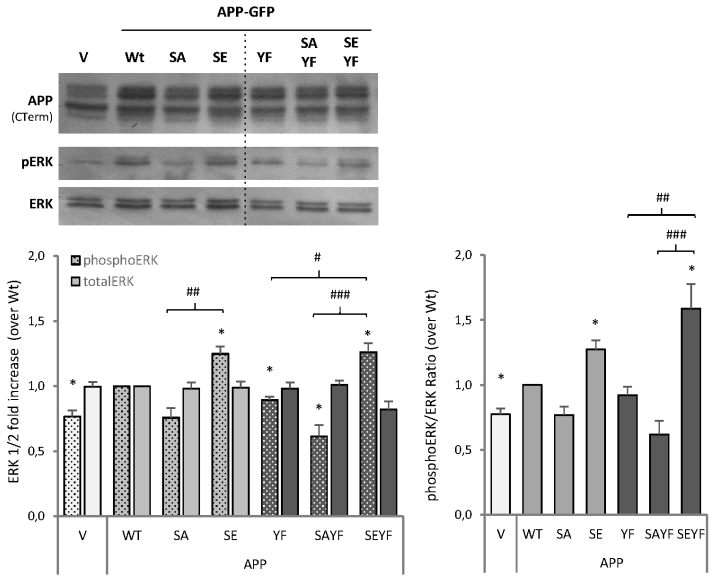

Figure B.14 - **APP S655E-induced ERK activation is not decreased by APP tyrosine 682 dephosphorylation.** SH-SY5Y cells were either 24h transfected with the GFP empty vector ('V'), or the APP-GFP cDNAs: wild-type ('Wt'), S655A mutant ('SA'), S655E mutant ('SE'), Y682F mutant ('YF'), or S655A and S655E double mutants additionally mutated in the APP tyrosine 682 to phenylalanine ('SAYF' and 'SEYF', respectively), to mimic Y682 constitutive dephosphorylation. Immunoblots of cell lysates were probed with the antibody for the APP C-terminal ('APP CTerm'), phospho-ERK1/2 ('pERK'), and total ERK 1/2 ('ERK'). pERK and total ERK were plotted as fold increases of APP-Wt samples. pERK/ERK ratio is shown on the right side. n=4 independent assays. * $p<0.05$ against control condition 'APP-Wt', established as 1.0, by one-way ANOVA followed by the Dunnet's post-test. Note that for the pERK/ERK ratio, APP-SA and APP-SAYF exhibited p-values =0.0542 and =0.053, respectively. # $p<0.05$, ## $p<0.01$, ### $p<0.001$ by one-way ANOVA followed by the Tukey's post-test. Note that for the phosphoERK levels in APP-SE and SEYF transfected cells were also significantly different from the empty vector 'V' cells ($p<0.01$); APP-SA from SEYF ($p<0.01$); APP-SE from YF ($p<0.05$) and from SAYF ($p<0.001$). Additionally, for the pERK/ERK ratio, APP-SEYF is also significantly different from the empty vector 'V' ($p<0.01$); APP-SA from SEYF ($p<0.01$); and APP-SE from SAYF ($p<0.001$).

6.4.7. APP and EGF-EGFR interplay in cortical neurons differentiation

Based on our results in the neuronal-like cell model, we pursued the interplay between APP and EGF-EGFR signaling in neuronal differentiation. Dissociated mouse cortical embryonic neurons were transfected at 5 days in vitro (DIV) with either the GFP empty vector or the APP-GFP cDNAs (APPWt, APPSA or APPSE), and incubated with EGF in the presence or absence of the EGFR inhibition up to 6 DIV.

In vector GFP control neurons, EGF stimulation ('GFP+EGF') or the inhibition of EGFR results in a slightly, not significant, increase in the number of primary neurites per neuron comparing to GFP alone, and the presence of the EGFR inhibitor blocks this increase (Figure B.15 A, and see Supplementary Figure B.7 A for representative tracings). Such tendency was translated by an increase in the number of dendrites (both primary dendrites and dendrite branches, Figure B.15 C and D), while the presence of the EGFR inhibitor abolishes this increase. Simultaneously, EGF tends to decrease the length of primary neurites (Figure B.15 B). The total length of the dendritic

tree does not change with EGF treatment, while it tends to decrease in the EGFR inhibitor condition (Figure B.15 E). Of note, EGF treatment of GFP-expressing neurons reduces axon length without affecting the number of axonal branches (Supplementary Figure B.7 B).

Looking now to the APP overexpressing neurons, in the absence of any other treatment APP overexpression tends to increase the number of primary neurites (Figure B.15 A), and the number of neurites branches (data not shown), while slightly decreasing their length (Figure B.15 B). The increase in the number of neurites appears to be dependent on the status of APP S655 phosphorylation since the APPSA dephosphomutant has similar values as the GFP expressing neurons, while APPSE is similar to APPWt (Figure B.15 A). Such behavior is translated to the number of dendrites, either primary dendrites or of its branches: APPWt and the SE phosphomimetic mutant tend to increase dendrites' number (when compared to GFP control neurons), while APPSA levels are similar to the GFP control (Figure B.15 C and D). These differences are maintained in the dendritic tree's total length (Figure B.15 E). Of note, all APPs similarly decrease the axon length (when compared to GFP), but APPWt and S655E do not induce alterations in axonal branching, while APPSA decreases all parameters related to axonal branching (Supplementary Figure B.7 B and C).

Intriguingly, APP overexpression in combination with the EGF treatment leads to a significant reduction in the number of neurites - primary neurites and neurites branches (Figure B.15 A and D). This decrease is translated to the number of dendrites– primary dendrites and dendritic branches (Figure B.15 C and D) – and axonal branches (Supplementary Figure B.7 B). In general, APPSA shows the highest decreases and APPSE was similar or less affected (for instance in primary neurites and primary dendrites) than APPWt. No major effects of APP overexpression combined with EGF was seen on the neurites' mean length (not shown), but in the presence of EGF, all APPs reduce even more the dendritic tree's total length (Figure B.15 E) and the axon's mean length (Supplementary Figure B.15 C), particularly APPSA. Such behavior was also seen for total axon length (data not shown).

The number of neurites - primary neurites and their branches - is reverted to APP "basal" levels by the presence of the EGFR inhibitor (Figure B.15 A, and data not shown). However, the mean length of primary neurites is significantly decreased when compared to non-EGF treated conditions (data not shown). Noteworthy, the sum length of neurite branches also shows some signs of "recovery" when compared to single treatment with EGF, with APPSE reverting to non-treated levels (Figure B.15 B). The number of dendrites (primary and branches) returns back to APP basal levels when the neurons were treated with both EGF and the EGFR inhibitor (Figure B.15 C and D); however, the dendritic tree total length does not recover (Figure B.15 E) since, in general, the dendrites' mean length tends to be smaller (data not shown). Of note, the axon length does not

seem to change, but the number of axonal branches increases in comparison to APPs combined with EGF (Supplementary Figure B.7 B and C).

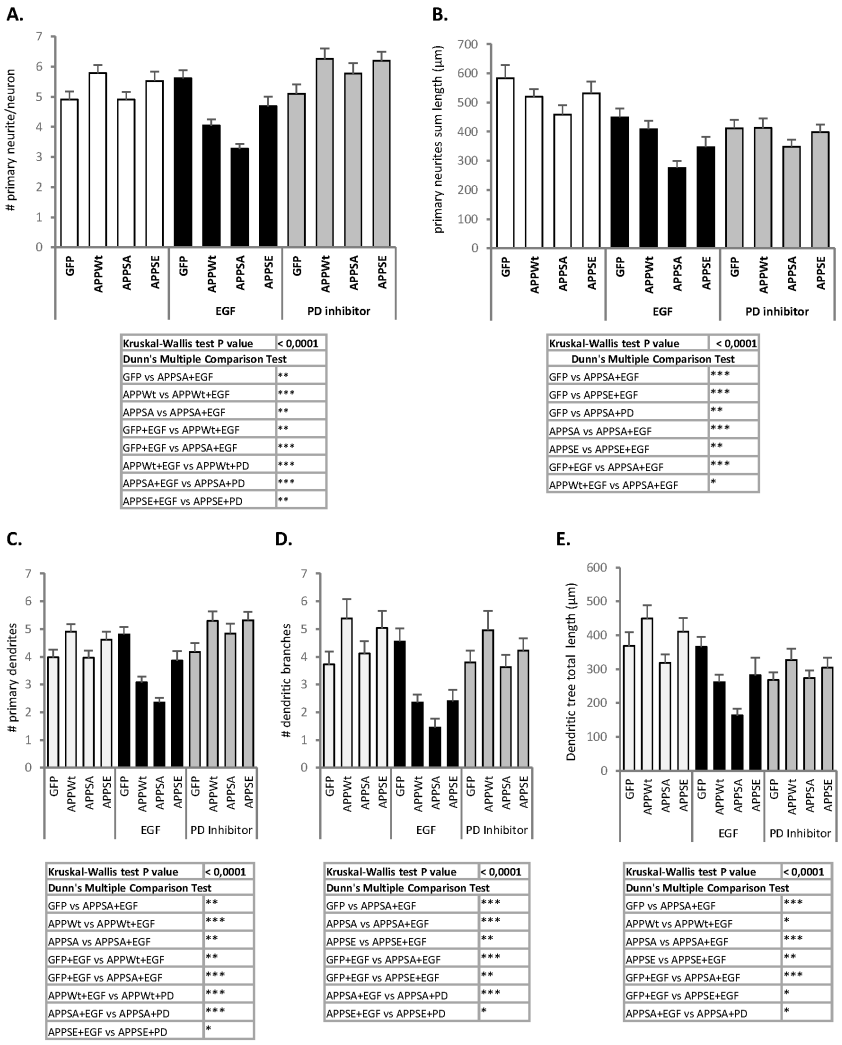

Kruskal-Wallis test P value	< 0,0001
Dunn's Multiple Comparison Test	
GFP vs APPSA+EGF	**
APPWt vs APPWt+EGF	***
APPSA vs APPSA+EGF	**
GFP+EGF vs APPWt+EGF	**
GFP+EGF vs APPSA+EGF	***
APPWt+EGF vs APPWt+PD	***
APPSA+EGF vs APPSA+PD	***
APPSE+EGF vs APPSE+PD	**

Kruskal-Wallis test P value	< 0,0001
Dunn's Multiple Comparison Test	
GFP vs APPSA+EGF	***
GFP vs APPSE+EGF	***
GFP vs APPSA+PD	**
APPSA vs APPSA+EGF	***
APPSE vs APPSE+EGF	**
GFP+EGF vs APPSA+EGF	***
APPWt+EGF vs APPSA+EGF	*

Kruskal-Wallis test P value	< 0,0001
Dunn's Multiple Comparison Test	
GFP vs APPSA+EGF	**
APPWt vs APPWt+EGF	***
APPSA vs APPSA+EGF	**
GFP+EGF vs APPWt+EGF	**
GFP+EGF vs APPSA+EGF	***
APPWt+EGF vs APPWt+PD	***
APPSA+EGF vs APPSA+PD	***
APPSE+EGF vs APPSE+PD	*

Kruskal-Wallis test P value	< 0,0001
Dunn's Multiple Comparison Test	
GFP vs APPSA+EGF	***
APPSA vs APPSA+EGF	***
APPSE vs APPSE+EGF	**
GFP+EGF vs APPSA+EGF	***
GFP+EGF vs APPSE+EGF	**
APPSA+EGF vs APPSA+PD	***
APPSE+EGF vs APPSE+PD	*

Kruskal-Wallis test P value	< 0,0001
Dunn's Multiple Comparison Test	
GFP vs APPSA+EGF	***
APPWt vs APPWt+EGF	*
APPSA vs APPSA+EGF	***
APPSE vs APPSE+EGF	**
GFP+EGF vs APPSA+EGF	***
GFP+EGF vs APPSE+EGF	*
APPSA+EGF vs APPSA+PD	*

Figure B.15 - **APP and EGF-EGFR signaling in mouse cortical neuronal differentiation.** Embryonic primary cortical neurons at 5 DIV were transfected with the GFP empty vector (GFP), or the APP-GFP cDNAs: wild-type ('APP-Wt'), S655A mutant ('APP-SA'), S655E mutant ('APP-SE'). A subset of cells was incubated with 100 ng/mL EGF after transfection medium change (21h of incubation before fixation), and a third group of cells was treated with the PD168393 EGFR inhibitor 3h before the same EGF stimulation treatment. Morphometric analyses of cortical primary neurons were performed: **A.** Number of primary neurites (neurites arising directly from the cell soma) per neuron. **B.** Primary neurites sum length per neuron. **C.** Number of primary dendrites (arising directly from the cell soma) per neuron. **D.** The number of dendrite branches (any branch arising from a primary dendrite) per neuron. **E.** Dendritic tree total length was calculated as the sum length of the primary dendrites and dendrite branches per neuron. n=50 neurons analyzed for each condition. * $p<0.05$, ** $p<0.01$, *** $p<0.001$ by the Kruskal-Wallis test followed by the Dunn's multicomparison post-test, as indicated in the table below each graph.

6.5. Discussion

APP and proEGF are both type 1 transmembrane glycoproteins, co-expressed in several tissues and cells, and display some functional overlap. Here we proved that APP and proEGF can form complexes, including in brain cortex (Figure B.8). Pull down of APP, either of the GFP moiety of exogenous APP-GFP or of endogenous APP, using anti-APP N-terminal antibody, co-immunoprecipitated different proEGF forms. This proEGF forms may derive from glycosylation on at least 10 glycosilation sites, and from alternative splicing, as 3 isoforms have already been described for proEGF. Furthermore, different molecular weight immunoreactive bands of proEGF in cell lysates, have been shown to result not only from different glycosylated forms but also from proEGF cleavage in the N-terminal distal part of the prodomain [50]. We believe that APP might interact with different forms of proEGF, that result in different immunoreactive bands after co-immunoprecitation depending on the cell type used, lysis buffer, loading buffer and gel conditions.

The existence of an APP-proEGF complex can meet existing models on the regulation of APP processing and signaling [51]. By one hand, we and others have shown that EGF stimulation induce the release of sAPP through activation of EGFR (Figure B.10 A), a mechanism that might be dependent on PKC activity and/or ERK1/2 activation [33, 52]. On the other hand, APP could be further modulated through direct interaction with a membrane-bound ligand, as proEGF, affecting e.g. the conformation of the intracellular domain of APP and APP affinity for interacting proteins, which in turn could alter APP localization and/or promote specific cleavage events of APP. Within the same rationale, APP interaction with proEGF could influence the cleavage of the membrane-bound ligand into EGF mature growth factor and modulate EGFR signaling events. We tested this hypothesis indirectly, by studying the proEGF protein levels on cell lysates and conditioning medium after 24h of APP overexpression. Although we could not detect significant changes on proEGF or soluble proEGF after APP overexpression, this hypothesis should not be excluded for different time scales, cell models, or *in vivo* systems. It would be very interesting to explore this situation and to test APP binding to other EGF-family growth factors.

Using the neuronal-like SH-SY5Y cell model, we proceed to test the existence of a functional interaction between APP and the growth factor EGF. No alteration in cell proliferation was found between EGF stimulated versus non-stimulated cells, either in APP transfected cells or control cells. It seems that in SH-SY5Y cells, the general described mitogenic effect of EGF does not occur. This is concordant with previous results showing unaltered cell proliferation after EGF treatment, either in the presence or absence of serum, in the same cell line [53]. EGF-stimulated cells tended to have higher number of cells comparing to the non-stimulated ones, but since there was no alteration in cell proliferation, EGF is most probably promoting cell survival.

Morphometric analyses of SH-SY5Y cells 24h after APP overexpression showed that the combination with EGF treatment accelerates neurite outgrowth, the emergence and elongation of cellular processes (Figure B.9). Combined treatment significantly increases the number of processes per cell (including of longer processes), and processes' mean length. Although APP alone is able to significantly increase the number of processes longer than 20 μm per cell comparing to control empty vector, APP combined with EGF increases the number of processes longer than 35 μm per cell above control, and above conditions of EGF treatment only and APP overexpression only. The neuronal-like differentiation induced by APP and EGF combined treatment was accompanied by an increase in ERK1/2 activation. Previous work has demonstrated that EGFR activation triggers neurite outgrowth of neuroblastoma cells potential via activation of the PI3K-Akt and MEK-ERK1/2 pathways [54, 55]. As expected, EGF treatment in the presence of EGFR inhibitor decreases all the parameters to similar or slightly below control empty vector levels. Interestingly, in APP overexpressing cells the presence of the EGFR inhibitor significantly decreases the number of >20 μm (and >35 μm) processes comparing to not only to the APP+EGF condition but also to the APP overexpression alone, suggesting that EGFR activation is implicated, at least partially, in the role played by APP in neurite outgrowth. Results on pERK/ERK ratio (and BIII-tubulin protein levels, data not shown) further support this conclusion.

The observed morphologic and signaling alterations seem to be accompanied by alterations in APP protein levels and in its processing. EGF stimulation significantly increases APP full-length protein levels and sAPP release, whereas previous EGFR inhibition blocked this effect. In APP overexpressing cells the protein levels of both total sAPP and sAPPalpha significantly decrease bellow control levels (APP transfection only) in the presence of the EGFR inhibitor. Others have shown that APP cleavage into sAPP is necessary for APP-induced neurite outgrowth [40, 56], and might be in part regulated by EGFR and ERK1/2 activation [52]. APP overexpression, here shown to activate ERK1/2 and to modulate EGFR protein levels, is suggestive of a positive-feedback pathway culminating in sAPP release, ERK1/2 activation and neurite outgrowth in SH-SY5Y cells.

Indeed, APP is able to increase the cellular levels of EGFR, potentially via a mechanism involving APP-EGFR binding and APP-induced altered EGFR trafficking. At steady state, when the majority of EGFR is expected to be unliganded, only a small percentage of EGFR are in transit in the endocytic pathway and, in general, are rapidly recycled back to the plasma membrane (PM). The constitutive internalization of the receptor establishes EGFR surface expression and its potential to signal when presented with ligand [57]. Upon EGF binding to EGFR, specific autophosphorylation sites recruit adaptor protein Grb2, which in turn brings SOS to interact with and activate Ras at the PM. Activates Ras initiates the RAF-MEK-ERK1/2 signaling cascade. Grb2 can additionally bind EGFR through Shc, also stimulating the Ras signaling pathway. Active EGFR can signal from the

PM and from endosomes, since endocytic trafficking might be required for optimal activity of some signal transducers and to propagate specific signals. Thus, the duration and intensity of the EGFR-ERK1/2 signaling can be modulated by receptor expression levels at the PM, by its endocytic trafficking, and by its subsequent fate: recycling or degradation [30, 49]. Here we show that APP overexpression increases the protein levels of EGFR in basal conditions, and partially impairs the usual downregulation of the EGFR protein after EGF-stimulation. This particular effect of APP seems independent of S655 phosphorylation and sAPP levels. Additionally, we have shown that APP interacts with EGFR, and that endogenous EGFR colocalizes with APP-GFP in cytoplasmic vesicles. APP interaction with a chimeric EGFR molecule was shown by Petschnigg et al., and the interaction seems to be stronger with phosphorylated EGFR, as demonstrated using a constitutive kinase active EGFR chimera mutant [58]. Importantly, we proved that APP impacts on EGFR trafficking, and subsequently in its levels, fate, active state, and signaling rate. At steady state most of the EGFR should be at the cell surface, but APP overexpression relocates EGFR molecules to early endosomes. This is demonstrated by the higher percentage of EGFR (and EGF) colocalization with Texas Red-Transferrin and with Rab5, in APP transfected cells. Accordingly, recent reports show that APP interacts with the Rab5 binding protein APP-BP1, and with the Rab5 effector APPL1, and that APP up-regulation can induce Rab5 over-activation and thus accelerates endocytosis [59, 60].

We have also demonstrated that particular events of the EGFR intracellular trafficking might be differentially affected by the APP S655 phosphorylation status. S655 phosphorylation, at the APP's functional motif YTSI, has been previously shown to regulate APP's endocytic route and fate. Specifically, the S655A dephosphomimetic mutant ('SA') is less endocytosed, while the S655E phosphomimetic mutant ('SE') presents slightly higher rate of membranar endocytosis and increased recycling (higher rate of traffic between the TGN and the PM). APPSA-containing vesicles are more targeted towards lysosomes, while APP phosphorylation at S655 partially rescues APP from degradation [4, 5]. This APP phosphorylation site also promotes sAPP release, and data from our group suggests it might be implicated in neuronal differentiation ([61], Dias R et al, submitted). Results here gathered indicate that, in general, all the three APP species used increased EGFR colocalization with the early endocytic marker Rab5, and all increased total EGFR protein levels over vector-transfected cells, even in EGF stimulation conditions. However, the fate of the increased half-lived EGFR protein may be different. While APPSE showed the highest colocalization with EGFR and the highest increase of EGFR colocalization with Rab5, APPSA increased the presence of EGFR in LAMP2-positive vesicles and fail to increase the total level of EGFR phosphorylation above vector-transfected cells as APPWt and APPSE appear to do (PhosTag gel at basal conditions, see Figure B.11 and Figure B.12).

Mechanisms that increase the duration of pEGFR and/or slow EGFR degradation might shift ERK1/2 signal from transient to sustained activation and promote neuronal differentiation in response to EGF [62-64]. Such behaviour might thus be favoured by APP phosphorylation at S655, while APP S655 dephosphorylation seems to promote EGFR inactivation and late endosomes/lysosomal targeting. Indeed, when at the sorting early endosome, EGFR can be targeted to recycling to the PM via Rab11-positive vesicles, or be targeted to intraluminal vesicles (ILV) of multivesicular bodies (MVB). This later occurs upon ubiquitinated EGFR recognition by the 'endosomal sorting complexes required for transport' (ESCRT) machinery, but requires prior receptor deubiquitination. Sorting onto ILVs already physically removes the tyrosine kinase domain from cytosolic substrates, and is followed by fusion with lysosomes, for cargo degradation [49, 65]. In the face of similar percentage of EGFR colocalization with LAMP2 and Rab4 for APPSE as for APPWt, but higher percentage of EGFR colocalization with Rab5 and increased ERK signal promotion (discussed below) for APPSE, the hypothesis that APPSE increases EGFR residence in the endosomal outer membrane and diverts EGFR from being sorted into ILV during MVB formation, gains some evidence.

APPSA, by its turn, would increase EGFR sorting into MVB and ILV, for subsequent lysosome targeting and degradation. Accordingly, MVB/late endosomes can already present the LAMP2 marker and APPSA showed increased EGFR colocalization with the late endosome/lysosome LAMP2. The fact that our immunoblot results showed impaired EGFR degradation for all APP species might indicate decreased EGFR de/ubiquitination, impaired sorting into ILVs, and/or delayed MVB maturation into/fusion with lysosome. The impairment of lysosome function and accumulation of endocytic cargos within enlarged late endosomes is consistently described to follow the APP-induced Rab5 over-activation and accelerated endocytosis [59, 60]. We also hypothesize that APP interaction with APPL1, a downstream effector of EGF-EGFR signaling that impairs EGF-induced EGFR lysosomal degradation when overexpressed, stabilizes both APPL1 and EGFR proteins in early and late endosomes [66]. Alternatively, APP might regulate EGFR ubiquitination and targeting to degradation via Grb2 interaction, since Grb2 mediates EGFR binding to the ubiquitin-protein ligase CBL [30]. APP might also influence receptor ubiquitination by binding to the described CBL inhibitors lipoprotein receptor-related protein LRP1 and/or the tyrosine kinase c-Src [9, 67, 68].

The deubiquitination of EGFR, necessary to occur prior translocation into the ILVs, might also be modulated by APP interaction with the deubiquitinating enzyme UCH-L1 [69]. Of note, in neurons from the Swedish mutant APP transgenic mice, increased intracellular abeta was linked to decreased UCH-L1 and proteasome activity, and consequently impaired degradation of EGFR following EGF stimulation [34].

Consistent with increased level of total EGFR phosphorylation, APPSE was observed to particularly increase signalling downstream EGFR. ERK1/2 signalling, resulting from EGFR and other growth factors signalling, is crucial for cortical development. Specific ERK1/2 functions seem to include the control of cortical neural progenitor proliferation, fate determination, and differentiation [70]. Abnormally diminished ERK activity, early in cortical development, significantly impact cortical cytoarchitecture due to alterations in the cellular composition of the postnatal cortex, and abnormal axon length and dendritic arborisation [71]. Here we show that combined APP overexpression and EGF treatment results in amplified ERK1/2 activation in an APP S655 phosphorylation- dependent manner. APP phosphomimicking mutant, S655E, is associated with increased ERK activation either in basal or EGF-stimulated conditions, while the dephosphomimicking mutant, S655A, has similar levels of ERK activation to control cells (Figure B.13). Since, phosphorylation of Y682, located at the YENPTY motif of APP cytodomain, mediates APP binding to adaptor proteins Shc and Grb2, linking APP to theERK1/2 signalling pathway [9], we further analysed its role in S655E-mediated ERK1/2 activation. Opposing this hypothesis, an APP double mutant, constitutively dephosphorylated at Y682 in association with the S655E mutation, failed to decrease ERK activation (Figure B.14). Results suggest that APP phosphorylated at S655 could be using a different mechanism for ERK1/2 activation, other than via direct recruitment of Grb2 and Shc. Curiously, APPSE overexpression leads to decreased protein levels of endogenous Grb2 and Shc, while APPSA show increased levels of these proteins.

Under different cellular contexts, specific APP phosphorylation events could modulate compartmentalization and duration of phosphoERK1/2 signalling to achieve specific outcomes [72, 73]. For instance, Y682 phosphorylation of full-length APP molecules might promote direct binding to Grb2 and link ERK activation to cell proliferation. On the other hand, upon apoptotic stimulus, ERK activation seems to result from Y682 phosphorylated APP-CTFs that complex with both Shc and Grb2, a situation that might occur in AD [74-76]. In the case of S655 phosphorylation, APP could be channelling ERK1/2 activation to neuronal differentiation events. This might involve binding to different ERK scaffolds or the modulation of receptor tyrosine kinases, like the here proposed EGFR.

In order to analyze a role for APP phosphorylation and EGF in neuronal differentiation, cultured cortical neurons were used. These are described to express EGFR, and it has been shown that EGF stimulates survival and neurite outgrowth of rat cerebral cortical neurons [77]. More recently, EFG was shown to stimulate axon extension of mouse spinal cord neurons during development [78]. Our results show that, in general, EGF treatment increases the number of dendrites (primary and branches) without changing the total dendritic tree length. The EGFR inhibitor blocks the effect of EGF on dendrites number. Furthermore, in apparently EGF stimulation-independent effects, EGFR

inhibition 1) tends to decrease the total length of the dendritic tree, potentially via diminished dendrites' mean length; and 2) tended to increase the number of axonal branches. Similar results were presented by others and related to impaired axonal pruning [79], and might implicate other EGFR family member(s) since the inhibitor used can also suppress the kinase activity of erbB2 and erbB4 [80].

Both EGF and EGFR inhibitor slightly decreased the axon length, suggesting that promotion of the number of dendrites and of axonal branches are events that impair axon elongation.

APPs overexpression, particularly of APPWt and APPSE, mainly increases the number of primary neurites and neurite branches. These mainly translate to increases in the number of primary dendrites and dendritic branches, in a S655 phosphorylation-dependent manner, with no apparent alteration in the number of axonal branches. Of note, APP overexpression, independently of S655 phosphorylation, also tended to decrease the mean length of primary neurites (including the axon), although with no alteration in the mean length of the neurites' branches.

Intriguingly, APP overexpression in combination with EGF treatment led to a significant reduction in the number of primary neurites and neurite branches, although with a notorious dependency on the APP S655 phosphorylation state. The number of primary neurites and neurite branches per neuron is reverted to APP "basal" levels in the presence of the EGFR inhibitor. In general, there were no major effects of APP combined with EGF on neurites' mean length, but combined treatment reduced markedly the axon's mean length.

In summary, APPWt and APPSE contribute to dendritogenesis, while APPSA does not. The surprisingly decreased number of neurites for APP overexpression in combination with EGF, brought to our attention that in cortical primary cultures both effects might involve mutually exclusive signaling pathways, or the resulting increase in signaling might reach a limit from which it is detrimental for neurite outgrowth, an idea explored in other reports [26, 81]. Furthermore, the quality and duration of the signaling generated by the combination of APP and EGF might be promoting a different output, i.e. neural progenitor's proliferation and/or cell survival [82]. This is consistent with our observations that EGF treatment always led to more GFP expressing neurons per visual field, while the presence of the EGFR inhibitor was more associated with GFP expressing neurons showing signs of degeneration.

6.6. References

1. Nhan, H.S., K. Chiang, and E.H. Koo, *The multifaceted nature of amyloid precursor protein and its proteolytic fragments: friends and foes.* Acta Neuropathol, 2015. **129**(1): p. 1-19.
2. Lichtenthaler, S.F., C. Haass, and H. Steiner, *Regulated intramembrane proteolysis--lessons from amyloid precursor protein processing.* J Neurochem, 2011. **117**(5): p. 779-96.
3. Muresan, Z. and V. Muresan, *The amyloid-beta precursor protein is phosphorylated via distinct pathways during differentiation, mitosis, stress, and degeneration.* Mol Biol Cell, 2007. **18**(10): p. 3835-44.
4. Vieira, S., et al., *Retrieval of the Alzheimer's amyloid precursor protein from the endosome to the TGN is S655 phosphorylation state-dependent and retromer-mediated.* Molecular Neurodegeneration, 2010. **5**(1): p. 40.
5. Vieira, S., et al., *S655 phosphorylation enhances APP secretory traffic.* Molecular and Cellular Biochemistry, 2009. **328**(1): p. 145-154.
6. Rebelo, S., et al., *Tyr687 dependent APP endocytosis and Abeta production.* J Mol Neurosci, 2007. **32**(1): p. 1-8.
7. Pastorino, L., et al., *The prolyl isomerase Pin1 regulates amyloid precursor protein processing and amyloid-beta production.* Nature, 2006. **440**(7083): p. 528-34.
8. Barbagallo, A.P., et al., *Tyr(682) in the intracellular domain of APP regulates amyloidogenic APP processing in vivo.* PLoS One, 2010. **5**(11): p. e15503.
9. Tamayev, R., D. Zhou, and L. D'Adamio, *The interactome of the amyloid beta precursor protein family members is shaped by phosphorylation of their intracellular domains.* Mol Neurodegener, 2009. **4**: p. 28.
10. Small, S.A. and S. Gandy, *Sorting through the Cell Biology of Alzheimer's Disease: Intracellular Pathways to Pathogenesis.* 2006. **52**(1): p. 15-31.
11. Westmark, C.J., *What/'s hAPPening at synapses[quest] The role of amyloid [beta]-protein precursor and [beta]-amyloid in neurological disorders.* Mol Psychiatry, 2013. **18**(4): p. 425-434.
12. Muller, U.C. and H. Zheng, *Physiological functions of APP family proteins.* Cold Spring Harb Perspect Med, 2012. **2**(2): p. a006288.
13. Demars, M.P., et al., *Soluble amyloid precursor protein: a novel proliferation factor of adult progenitor cells of ectodermal and mesodermal origin.* Stem Cell Res Ther, 2011. **2**(4): p. 36.
14. Young-Pearse, T.L., et al., *A critical function for beta-amyloid precursor protein in neuronal migration revealed by in utero RNA interference.* J Neurosci, 2007. **27**(52): p. 14459-69.
15. Hoe, H.S., et al., *Interaction of reelin with amyloid precursor protein promotes neurite outgrowth.* J Neurosci, 2009. **29**(23): p. 7459-73.
16. Sosa, L.J., et al., *Amyloid precursor protein is an autonomous growth cone adhesion molecule engaged in contact guidance.* PLoS One, 2013. **8**(5): p. e64521.
17. Tyan, S.H., et al., *Amyloid precursor protein (APP) regulates synaptic structure and function.* Mol Cell Neurosci, 2012. **51**(1-2): p. 43-52.
18. Weyer, S.W., et al., *APP and APLP2 are essential at PNS and CNS synapses for transmission, spatial learning and LTP.* EMBO J, 2011. **30**(11): p. 2266-80.
19. G Carpenter, a. and S. Cohen, *Epidermal Growth Factor.* Annual Review of Biochemistry, 1979. **48**(1): p. 193-216.
20. Zeng, F. and R.C. Harris, *Epidermal growth factor, from gene organization to bedside.* Semin Cell Dev Biol, 2014. **28**: p. 2-11.
21. Parries, G., et al., *The human urinary epidermal growth factor (EGF) precursor. Isolation of a biologically active 160-kilodalton heparin-binding pro-EGF with a truncated carboxyl terminus.* J Biol Chem, 1995. **270**(46): p. 27954-60.
22. Nelson, A.D., M. Suzuki, and C.N. Svendsen, *A high concentration of epidermal growth factor increases the growth and survival of neurogenic radial glial cells within human neurosphere cultures.* Stem Cells, 2008. **26**(2): p. 348-55.
23. Yamada, M., T. Ikeuchi, and H. Hatanaka, *The neurotrophic action and signalling of epidermal growth factor.* Prog Neurobiol, 1997. **51**(1): p. 19-37.
24. Abe, Y., H. Nawa, and H. Namba, *Activation of epidermal growth factor receptor ErbB1 attenuates inhibitory synaptic development in mouse dentate gyrus.* Neurosci Res, 2009. **63**(2): p. 138-48.
25. Wagner, B., et al., *Neuronal survival depends on EGFR signaling in cortical but not midbrain astrocytes.* EMBO J, 2006. **25**(4): p. 752-62.

26. Caric, D., et al., *EGFRs mediate chemotactic migration in the developing telencephalon.* Development, 2001. **128**(21): p. 4203-16.
27. Siddiqui, S., et al., *Central role of the EGF receptor in neurometabolic aging.* Int J Endocrinol, 2012. **2012**: p. 739428.
28. Oda, K., et al., *A comprehensive pathway map of epidermal growth factor receptor signaling.* Mol Syst Biol, 2005. **1**: p. 2005 0010.
29. Di Guglielmo, G.M., et al., *Compartmentalization of SHC, GRB2 and mSOS, and hyperphosphorylation of Raf-1 by EGF but not insulin in liver parenchyma.* EMBO J, 1994. **13**(18): p. 4269-77.
30. Goh, L.K., et al., *Multiple mechanisms collectively regulate clathrin-mediated endocytosis of the epidermal growth factor receptor.* J Cell Biol, 2010. **189**(5): p. 871-83.
31. Roepstorff, K., et al., *Differential effects of EGFR ligands on endocytic sorting of the receptor.* Traffic, 2009. **10**(8): p. 1115-27.
32. Refolo, L.M., et al., *Nerve and epidermal growth factors induce the release of the Alzheimer amyloid precursor from PC 12 cell cultures.* Biochem Biophys Res Commun, 1989. **164**(2): p. 664-70.
33. Slack, B.E., et al., *Rapid stimulation of amyloid precursor protein release by epidermal growth factor: role of protein kinase C.* Biochem J, 1997. **327 (Pt 1)**: p. 245-9.
34. Almeida, C.G., R.H. Takahashi, and G.K. Gouras, *Beta-amyloid accumulation impairs multivesicular body sorting by inhibiting the ubiquitin-proteasome system.* J Neurosci, 2006. **26**(16): p. 4277-88.
35. Zhang, Y.W., et al., *Presenilin/gamma-secretase-dependent processing of beta-amyloid precursor protein regulates EGF receptor expression.* Proc Natl Acad Sci U S A, 2007. **104**(25): p. 10613-8.
36. da Cruz, E.S.O.A., et al., *A model system to study intracellular trafficking and processing of the Alzheimer's amyloid precursor protein.* Neurodegener Dis, 2004. **1**(4-5): p. 196-204.
37. Martins, F., et al., *BRI2 and BRI3 are functionally distinct phosphoproteins.* Cell Signal, 2016. **28**(1): p. 130-44.
38. Zheng, Y., et al., *Temporal regulation of EGF signalling networks by the scaffold protein Shc1.* Nature, 2013. **499**(7457): p. 166-71.
39. Bolte, S. and F.P. Cordelieres, *A guided tour into subcellular colocalization analysis in light microscopy.* J Microsc, 2006. **224**(Pt 3): p. 213-32.
40. da Rocha, J.F., O.A. da Cruz e Silva, and S.I. Vieira, *Analysis of the amyloid precursor protein role in neuritogenesis reveals a biphasic SH-SY5Y neuronal cell differentiation model.* J Neurochem, 2015. **134**(2): p. 288-301.
41. Meijering, E., *Neuron tracing in perspective.* Cytometry A, 2010. **77**(7): p. 693-704.
42. Popko, J., et al., *Automated analysis of NeuronJ tracing data.* Cytometry A, 2009. **75**(4): p. 371-6.
43. Coombs, J., et al., *Morphological properties of mouse retinal ganglion cells.* Neuroscience, 2006. **140**(1): p. 123-36.
44. Romero-Calvo, I., et al., *Reversible Ponceau staining as a loading control alternative to actin in Western blots.* Anal Biochem, 2010. **401**(2): p. 318-20.
45. Farmer, S.R., et al., *Regulation of actin mRNA levels and translation responds to changes in cell configuration.* Mol Cell Biol, 1983. **3**(2): p. 182-9.
46. Dittmer, A. and J. Dittmer, *Beta-actin is not a reliable loading control in Western blot analysis.* Electrophoresis, 2006. **27**(14): p. 2844-5.
47. Castaño, Z. and R.M. Kypta, *Housekeeping Proteins: Limitations as References During Neuronal Differentiation* The Open Neuroscience Journal, 2008. **2**: p. 36-40.
48. Turner, P.R., et al., *Roles of amyloid precursor protein and its fragments in regulating neural activity, plasticity and memory.* Progress in Neurobiology, 2003. **70**(1): p. 1-32.
49. Tomas, A., C.E. Futter, and E.R. Eden, *EGF receptor trafficking: consequences for signaling and cancer.* Trends Cell Biol, 2014. **24**(1): p. 26-34.
50. Le Gall, S.M., et al., *Regulated cell surface pro-EGF ectodomain shedding is a zinc metalloprotease-dependent process.* J Biol Chem, 2003. **278**(46): p. 45255-68.
51. Jacobsen, K.T. and K. Iverfeldt, *Amyloid precursor protein and its homologues: a family of proteolysis-dependent receptors.* Cell Mol Life Sci, 2009. **66**(14): p. 2299-318.
52. Mills, J., et al., *Regulation of amyloid precursor protein catabolism involves the mitogen-activated protein kinase signal transduction pathway.* J Neurosci, 1997. **17**(24): p. 9415-22.
53. da Motta, L.A., et al., *Effects of epidermal growth factor on the [3H]-thymidine uptake in the SK-N-SH and SH-SY5Y human neuroblastoma cell lines.* Arq Neuropsiquiatr, 1997. **55**(3A): p. 444-51.

54. Evangelopoulos, M.E., J. Weis, and A. Kruttgen, *Signalling pathways leading to neuroblastoma differentiation after serum withdrawal: HDL blocks neuroblastoma differentiation by inhibition of EGFR.* Oncogene, 2005. **24**(20): p. 3309-18.
55. Evangelopoulos, M.E., J. Weis, and A. Kruttgen, *Mevastatin-induced neurite outgrowth of neuroblastoma cells via activation of EGFR.* J Neurosci Res, 2009. **87**(9): p. 2138-44.
56. Young-Pearse, T., et al., *Secreted APP regulates the function of full-length APP in neurite outgrowth through interaction with integrin beta1.* Neural Development, 2008. **3**(1): p. 15.
57. Rush, J.S. and B.P. Ceresa, *RAB7 and TSG101 are required for the constitutive recycling of unliganded EGFRs via distinct mechanisms.* Molecular and Cellular Endocrinology, 2013. **381**(1–2): p. 188-197.
58. Petschnigg, J., et al., *The mammalian-membrane two-hybrid assay (MaMTH) for probing membrane-protein interactions in human cells.* Nat Meth, 2014. **11**(5): p. 585-592.
59. Laifenfeld, D., et al., *Rab5 mediates an amyloid precursor protein signaling pathway that leads to apoptosis.* J Neurosci, 2007. **27**(27): p. 7141-53.
60. Kim, S., et al., *Evidence that the rab5 effector APPL1 mediates APP-betaCTF-induced dysfunction of endosomes in Down syndrome and Alzheimer's disease.* Mol Psychiatry, 2016. **21**(5): p. 707-16.
61. Rocha, J.F., S.I. Vieira, and O.A.B.d.C.e. Silva, *APP Phosphorylation at S655 Correlates with F-actin Cytoskeleton Dynamics—Relevance in Neuronal Differentiation.* Microscopy and Microanalysis, 2012. **18**(SupplementS5): p. 57-58.
62. Marshall, C.J., *Specificity of receptor tyrosine kinase signaling: transient versus sustained extracellular signal-regulated kinase activation.* Cell, 1995. **80**(2): p. 179-85.
63. Traverse, S., et al., *EGF triggers neuronal differentiation of PC12 cells that overexpress the EGF receptor.* Curr Biol, 1994. **4**(8): p. 694-701.
64. Takebayashi, M., T. Hayashi, and T.P. Su, *Sigma-1 receptors potentiate epidermal growth factor signaling towards neuritogenesis in PC12 cells: potential relation to lipid raft reconstitution.* Synapse, 2004. **53**(2): p. 90-103.
65. Haglund, K. and I. Dikic, *The role of ubiquitylation in receptor endocytosis and endosomal sorting.* Journal of Cell Science, 2012. **125**(2): p. 265-275.
66. Lee, J.R., et al., *Adaptor protein containing PH domain, PTB domain and leucine zipper (APPL1) regulates the protein level of EGFR by modulating its trafficking.* Biochem Biophys Res Commun, 2011. **415**(1): p. 206-11.
67. Donepudi, M. and M.D. Resh, *c-Src trafficking and co-localization with the EGF receptor promotes EGF ligand-independent EGF receptor activation and signaling.* Cell Signal, 2008. **20**(7): p. 1359-67.
68. Takayama, Y., et al., *Low density lipoprotein receptor-related protein 1 (LRP1) controls endocytosis and c-CBL-mediated ubiquitination of the platelet-derived growth factor receptor beta (PDGFR beta).* J Biol Chem, 2005. **280**(18): p. 18504-10.
69. Cottrell, B.A., et al., *A Pilot Proteomic Study of Amyloid Precursor Interactors in Alzheimer's Disease.* Annals of neurology, 2005. **58**(2): p. 277-289.
70. Samuels, I.S., S.C. Saitta, and G.E. Landreth, *MAP'ing CNS Development and Cognition: an ERKsome process.* Neuron, 2009. **61**(2): p. 160-167.
71. Pucilowska, J., et al., *Disrupted ERK Signaling during Cortical Development Leads to Abnormal Progenitor Proliferation, Neuronal and Network Excitability and Behavior, Modeling Human Neuro-Cardio-Facial-Cutaneous and Related Syndromes.* The Journal of Neuroscience, 2012. **32**(25): p. 8663-8677.
72. Ishii, A., et al., *Strength of ERK1/2 MAPK Activation Determines Its Effect on Myelin and Axonal Integrity in the Adult CNS.* J Neurosci, 2016. **36**(24): p. 6471-87.
73. Wainstein, E. and R. Seger, *The dynamic subcellular localization of ERK: mechanisms of translocation and role in various organelles.* Curr Opin Cell Biol, 2016. **39**: p. 15-20.
74. Russo, C., et al., *Signal transduction through tyrosine-phosphorylated C-terminal fragments of amyloid precursor protein via an enhanced interaction with Shc/Grb2 adaptor proteins in reactive astrocytes of Alzheimer's disease brain.* J Biol Chem, 2002. **277**(38): p. 35282-8.
75. Venezia, V., et al., *Apoptotic cell death and amyloid precursor protein signaling in neuroblastoma SH-SY5Y cells.* Ann N Y Acad Sci, 2004. **1030**: p. 339-47.
76. Nizzari, M., et al., *Amyloid precursor protein and Presenilin1 interact with the adaptor GRB2 and modulate ERK 1,2 signaling.* J Biol Chem, 2007. **282**(18): p. 13833-44.
77. Kornblum, H.I., et al., *Epidermal growth factor and basic fibroblast growth factor: effects on an overlapping population of neocortical neurons in vitro.* Brain Res, 1990. **535**(2): p. 255-63.

78. Tsai, N.P., et al., *Kappa opioid receptor contributes to EGF-stimulated neurite extension in development.* Proc Natl Acad Sci U S A, 2010. **107**(7): p. 3216-21.
79. Zschatzsch, M., et al., *Regulation of branching dynamics by axon-intrinsic asymmetries in Tyrosine Kinase Receptor signaling.* Elife, 2014. **3**: p. e01699.
80. Fry, D.W., et al., *Specific, irreversible inactivation of the epidermal growth factor receptor and erbB2, by a new class of tyrosine kinase inhibitor.* Proc Natl Acad Sci U S A, 1998. **95**(20): p. 12022-7.
81. Duchek, P. and P. Rorth, *Guidance of cell migration by EGF receptor signaling during Drosophila oogenesis.* Science, 2001. **291**(5501): p. 131-3.
82. Ayuso-Sacido, A., et al., *Activated EGFR signaling increases proliferation, survival, and migration and blocks neuronal differentiation in post-natal neural stem cells.* J Neurooncol, 2010. **97**(3): p. 323-37.

6.7. Supplementary Data

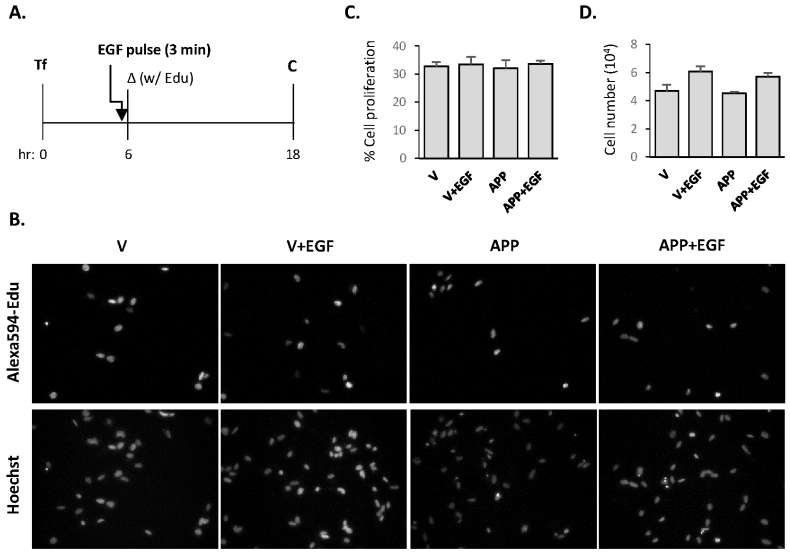

Supplementary Figure B.4 - **Effect of EGF and APP on SH-SY5Y cell proliferation and survival.** SH-SY5Y cells were either transfected with the GFP empty vector ('V') or wild-type APP-GFP cDNA ('APP'), exposed or not for 3 min to 100 ng/mL human recombinant EGF ('V+EGF' and 'APP+EGF'). n=3 independent assays. **A.** Experimental approach schematics. **B.** Representative epifluorescence microphotographs of cells tested with the Click-iT® EdU Alexa Fluor® imaging kit. **C.** Percentage of cell proliferation was calculated by scoring the number of EdU Alexa Fluor® 594 positive cells versus the total number of Hoechst 33342 positive cells. **D.** Total cell number - the number of cells (Hoechst positive) was scored.

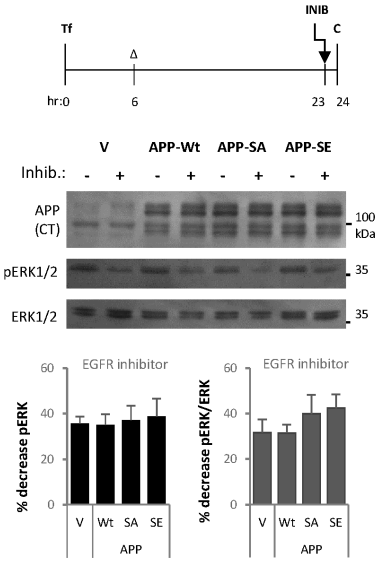

Supplementary Figure B.5 - **EGFR inhibition reduces ERK activation independently of the transfected APP species**. SH-SY5Y cells were either 24h transfected with the GFP empty vector ('V'), or the APP-GFP cDNAs: wild-type ('APP-Wt'), S655A mutant ('APP-SA'), S655E mutant ('APP-SE'). Before cell harvesting the treatment group was exposed for 10 µM EGFR inhibitor PD168393 for 1 hour. Immunoblots of cell lysates were probed with the antibody for the APP C-terminal, phospho-ERK1/2 ('pERK'), and total ERK 1/2 ('ERK'). Of note, all the lanes are from the same blot but were rearranged into the present order. The percentage of decrease in the pERK protein levels and pERK/ERK ratio was calculated in relation to the corresponding cDNA in non-EGFR Inhibitor treated conditions.

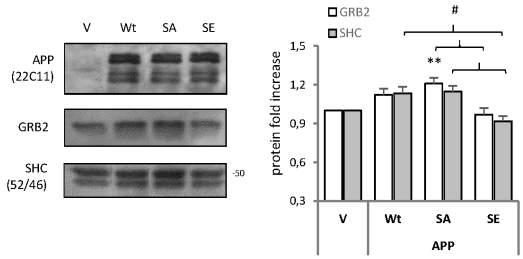

Supplementary Figure B.6 - **S655 APP phosphorylation and the levels of the adaptor proteins Grb2 and Shc**. SH-SY5Y cells were transiently overexpressing the empty GFP vector (V) or the APP-GFP cDNAs: wild-type ('Wt'), S655A mutant ('SA'), S655E mutant ('SE'). Immunoblots of cell lysates were probed with the antibodies for the adaptor proteins GRB2 and SHC, and their protein levels plotted as fold increases of empty vector lysates ('V'). n=6. ** $p<0.01$ against control condition 'V', established as 1.0, by one-way ANOVA followed by the Dunnet's post-test. # $p<0.05$ for indicated conditions by one-way ANOVA followed by the Tukey's post-test. Of note, all the lanes are from the same blot but were rearranged into the present order.

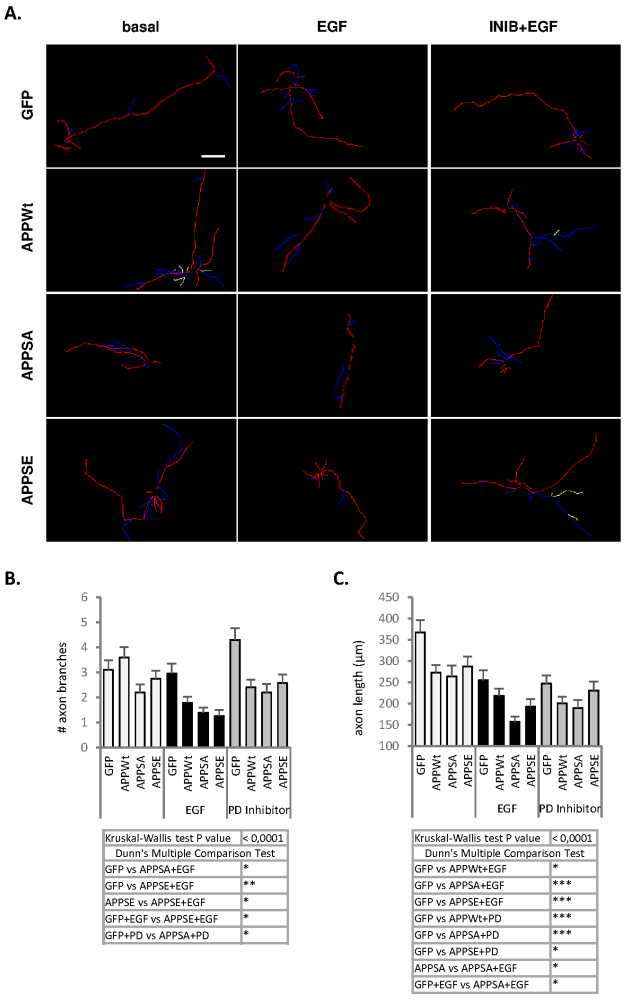

Kruskal-Wallis test P value	< 0,0001
Dunn's Multiple Comparison Test	
GFP vs APPSA+EGF	*
GFP vs APPSE+EGF	**
APPSE vs APPSE+EGF	*
GFP+EGF vs APPSE+EGF	*
GFP+PD vs APPSA+PD	*

Kruskal-Wallis test P value	< 0,0001
Dunn's Multiple Comparison Test	
GFP vs APPWt+EGF	*
GFP vs APPSA+EGF	***
GFP vs APPSE+EGF	***
GFP vs APPWt+PD	***
GFP vs APPSA+PD	***
GFP vs APPSE+PD	*
APPSA vs APPSA+EGF	*
GFP+EGF vs APPSA+EGF	*

Supplementary Figure B.7 - **Representative images of the neurite tracings and cortical neurons axonal parameters.** Embryonic primary cortical neurons at 5 DIV were transfected with the GFP empty vector (GFP), or the APP-GFP cDNAs: wild-type ('APP-Wt'), S655A mutant ('APP-SA'), S655E mutant ('APP-SE'). A subset of cells was incubated

Supplementary Figure B.7 (continuation) - with 100 ng/mL EGF after transfection medium change (21h of incubation before fixation), and a third group of cells was treated with the PD168393 EGFR inhibitor 3h before the same EGF stimulation treatment. **A.** MAP2- or BIII Tubulin-positive, GFP expressing mouse cortical primary neurons were traced using the NeuronJ. Tracings are color coded: the primary neurites that arise directly from the cell soma are in red; the secondary neurites that emanate from a primary neurite are in blue; the tertiary neurites that arise from a secondary neurite and in yellow. Secondary and tertiary neurites were grouped as neurite branches for the morphometric quantifications. Scale bar = 50 µm. **B.** The number of axonal branches per neuron. **C.** The mean axon length calculated based on the length of the longest neurite considered here as the axon. * $p<0.05$, ** $p<0.01$, *** $p<0.001$ by the Kruskal-Wallis test followed by the Dunn's multicomparison post-test, as indicated in the table below each graph.

Supplementary Table B.1 – Neuronal morphometric parameters analyzed.

Parameters directly obtained by the NeuronJ pluggin analyses	
# neurites	Total count of neurites traced per neuron
Neurites total length	The sum of the length of all the neurites traced per neuron
Neurites mean length	The mean length of all the neurites traced per neuron
Parameters obtained by the NeuronJ pluggin but dependent on the user assessment	
# primary neurites	Number of neurites arising directly from the cell soma per neuron
Primary neurites total length	The sum of the length of all primary neurites traced per neuron
Primary neurites mean length	The mean length of all primary neurites traced per neuron
# neurite branches	Sum of the number of secondary (branches from a primary neurite), tertiary (branches from a secondary neurite), and quaternary (branches from a tertiary neurites) neurites per neuron
Neurite branches total length	The sum of the length of all neurite branches per neuron
Neurite branches mean length	The mean length of all neurite branches traced per neuron
Parameters inferred or estimated	
"Theoretical" axon mean length	The longest neurite – maximum tracing length value – of a neuron was consider the axon.
# axonal branches	Number of neurites (secondary and/or tertiary neurites) branching from the longest neurite per neuron.
Total axon length	The sum of the length of the axon and all its branches.
# Primary dendrites	Number of dendrites per neuron. Obtained by subtracting an axon and the number of neurite branches to the total neurite count.
# dendritic branches	Obtained by subtracting the number of axon branches to the neurite branches total count, per neuron.
Dendritic tree total length	Obtained by subtracting the "total axon length" to "Neurites total length".

7. Analysis of an Alzheimer's Amyloid Precursor Protein (APP)-S655 phosphorylation differential interactome with potential functions in neuronal differentiation

Joana F. da Rocha[1,2], J. Mirjam A. Damen[3], Patrícia Correia[1], Odete A. B. da Cruz e Silva[2], A. F. Maarten Altelaar[3], Sandra I. Vieira*[1,2]

[1]Cell Differentiation and Regeneration group, Institute of Biomedicine (iBiMED), Department of Medical Sciences, Universidade de Aveiro, Campus de Santiago, 3810-193 Aveiro, Portugal;

[2]Neurosciences and Signalling group, Institute of Biomedicine (iBiMED), Department of Medical Sciences, Universidade de Aveiro, Campus de Santiago, 3810-193 Aveiro, Portugal.

[3]Biomolecular Mass Spectrometry and Proteomics, Bijvoet Centre for Biomolecular Research and Utrecht Institute for Pharmaceutical Sciences, University of Utrecht, Utrecht, The Netherlands

*E-mail: sivieira@ua.pt; Tlf:(+351) 234 247 256; Fax:(+351) 234 372 587

7.1. Abstract

APP has been described to be determinant for neuronal development and function, not only in its full-length conformation but also after proteolytic cleavage events in the form of several biological peptides. Furthermore, APP phosphorylation tightly regulates its trafficking, proteolysis, protein-protein binding, and consequently its several functions. One possible APP phosphorylation site is the S655 residue located in the basolateral sorting motif YTSI. Some lines of evidence indicate that phosphoS655 potentially modulates APP-mediated neuronal differentiation. In the present work, we used RA-differentiated SH-SY5Y cells overexpressing Wt or S655 phosphomutants APP-GFP cDNAs, and immunoprecipitate the specific APP species and their respective interacting partners. After protein identification by mass spectrometry we were able to characterize APP-phosphoS655/dephosphoS655 interactomes potentially involved in neuronal differentiation events. The APP-dephosphoS655 interactome was particularly enriched in actin binding proteins what correlated with a cortical actin phenotype, while the APP-phophoS655 interactome presented specific binding partners that correlate well with neurite outgrowth output.

7.2. Introduction

The Amyloid Precursor Protein (APP) is mainly studied for its association with the Alzheimer's disease (AD). This transmembrane protein is dynamically sorted through the membranes of intracellular organelles and the plasma membrane. During its trafficking the full-length APP protein suffers proteolytic cleavages by proteases into some functional peptides. Briefly, alpha-secretases generate the sAPPalpha and a membrane tethered C-terminal fragment (CTF), whereas cleavage by beta-secretase releases the sAPPbeta. The resulting CTFs of both pathways are subsequently processed by the gamma-secretase complex to produce the p3 or Abeta peptides, respectively, and the intracellular AICD fragment [1].

Several crucial physiological roles have been attributed to the complex APP molecule. Particularly, APP has been described to be determinant for neuronal development and function, with attributed functions in cell migration [2], neuritogenesis [3, 4] and synaptic plasticity [5, 6]. Several of these functions have been attributed not only to the full-length protein but also to its proteolytic fragments [7-10]. However, contradictory results have been reported regarding the benefits of knocking-down or overexpressing APP, and its role in neuronal development is far from being clarified [11, 12] and most possible involves its regulation through post-translational modifications.

As a phosphoprotein, APP phosphorylation tightly regulates its trafficking [13], proteolysis [14], and protein-protein binding [15]. One possible APP phosphorylation site is the S655 residue located in the basolateral sorting motif ^{653}YTSI^{656}. Phosphorylation at S655 has been observed to occur in mature APP molecules in cultured cell lines and rat cortex [16]. In human hippocampus of AD patients it was reported the existence of phosphoS655 APP-CTFs [14]. Additionally, this phosphorylation site is the only APP Ser/Thr residue described to be phosphorylated by PKC [16, 17]. NMR analyses showed that APP phosphorylation at S655 induces significant local conformational changes in the APP C-terminus at and downstream the ^{653}YTSI^{656} motif, potentially regulating protein-protein interactions at those regions [18].

We have collected several data indicating that phosphoS655 potentially modulates APP-mediated neuronal differentiation. Mechanisms underlying this modulation may involve altered APP trafficking to and from the plasma membrane and subsequent increased APP cleavage to its neuritogenic fragment sAPP [13, 19], altered APP-mediated cytoskeleton rearrangements [20], promotion of intracellular signaling events (i.e. amplified ERK1/2 activation), and differential binding to neurotrophic effectors (Dias R., et al, 2016 and da Rocha J.F., et al, 2016 unpublished data) .

The work here reported aimed to identify specific protein binding partners of phosphoS655 and dephosphoS655 APP, particularly those potentially involved in neuronal differentiation events. To

this end, we used the neuritogenic cellular model retinoic acid (RA)-differentiated SH-SY5Y cells transiently overexpressing APP-GFP S655 phosphomutants (S655A and S655E). The differentiation days 3 and 7 were chosen as they represent two distinct periods of RA-induced SH-SY5Y neuronal differentiation. In the first one, more related to an increase in the number of pre-neuritic projections, APP levels rise but holo APP is cleaved at a higher rate into sAPP. Neurites appear more abundantly during the second period, related to neuritic elongation and to the stabilization of longer neurites in a holo APP-assisted manner [21].

The GFPTrap assay was used to immunoprecipitate APP-GFP proteins and their respective interacting partners, which were identified by mass spectrometry (MS). In general, we found a special enrichment in RNA-binding proteins linking APP neuronal differentiation role with regulation of mRNA processing (splicing, decay and translation). This RNA regulatory proteins were found for both the phosphoS655 and dephosphoS655 categories, but particularly enriched in the later. The dephosphoS655 APP interactome was also enriched in energy metabolism related proteins, and in actin-binding proteins, what correlated with a cortical actin phenotype. The phophoS655 APP interactome presented a reduced number of protein interactors, when compared to the other categories, denoting a higher degree of functional specificity. The phosphoS655 APP interactome included proteins involved in the regulation of proliferation, survival and differentiation, and in various signaling pathways that appear to promote cell fate, neurite outgrowth and neuronal maturation.

7.3. Material and Methods

7.3.1. SH-SY5Y cell culture and differentiation

The SH-SY5Y human neuroblastoma cell line was maintained in minimum essential media/F12 medium supplemented with 10% fetal bovine serum. Before differentiation, cell culture was enriched in the neuroblastic N-type of cells (immature nerve cells that are RA-differentiated into neuronal-like cells), on the basis of their lower substrate adherence comparing to the S-type cells [21]. For the experiments N-type enriched 30000 cells/cm^2 were plated onto 100 mm culture plates. The day after, cells were incubated with 10 μM RA complete medium to start neuronal-like differentiation. New cell medium supplemented with 10 μM RA was added every other day. Cells were kept under humidified, 37ºC, 5% CO_2 incubator.

7.3.2. Cell Transfection

Previously produced human APP isoform 695 ("APPWt") cDNA, and the respective S655 phosphomutants, Serine 655 to Alanine (S655A, "APPSA") or to Glutamate (S655E, "APPSE") fused in frame with GFP in the pEGFP-N1 mammalian expression vector, were used [22]. The "empty" pEGFP-N1 expression vector was used as control. Cells were transfected at day 3 or day 6 of differentiation, and collected 24h after transfection. These time points were chosen as key regulatory differentiation periods, based on previous data obtained by us on time-dependent APP-induced neuritogenic alterations [21]. Cell transfections were carried out with the TurboFect™ reagent according to the manufacter's instructions (Fermentas Life Sciences). Briefly, for each monolayer of cells grown in 100 mm plates, 9 μg of DNA, either eGFP-N1 empty vector or APPs-GFP cDNA, were diluted in 900 μL of serum-free growth medium. After a brief vortex, 18 μL of TurboFect™ were added to the diluted DNA. The mixture was vortexed and incubated for 15-20 min at room temperature (RT), after what this mixture was added dropwise with gently rocking. Cells were further incubated for 6h at 37ºC in a CO_2 incubator, after which medium was changed. After 24h, the efficiency of cell transfections was confirmed by visualization of GFP expressing cells with the Olympus IX81 inverted epifluorescence microscope. The experiments were performed in duplicate.

7.3.3. GFP Trap IP assays

Pull down of the GFP moiety was performed by GFP-trap® (Chromotek) according to the manufacturer. After transfection, SH-SY5Y cells were washed in PBS, and 1 mL of ice-cold PBS with 1x PMSF (dilute stock 1:100). Cells were collected with a scrapper to a microtube and immediately placed on ice. Subsequent steps were always performed at 4ºC. The samples were

centrifuged for 5 min at 3000 g, and the supernatant removed. Cell pellet was lysed with 500 µL non-denaturant Lysis buffer (10 mM Tris HCl pH 7.5, 0.5 mM EDTA, 0.5% Gepac-ca-630, 150 mM NaCl, 1 mM PMSF) supplemented with protease inhibitors cocktail (Sigma-Aldrich), 1 mM NaF, and 10 mM Sodium Orthovanadate, for 30 min. During this time, GFP-TRAP beads (Chromotek) were resuspended in wash buffer, centrifuged at 13000 g for 1 min. Samples were then centrifuged for 5 min at 20000 g, and an aliquot of 25 µL of supernatant transferred to a new microtube ('cells lysates') for transfection assessment via immunoblot procedures. The remaining supernatant was incubated with the GFP-TRAP beads (25 µL for sample) and incubated for 3h with orbital shaking. The beads were magnetically separated until supernatant was clear, and ressuspended in wash buffer. Magnetic separation and washing step were repeated 4 times. Beads were finally ressuspended in 100 µL 2x SDS-sample buffer and boiled for 10 min at 95ºC to dissociate immunocomplexes from GFPTrap beads. After vortexed, beads were magnetically separated, and the supernatant transferred to a new microtube. Samples were immediately stored at -20ºC for later mass spectrometry.

7.3.4. Mass spectrometry (MS)

The MS experiments were performed under the PRIME-XS consortium in collaboration with the Biomolecular Mass Spectrometry and Proteomics group at Utrecht University.

The samples were defrosted, 45 µL of each sample were loaded on a 12% SDS-PAGE gel (Bio-Rad 345-0117) and run for 2h under a constant amperage of 20 mA. Afterwards the gel was fixed for 30 min in 40% MeOH, 10% HAc solution. Subsequently the gel was stained with coomassie (Gelcode blue stain, Pierce). Each lane was divided in 3 equal gel bands. These gel bands were excised and cut into small (approximately 1 mm^3) pieces. The gel pieces were washed, in-gel reduced with 6.5 mM dithiothreitol (RT, 60 min), alkylated with 54 mM iodoacetamide (dark, RT, 30 min), and digested by adding trypsin at a concentration of 3 ng/µL (overnight at 37 °C) as described in [23].

After the incubation, peptides were extracted with 100% acetonitrile (Biosolve) and dried by vacuum centrifugation. The peptides were dissolved in 45 µl 10% Formic acid and spun for 10 min at 20000 rpm prior to analysis. 20 µl of each sample was analyzed on a Q exactive plus (Thermo Fisher Scientific, Bremen) connected to Thermo Scientific EASYnLC 1000 (Thermo Fisher Scientific, Bremen). All columns were packed in-house. The trap column was a double fritted 100 µm inner diameter capillary with a length of 20 mm (Dr Maisch Reprosil C18, 3 µm). The analytical column (Agilent Poroshell EC-C18, 2.7 µm) had an id of 75 µm and a length of 50 cm, and was heated to 40°C.

Trapping of the sample was performed at a flow rate of 100 nl/min for 10 min in solvent A (0.1 % Formic acid in water) and elution was achieved with a gradient of 7–38% B (0.1% Formic acid 100% acetonitrile) in 75 min, 38–100% B in 3min, 100% B for 2min at a maximum pressure of 800 bar. Nano spray was achieved using a distally coated fused silica emitter (made in-house, o.d. 375 µm; i.d. 20 µm) biased to 1.7kV. The mass spectrometer was operated in the data dependent mode to automatically switch between MS and MS/MS. MS full scan spectra were acquired from m/z 375–1600 after accumulation to a target value of 3x106. Up to ten most intense precursor ions were selected for fragmentation. HCD fragmentation was performed at normalised collision energy of 25% after the accumulation to a target value of 5x104. MS/MS was acquired at a resolution of 17500.

7.3.5. Data analysis and bioinformatics

IP samples of N1-eGFP transfected cells were used as negative controls. A list of 180 proteins were identified in N1-eGFP samples (including replicates of both differentiation days) and established as false positives – proteins that bind nonspecifically to the GFPTrap beads and/or to the GFP fusion tag – being excluded from the APP interactomes. Exceptions were considered when the ratio between the number of peptide spectrum matches (PSM) for a given protein in an APP sample and the PSM in the N1-eGFP sample of the same differentiation day, was equal or higher than 2.0. Additionally, we directly excluded well described common MS contaminants [24], and proteins characteristic of hair, skin/epidermis, tongue and gums that are highly probable contaminants (KRT33A, KRT78, KRT85, KRT14, KRT5, KRT3, KRT31, KRT32, KRT33B, KRT35, KRT36, KRT4, KRT77, KRT8, FLG2, HRNR, SPRR1A, SPRR3, KRT17). In this manner, for each APP species (Wt, S655A, S655E) in a specific differentiation day (days 3 and 7) we generated a "cleaned list" of potential interactors.

Following, based on the condition in which the potential interactor was pull-downed and detected by MS, we divided the APP potential interactors in the following categories: 1) Total APP interactors – all interactors experimentally identified, independent of the experimental condition; 2) Interactors that bind APP independently of its S655 phosphorylation status. This category includes interactors that are common to all APP backgrounds (APPWt, APPSA, and APPSE) or common to both S655 phosphorylation mutants (APPSA and APPSE). 3) Interactors that bind APP in a S655 phosphorylation status dependent manner; this is further divided in the subcategories: 3a) APP S655 dephospho interactome (interactors present uniquely in APPSA, or common to APPWt and APPSA conditions); and 3b) APP S655 phospho interactome (interactors present uniquely in APPSE or common to APPWt and APPSE conditions).

Protein lists' comparison was performed using a Venn diagram tool available online – jvenn (http://bioinfo.genotoul.fr/jvenn) [25].

Construction of protein-protein interactions (PPI) networks was performed using the Cytoscape software (version 3.4.0). Protein-protein data was retrieved from the International Molecular Exchange (IMEx) consortium partners only [26]. The HIPPIE database was used for retrieving additional human APP PPI data (downloaded on June 27, 2016). This database is regularly updated by incorporating interaction data from major expert-curated experimental PPI databases (such as BioGRID, HPRD, IntAct, and MINT). To the 1111 APP protein interactors retrieved from HIPPIE, we added interacting proteins from a published APP interactome [27], and imported the final curated APP PPI list into Cytoscape to add information on APP interactors to the constructed networks. In the PPI networks proteins are represented by their gene names as retrieved by the databases.

Functional enrichment analysis of Gene Ontology categories (Biological Processes and Molecular Function), and Kyoto Encyclopedia of Genes and Genomes (KEGG) were performed using the Cytoscape app ClueGO, version 2.2.6 [28]. Complementarily, the Panther overrepresentation test was performed [29]. For both analysis, the overall set of human protein-coding genes was used as reference set, and only enriched functions with a P value < 0.05 (including Bonferroni-correction) were considered.

Functional classification of single proteins lists was performed by Panther functional classification analysis [29]. Proteins annotated with GO terms related to brain development, neuron function, neurogenesis, neuronal differentiation and/or related events (cytoskeleton organization, cell adhesion, and cell migration), and related signaling pathways, were selected as interactors of interest. The Uniprot [30] and PubMed databases were manually searched for each of the interactors of interest to verify involvement in neuronal differentiation. The association of selected proteins with brain alterations and disorders, especially brain development and neurodegenerative diseases, was verified using the Mouse Genome Informatics database (http://www.informatics.jax.org/) [31] and, in the human context, the OMIM (http://omim.org/) and the Uniprot databases. Identification of the brain specific or brain enriched proteins was performed using The Human Protein Atlas database [32]. Figure 1, gives an overview of the methodological approach used, from cells differentiation to bioinformatics analysis.

7.3.6. Cell morphology studies: immunocytochemistry, microscopy and image analysis

Cells grown on coverslips were fixed with a 4% paraformaldehyde PBS solution (PFA) for 20 min and, upon three washes with PBS, coverslips were permeabilized with a 0,2% TRITON PBS solution (10 min), for subsequent immunocytochemistry analysis. Briefly, cells were first blocked

for 30 min-1h with 5% bovine serum albumin in PBS, then incubated with specific primary antibodies, and finally incubated with the fluorophore conjugated-secondary antibodies. Preparations were washed with PBS, mounted with Vectashield® mounting media with or without DAPI (Vector Labs). Alexa Fluor 568 Phalloidin was diluted in the secondary antibody solution for the specified conditions.

Cells visualization was performed either by epifluorescence and phase contrast (PhC) illumination microscopy under an Olympus IX-81 motorized inverted microscope equipped with a LCPlanFl 20x/0.40 objective lens, or by confocal microscopy using a LSM 510 META confocal microscope (Zeiss) and a 63x oil objective

Morphometric analysis of cells was performed on ~30 random digitized images per sample, with an average of 40 transfected cells per biological replica of each condition being analyzed. Transfected cells were identified by GFP expression, measurements were performed on matching PhC microphotographs.

7.4. Results

The main aim of this study was the identification of APP protein interactors dependent on its S655 phosphorylation state. RA-differentiated SH-SY5Y cells overexpressing Wt or S655 phosphomutants APP-GFP cDNAs were used as the protein pool. The GFPTrap assay was used to immunoprecipitate the specific APP proteins (Wt, SA, and SE) and their respective interacting partners, which were subsequently identified by mass spectrometry (Figure B.16 and Supplementary Table B.2).

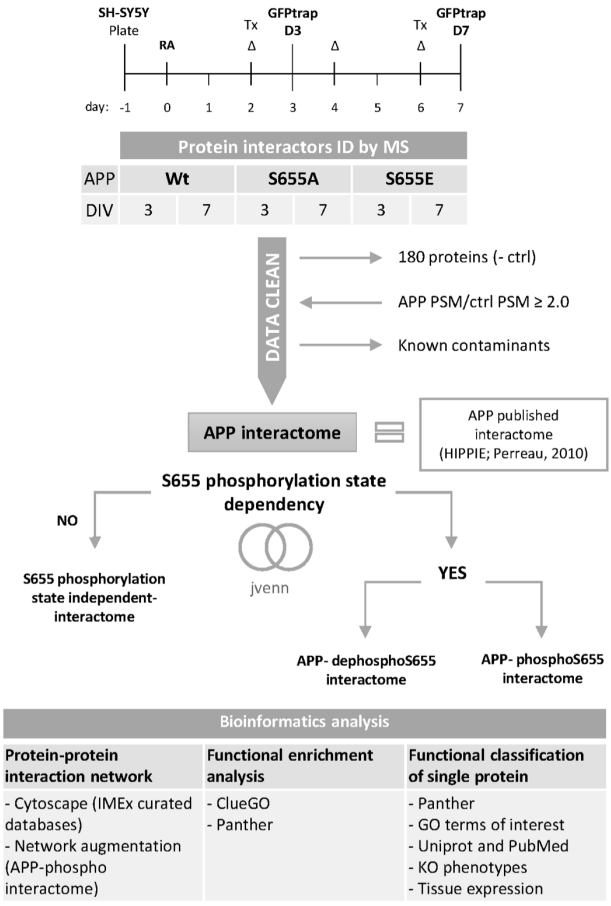

Figure B.16 - **Methodological approach schematic representation.** SH-SY5Y cells, differentiated for 3 and 7 days with 10 μM RA, and overexpressing Wt or S655 phosphomutants APP-GFP cDNAs by 24h transient transfection, were used as the protein pools to identify APP S655 interactors. The GFPTrap assay was used to immunoprecipitate the specific APP (Wt, SA, and SE) proteins and their respective interacting partners, which were subsequently identified by mass spectrometry. The list of identified proteins was pre-processed ('cleaned') to exclude unspecific protein interactors and potential contaminants. Before bioinformatics analysis, the interacting proteins were grouped based on their appearance or not in specific APP S655 phosphorylation groups (Wt, SA, SE).

Some proteins were identified only in the APP-GFP pull-down samples and never in the controls (cells expressing the N1-eGFP empty vector on day 3 and day 7), and other proteins were enriched in the APP-GFP conditions and were also considered potential APP interactors (PSM ratio between APP samples and N1-eGFP ≥ 2.0). In this manner, after a processing step to clean unspecific and

contaminant proteins, we obtained a list of 456 potential APP protein interactors (including APP), of which 105 were already described as APP interactors.

As shown in Figure B.17, APPWt show a decrease in the number of interactors (almost half) from day 3 to day 7. On differentiation day 3 (D3), APPWt and APPSA have a similar number of interactors, and most are shared between these two conditions. From day 3 to day 7, APPSA shows a small increase in the number of protein interactors. Very interestingly, on differentiation day 7 (D7), APPSA more than triplicates the number of unique interactors (and decreases the number of interactors shared with APPWt). APPSE is the condition with the lowest number of interactors. This APP species roughly maintains the number of interactors from D3 to D7 (a minor decrease from 90 to 74 was noted), including similar numbers of unique interactors between days.

Based on the condition where the putative APP interactor was detected, we divided the APP protein interactors in 3 categories: 1) Total APP interactors (D3 = 289, D7 = 345), which includes all APP interactors identified in this work; 2) APP interactors whose interaction seems independent of the S655 phosphorylation status; and 3) APP interactors dependent of the APP S655 phosphorylation status, this subdivided in the dephosphoS655 APP interactome, and the phosphoS655 APP interactome. Of note, some proteins are included in an APPS655 phosphorylation-dependent category at the first differentiation day, and in a different category at the last differentiation day (Supplementary Table B.3).

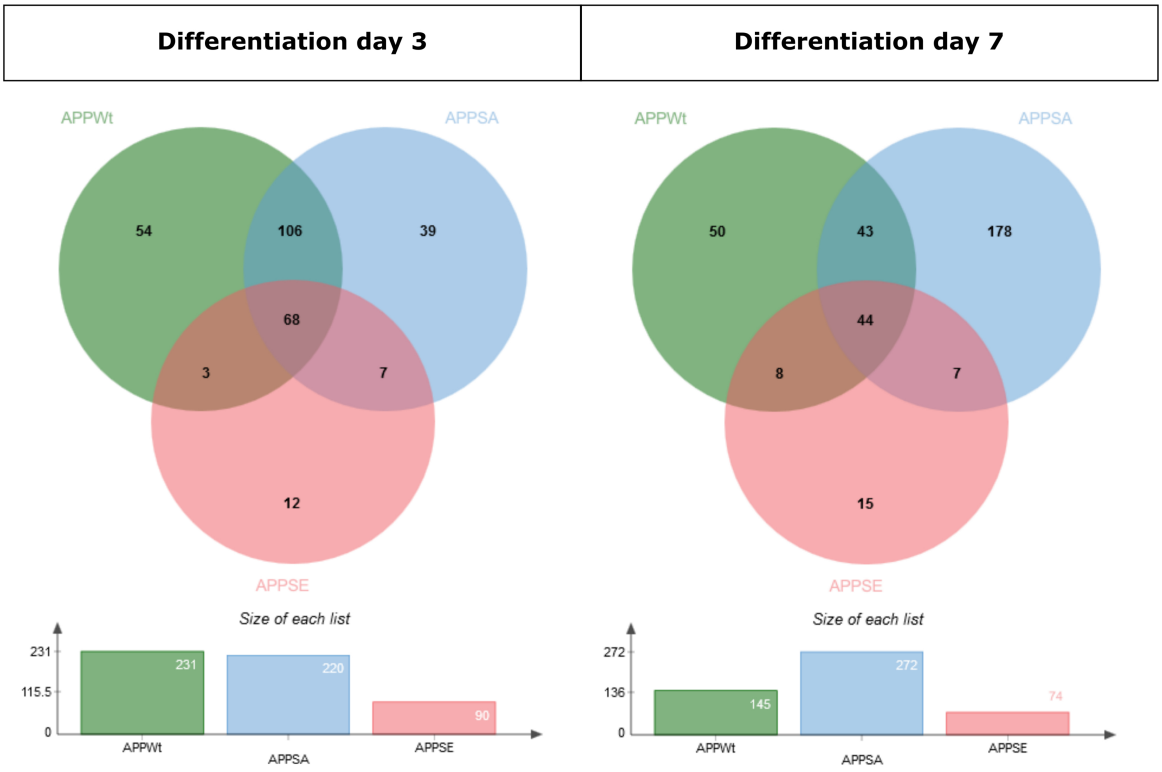

Figure B.17 - **Total APP protein interactors detected by MS.** Venn's diagrams presenting the numbers of interactors experimentally detected in the three pull-downs (of APPWt and the S655 phosphomimetic mutants, APPSA and APPSE), and the intersections between these conditions, at both differentiation days (3 and 7).

7.4.1. Total APP interactors with differentiation time

We considered as "Total" APP interactors all the proteins detected, independently of the APP nature (Wt, SA, or SE). This category was created to allow a general view of the dynamics of the APP interactome with the differentiation time (Figure B.18). The list of proteins identified on D3 included APP itself and 289 different APP protein interactors, 63 of which already described as APP interactors. Almost half of these interactors are nucleic-acid binding proteins (mainly RNA binding proteins, RBP). Other represented protein classes include cytoskeletal proteins (7.6% of the D3 protein list, with similar numbers of actins, microtubules (MTs), and intermediate filaments (IFs)), enzyme modulators (6.0% of proteins; mainly G-proteins and G-protein modulators), hydrolases (4.6%), and transcription factors (TFs; 5.0%). Differentiation D7 included 345 different APP protein interactors and APP itself, 86 of which were known APP interactors. Like in D3, the majority of proteins belong to the nucleic-acid binding protein class (mainly RBP), followed by cytoskeletal proteins (9.6% of D7 proteins; half of which belong to the actin family), enzyme modulators (5.9%; mainly G-proteins and G-protein modulators), chaperons (5.9%; comprising

Hsp90 family and chaperonin family members), oxidoreductases (4.5%), transferases (3.7%), hydrolases (3.7%), TFs (3.7%), calcium-binding proteins (3.1%), and signaling molecules (2.8%).

The APP interactor network is dynamic with time of differentiation. 180 APP interactors (including APP) are shared between differentiation days 3 and 7 (Figure B.18 A). The remaining (~40% at D3 and ~50% at D7) are protein interactors specific of each differentiation day. In order to test if the APP interactome could be assigned to specific functions depending on the differentiation day we performed cluster comparison functional enrichment analysis using the Cytoscape app ClueGO (Figure B.18 B). For both differentiation days, a large number of proteins are associated with RNA and mRNA binding, leading to enrichment in these functions. Common enriched functions include RNA biosynthetic and metabolic processes, gene expression, RNA splicing, ribonucleoprotein complex biogenesis and organization, and protein target to endoplasmic reticulum (ER).

Very interestingly, while D3 is assigned to negative regulation of mRNA metabolic processing and RNA splicing, and to negative regulation of telomere maintenance via telomere lengthening, D7 is associated with positive regulation of the same functions (Table B.1 and Figure B.18 B).

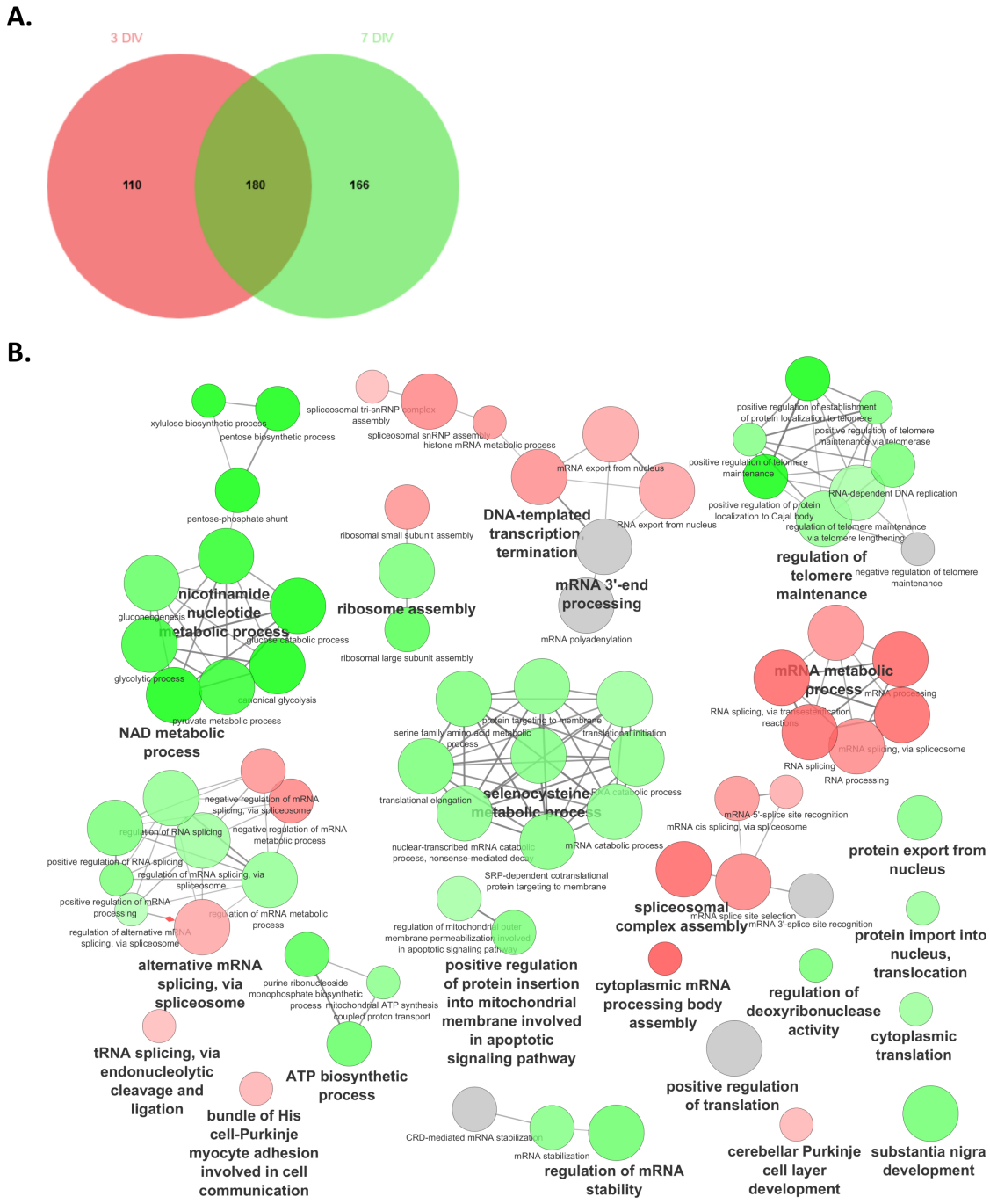

Figure B.18 - **Comparison of Total APP interactors at differentiation days 3 (D3) and 7 (D7). A.** The number of Total APP interactors identified for each differentiation day (APP included). **B.** Biological processes gene ontology (GO) terms specifically enriched at D3 (red color) or D7 (green color). Grey color indicates non-specific GO terms, meaning the two differentiation days display similar % of genes attributed to the functional term. The enrichment analysis was performed using the Cytoscape app ClueGO cluster analysis. Only terms with pvalue < 0.05 are represented.

Table B.1 - **Examples of enriched biological processes differentially attributed to APP 'Total' interactors depending on the differentiation day (D3 versus D7).** The enrichment analysis was performed using the Cytoscape app ClueGO. Pvalue, calculated p value that includes Bonferroni step down correction.

Biological Process (GO term)	Enriched at *(Pvalue)*	%Genes D3	%Genes D7	Genes Cluster at D3	Genes Cluster at D7
stress granule assembly	**D3** *(230.0E-6)*	**77.40**	46.44	ATXN2, ATXN2L, CIRBP, DDX3X, PUM2	ATXN2L, CIRBP, DDX3X
negative regulation of mRNA processing	**D3** *(49.0E-3)*	**73.25**	58.60	HNRNPA2B1, HNRNPK, RBMX, SFSWAP, U2AF2	HNRNPA2B1, HNRNPK, RBMX, U2AF2
negative regulation of mRNA splicing, via spliceosome	**D3** *(9.5E-3)*	**73.25**	58.60	HNRNPA2B1, HNRNPK, RBMX, SFSWAP, U2AF2	HNRNPA2B1, HNRNPK, RBMX, U2AF2
negative regulation of telomere maintenance via telomere lengthening	**D3** *(36.0E-3)*	**71.24**	53.43	HNRNPA1, HNRNPC, HNRNPU, PARP1	HNRNPA1, HNRNPC, HNRNPU
cerebellar Purkinje cell layer development	**D3** *(49.0E-3)*	**66.17**	49.63	ATXN2, HSPA5, LDB2, MYH10	AARS, HSPA5, MYH10
canonical glycolysis	**D7** *(2.8E-6)*	0.00	**100.00**	-	ALDOA, ENO1, ENO3, GAPDH, GPI, PFKM, PGAM2, PGK1, PKM, TPI1
protein localization to nuclear body/Cajal body/telomere	**D7** *(3.7E-3)*	0.00	**100.00**	-	CCT2, CCT4, CCT5, CCT8
ATP generation from ADP	**D7** *(140.0E-6)*	8.33	**91.67**	OGT	ALDOA, ENO1, ENO3, GAPDH, GPI, LDHA, PFKM, PGAM2, PGK1, PKM, TPI1
gluconeogenesis	**D7** *(18.0E-6)*	20.88	**83.53**	KHSRP, OGT, SOGA1	ALDOA, ENO1, ENO3, GAPDH, GPI, KHSRP, MDH2, PC, PGAM2, PGK1, SLC25A1, TPI1
substantia nigra development	**D7** *(1.7E-6)*	43.85	**80.40**	ACTB, ATP5F1, CALM1, HSPA5, INA, YWHAQ	ACTB, BASP1, CALM1, CKB, ENO3, G6PD, HSPA5, INA, LDHA, YWHAE, YWHAQ
positive regulation of mRNA processing	**D7** *(13.0E-3)*	51.88	**77.82**	HSPA8, PABPC1, RBMX, SNW1	HSPA8, PABPC1, RBMX, SNRNP70, SNW1, TRA2B
positive regulation of mRNA splicing, via spliceosome	**D7** *(2.8E-3)*	46.44	**77.40**	HSPA8, RBMX, SNW1	HSPA8, RBMX, SNRNP70, SNW1, TRA2B
positive regulation of telomere maintenance via telomere lengthening	**D7** *(15.0E-3)*	30.69	**76.73**	AURKB, HNRNPA1	CCT2, CCT4, CCT5, CCT8, HNRNPA1
positive regulation of mitochondrial membrane permeability involved in apoptotic process	**D7** *(29.0E-3)*	57.96	**69.56**	SFN, SLC25A5, YWHAB, YWHAG, YWHAQ	SFN, YWHAB, YWHAE, YWHAG, YWHAQ, YWHAZ

Other functions particularly enriched at D3 include stress granule assembly and cerebellar Purkinje cell layer development, although D7 also presented interactors involved in these functions. Differentiation D7 presented enriched biological processes to which there are no or few associated

proteins present in D3, like protein localization to nuclear body, to Cajal body, and to telomere; glycolysis; and ATP generation from ADP. Other highly enriched at D7 include gluconeogenesis; substantia nigra development; and positive regulation of mitochondrial membrane permeability involved in apoptotic process, besides the above mentioned positive regulation of mRNA processing and telomere maintenance (Table B.1 and Figure B.18 B). Table B.2 presents Molecular Function terms with particular interest for neuronal differentiation specifically enriched on D7. The higher number of proteins associated with the cytoskeleton, particularly actin and actin filaments binding proteins, is notorious.

Table B.2 - **'Total' APP interactors: examples of enriched Molecular Function gene ontology terms attributed to differentiation day 7 (D7).** The enrichment analysis was performed using the Cytoscape app ClueGO. Pvalue, p value that includes Bonferroni step down correction**.**

Molecular Function (GO term)	*Pvalue*	%Genes D3	%Genes D7	Genes Cluster at D3	Genes Cluster at D7
protein kinase C inhibitor activity	2.9E-3	45.51	68.26	SFN, YWHAG	HSPB1, SFN, YWHAG
cytoskeletal protein binding	64.0E-6	44.38	72.63	ACTB, CALM1, CAMSAP2, CAMSAP3, DLG1, EEF2, EMD, EPB41, FUS, HNRNPK, KTN1, MAGI1, MAP4, MYH10, MYH9, MYO1B, PLEC, RPS3, RTCB, S100A8, SHROOM3, SYNPO2	ACTB, ACTN1, ACTN4, ALDOA, ANXA2, CALD1, CALM1, CAPZB, CCT5, CFL1, EEF2, EMD, FKBP4, FLNA, FLNB, FMR1, FUS, GAPDH, HNRNPK, KIF26A, LASP1, MAP1B, MSN, MYH10, MYH9, PFN1, PLEC, RPS3, S100A4, S100A6, SHROOM3, STMN1, TLN1, TMSB4X, TPM4, VCL
actin filament binding	4.1E-3	37.34	82.16	EEF2, MYH10, MYH9, MYO1B, SHROOM3	ACTN1, ACTN4, CAPZB, EEF2, FLNA, LASP1, MYH10, MYH9, SHROOM3, TLN1, VCL
actin binding	4.1E-3	33.74	82.49	EEF2, EMD, EPB41, MYH10, MYH9, MYO1B, PLEC, SHROOM3, SYNPO2	ACTN1, ACTN4, ALDOA, CALD1, CAPZB, CFL1, EEF2, EMD, FLNA, FLNB, LASP1, MSN, MYH10, MYH9, PFN1, PLEC, S100A4, SHROOM3, TLN1, TMSB4X, TPM4, VCL

Additionally, KEGG enrichment analysis attributed as main pathways for D3: mRNA surveillance (Pvalue, p = 200.0E-9) and spliceosome (p = 8.0E-42); for D7 it attributed as main pathways: spliceosome (p = 8.0E-42), ribosome (p = 2.2E-21), RNA degradation (p = 550.0E-6), glycolysis and gluconeogenesis (p = 890.0E-9), and pentose phosphate pathway (p = 600.0E-6). The Panther overrepresentation test was also performed (Supplementary Table B.4). In most cases this analysis confirmed the results obtained by ClueGo, but also highlighted functions in cell adhesion (including via cadherin) and in Parkinson disease pathway for both differentiation days. Further, D3 interactors might be more associated with MTs-based processes, while D7 interactors are enriched in the cytoskeleton regulation by Rho GTPases pathway.

To evaluate how the APP interactors identified by our system were interconnected, we constructed PPI networks using Cytoscape software, and by importing data on the relation between these proteins from public databases, as explained in the Methods section. For differentiation D3, we were able to map 284 of the interactors with 760 edges (connections between nodes). 56 (~20%) nodes were found to be isolated, and the network had a mean clustering coefficient (a measure of how nodes are interconnected, that ranges from 0 to 1) of 0.198. APP was connected to 62 protein interactors, representing known APP interactors. Based on node degree (k, the number of proteins that interact with a specific protein within the network) [33], the following proteins are highlighted: SNW1 (k = 91), HNRNPU (k = 38), SF1 (k = 38), YWHAG (k = 33), and SF3A2 (k = 47). For differentiation D7, we were able to map 342 of the interactors with 1059 edges. 47 (~14%) nodes were isolated, and the network had a mean clustering coefficient of 0.256. APP was connected to 96 reported protein interactors. Node degree analysis highlighted the same proteins as in day 3: SNW1 (k = 106), HNRNPU (k =46), SF1 (k = 30), YWHAG (k = 31), and SF3A2 (k = 45), and additionally highlighted the following proteins: YWHAZ (k = 93), NPM1 (k = 38), RPL10 (k = 30). The generated PPI networks are not shown due to space restrictions.

7.4.2. APP interactors independent of the S655 phosphorylation state

This category included interactors common to the three APP backgrounds (APPWt, APPSA, and APPSE) plus interactors common to both S655 phosphorylation mutants (APPSA and APPSE), at a specific differentiation day. Since these proteins interact with both dephosphomimetic and phosphomimetic mutants of S655, they most probably interact with APP independently of its S655 phosphorylation status. For differentiation D3 we retrieved 75 potential interactors (68 common to the three conditions +7 common to both S655 mutants), and for differentiation D7, 51 (44+7) proteins, indicating a decrease in the number of interactors independent of S655 phosphorylation state with differentiation time. The two differentiation time periods shared 22 APP protein interactors. For both differentiation days, the majority of proteins are nucleic-acid binding proteins (~60.0% of proteins), mainly RBP. At D3, the other most represented protein classes are TFs (8.1% of proteins) and cytoskeletal proteins (6.8%; mainly IFs, but also MTs). In Day 7, enzyme modulators (9.6%), cytoskeletal proteins (5.8%; with IFs and MTs), and signaling molecules (5.8%) are the main protein classes represented.

The protein-protein interaction sub-network of differentiation D3 presented 75 nodes (APP included) with 68 edges (Figure B.19 A). Of note, one entry was not mapped by Cytoscape and we found that the uniprot accession number has been deleted. This D3 sub-network had 22 isolated nodes (29%), and a mean clustering coefficient of 0.14. Within this sub-network, APP presented 19 known protein interactors; the other two major clusters have as central nodes SF1 (with k = 10),

EWSR1 (with k = 7), and SNRPB (with k = 6). For differentiation D7, the PPI sub-network included 52 nodes (considering APP, and excluding one deleted entry as above; Figure B.19 B). This sub-network had 19 isolated nodes (~36%). APP presented 8 known protein interactors, and again SF1 was highlighted by the number of direct known interactors (k = 10), followed by PUF60 with k = 7.

Functional enrichment analysis, either using ClueGO or Panther, did not attributed gene ontology terms with interest for neuronal differentiation. Even if we increase the input list to include the protein interactors only identified in the APPWt condition, the majority of the attributed functions are related to ribonucleoprotein and spliceosomal complex assembly, regulation of RNA splicing, translation and translation regulation, with some specificities depending on the differentiation day (Supplementary Table B.5).

Nevertheless, we performed functional annotation of individual proteins. Based on the assigned gene ontology, followed by literature search on PubMed and study of the association with brain anomalies, we were able to select a list of a few APP protein interactors with special interest for neuronal differentiation, which included e.g. ELAV-like protein 4 (ELAVL4) and Caprin-1 (CAPRIN1) (Table B.3).

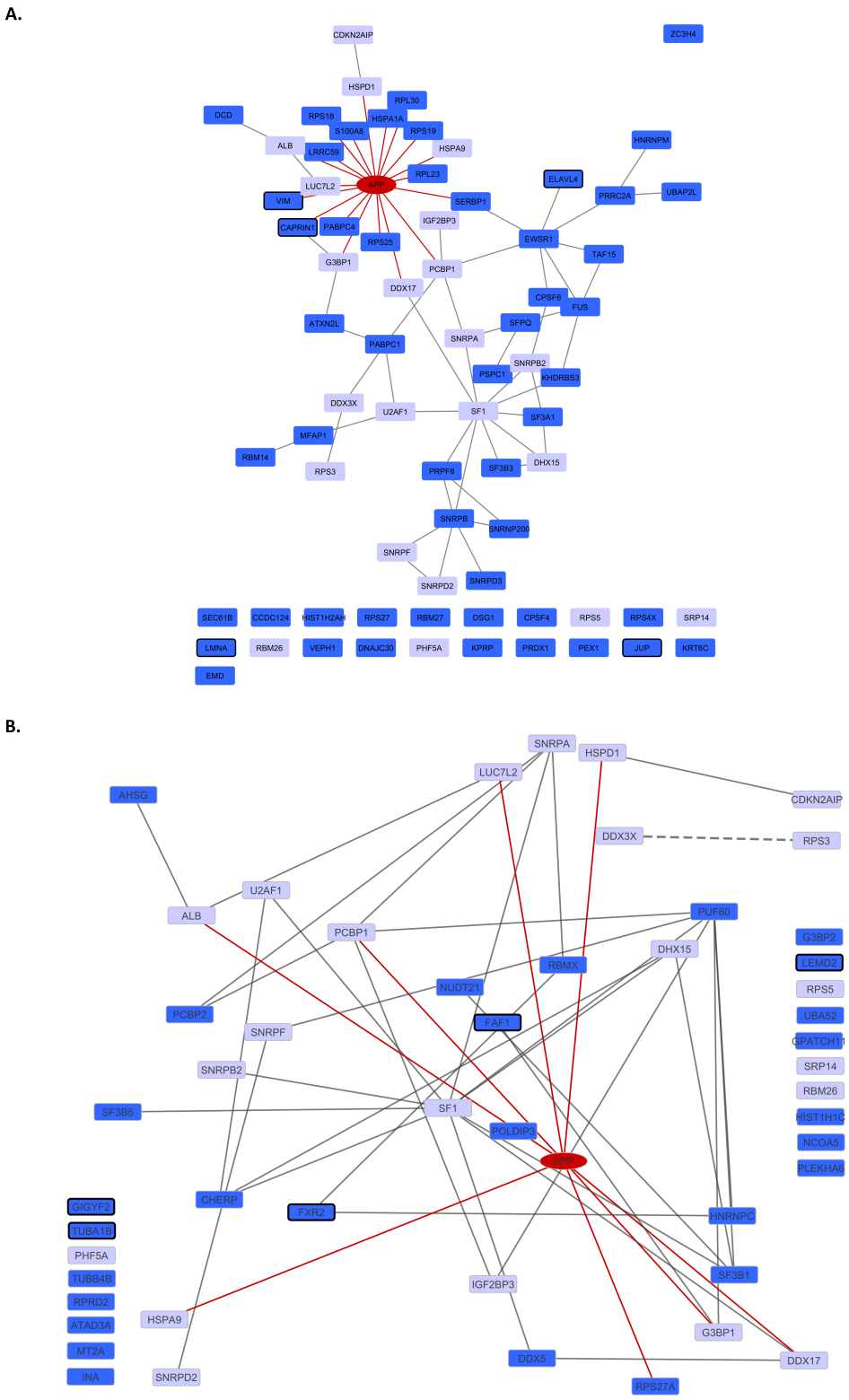

Figure B.19 - **APP S655 phosphorylation state independent protein-protein interaction sub-network for differentiation days 3 (A.) and 7 (B.).** Black marked nodes indicate APP interactors with a potential high level of interest for neuronal differentiation studies. APP is presented in red, bound to already reported APP interactors (by red edges). Light blue nodes indicate protein interactors shared by both differentiation days.

Table B.3 - **APP interactors independent of the S655 phosphorylation state with potential interest for neuronal differentiation.** From the interactors' list specific of each differentiation day, proteins were selected based on functional annotations directly related to brain development, neuron function, neurogenesis, and/or neuronal differentiation related events (cytoskeleton organization, cell adhesion, and cell migration) and signaling pathways. In bold are the UniProt accession number of newly identified APP interactors. The gene ontology (GO) terms determinant for the selection are described in the biological process column. Node degree ('k'), is the number of APP interactors that the protein presents and refers to the position of the protein inside the protein-protein interaction network that includes all the interactors identified for each differentiation day. 'Ref', indicates references retrieved from the PubMed supporting the role of the indicated interactor in neuronal differentiation. 'Mammalian phenotype/human diseases', KO mouse phenotypes were searched on Jackson Laboratories mouse knockout database, and human diseases retrieved from UniProt and other indicated references. 'Expression', brain enrichment or altered expression in RA-differentiated SH-SY5Y cells are indicated. 'Dif.' – differentiation; 'Reg.' – regulation; 'PM' – plasma membrane.

Uniprot nr	Gene name and symbol	k	Biological Process	Ref.	Mammalian phenotype/ human diseases	Expression
				D3		
P26378	ELAV-like protein 4; ELAVL4	**1**	Learning (GO:0007612); dendrite morphogenesis (GO:0048813).	[34]	increased neuron apoptosis; abnormal nervous system development, and neuron dif. [35].	Tissue enhanced (cerebral cortex); RA dif. SH-SY5Y regulated gene [36].
Q14444	Caprin-1; CAPRIN1	**1**	positive reg. of dendrite morphogenesis (GO:0050775) and of dendritic spine morphogenesis (GO:0061003); cell dif.(GO:0030154).	[37]	increased neuron apoptosis; abnormal neuron physiology; abnormal dendrite and synapse morphology; abnormal miniature excitatory postsynaptic currents [38].	
P08670	Vimentin; VIM	**12**	negative reg. of neuron projection development (GO:0010977); Bergmann glial cell dif. (GO:0060020); movement of cell or subcellular component (GO:0006928); intermediate filament organization (GO:0045109).	[39]	abnormal Purkinje cell dendrite morphology [40].	RA dif. SH-SY5Y regulated gene [36, 41]. *Neuronal precursors (replaced by Nfs in post-mitotic neurons)[42].*
P02545	Prelamin-A/C; LMNA	**4**	reg. of cell migration (GO:0030334); establishment or maintenance of microtubule cytoskeleton polarity (GO:0030951).	[43]	abnormal cholinergic neuron morphology [44]; axonal neuropathy Charcot-Marie-Tooth disorder type 2 in humans.	
P14923	Junction plakoglobin; JUP	**2**	cell adhesion (GO:0007155); desmosome assembly (GO:0002159); adherens junction assembly (GO:0034333) and organization (GO:0034332); cytoskeletal anchoring at PM(GO:0007016); cell migration (GO:0016477); reg. of cell proliferation (GO:0042127); positive reg. of canonical Wnt signaling.	[45]		RA dif. SH-SY5Y regulated gene [41].

D7						
Q6Y7W6	PERQ amino acid-rich with GYF domain-containing protein 2; GIGYF2	**6**	post-embryonic development (GO:0009791); spinal cord motor neuron dif. (GO:0021522); homeostasis of number of cells within a tissue (GO:0048873); cell-cell adhesion (GO:0098609)	[46]	motor neuron degeneration; abnormal neuron number ; postnatal lethality, incomplete penetrance; neonatal lethality, incomplete penetrance [47]; Involvement in Parkinson disease 11.	
Q8NC56	LEM domain-containing protein 2; LEMD2	**3**	Neurogenesis (GO:0022008); negative reg. of MAPK cascade (GO:0043409); negative reg. of BMP signaling pathway (GO:0030514).	-	abnormal embryonic neuroepithelium morphology, increased apoptosis and decreased proliferation; impaired neuron dif.; absent embryonic telencephalon; abnormal dorsal root ganglion, and retinal neuronal layer morphology; embryonic lethality during organogenesis, complete penetrance [48].	
P51116	Fragile X mental retardation syndrome-related protein 2; FXR2	**7**	*positive translation reg. of PSD95 mRNA (mouse hippocampus); role in neuronal dendritic development (binds, stabilizes, and enhances GluA1 mRNA expression); FXR2 deficiency in dendate gyrus neural stem cells enhances cell proliferation and dif. (by reg. Noggin expression)*.	[49-51]	hyperactivity; abnormal locomotor activity, sensimotor gating, and cognitive function; altered hippocampal synaptic plasticity [52-54].	*High expression in the brain* [55].
Q9UNN5	FAS-associated factor 1; FAF1	**3**	cytoplasmic sequestering of NF-kB (GO:0007253); reg. of cell adhesion (GO:0030155); positive reg. of extrinsic apoptotic signaling pathway via death domain receptors (GO:1902043)	[56]	embryonic lethality before implantation, complete penetrance; decreased susceptibility to dopaminergic neuron neurotoxicity; embryonic lethality, complete penetrance [57, 58].	
P68363	Tubulin alpha-1B chain; TUBA1B	**1**	microtubule cytoskeleton organization (GO:0000226); cytoskeleton organization (GO:0007010)	-	abnormal cerebral cortex (including visual, auditory, and somatosensory), hippocampus, and dentate gyrus morphology; abnormal hippocampal mossy fiber morphology; abnormal neuronal migration, neuron morphology, and dendrite morphology; decreased number and abnormal hippocampus pyramidal cell layer; abnormal cortex pyramidal cell morphology; several altered behaviors and cognitive functions [59, 60]; gene mutations cause Lissencephaly.	
Q16352	Alpha-internexin; INA	0	nervous system development (GO:0007399); substantia nigra development (GO:0021762); cell dif. (GO:0030154); NF cytoskeleton organization (GO:0060052); intermediate filament cytoskeleton organization (GO:0045104)	[61]		Group enriched (adrenal gland, cerebral cortex)

7.4.3. The dephosphoS655 APP interactome

This category included protein interactors uniquely identified in APPSA, and the interactors present in both APPWt and APPSA conditions. Since APPWt can be either phosphorylated or dephosphorylated at S655, the detection of the same protein interaction in APPWt and in the dephosphomimetic S655A mutant most probably indicates that this interaction happens when APP is S655 dephosphorylated. On differentiation D3, this category comprised 147 APP protein interactors (39 + 106). Again, most identified proteins are nucleic-acid binding proteins (40.7%; mainly RBP). The second most represented protein class is cytoskeletal proteins (8.3%; similar numbers of actin, MTs, and IFs), and enzyme modulators (8.3%), followed by hydrolases (6.9%), and TFs (5.5%). On differentiation D7, the total number of APP protein interactors detected increased to 222 (178 +43). 34.5% of these proteins are nucleic-acid binding proteins, 11.6% are cytoskeletal proteins (mainly from the actin family), 8.6% are chaperones, 6.9% are oxidoreductases, 5.2% are enzyme modulators (mainly small GTPases), and 4.7% are transferases. The two differentiation days share 49 APP protein interactors.

The differentiation D3 PPI sub-network presented 144 nodes (3 identified protein interactors were not mapped by the software) and 312 edges. This network had 35 isolated nodes (~24%), and an overall cluster coefficient of 0.172. APP gathered 28 already known interactions. Other important proteins based on node degree were: SNW1 (k = 52), SF3A2 (k = 27), HNRNPU (k = 23), HNRNPA1 (k = 18), and YWHAG (k = 16). The differentiation D7 sub-network had 218 nodes, of which 28 were isolated nodes (~13%), and 576 edges with an average clustering coefficient of 0.292. Within this sub-network APP presented 74 known protein interactors. Also, highlighted by their node degree are: YWHAZ (k = 77), SNW1 (k = 61), ACTB (k = 34), HRNPN4 (k = 33), NPM (k = 29), and RPL10 (k = 28). These D3 and D7 PPI networks are not presented as figures due to space restrictions.

Figure B.20 A and B show the results obtained for differentiation D3 functional enrichment analysis of the dephosphoS655 APP interactome. Enriched biological process gene ontology terms are mainly related to regulation of mRNA processing and translation (Figure B.20 A). KEGG enrichment analysis (Figure B.20 B) showed that, in addition to a role in ribosome, spliceosome, and mRNA surveillance, this group might have an involvement in tight-junction and in the Hippo signaling pathway. Molecular functions not included in Figure B.20 but also found enriched are: neural nucleus development (p = 510.0E-6) and substantia nigra development (p = 99.0E-6) with the following associated gene names: ACTB, CALM1/2/3, HSPA5, INA, YWHAQ. Additionally, the Panther overrepresentation analysis (Supplementary Table B.6) assigned a function as

structural constituent of cytoskeleton, cytoskeleton regulation by RhoGTPases, cell-cell adhesion via cadherin binding, and a relation to Parkinson disease.

The results obtained for differentiation D7 functional enrichment analysis (Figure B.20 C and D) also assigned a role in substantia nigra development (p = 170E-9) and in negative regulation of MT polymerization (p = 11E-3). Functional enrichment in regulation of protein localization to Cajal body, and in energy metabolism, indicates that these functions (above observed when analyzing the total APP interactome, can be mainly attributed to the dephosphoS655 APP interactome. In Figure B.20 D we can see the enriched KEGG functions attributed to this D7 S655A group, highlighting transcription and translation-related regulatory pathways, and energy metabolism. The Panther overrepresentation analysis (Supplementary Table B.6), attributed similar functions as the ones of day 3, and reinforced the results obtained by ClueGo. This analysis further highlighted functions in actin filament binding and actin binding. Of note, both analyses attributed PKC inhibitor activity (ClueGO Pvalue = 100E-6) due to the presence of HSPB1, SFN, and YWHAG. Functional annotation of individual proteins allowed to select dephosphoS655 APP protein interactors that might be of special interest for neuronal differentiation. The selection criteria applied indicated 11 protein interactors shared by D3 and D7 (Table B.4), 10 unique for differentiation D3 (Table B.5), and 25 unique for differentiation D7 (Table B.6 and Supplementary Table B.7).

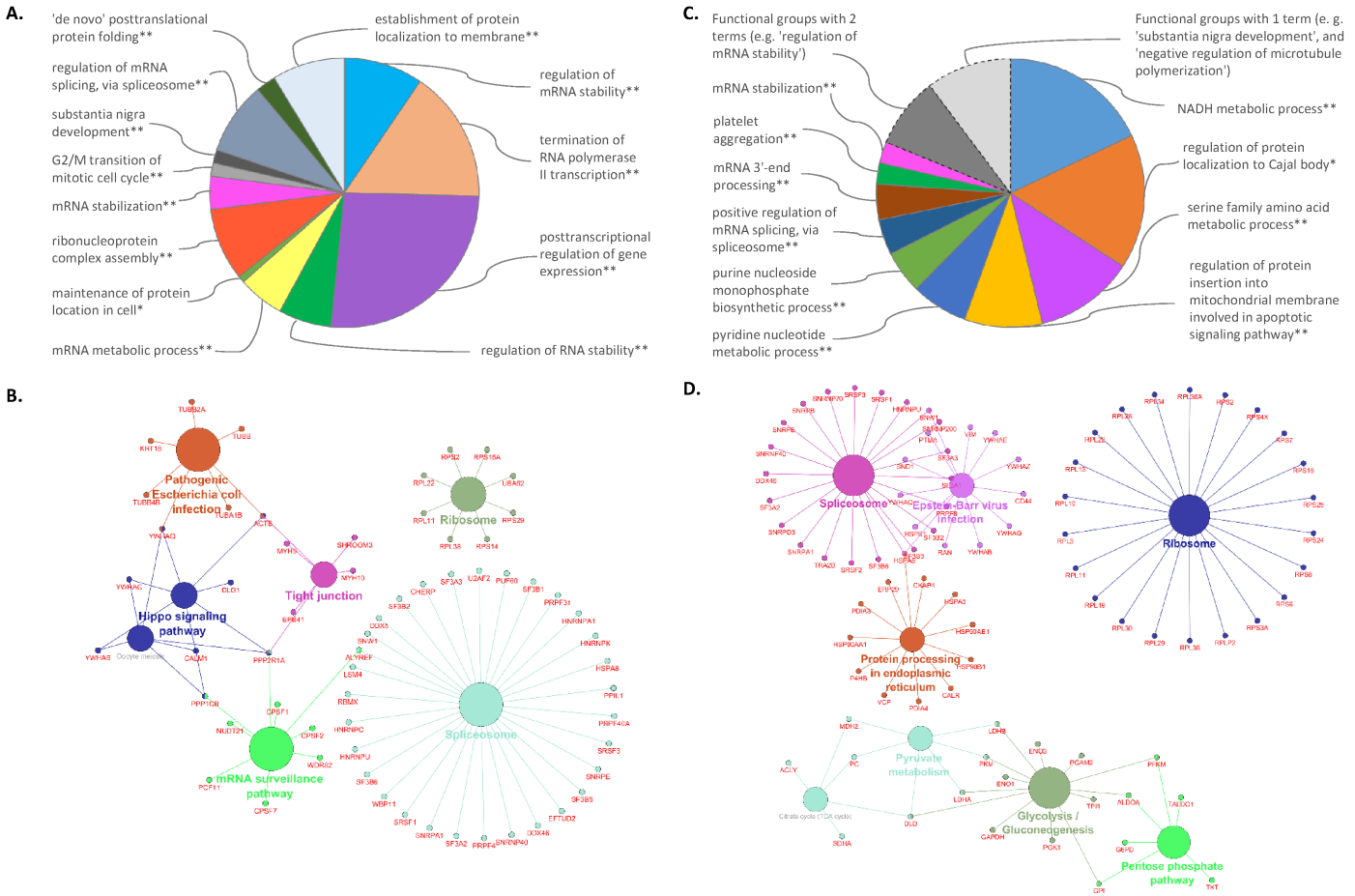

Figure B.20 - **Functional annotation analysis of the dephosphoS655 APP interactome. A.** Pie chart representation of the biological process functional groups attributed to differentiation day 3 (D3). **B.** Enriched pathways (KEGG) gene ontology terms attributed to differentiation day 3 (D3). **C.** Pie chart representation of the biological process functional groups attributed to differentiation day 7 (D7). **D.** Enriched pathways (KEGG) gene ontology terms attributed to D7. The enrichment analysis was performed using the Cytoscape app ClueGO, and only terms with pvalue < 0.05 are represented; each group was named accordingly to the most significant GO term. Gene's names were added using the CluePedia app**.**

Table B.4 - **APP interactors associated with dephosphoS655 present in both differentiation days 3 and 7, and with potential interest for neuronal differentiation.** Proteins were selected based on functional annotations directly related to brain development, neuron function, neurogenesis, and/or neuronal differentiation related events (cytoskeleton organization, cell adhesion, and cell migration) and signaling pathways. In bold are the UniProt accession number of newly identified APP interactors. The gene ontology (GO) terms determinant for the selection are described in the biological process column. Node degree ('k'), is the number of APP interactors that the protein presents and refers to the position of the protein inside the protein-protein interaction network that includes all the interactors identified in the S655A conditions at differentiation days 3 and 7, respectively. 'Ref', indicates references retrieved from the PubMed supporting the role of the indicated interactor in neuronal differentiation. 'Mammalian phenotype/human diseases', KO mouse phenotypes were searched on Jackson Laboratories mouse knockout database, and human diseases retrieved from UniProt and other indicated references. 'Expression', brain enrichment or altered expression in RA-differentiated SH-SY5Y cells are indicated. 'Dif.' – differentiation; 'Reg.' – regulation; 'PM' – plasma membrane; 'AD' - Alzheimer's disease; 'PD' – Parkinson's disease.

Uniprot nr	Gene name and symbol	k at D3 / D7	Biological Process	Ref	Mammalian phenotype/ human diseases	Expression
Q9H0D6	5'-3' exoribonuclease 2; XRN2	4 / 5	hippocampus development (GO:0021766); neuron dif. (GO:0030182); cell growth (GO:0016049)	[62, 63]		
P15884	Transcription factor 4; TCF4	5 / 3	positive regulation of neuron dif. (GO:0045666); nervous system development (GO:0007399); cell dif. (GO:0030154)	[64, 65]	abnormal brain development [66]; Pitt-Hopkins mental retardation Syndrome; schizophrenia susceptibility gene	
Q13573	SNW domain-containing protein 1; SNW1	89 / 106	positive regulation of neurogenesis (GO:0050769); Notch signaling pathway (GO:0007219); positive regulation of TGFBR signaling (GO:0030511); regulation of RAR signaling (GO:0048385);	[67, 68]		
P11021	78 kDa glucose-regulated protein; HSPA5	11 / 20	cerebellum structural organization (GO:0021589); cerebellar Purkinje cell layer (GO:0021680), and substantia nigra development (GO:0021762); positive regulation of cell migration (GO:0030335); negative regulation of TGFBR signaling (GO:0030512); negative regulation of apoptotic process (GO:0043066); cell-cell adhesion (GO:0098609)	[69-71]	abnormal cerebral cortex morphology and stratification; abnormal hippocampus and cerebellum morphology; abnormal brain white matter and internal capsule morphology; abnormal neuron dif. and proliferation [69]	APP-KO (prefrontal cortex) down-regulated gene [72]; RA dif SH-SY5Y regulated gene [36].

Uniprot nr	Gene name and symbol	k at D3 / D7	Biological Process	Ref	Mammalian phenotype/ human diseases	Expression
P35580	Myosin-10; MYH10	3 / 3	brain development (GO:0007420); cerebellar Purkinje cell layer development (GO:0021680); neuron migration (GO:0001764); neuron projection development (GO:0031175); axonogenesis (GO:0007409); axon guidance (GO:0007411); substrate-dependent cell migration, cell extension (GO:0006930); cell adhesion (GO:0007155); cell proliferation (GO:0008283); regulation of cell shape (GO:0008360); actin filament-based movement (GO:0030048); actomyosin structure organization (GO:0031032); actin cytoskeleton organization (GO:0030036)	[73, 74]	abnormal neuronal migration; abnormal Purkinje cell dendrite morphology [75, 76]	Id as APP interactor in mouse brain [77].
P07196	Neurofilament light polypeptide; NEFL	3 / 4	neuron projection morphogenesis (GO:0048812); positive regulation of axonogenesis (GO:0050772); axon development (GO:0061564); regulation of axon diameter (GO:0031133); PNS axon regeneration (GO:0014012); spinal cord (GO:0021510), hippocampus (GO:0021766), and cerebral cortex development (GO:0021987); negative regulation of neuron apoptotic process (GO:0043524); anterograde (GO:0008089) and retrograde (GO:0008090) axonal transport; NF bundle assembly (GO:0033693); NF cytoskeleton organization (GO:0060052); MAPK cascade (GO:0000165); MT cytoskeleton organization(GO:0000226); intermediate filament polymerization or depolymerization (GO:0045105)	[78]	Demyelinating neuropathy Charcot-Marie-Tooth disease 1F, and axonal neuropathy Charcot-Marie-Tooth disease 2E	Tissue enriched (cerebral cortex)
P61981	14-3-3 protein gamma; YWHAG	28 / 31	regulation of neuron dif. (GO:0045664); regulation of synaptic plasticity (GO:0048167); cellular response to insulin (GO:0032869); membrane organization (GO:0061024); positive regulation of protein insertion into mitochondrial membrane involved in apoptotic signaling pathway (GO:1900740)	[79, 80]		Increased expression in AD, decreased in Down Syndrome, present in Lewy bodies in PD [79]. Id as APP interactor in mouse brain [77].
P62158	Calmodulin; CALM1/2/3	2 / 5	*NT release; regulates expression of synaptic proteins; mediates calcium signal involved in growth cone guidance and dendrite growth*	[81, 82]	Downregulated in AD substantia nigra samples [83].	

Uniprot nr	Gene name and symbol	k at D3 / D7	Biological Process	Ref	Mammalian phenotype/ human diseases	Expression
P11142	Heat shock cognate 71 kDa protein; HSPA8	7 / 10	neurotransmitter secretion (GO:0007269); regulation of cell cycle (GO:0051726); cell-cell adhesion (GO:0098609)	[71, 84]		
P35579	Myosin-9; MYH9	11 / 23	cell morphogenesis involved in dif. (GO:0000904); regulation of cell shape (GO:0008360); cell adhesion(GO:0007155); integrin-mediated signaling (GO:0007229); actin filament-based movement (GO:0030048); actomyosin structure organization (GO:0031032); actin cytoskeleton reorganization (GO:0031532); negative regulation of actin filament severing (GO:1903919)	[73]		Id as APP interactor in mouse brain [77].
Q15149	Plectin; PLEC	7 / 7	hemidesmosome assembly (GO:0031581); cell-cell adhesion (GO:0098609)	[85, 86]		

Table B.5 - **DephosphoS655 APP associated protein interactors present only in differentiation day 3, and with potential interest for neuronal differentiation.** Proteins were selected based on functional annotations directly related to brain development, neuron function, neurogenesis, and/or neuronal differentiation related events (cytoskeleton organization, cell adhesion, and cell migration) and signaling pathways. In bold are the UniProt accession number of newly identified APP interactors. The gene ontology terms determinant for the selection are described in the biological process column. Node degree ('k'), is the number of interactors the protein presents and refers to the position of the protein inside the protein-protein interaction network that includes all the interactors identified for differentiation day 3. 'Ref', indicates references retrieved from the PubMed supporting the role of the indicated interactor in neuronal differentiation. 'Mammalian phenotype/human diseases', KO mouse phenotypes were searched on Jackson Laboratories mouse knockout database, and human diseases retrieved from UniProt and other indicated references. 'Expression', brain enrichment or altered expression in RA-differentiated SH-SY5Y cells are indicated. 'Dif.' – differentiation; 'Reg.' – regulation; 'PM' – plasma membrane; 'PD' – Parkinson's disease.

Uniprot nr	Gene name and symbol	K D3	Biological Process	Ref	Mammalian Phenotype	Expression
Q6Y7W6	PERQ amino acid-rich with GYF domain-containing protein 2; GIGYF2	7	post-embryonic development (GO:0009791); spinal cord motor neuron dif. (GO:0021522); insulin-like growth factor receptor signaling (GO:0048009); homeostasis of number of cells within a tissue (GO:0048873); cell-cell adhesion (GO:0098609)	[46]	motor neuron degeneration; impaired coordination; abnormal movement; neurodegeneration; abnormal neuron number; postnatal lethality, incomplete penetrance; neonatal lethality, incomplete penetrance [47]; Involvement in PD 11.	

Uniprot nr	Gene name and symbol	KD3	Biological Process	Ref	Mammalian Phenotype	Expression
Q8NC56	LEM domain-containing protein 2; LEMD2	2	neurogenesis(GO:0022008); negative reg. of MAPK cascade (GO:0043409); negative reg. of BMP signaling (GO:0030514)	-	increased apoptosis, decreased cell proliferation and abnormal morphology of embryonic neuroepithelium; absent embryonic telencephalon; abnormal retinal neuronal layer, and dorsal root ganglion morphology; impaired neuron dif.; embryonic lethality during organogenesis, complete penetrance [48].	
P51116	Fragile X mental retardation syndrome-related protein 2; FXR2	11	positive translation reg. of PSD95 mRNA (mouse hippocampus); role in neuronal dendritic development (binds, stabilizes, and expression enhancement of GluA1 mRNA); FXR2 deficiency in dendate gyrus neural stem cells enhances cell proliferation and dif. (by reg. Of Noggin expression)	[49-51]	hyperactivity; abnormal locomotor activity, sensimotor gating, and cognitive function; altered hippocampal synaptic plasticity [52-54].	*High expression in the brain* [55].
P61978	Heterogeneous nuclear ribonucleoprotein K; HNRNPK	20	CNS (GO:0007417) and PNS (GO:0007422) development; cerebellum (GO:0021549), hippocampus (GO:0021766), and cerebral cortex development (GO:0021987); positive reg. of neuron projection development (GO:0010976); positive reg. of dendrite extension (GO:1903861), dendritic spine development (GO:0060999), synapse maturation (GO:0090129), synaptic transmission (GO:0050806), and long-term synaptic potentiation (GO:1900273); negative reg. of branching morphogenesis of a nerve (GO:2000173); aging (GO:0007568); cellular response to insulin (GO:0032869); negative reg. of apoptotic process (GO:0043066).	[87, 88]	Au-Kline syndrome (intellectual disability).	
Q8TF72	Protein Shroom3; SHROOM3	4	cell morphogenesis (GO:0000902); neural tube closure (GO:0001843); reg. of cell shape (GO:0008360).	[89-91]	open neural tube in 100% of mice, which leads to exposure of the forebrain neuroepithelium (exencephaly) [92].	

Uniprot nr	Gene name and symbol	KD3	Biological Process	Ref	Mammalian Phenotype	Expression
Q12959	Disks large homolog 1; DLG1	0	nervous system development (GO:0007399); chemical synaptic transmission (GO:0007268); reg. of myelination (GO:0031641); receptor localization to synapse (GO:0097120); APP metabolic process (GO:0042982); establishment or maintenance of cell polarity (GO:0007163); positive reg. of cell proliferation (GO:0008284); reg. of cell shape (GO:0008360); positive reg. of actin filament polymerization (GO:0030838); cortical actin cytoskeleton organization (GO:0030866); cortical MT organization (GO:0043622); negative reg. of ERK1 and ERK2 (GO:0070373); bicellular tight junction assembly (GO:0070830); reg. of NIK/NF-kB signaling (GO:1901222).	[93]	abnormal dendrite morphology [94].	
P21741	Midkine; MDK	0	cerebral cortex (GO:0021987), hippocampus (GO:0021766), dentate gyrus (GO:0021542), and cerebellar granular layer development (GO:0021681); short-term memory (GO:0007614); Notch signaling pathway (GO:0007219); cell migration (GO:0016477); cell dif. (GO:0030154); negative reg. of neuron apoptotic process (GO:0043524).	[95, 96]	abnormal hippocampus development [97].	
Q8NFD5	AT-rich interactive domain-containing protein 1B; ARID1B	0	nervous system development (GO:0007399)	[98]	Coffin-Siris syndrome (malformations of the CNS, intellectual disability and speech impairment).	
Q16352	Alpha-internexin; INA	0	nervous system development (GO:0007399); substantia nigra development (GO:0021762); cell dif. (GO:0030154); NF cytoskeleton organization (GO:0060052); intermediate filament cytoskeleton organization (GO:0045104)	[61]		Group enriched (adrenal gland, cerebral cortex)
Q6DN90	IQ motif and SEC7 domain-containing protein 1; IQSEC1	0	reg. of ARF protein signal transduction (GO:0032012); positive reg. of GTPase activity (GO:0043547); actin cytoskeleton organization (GO:0030036)	[99]		

Table B.6 - **DephosphoS655 APP associated protein interactors present only in differentiation day 7, and with potential interest for neuronal differentiation.** Proteins were selected based on functional annotations directly related to brain development, neuron function, neurogenesis, and/or neuronal differentiation related events (cytoskeleton organization, cell adhesion, and cell migration) and signaling pathways. In bold are the UniProt accession number of newly identified APP interactors. The gene ontology (GO) terms determinant for the selection are described the biological process column. Node degree ('k'), is the number of interactors the protein presents and refers to the position of the protein inside the protein-protein interaction network that includes all the interactors identified for differentiation day 7. 'Ref', indicates references retrieved from the PubMed supporting the role of the indicated interactor in neuronal differentiation. 'Mammalian phenotype/human diseases', KO mouse phenotypes were searched on Jackson Laboratories mouse knockout database, and human diseases retrieved from UniProt and other indicated references. 'Expression', brain enrichment or altered expression in RA-differentiated SH-SY5Y cells are indicated. 'Dif.' – differentiation; 'Reg.' – regulation; 'PM' – plasma membrane; 'AD' - Alzheimer's disease; 'PD' – Parkinson's disease.

Uniprot nr	Gene name and symbol	k	Biological Process	Ref	Mammalian Phenotype	Expression
P16949	Stathmin; STMN1	2	cell dif. (GO:0030154); nervous system development (GO:0007399); neuron projection development (GO:0031175); axonogenesis (GO:0007409); brain development (GO:0007420); reg. of cytoskeleton organization (GO:0051493); reg. of MT polymerization or depolymerization (GO:0031110); MT depolymerization (GO:0007019); negative reg. of MT polymerization (GO:0031115).	[100]	abnormal nervous system morphology; abnormal brain morphology; axon degeneration; demyelination [101].	
P09382	Galectin-1; LGALS1	2	negative reg. of neuron projection development (GO:0010977); response to axon injury (GO:0048678); negative reg. of cell-substrate adhesion (GO:0010812); reg. of apoptotic process (GO:0042981); positive reg. of I-kB kinase/NF-kB signaling (GO:0043123)	[102]	abnormal dorsal root ganglion, sensory neuron, nociceptor, mechanoreceptor, and olfactory sensory neuron morphology [103, 104]; increased number of neural precursor cells; impaired memory formation [105].	
P62826	GTP-binding nuclear protein Ran; RAN	4	hippocampus development (GO:0021766); actin cytoskeleton organization (GO:0030036); cell division (GO:0051301); cell-cell adhesion (GO:0098609)	[106]		

Uniprot nr	Gene name and symbol	k	Biological Process	Ref	Mammalian Phenotype	Expression
Q06787	Fragile X mental retardation protein 1; FMR1	1	positive reg. of dendritic spine development (GO:0060999); negative reg. of long term synaptic depression (GO:1900453); negative reg. of synaptic vesicle exocytosis (GO:2000301); positive reg. of receptor internalization (GO:0002092); glutamate receptor signaling (GO:0007215); positive reg. of filopodium assembly(GO:0051491)	[37, 49, 82]	decreased Purkinje cell number, and abnormal morphology; abnormal brain morphology; abnormal CNS synaptic transmission; abnormal hippocampal mossy fiber and pyramidal cells morphology; abnormal nerve fiber response; abnormal neuronal precursor proliferation; abnormal neuron dif., and dendritic spine morphology; abnormal learning/memory/conditioning [53, 54, 107-109] ; gene mutations cause fragile X syndrome; Fragile X tremor/ataxia syndrome.	*High expression in the brain* [55].
P62258	14-3-3 protein epsilon; YWHAE	8	neuron migration (GO:0001764); substantia nigra (GO:0021762), hippocampus (GO:0021766), and cerebral cortex development (GO:0021987); hippo signaling (GO:0035329); membrane organization (GO:0061024); cell-cell adhesion (GO:0098609)	[79, 110]	abnormal neuronal migration; abnormal hippocampus pyramidal cell layer; perinatal lethality, complete penetrance; perinatal lethality, incomplete penetrance [111]; gene deletion in Miller-Dieker syndrome;	Increased expression in AD, present in Lewy bodies in Parkinson disease PD [79]. Id as APP interactor in mouse brain [77].
P63104	14-3-3 protein zeta/delta; YWHAZ	93	negative reg. of apoptotic process (GO:0043066); membrane organization (GO:0061024); positive reg. of protein insertion into mitochondrial membrane involved in apoptotic signaling pathway (GO:1900740); cell-cell adhesion(GO:0098609)	[79, 110]	abnormal neuronal migration; abnormal dendrite morphology; abnormal hippocampus pyramidal cell layer; abnormal hippocampus granule cell morphology; ectopic hippocampus pyramidal cells; postnatal lethality, incomplete penetrance [112];	Present in AD tangles, and Lewy bodies in PD [79]. Id as APP interactor in mouse brain [77].

Uniprot nr	Gene name and symbol	k	Biological Process	Ref	Mammalian Phenotype	Expression
P27797	Calreticulin; CALR	4	negative reg. of neuron dif. (GO:0045665); cell cycle arrest (GO:0007050); positive reg. of cell proliferation (GO:0008284), and of substrate adhesion-dependent cell spreading (GO:1900026); cortical actin cytoskeleton organization (GO:0030866); reg. of apoptotic process (GO:0042981); negative reg. of RAR signaling pathway (GO:0048387); positive reg. of NIK/NF-kB signaling(GO:1901224)	[113]	*Brain defects: defects in neural tube closure and exencephaly [114].*	
P46821	MT-associated protein 1B; MAP1B	1	nervous system development (GO:0007399); positive reg. of axon extension (GO:0045773); axonogenesis (GO:0007409); dendrite development (GO:0016358); MT cytoskeleton organization(GO:0000226); MT bundle formation(GO:0001578);	[82, 115]		Tissue enhanced (cerebral cortex)
P80723	Brain acid soluble protein 1; BASP1	3	substantia nigra development (GO:0021762)	[116]	abnormal cerebral cortex and hippocampus morphology; abnormal Schwann cell morphology; abnormal neuron morphology and axon extension; abnormal motor nerve collateral sprouting; postnatal lethality, incomplete penetrance [117].	Tissue enhanced (cerebral cortex)
P23528	Cofilin-1; CFL1	6	reg. of dendritic spine morphogenesis (GO:0061001); actin filament depolymerization (GO:0030042); Rho protein signal transduction (GO:0007266); reg. of cell morphogenesis (GO:0022604); actin cytoskeleton organization (GO:0030036); negative reg. of apoptotic process (GO:0043066)	-	abnormal neural tube morphology; premature neuronal precursor dif. and abnormal proliferation; abnormal neuron dif., axon extension, and neurite morphology; postnatal lethality, incomplete penetrance; prenatal lethality, complete penetrance; enlarged brain ventricles; decreased embryonic neuroepithelium thickness [118, 119].	
O43175	D-3-phosphoglycerate dehydrogenase; PHGDH	1	brain (GO:0007420) and spinal cord development (GO:0021510); glial cell development (GO:0021782); neural tube development (GO:0021915); neuron projection development (GO:0031175); neurogenesis(GO:0022008); GABA metabolic process (GO:0009448)	[120]	decreased brain size; abnormal embryonic neuroepithelial layer dif.; absent cerebellum; abnormal brain development; exencephaly; decreased brain weight; abnormal neuron dif.; embryonic lethality during organogenesis, complete penetrance [121]; Neu-Laxova syndrome 1 (CNS anomalies: lissencephaly, cerebellar hypoplasia and/or	

Uniprot nr	Gene name and symbol	k	Biological Process	Ref	Mammalian Phenotype	Expression
					abnormal/ agenesis of the corpus callosum), Phosphoglycerate dehydrogenase deficiency (microcephaly, psychomotor retardation).	
P08670	Vimentin; VIM	16	negative reg. of neuron projection development (GO:0010977); movement of cell or subcellular component (GO:0006928); intermediate filament organization (GO:0045109); Bergmann glial cell dif. (GO:0060020); SMAD protein signal transduction (GO:0060395)	[39]	abnormal Purkinje cell dendrite morphology [40].	RA dif SH-SY5Y regulated gene [36, 41].
P62995	Transformer-2 protein homolog beta; TRA2B	8	cerebral cortex regionalization (GO:0021796); embryonic brain development (GO:1990403)	-	*conditional KO mouse: extensive apoptosis of NPC, defects in dif. of cortical layers and development of projection neuron axons, massive apoptosis in the ventricular layers of the cortex, die immediately after birth* [122, 123].	
P06748	Nucleophosmin; NPM1	38	reg. of neuron apoptotic process (GO:0043523); cell aging (GO:0007569); positive(GO:0008284) and negative (GO:0008285) reg. of cell proliferation; negative reg. of apoptotic process (GO:0043066); positive reg. of NF-kB transcription factor activity (GO:0051092)	[124]	abnormal brain morphology [125].	

7.4.4. The phosphoS655 APP interactome

This category included interactors present uniquely in the APPSE condition, and the interactors common to both APPWt and APPSE conditions. On differentiation D3 we were able to identify 15 APP protein interactors specific of phosphorylated APP655 at this time point, and at differentiation D7 we identified 23 APP S655E protein interactors. Comparing with the other aforementioned groups, this category had considerably less protein interactors. The sub-networks were mainly composed of isolated nodes, and functional enriched analysis did not retrieve any significant results. For these reasons, specifically for the phosphoS655 APP interactome, we performed network augmentation by increasing our protein-protein interaction network with known protein partners (in blue) of our protein interactors input list (in pink). To control the network complexity, we only add blue nodes with a minimum node degree of 2 (i.e., proteins that bind to at least two of our experimentally identified interactors). Differentiation day 3 "augmented" network had 46 nodes with 96 edges (Figure B.21 A; note that the interactor UPS17L3, Uniprot accession number A6NCW0, a described APP interactor also detected by us, was not mapped by the cystoscape). APP connected to 15 known protein interactors, 4 of which now identified by us as S655-phosphorylation dependent: CNBP, COL14A1, FAM184A, and PRDX2. Other protein interactors identified by us which stand out based on their node degree included: histone H4 (k = 18) and histone H1.2 (k = 16), and PRDX2 (k = 17). The differentiation D7 "augmented" network had 126 nodes with 278 edges (Figure B.22 A; note that the interactors DNAH12 and IGHV3, Uniprot accession number Q6ZR08 and P01765, were not mapped by the cystoscape). APP connected to 15 already described protein interactors, 5 of which here identified by us as S655 phosphorylation dependent: CAPRIN1, CLP1, FUBP3, HNRNPA1, RPS14. Within this network, detected protein interactors highlighted due to their high node degree include: HNRNPA1 (k = 49), PPPICB (k = 35), and the ribosomal proteins RPS14 (k = 33), RPS27 (k = 19), RPL12 (k = 21), and RBM14 (k = 18). Curiously, some proteins attributed by network augmentation have been also identified in this work, although allocated to a different S655 phosphorylation category. Interestingly, functional enrichment analysis of the phosphoS655 APP interactome after network augmentation assigned modulatory roles in various relevant signaling pathways (as neurotrophic and apoptotic signaling) to the D3 and D7 interactors (Figure B.21 B; Figure B.22 B; Table B.7). These include roles in the FoxO signaling pathway, in the regulation of EGFR signaling, response to NGF signaling, and beta-tubulin binding/GABA receptor binding (these last functions relate to the presence of GABARAP, GABARAPL1, and GABARAPL2). Interestingly, D7 had a high number of proteins associated with: cell response to TGFbeta, signal transduction by p53 class mediator and negative

regulation of cell death (Table B.7); TNF signaling pathway (p = 9.4E-3), tight junction (p = 700E-6) and focal adhesion (p = 8.5E-3) (Figure B.22 B).

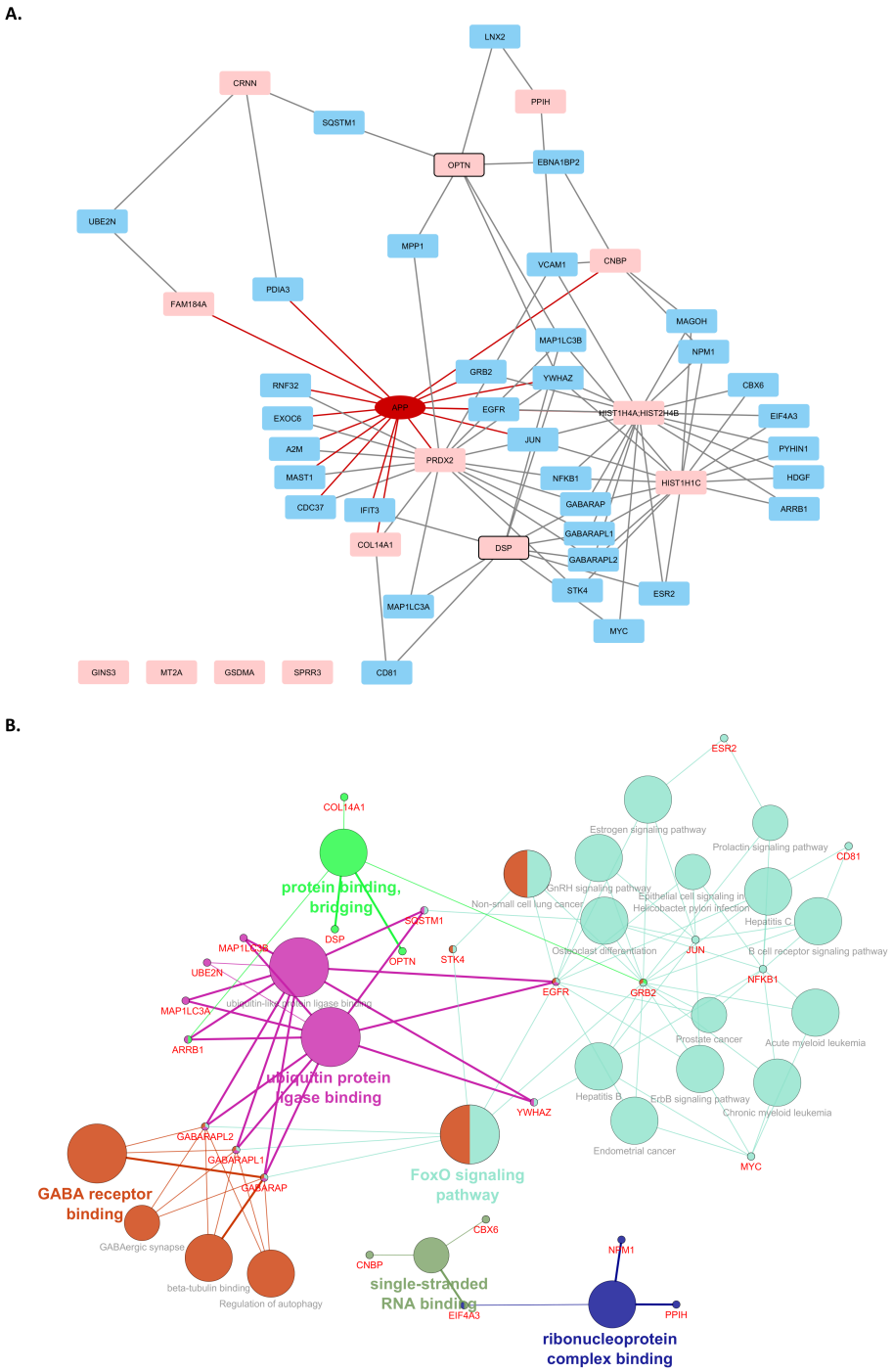

Figure B.21 - **PhosphoS655 APP interactome at differentiation day 3. A.** Expanded phosphoS655 APP protein-protein interaction network. APP interacting proteins experimentally identified in this work are presented in pink. The protein-protein interaction network was augmented to include known interactors of the identified proteins (nodes in blue); to reduce complexity, only blue nodes with a minimum node degree of 2 were maintained and here presented. Black marked nodes indicate APP interactors that might have special interest for neuronal differentiation studies. **B.** Enriched molecular functions and KEGG pathways gene ontology terms. The enrichment analysis was performed using the Cytoscape app ClueGO; only terms with pvalue < 0.05 are represented. The genes associated with each term were added using the CluePedia app.

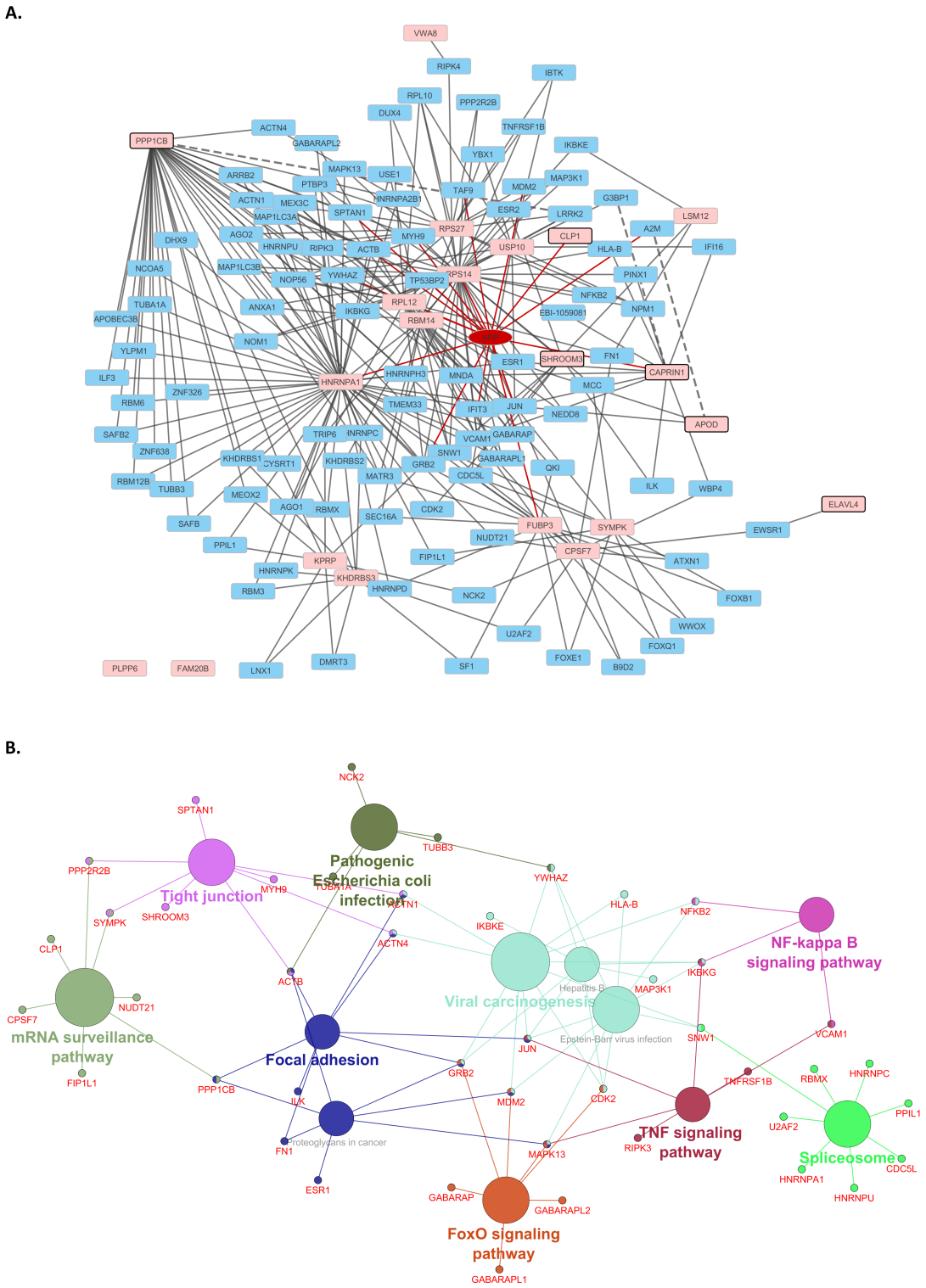

Figure B.22 - **PhosphoS655 APP interactome at differentiation day 7. A.** Expanded phosphoS655 APP protein-protein interaction network. APP interacting proteins experimentally identified in this work are presented in pink. The protein-protein interaction network was augmented to include known interactors of the identified proteins (nodes in blue), which bind to at least two of the here identified APP interactors (blue nodes with a minimum node degree of 2). Black marked nodes indicate the APP interactors that might have special interest for neuronal differentiation studies. **B.** Enriched KEGG pathways gene ontology terms. The enrichment analysis was performed using the Cytoscape app ClueGO, only terms with pvalue < 0.05 are represented. The genes associated with each term were added using the CluePedia app.

Table B.7 - **Enriched biological processes (BP) and molecular functions (MF) attributed to the phospho655 APP interactome and with interest for neuronal differentiation.** The enrichment analysis was performed using the Cytoscape app ClueGO. D3 and D7, differentiation days 3 and 7, respectively. GO term, the enriched term attributed. GO source, the gene ontology sources, namely molecular function (MF), biological processes (BP), and KEGG pathways. Pvalue, calculated pvalue with Bonferroni correction; % genes, percentage of proteins (here by the gene name) associated to the attributed enriched term; ID, the gene names of the proteins associated with the attributed enriched terms. EGFR, Epidermal growth factor receptor; NGF, Nerve growth factor; TGF, Transforming growth factor.

Dif. day	GO term	GO source	PValue	% Genes	ID
D3	regulation of EGFR signaling pathway	BP	1.4E-3	4.94	APP, EGFR, ESR2, GRB2
	cellular response to NGF stimulus	BP	2.6E-3	7.89	APP, EIF4A3, NFKB1
	receptor internalization	BP	12.0E-3	3.45	ARRB1, CD81, GRB2
D7	regulation of EGFR signaling pathway	BP	27.0E-3	6.17	APP, ESR1, ESR2, GRB2, NCK2
	positive regulation of actin filament polymerization	BP	32.0E-3	3.00	GRB2, MAP3K1, NCK2
	cellular response to TGFbeta stimulus	BP	49.0E-3	3.01	ARRB2, FN1, JUN, MAP3K1, NEDD8, PPP1CB, SNW1, WWOX
	intracellular estrogen receptor signaling pathway	BP	41.0E-3	7.84	ESR1, ESR2, RBM14, SAFB
	cellular response to estrogen stimulus	BP	24.0E-3	9.30	ESR1, ESR2, HNRNPD, MDM2
	signal transduction by p53 class mediator	BP	41.0E-3	3.59	CDK2, MDM2, SNW1, TAF9, TP53BP2, USP10, WWOX
	intrinsic apoptotic signaling pathway	BP	10.0E-3	3.12	IKBKE, LRRK2, NCK2, RIPK3, SNW1, TAF9, TNFRSF1B, TP53BP2, WWOX, YWHAZ
	negative regulation of neuron death	BP	38.0E-3	3.65	ESR1, ESR2, FOXB1, IKBKG, ILK, JUN, LRRK2
	posttranscriptional gene silencing by RNA	BP	3.6E-3	9.80	AGO1, AGO2, CLP1, HNRNPA2B1, RBM3
	production of miRNAs involved in gene silencing by miRNA	BP	3.3E-3	16.00	AGO1, AGO2, HNRNPA2B1, RBM3
	GABA receptor binding	MF	4.2E-3	20.00	GABARAP, GABARAPL1, GABARAPL2
	beta-tubulin binding	MF	30.0E-3	8.11	GABARAP, GABARAPL1, GABARAPL2
	cell adhesion molecule binding	MF	30.0E-3	3.00	ACTN1, ACTN4, FN1, ILK, RPL10, VCAM1
	integrin binding	MF	4.5E-3	5,17	ACTN1, ACTN4, FN1, ILK, RPL10, VCAM1
	p53 binding	MF	4.2E-3	6,94	MDM2, TAF9, TP53BP2, USP10, YBX1
	receptor signaling protein serine/threonine kinase activity	MF	22.0E-3	5,80	IKBKE, MAP3K1, MAPK13, RIPK3

Functional annotation of individual protein interactors here detected, allowed to discriminate phosphoS655 APP protein interactors that might be of special interest for neuronal differentiation studies (Table B.8). Since some of the interactors belong to another category at a different differentiation day (Supplementary Table B.3), the interactors were divided into ‘exclusive’ or ‘enriched at a given time point of differentiation. In general, functional annotation of individual proteins revealed that from the 11 exclusive phosphoS655 APP interactors identified at D3, 8 (GINS3, DSP, USP17L3, GSDMA, OPTN, CRNN, COL14A1, SPRR3) (73%) can be associated to the regulation of epithelial cell division, apoptosis and differentiation. Other 2 are involved in

mRNA processing: PPIH, a chaperone involved in RNA splicing, and CNBP, a zinc finger protein that binds translation-related mRNAs in response to growth factors and heat shock. The four D3-enriched phospho655 interactors include 2 histones that are associated with negative regulation of cell growth (HIST1H4A, and HIST1H1C), and 2 interactors involved in redox regulation, cellular response to drug and regulation of cell growth: MT2A, and Peroxiredoxin-2. From the 23 proteins that only interact with S655E APP at D7, 9 are exclusive phosphoS655 APP interactors, and 14 are enriched at this time point. From the 9 exclusive phosphoS655 APP interactors identified at D7, 3 are involved in mRNA maturation and translation: 2 polyadenylation complex members/factors that may also regulate mRNA decay (SYMPK, CLP1), and a 60S ribossomal protein (RPL12). DNAH12 is a dynein, and the remaining 4 exclusive interactors appear to regulate (directly or indirectly) cell signaling: FAM20B catalyzes proteoglycans; PLPP6 is a phospholipid phosphatase that decreases the rate of phosphatidylinositol synthesis; ApoD is involved in lipid metabolism; FUBP3 binds to the 3'-UTR of FGF9 mRNA and promotes the expression of FGF9 [126]. Nine of the 14 (64.3%) D7-enriched phospho655 interactors are RNA binding and RNA processing/translation regulators: RPS14, RPS27, CPSF7, CLP1, FUBP3, KHDRBS3, RPL12, CAPRIN1, and ELAVL4. We considered three phosphoS655 APP protein interactors to be of particular interest for neuronal differentiation events at D3, and five (2 exclusive and 3 enriched) at D7 (Table B.8). Of note, on D3 all the three assigned proteins are one node away from PRDX2, a protein with high node degree, within the "augmented" network (see Figure B.21 A). On D7, SHROOM3 and CAPRIN1 are connected by integrin-linked protein kinase (ILK).

7.4.5. APP S655 phosphomimetic mutants are associated with specific cell phenotypes

To complement our APP interactome results, we analyzed cell morphology parameters related with neuronal-like differentiation. From the F-actin analysis, we distinguished three different phenotypes accordingly to the organization of the actin filaments: a fibrous phenotype with cells that shown mainly long actin stress fibers that cross all cell ('Fibers', Figure B.23 A); a cortical phenotype, where it is visible disorganization of actin fibers within the cell body and clumping of F-actin at the periphery, beneath the plasma membrane ('Cortical', Figure B.23 A); and an intermediate phenotype, showing less stress fibers and some spots of F-actin polymerization within the cell body ('Intermediate', Figure B.23 A). Very interestingly, the three phenotypes showed different patterns of F-actin distribution according with each APP cDNA. Thus, for S655A APP-GFP transfected cells differentiated for 4 days, stabilization of stress fibers was more affected, as these cells showed higher number of cortical cells at the expense of intermediate and fibers phenotypes (Figure B.23 A). S655E APP-GFP presented was the APP cDNA less affected comparing to control N1 –EGFP expressing cells, for this differentiation time period. We further

proceed to characterize the neuronal-like differentiation, and measure the number of processes per cell by category, namely: all processes of all sizes ('Total'), processes higher than 20 µm, and processes higher than 35 µm (Figure B.23 B). In general, S655E APP-GFP expression favors the elongation of processes and shows higher percentage of differentiated cells (Figure B.23).

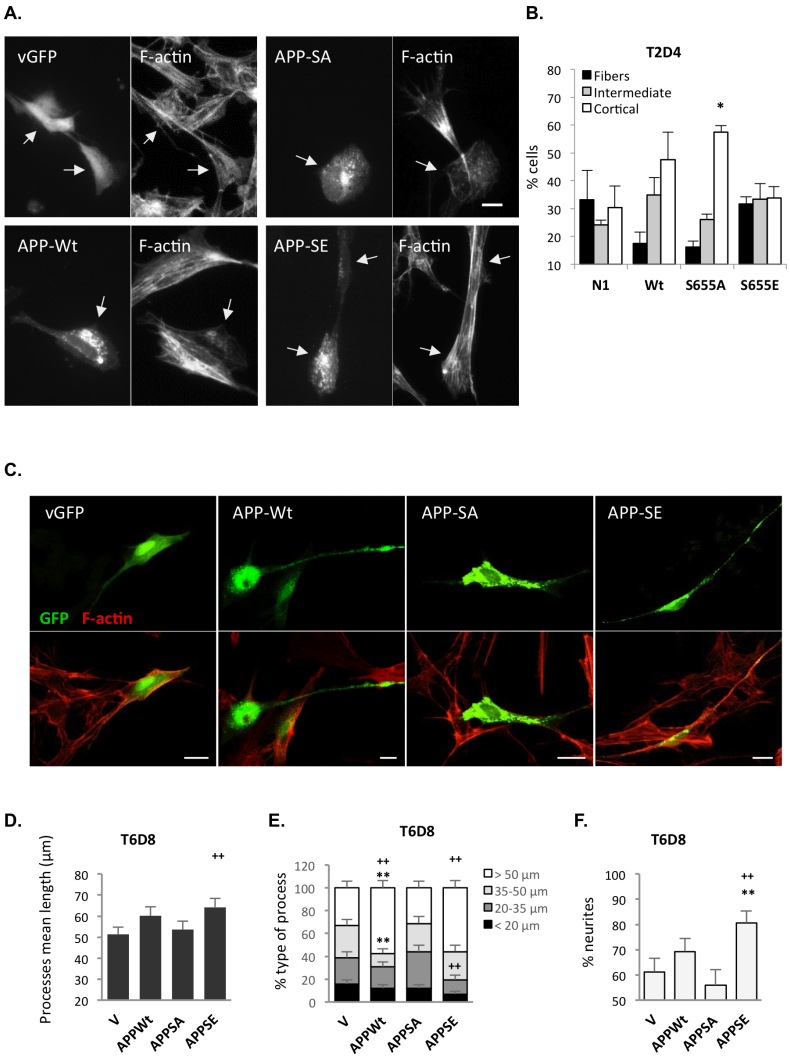

Figure B.23 - **Effects of overexpressing the APP S655 phosphomimetic mutants S655A and S655E in SH-SY5Y differentiation. A.** Cells were differentiated with 10 µM RA for 2 days and transfected for the last 48h with the different APP cDNAs to analyse their effect on filamentous actin (F-actin) distribution. Scale bar, 10 µm. Arrows indicate transfected cells presenting actin depolymerization. **B.** Cells were scored based on their F-actin organization: Fibers, presence of F-actin stress fibers throughout the cell; Cortical, F-actin fibers accumulated at the cell periphery and short disorganized fibers within the cell body; Intermediate, not entirely cortical, and exhibiting reduced number of stress fibers together with F-actin spots within the cell body. Results are show as a percentage of the total number of cells (75-100 cells analysed per replica, at least 3 independent replicas). *, p <0.05. **C.** Cells were exposed to 10 µM RA for 6 days and transfected for the last 48h with the different APP cDNAs to analyse their effect on neurite elongation. Scale bar, 20 µm. **D.** Processes ≥20 µm were measured and their mean length calculated. */#, p<0.05 by unpaired t-test (after Ln transformation of data) against control empty vector or APPSA, respectively. **E.** Processes were categorized accordingly to their length, and the percentage of the different types calculated in relation to the total number of processes per cell. Processes ≥35 µm are considered differentiated neurites. */#, p<0.05; **/##, p<0.01 by Mann Whitney test against control empty vector or APPSA, respectively. Note that for 20-35 µm processes, APPSA vs APPWt had p=0.0536; for 35-50 µm processes APPWt vs APPSE or APPSA had p=0.0513 and p=0.0556, respectively. **F.** The percentage of neurites per cell. **/##, p<0.01 by Mann Whitney test against control empty vector or APPSA, respectively. Note that APPWt against APPSE had p=0.0596.

Table B.8 - **PhosphoS655 APP protein interactors with potential interest for neuronal differentiation.** From the total phosphoAPP interactome, proteins were selected based on functional annotations directly related to brain development, neuron function, neurogenesis, and/or neuronal differentiation related events (cytoskeleton organization, cell adhesion, and cell migration) and signaling pathways. In bold are the UniProt accession number of newly identified APP interactors. The gene ontology (GO) terms determinant for the selection are described in the biological process column. Node degree ('k'), is the number of interactors the protein presents and refers to the position of the protein inside the protein-protein interaction network that includes all the interactors identified for each differentiation day. 'Ref', indicates references retrieved from the PubMed supporting the role in neuronal differentiation. 'Mammalian phenotype/human diseases', KO mouse phenotypes were searched on Jackson Laboratories mouse knockout database, and human diseases retrieved from UniProt and other indicated references. 'Expression', brain enrichment or altered expression in RA-differentiated SH-SY5Y cells are indicated. 'Dif.' – differentiation; 'Reg.' – regulation; 'PM' – plasma membrane.

Uniprot nr	Gene name and symbol	k	Biological Process	Ref	Mammalian Phenotype	Expression
phosphoS655 exclusive interactors at D3						
Q96CV9	Optineurin; OPTN	4	negative regulation of receptor recycling (GO:0001920); negative regulation of I-kappaB kinase/NF-kappaB	[127-129]	Amyotrophic lateral sclerosis type 12	Found in disease-specific bodies or inclusions in a variety of neurodegenerative conditions [130].
P15924	Desmoplakin; DSP	2	desmosome (GO:0002934) and adherens junction organization (GO:0034332); protein localization to adherens junction (GO:0071896); intermediate filament cytoskeleton organization (GO:0045104)	[86, 131]	Conditional KO in motoneurons (evaluation 7 days after quadriceps femoris nerve crush): delayed axon extension; abnormal sciatic nerve morphology (worse sciatic functional index, slower recovery, worse toe spreading); impaired ability to fire action potentials and decreased nerve conduction velocity; reduced number and delayed regeneration of motor fibers [131]	
P62633	Cellular nucleic acid-binding protein; CNBP	9	cholesterol biosynthetic process (GO:0006695); positive regulation of cell proliferation (GO:0008284); positive regulation of transcription, DNA-templated (GO:0045893)	[132, 133]	abnormal cephalic neural fold, and embryonic neuroepithelium morphology; decreased embryonic neuroepithelial cell proliferation; decreased forebrain size, absent diencephalon and telencephalon [134].	
phosphoS655 exclusive interactors at D7						
Q92989	Polyribonucleotide 5'-hydroxyl-kinase Clp1; CLP1	1	cerebellar cortex development (GO:0021695)	[135]	motor neuron degeneration; decreased motor neuron number; decreased brain weight; increased neuron apoptosis; abnormal axon morphology; axon degeneration; thin cerebral cortex; decreased neuron number; neonatal lethality, complete penetrance; embryonic lethality, complete penetrance; lethality, complete penetrance [136]; Pontocerebellar hypoplasia 10 [137].	

Uniprot nr	Gene name and symbol	k	Biological Process	Ref	Mammalian Phenotype	Expression
P05090	Apolipoprotein D; APOD	0	brain development (GO:0007420); PNS axon regeneration (GO:0014012); tissue regeneration (GO:0042246); response to axon injury (GO:0048678); negative regulation of focal adhesion assembly (GO:0051895)	[138, 139]	abnormal motor learning, abnormal spatial learning, abnormal spatial reference memory, decreased vertical activity, and hypoactivity; increase in levels of lipid peroxides in the brain (not in the lung) [140].	Up-regulated during brain aging and in many neurodegenerative diseases [141, 142].
phosphoS655-enriched interactors at D7						
P26378	ELAV-like protein 4; ELAVL4	0	learning (GO:0007612); dendrite morphogenesis (GO:0048813)	[34]	increased neuron apoptosis; abnormal nervous system development; abnormal neuron differentiation [35].	Tissue enhanced (cerebral cortex); RA dif SH-SY5Y regulated gene [36].
Q8TF72	Protein Shroom3; SHROOM3	4	cell morphogenesis (GO:0000902); neural tube closure (GO:0001843); regulation of cell shape (GO:0008360)	[89-91]	open neural tube in 100% of mice, which leads to exposure of the forebrain neuroepithelium (exencephaly) [92].	
Q14444	Caprin-1; CAPRIN1	1	positive regulation of dendrite morphogenesis (GO:0050775) and dendritic spine morphogenesis (GO:0061003); cell differentiation (GO:0030154)	[37]	increased neuron apoptosis; abnormal miniature excitatory postsynaptic currents; abnormal neuron physiology; abnormal dendrite morphology; abnormal synapse morphology [38].	

7.5. Discussion

APP S655 phosphorylation is known to occur in healthy neurons and in AD patients. However, the molecular function(s) and mechanisms triggered by this phosphorylation remain elusive. Our group has been gathering experimental evidences on specific roles for this phosphorylation using S655 phosphomimetic APP mutants. In order to begin to unravel the APP protein effectors and regulators involved in such roles, we start to characterize the S655 phosphorylation-dependent APP interactome. SH-SY5Y cells were differentiated with retinoic acid to a neuronal-like phenotype, and transfected at two different time periods with either APPWt or APPS655A/E phosphomimetic mutants. All these exogenously expressed APP proteins correspond to the neuron-enriched APP isoform 695. The APP proteins and their respective interaction partners were isolated by GFP-trap, and identified by MS. By comparing the interactomes of APPWt, APPS65A, and APPS655E we were able to obtain differential (sub)interactomes based on the dependency on the S655 phosphorylation state with differentiation time: the APP S655 phosphorylation-independent interactome, the dephosphoS655 APP interactome, and the phosphoS655 APP interactome. The 'Total' APP interactome resulted from the addition of all the interactors here experimentally identified.

The methodology applied has some limitations that should be stated. The first one is related to the use of APP overexpression that might lead to incorrect subcellular localization and unspecific binding; nevertheless, the immunoprecipitation takes place in vitro, after cells lyses, what increases the probability of protein-protein interaction. Secondly, the GFP-fusion tag is located in the APP C-terminal. Since APP suffers proteolytic cleavages that originate different APP C-terminal fragments, when we perform the GFP pull-down we isolated not only full length APP-GFP and its interactors, but also the different APP C-terminal fragments, including AICD, and their interactors. Furthermore, we cannot exclude the possibility that the presence of the GFP-fusion tag could impair some interactions. A third limitation derives from the cell model applied. Although very attractive because of its human origin, ease of access, and the lack of ethical concerns, RA-differentiated SH-SY5Y cells only mimic to a certain extent neuronal differentiation events and function. Specifically, RA-differentiated SH-SY5Y cells have been shown, by genome-wide transcriptional analysis, to share some characteristics with dopaminergic neurons [36]. We also have to consider that neuronal differentiation events will have many variants depending on the cell type. Other limitations to consider are related to the MS technique and the fact that the analysis was performed from extracts. For example, this technique does not distinguish a direct interaction from an indirect one, and might detect protein-protein interactions that do not occur in vivo just by bringing together proteins that exist in different subcellular compartments. MS is also described as

biased toward proteins of high expression, and thus might fail to identify interactors of lower expression. Additionally, the obtained interactomes most probably miss some interactions between APP and membrane proteins and nuclear proteins due to their typical poor solubilization under these conditions, and might lack weak or transient interactions. Because of the aforementioned reasons, the interactomes presented in this work are not complete, and all the detected protein interactors are "potential interactors" that will need further validation.

In general, we detected more APP protein interactors at D7 than at D3 ('Total' APP interactors). Accordingly, the differentiation day 7 PPI network is more complex than day 3, showing more nodes (342 at D7 vs 284 at D3) and edges (1059 vs 760), smaller percentage of isolated nodes (14% vs 20%), and higher clustering coefficient (0.256 vs 0.198). This behavior is also visible for the dephosphoS655 APP and the phosphoS655 APP interactomes, separately. Contrarily, the APP interactome independent of S655 phosphorylation show a decrease in the number of interactors from D3 to D7. Noteworthy, if we look at the specific experimental conditions, while APPWt and APPSA shared a high number of protein interactors at D3, APPSA more than triplicates the number of unique interactors from D3 to D7. The change in the number of APP protein interactors attractively suggests that modulation of APP S655 phosphorylation is more tightly controlled at later differentiation periods. The smaller number of phosphoS655 interactors indicates that S655 phosphorylation leads to a functional sub-specialization (and/or enrichment of sub-specializations), as expected.

Functional enrichment analysis results showed that the most significant attributed functions to the APP protein interactors are related to ribonucleoprotein and spliceosomal complex assembly and organization, RNA biosynthesis, RNA metabolism, RNA splicing and regulation of RNA splicing, translation regulation, and gene expression. Consistent with a role in such functions is the fact that the majority of APP interactors detected by us are RBP (including mRNA processing/mRNA splicing factors, ribosomal proteins, ribonucleoproteins, translation factors, RNA helicases). Additionally, several APP protein interactors belong to the class of DNA-binding proteins and TFs. One study involving transcriptome profiling of HEK 293 cells stable overexpressing human APP shows that several of the differentially regulated genes are involved in DNA replication, transcription and translation regulation (including RNA splicing and ribosome biogenesis). Specifically, they show that upregulated genes were involved in regulation of transcription and negative regulation of translation, and downregulated genes were involved in DNA replication, DNA-dependent transcription, and translation [143]. Transcriptome profiling of pre-frontal cortex of adult APPKO mice also show that differentially expressed genes are involved in regulation of transcription (either negative or positive) [72].

The AICD fragment of APP has been shown to be involved in the regulation of gene transcription, although this issue is still controversial. AICD is known to translocate to the nucleus to form a transcriptionally active complex in combination with Fe65 and the histone acetyltransferase Tip60 [144-146]. Besides its implication in gene transcription regulation, it was already suggested by co-localization studies that APP C-terminal fragments accumulate in the intranuclear splicing factor compartments [147].

The human brain is the tissue with the highest level of alternatively spliced transcripts, and this process affect all aspects of neurodevelopment and function [148]. Also, defects in alternative splicing have been implicated in neurological and neurodegenerative diseases [149]. Alternative splicing is thus an important APP function that can affect various physiological processes and should be further studied. Different alternative splicing choices can alter the structure and activity of a protein, alter mRNA localization, translation or decay, and impact the overall expression of a newborn protein. Splicing of a given alternative exon can be affected by multiple RBP, and RBPs interact dynamically with mRNA, controlling all aspects of mRNA posttranscriptional fate, including translation, surveillance and decay [149]. Indeed, RBP actions occur not only in the nucleus but also in the cytoplasm. Cytoplasmic actions comprise translation control via transcript stabilization, regulation of microRNA binding, regulation of mRNA transport and differential localization. These aspects are very important in neurons, where the correct transport, target and local translation of mRNA are determinant for neuronal polarity and synaptic plasticity. The transcripts of splicing regulators or other RNA binding proteins often contain an alternative exon that is controlled by the protein itself or by other RBP. Splicing regulators extensively modulate each other's activity, as well as control the activity of transcriptional regulators. APP might bind different RBPs to modulate their function and/or APP could be part of messenger ribonucleoprotein complexes, influencing the cellular fates of different mRNAs [150, 151].

On differentiation D3, the S655 phosphorylation-independent APP interactome included the ELAVL4 protein (Table B.3, D3), a splicing regulatory protein specific of neurons [150]. This protein regulates, via different post-transcriptional effects, several mRNAs whose protein products (like GAP-43, Tau, AchE, PSD95, Homer 1a, neuritin and CamKIIα) have key roles in neurons. ELAVL4 has been implicated in neurogenesis, neuronal survival, and synaptic plasticity during learning and memory [150]. Besides the brain phenotype demonstrated by an *Elavl4* mouse KO (see Table B.3), this protein has been implicated in several human CNS disorders, namely Alzheimer's and Parkinson's diseases, schizophrenia, amyotrophic lateral sclerosis, and epilepsy [34]. Inside the D3 network, ELAVL4 binds the transcription repressor Ewing Sarcoma Protein Ewsr1, also allocated to the same category. *Ewsr1* KO mouse display a very high post-natal

lethality, while in Zebrafish the gene knockdown led to p53-mediated apoptosis in the brain and the spinal cord [152].

Additionally, in the same differentiation day and in the same APP interactome category, we identified the previously described APP interactors Caprin-1 and G3BP1, which also interact with each other. Both proteins are described to be part of ribonucleoprotein complexes like RNA granules and Stress granules [149, 153]. Caprin-1 has been implicated in the control of local translation required for synaptic plasticity [38], with part of its actions performed in collaboration with one of the best known RBP, the synaptic functional regulator FMR1 (FMRP) [37]. The interaction between the FMRP protein and APP was also detected by us, at differentiation D7 in the dephosphoS655 APP interactome. This protein binds to approximately 5% of all transcripts present in the mammalian brain, modulating several aspects of brain development and function [149]. Alterations in FMRP have been reported in several neurodevelopment and psychiatric disorders (Fragile X Syndrome, autism, schizophrenia, bipolar disorder, and major depression) [154]. Previous work has shown a link between APP and FMRP, with FMRP binding to and repressing the APP mRNA, and loss of FMRP (KO mouse) resulting in increased levels of APP [154]. Furthermore, RanBP9, a well described APP interactor [155], was described to interact with the c-terminal of FMR1 in the microtubule organizing center [156].

On differentiation D7, the S655 phosphorylation-independent APP interactome included the PERQ amino acid-rich with GYF domain-containing protein 2 (GIGYF2) and the Fragile X mental retardation syndrome-related protein 2 (FXR2). Both proteins have been implicated in the regulation of mRNA translation. The FXR2 protein is a selective RBP, paralog of the FMRP, with which it cooperates to regulate the translation of different mRNA targets (for example in the positive translation control of PSD95), controlling several aspects of locomotor activity, sensorimotor gating, and cognitive processes [53]. FXR2 also functions independently of FMRP [49]. GIGYF2 is an mRNA translation silencing protein that competes with the eukaryotic initiation factor 4E (eIF4E) and binds to the Argonaute protein AGO2, being part of mRNA silencing and decay complexes. Besides its role in mRNA translation, GIGYF2 functions in the CNS; the neurodegeneration observed in *Gigyf2* KO mice was related to the role of this protein in the regulation of endosome signaling, IGF-1 trafficking, and ERK1/2 activation [46, 47].

Curiously, at D3 the ELAVL4 and Caprin-1 proteins are allocated to the S655 phosphorylation independent category, while at D7 they are included in the phosphoS655 APP interactome (Supplementary Table B.3). The GIGYF2 and FXR2 proteins, above described as APP interactors' independent of S655 phosphorylation at D7, are included in the dephosphoS655 APP interactome on D3. This phenomenon, although indicative that the interaction with APP itself must be independent of the S655 phosphorylation, may also indicate that the different APP backgrounds

and/or the differentiation time might affect these protein levels (or the levels of bridge proteins), subcellular localization, and post-translational modifications, making the protein more specific or enriched in a different APPS655 category at different differentiation times. For example, protein levels of neuronal ELAVL are significantly decreased in the hippocampi of AD brain, and negatively correlate with the amount of Abeta [157]. On the other hand, APP phosphorylation at S655 has been associated to diminished Abeta production [13, 158]. Since neurons have higher rates of Abeta production, these might justify the specificity of the presence of ELAVL4 in the phosphoS655 APP interactome on the more mature neuronal-like cells of D7. Related to this, it would be very interesting to explore how APP and its S655 phosphorylation state alters the protein levels of different RBP, and the presence of APP in the different messenger ribonucleoprotein complexes (RNA granule, stress granule, polysome, miRISC, etc).

Functional enrichment analysis of the D7 dephosphoS655 APP interactome attributed as a significant biological process 'protein localization to nuclear body and Cajal body', due to the presence of different subunits of the chaperonin-containing TCP1 complex (CCT2, CCT4, CCT5, and CCT8). The main function of this complex appears to be in protein folding (including of actin and tubulin monomers), but recently it has been implicated in telomerase function and trafficking of telomerase and small Cajal body RNAs to Cajal bodies [159]. Although in our specific conditions the retrieval of the CCT proteins from a nuclear localization is less likely (due to poor nuclear solubilization), their detection as APP interactors is very interesting due to the previously reported APP association to Cajal bodies. Indeed, the well-established AICD-Fe65-TIP60 complex was described to be in close proximity with Cajal Bodies and PML bodies [146]. Other significant function specifically attributed to the dephosphoS655 APP interactome on differentiation D7 was glycolysis. Upon RA differentiation, SH-SY5Y cells increase their rate of glycolysis and there is an upregulation of genes involved in this pathway [160]. Neuronal differentiation events are very demanding in energetic terms, and a possible role for APP in the glycolysis pathway deserves future attention. For instance, it would be interesting to explore if APP and APP S655 phosphorylation have a role in metabolic reprogramming, namely in the transition from aerobic glycolysis in neural progenitor cells to neuronal oxidative phosphorylation [161]. A very interesting aspect of the D7 dephosphoS655 APP interactome was the high number of cytoskeleton proteins, especially from the actin family, which translated in an overrepresentation of functions like cytoskeleton organization, actin and actin filament binding (see Supplementary Table B.6). There is no question that alterations in cytoskeleton dynamics are of central importance for neuronal differentiation. Rearrangements of actin and microtubules both establishes and maintains polarity in neurons, but are also fundamental for other steps like neural progenitor's proliferation, neural migration, and vesicle trafficking [162, 163]. Concordantly, upon 4 days of RA exposure,

APPSA overexpression could be particularly associated with actin depolymerization and cortical actin distribution (Figure B.23 A). The APP interactors detected that belong to the family of actin binding and were already associated with neuronal differentiation events include: cofilin-1 (Table B.6), F-actin-capping protein subunit beta, profilin-1, filamin-A (and filamin-B), moesin, and thymosin beta-4 (Supplementary Table B.7). Interestingly, APP has been associated before with mobile membrane structures like actin-positive and cortactin-rich extending lamellipodia. The APP function in such structures seems to depend on the interaction of APP and Fe65 with the actin-associated protein Mena. Additionally, Mena is known to bind profiling [164, 165].

An additionally dephosphoS655 APP protein interactor that we found particularly interesting was the MT-destabilizing protein Stathmin. Stathmin expression is regulated during neuronal development, and this protein has been implicated in neuronal polarization by destabilizing the MT in minor neurites [166]. Overexpression of Stathmin in neurons of the subgranular zone (SGZ) and in primary cultured hippocampal neurons induced aberrant arborization of axons [167]. Stathmin appears to be crucial in adult SGZ neurogenesis by modulation of several MT-associated events, since proliferation and migration to differentiation [100].

Regarding the phosphoS655 APP interactome, a simple comparison of the number of APP interactors detected for the APPSA and for the APPSE, suggests that S655 phosphorylation commits APP to a more specific role by endorsing in a smaller number but specific protein interactions. This behavior might be associated with the more dynamic TGN-to-PM trafficking of APPSE, and it's increased processing by alpha-secretase [13, 19].

In line with our preliminary data correlating the overexpression of the phosphomimicking mutant, APPSE, with neurite elongation in SH-SY5Y cells (Figure B.23), we identified potential APP-phosphoS655 specific interactors that are strongly associated with neurite outgrowth (Table B.8). On D3 we considered desmoplakin (DSP), optineurin (OPTN), and cellular nucleic acid-binding protein (CNBP) particularly interesting. The protein desmoplakin (DSP), together with plakoglobin and members of the cadherin family, form the desmosomes where DSP functions as the cytoskeleton adaptor that anchors IFs to the plasma membrane. Forebrain-specific *Dsp* mouse mutants show decreased stem-cell proliferation rate in the dentate gyrus, and defective differentiation [168]. In this study, the authors suggest that DSP mediated cell–cell adhesion is important to establish the signaling pathway from neighboring cells to allow neuronal differentiation [168]. Concordantly, in spinal cord motor neurons, the DSP complex with N-cadherin, plakoglobin and vimentin appears to be a crucial process for axon regeneration and outgrowth in vitro and in vivo [131].

Within the constructed network, DSP is one node away from a known APP protein interactor and one of the proteins with the highest node degree, the Peroxiredoxin-2 protein (PRDX2; see Figure

B.21 A, DSP and PRDX2 share the MAP1A/1B light chain 3A as a protein interactor). This peroxidase, the most abundant neuronal peroxidedoxin, is involved in the response to oxidative stress, and its overexpression was described to be neuroprotective for dopaminergic neurons [169]. On the other hand, PRDX2 is one protein (MPP1) away from OPTN. OPTN seems to be involved in anterograde trafficking pathways, and can be found in recycling endosomes. In scratch wound assays, loss of OPTN results in the loss of EGFR from the plasma membrane facing the wound and reduces the number of cells extending lamellipodia into the scratch wound. In addition, the delivery of β1-integrin towards the front of the cell also seems affected [128]. In retinal ganglion cells, OPTN siRNAs increase the number of cells undergoing apoptotic cell death, and reduces the amount of secreted growth factors [170]. Transient knockdown of OPTN in zebrafish embryos resulted in abnormal morphology and defects in spinal motor axon guidance [129].

CNBP is a nucleic-acid binding protein involved in regulation of transcription, and most of the described putative CNBP target genes are related to embryonic developmental processes [132]. Specifically, CNBP appears to downregulate the transcription of Wnt [132]. This protein is required for forebrain formation during mouse, chick, and zebrafish embryogenesis by its ability to control proliferation and cell survival [133, 134, 171].

Curiously, three APP protein interactors (ELAV4, Caprin-1, and Shroom3) highlighted in this work for their potential role in neuronal differentiation, shift from the APP interactome independent of the S655 phosphorylation status and the APP- dephosphoS655 interactome on day 3, to the APP-phosphoS655 interactome on differentiation day 7. The presence of these protein in late differentiation periods in the APP- phosphoS655 interactome may support such phenotype. We already mentioned that Caprin-1 and ELAV4 are positive modulators of dendritogenesis and synaptic plasticity. Shroom3 is an actin binding protein, reported to bind f-actin and to modulate f-actin subcellular distribution, a function that is related to neural tube closure failure in Shroom3 KO mice [92]. Furthermore, this protein directly binds Rho kinase (ROCK), and the Shroom3-ROCK interaction has been shown to negatively regulate neurite outgrowth [89]. It will be interesting to test if pS655 APP binding to Shroom 3 prevents its interaction with ROCK, and promotes neurite outgrowth.

Apolipoprotein D (APOD), is another specific APP- phosphoS655 protein interactor that could be assisting the APPSE induced neuritogenesis. APOD is reported to be neuroprotective and neurotrophic [138, 140, 172]. This extracellular glycosylated lipocalin, binds and transports a variety of ligands (for example, RA, arachidonic acid, and the endocannabinoid anandamide). APOD levels are increased during prefrontal cortex maturation, and APOD is a consistently upregulated gene during brain aging in mammals. Regarding its potential neurotrophic role, APOD was shown to exert differentiating and synaptogenic effects in dorsal root ganglion neurons, and to

be necessary for the transcription factor p73 mediated [173], and for RA mediated- neurite outgrowth in SH-SY5Y cells [139]. Thus, the APP- phosphoS655 interactome includes interesting potential protein partners that could be assisting APP in the promotion of neurite outgrowth.

In line with the functional annotation of individual protein interactors, the functional enrichment analysis of the expanded phosphoS655 APP interactome linked APP interactors to several signaling pathways important for neuronal differentiation, namely FoxO [174], TGFbeta [175, 176], TNF [177], NF-kB [160], and estrogen signaling pathways [178] (Figure B.22, Figure B.23 and Table B.7), with some of these being functionally related [179].

All these data indicate roles for APP S655 phosphorylation in controlling cell proliferation and survival, as well as in the modulation of signaling pathways crucial for cell commitment to neuronal differentiation. Accordingly, we have observed that APPSE overexpression correlates with enhanced neurite elongation in SH-SY5Y cells (Figure B.23 B). Further work exploring some of these fascinating interactions will help to increase our knowledge on APP physiology, in particular its role in neuronal differentiation.

7.6. References

1. Andrew, R.J., et al., *A Greek Tragedy: The Growing Complexity of Alzheimer Amyloid Precursor Protein Proteolysis.* Journal of Biological Chemistry, 2016. **291**(37): p. 19235-19244.
2. Young-Pearse, T.L., et al., *A critical function for beta-amyloid precursor protein in neuronal migration revealed by in utero RNA interference.* J Neurosci, 2007. **27**(52): p. 14459-69.
3. Young-Pearse, T., et al., *Secreted APP regulates the function of full-length APP in neurite outgrowth through interaction with integrin beta1.* Neural Development, 2008. **3**(1): p. 15.
4. Hoe, H.S., et al., *Interaction of reelin with amyloid precursor protein promotes neurite outgrowth.* J Neurosci, 2009. **29**(23): p. 7459-73.
5. Tyan, S.H., et al., *Amyloid precursor protein (APP) regulates synaptic structure and function.* Mol Cell Neurosci, 2012. **51**(1-2): p. 43-52.
6. Weyer, S.W., et al., *APP and APLP2 are essential at PNS and CNS synapses for transmission, spatial learning and LTP.* EMBO J, 2011. **30**(11): p. 2266-80.
7. Chasseigneaux, S., et al., *Secreted amyloid precursor protein beta and secreted amyloid precursor protein alpha induce axon outgrowth in vitro through Egr1 signaling pathway.* PLoS One, 2011. **6**(1): p. e16301.
8. Stahl, R., et al., *Shedding of APP limits its synaptogenic activity and cell adhesion properties.* Front Cell Neurosci, 2014. **8**: p. 410.
9. Weyer, S.W., et al., *Comparative analysis of single and combined APP/APLP knockouts reveals reduced spine density in APP-KO mice that is prevented by APPsα expression.* Acta Neuropathologica Communications, 2014. **2**(1): p. 36.
10. Klevanski, M., et al., *The APP Intracellular Domain Is Required for Normal Synaptic Morphology, Synaptic Plasticity, and Hippocampus-Dependent Behavior.* J Neurosci, 2015. **35**(49): p. 16018-33.
11. Bergmans, B.A., et al., *Neurons generated from APP/APLP1/APLP2 triple knockout embryonic stem cells behave normally in vitro and in vivo: lack of evidence for a cell autonomous role of the amyloid precursor protein in neuronal differentiation.* Stem Cells, 2010. **28**(3): p. 399-406.
12. Aydin, D., S.W. Weyer, and U.C. Muller, *Functions of the APP gene family in the nervous system: insights from mouse models.* Exp Brain Res, 2012. **217**(3-4): p. 423-34.
13. Vieira, S., et al., *Retrieval of the Alzheimer's amyloid precursor protein from the endosome to the TGN is S655 phosphorylation state-dependent and retromer-mediated.* Molecular Neurodegeneration, 2010. **5**(1): p. 40.
14. Lee, M.-S., et al., *APP processing is regulated by cytoplasmic phosphorylation.* The Journal of Cell Biology, 2003. **163**(1): p. 83-95.
15. Tamayev, R., D. Zhou, and L. D'Adamio, *The interactome of the amyloid beta precursor protein family members is shaped by phosphorylation of their intracellular domains.* Mol Neurodegener, 2009. **4**: p. 28.
16. Gandy, S., A.J. Czernik, and P. Greengard, *Phosphorylation of Alzheimer disease amyloid precursor peptide by protein kinase C and Ca2+/calmodulin-dependent protein kinase II.* Proc Natl Acad Sci U S A, 1988. **85**(16): p. 6218-21.
17. Suzuki, T., et al., *Phosphorylation of Alzheimer amyloid precursor protein by protein kinase C.* Neuroscience, 1992. **48**(4): p. 755-61.
18. Ramelot, T.A. and L.K. Nicholson, *Phosphorylation-induced structural changes in the amyloid precursor protein cytoplasmic tail detected by NMR.* J Mol Biol, 2001. **307**(3): p. 871-84.
19. Vieira, S., et al., *S655 phosphorylation enhances APP secretory traffic.* Molecular and Cellular Biochemistry, 2009. **328**(1): p. 145-154.
20. Rocha, J.F., S.I. Vieira, and O.A.B.d.C.e. Silva, *APP Phosphorylation at S655 Correlates with F-actin Cytoskeleton Dynamics—Relevance in Neuronal Differentiation.* Microscopy and Microanalysis, 2012. **18**(SupplementS5): p. 57-58.
21. da Rocha, J.F., O.A. da Cruz e Silva, and S.I. Vieira, *Analysis of the amyloid precursor protein role in neuritogenesis reveals a biphasic SH-SY5Y neuronal cell differentiation model.* J Neurochem, 2015. **134**(2): p. 288-301.
22. da Cruz, E.S.O.A., et al., *A model system to study intracellular trafficking and processing of the Alzheimer's amyloid precursor protein.* Neurodegener Dis, 2004. **1**(4-5): p. 196-204.
23. Shevchenko, A., et al., *In-gel digestion for mass spectrometric characterization of proteins and proteomes.* Nat Protoc, 2006. **1**(6): p. 2856-60.
24. Keller, B.O., et al., *Interferences and contaminants encountered in modern mass spectrometry.* Anal Chim Acta, 2008. **627**(1): p. 71-81.

25. Bardou, P., et al., *jvenn: an interactive Venn diagram viewer.* BMC Bioinformatics, 2014. **15**(1): p. 293.
26. Orchard, S., et al., *Protein interaction data curation: the International Molecular Exchange (IMEx) consortium.* Nat Meth, 2012. **9**(4): p. 345-350.
27. Perreau, V.M., et al., *A domain level interaction network of amyloid precursor protein and Abeta of Alzheimer's disease.* Proteomics, 2010. **10**(12): p. 2377-95.
28. Bindea, G., et al., *ClueGO: a Cytoscape plug-in to decipher functionally grouped gene ontology and pathway annotation networks.* Bioinformatics, 2009. **25**(8): p. 1091-3.
29. Mi, H., et al., *Large-scale gene function analysis with the PANTHER classification system.* Nat. Protocols, 2013. **8**(8): p. 1551-1566.
30. *UniProt: a hub for protein information.* Nucleic Acids Res, 2015. **43**(Database issue): p. D204-12.
31. Bult, C.J., et al., *Mouse genome database 2016.* Nucleic Acids Res, 2016. **44**(D1): p. D840-7.
32. Uhlen, M., et al., *Proteomics. Tissue-based map of the human proteome.* Science, 2015. **347**(6220): p. 1260419.
33. Morris, J.H., et al., *Affinity purification-mass spectrometry and network analysis to understand protein-protein interactions.* Nat Protoc, 2014. **9**(11): p. 2539-54.
34. Bronicki, L.M. and B.J. Jasmin, *Emerging complexity of the HuD/ELAVl4 gene; implications for neuronal development, function, and dysfunction.* RNA, 2013. **19**(8): p. 1019-37.
35. Akamatsu, W., et al., *The RNA-binding protein HuD regulates neuronal cell identity and maturation.* Proc Natl Acad Sci U S A, 2005. **102**(12): p. 4625-30.
36. Korecka, J.A., et al., *Phenotypic characterization of retinoic acid differentiated SH-SY5Y cells by transcriptional profiling.* PLoS One, 2013. **8**(5): p. e63862.
37. Papoulas, O., et al., *dFMRP and Caprin, translational regulators of synaptic plasticity, control the cell cycle at the Drosophila mid-blastula transition.* Development, 2010. **137**(24): p. 4201-9.
38. Shiina, N., K. Yamaguchi, and M. Tokunaga, *RNG105 deficiency impairs the dendritic localization of mRNAs for Na+/K+ ATPase subunit isoforms and leads to the degeneration of neuronal networks.* J Neurosci, 2010. **30**(38): p. 12816-30.
39. Dubey, M., et al., *Reexpression of vimentin in differentiated neuroblastoma cells enhances elongation of axonal neurites.* J Neurosci Res, 2004. **78**(2): p. 245-9.
40. Colucci-Guyon, E., et al., *Cerebellar defect and impaired motor coordination in mice lacking vimentin.* Glia, 1999. **25**(1): p. 33-43.
41. Pezzini, F., et al., *Transcriptomic Profiling Discloses Molecular and Cellular Events Related to Neuronal Differentiation in SH-SY5Y Neuroblastoma Cells.* Cell Mol Neurobiol, 2016.
42. Yabe, J.T., et al., *Regulation of the transition from vimentin to neurofilaments during neuronal differentiation.* Cell Motil Cytoskeleton, 2003. **56**(3): p. 193-205.
43. Worman, H.J. and W.T. Dauer, *The Nuclear Envelope: An Intriguing Focal Point for Neurogenetic Disease.* Neurotherapeutics, 2014. **11**(4): p. 764-772.
44. Yang, S.H., et al., *Mice that express farnesylated versions of prelamin A in neurons develop achalasia.* Hum Mol Genet, 2015. **24**(10): p. 2826-40.
45. Mahendram, S., et al., *Ectopic gamma-catenin expression partially mimics the effects of stabilized beta-catenin on embryonic stem cell differentiation.* PLoS One, 2013. **8**(5): p. e65320.
46. Higashi, S., et al., *GIGYF2 is present in endosomal compartments in the mammalian brains and enhances IGF-1-induced ERK1/2 activation.* J Neurochem, 2010. **115**(2): p. 423-37.
47. Giovannone, B., et al., *GIGYF2 gene disruption in mice results in neurodegeneration and altered insulin-like growth factor signaling.* Hum Mol Genet, 2009. **18**(23): p. 4629-39.
48. Tapia, O., et al., *Nuclear envelope protein Lem2 is required for mouse development and regulates MAP and AKT kinases.* PLoS One, 2015. **10**(3): p. e0116196.
49. Guo, W., et al., *Fragile X Proteins FMRP and FXR2P Control Synaptic GluA1 Expression and Neuronal Maturation via Distinct Mechanisms.* Cell Rep, 2015. **11**(10): p. 1651-66.
50. Fernandez, E., et al., *FXR2P Exerts a Positive Translational Control and Is Required for the Activity-Dependent Increase of PSD95 Expression.* J Neurosci, 2015. **35**(25): p. 9402-8.
51. Guo, W., et al., *RNA-binding protein FXR2 regulates adult hippocampal neurogenesis by reducing Noggin expression.* Neuron, 2011. **70**(5): p. 924-38.
52. Bontekoe, C.J., et al., *Knockout mouse model for Fxr2: a model for mental retardation.* Hum Mol Genet, 2002. **11**(5): p. 487-98.
53. Spencer, C.M., et al., *Exaggerated behavioral phenotypes in Fmr1/Fxr2 double knockout mice reveal a functional genetic interaction between Fragile X-related proteins.* Hum Mol Genet, 2006. **15**(12): p. 1984-94.

54. Zhang, J., et al., *Altered hippocampal synaptic plasticity in the FMR1 gene family knockout mouse models.* J Neurophysiol, 2009. **101**(5): p. 2572-80.
55. Bakker, C.E., et al., *Immunocytochemical and biochemical characterization of FMRP, FXR1P, and FXR2P in the mouse.* Exp Cell Res, 2000. **258**(1): p. 162-70.
56. Cheng, K., L. Bai, and L. Belluscio, *Fas-associated factor 1 as a regulator of olfactory axon guidance.* J Neurosci, 2011. **31**(33): p. 11905-13.
57. Adham, I.M., et al., *Fas-associated factor (FAF1) is required for the early cleavage-stages of mouse embryo.* Mol Hum Reprod, 2008. **14**(4): p. 207-13.
58. Sul, J.W., et al., *Accumulation of the parkin substrate, FAF1, plays a key role in the dopaminergic neurodegeneration.* Hum Mol Genet, 2013. **22**(8): p. 1558-73.
59. Furuse, T., et al., *Behavioral and neuromorphological characterization of a novel Tuba1 mutant mouse.* Behav Brain Res, 2012. **227**(1): p. 167-74.
60. Keays, D.A., et al., *Mutations in α-Tubulin Cause Abnormal Neuronal Migration in Mice and Lissencephaly in Humans.* Cell, 2007. **128**(1): p. 45-57.
61. Zhao, J. and R.K. Liem, *alpha-Internexin and Peripherin: Expression, Assembly, Functions, and Roles in Disease.* Methods Enzymol, 2016. **568**: p. 477-507.
62. de Sousa, E., et al., *Developmental and functional expression of miRNA-stability related genes in the nervous system.* PLoS One, 2013. **8**(5): p. e56908.
63. Kinjo, E.R., et al., *A possible new mechanism for the control of miRNA expression in neurons.* Exp Neurol, 2013. **248**: p. 546-58.
64. D'Rozario, M., et al., *Type I bHLH Proteins Daughterless and Tcf4 Restrict Neurite Branching and Synapse Formation by Repressing Neurexin in Postmitotic Neurons.* Cell Rep, 2016. **15**(2): p. 386-97.
65. Chen, T., et al., *Tcf4 Controls Neuronal Migration of the Cerebral Cortex through Regulation of Bmp7.* Front Mol Neurosci, 2016. **9**: p. 94.
66. Flora, A., et al., *The E-protein Tcf4 interacts with Math1 to regulate differentiation of a specific subset of neuronal progenitors.* Proc Natl Acad Sci U S A, 2007. **104**(39): p. 15382-7.
67. Kang, M.R., et al., *Reciprocal roles of SIRT1 and SKIP in the regulation of RAR activity: implication in the retinoic acid-induced neuronal differentiation of P19 cells.* Nucleic Acids Res, 2010. **38**(3): p. 822-31.
68. Wu, M.Y., et al., *SNW1 is a critical regulator of spatial BMP activity, neural plate border formation, and neural crest specification in vertebrate embryos.* PLoS Biol, 2011. **9**(2): p. e1000593.
69. Favero, C.B., et al., *Mutation of the BiP/GRP78 gene causes axon outgrowth and fasciculation defects in the thalamocortical connections of the mammalian forebrain.* J Comp Neurol, 2013. **521**(3): p. 677-96.
70. Yang, Y., R.S. Turner, and J.R. Gaut, *The chaperone BiP/GRP78 binds to amyloid precursor protein and decreases Abeta40 and Abeta42 secretion.* J Biol Chem, 1998. **273**(40): p. 25552-5.
71. Chakrabarti, A. and D. Mukhopadhyay, *Novel adaptors of amyloid precursor protein intracellular domain and their functional implications.* Genomics Proteomics Bioinformatics, 2012. **10**(4): p. 208-16.
72. Aydin, D., et al., *Comparative transcriptome profiling of amyloid precursor protein family members in the adult cortex.* BMC Genomics, 2011. **12**: p. 160-160.
73. Gutzman, J.H., S.U. Sahu, and C. Kwas, *Non-muscle myosin IIA and IIB differentially regulate cell shape changes during zebrafish brain morphogenesis.* Developmental Biology, 2015. **397**(1): p. 103-115.
74. Ozkan, E.D., et al., *Input-specific regulation of hippocampal circuit maturation by non-muscle myosin IIB.* J Neurochem, 2015. **134**(3): p. 429-44.
75. Ma, X., et al., *A point mutation in the motor domain of nonmuscle myosin II-B impairs migration of distinct groups of neurons.* Mol Biol Cell, 2004. **15**(6): p. 2568-79.
76. Ma, X., et al., *Function of the neuron-specific alternatively spliced isoforms of nonmuscle myosin II-B during mouse brain development.* Mol Biol Cell, 2006. **17**(5): p. 2138-49.
77. Kohli, B.M., et al., *Interactome of the amyloid precursor protein APP in brain reveals a protein network involved in synaptic vesicle turnover and a close association with Synaptotagmin-1.* J Proteome Res, 2012. **11**(8): p. 4075-90.
78. Fernandez-Martos, C.M., et al., *Neurofilament light gene deletion exacerbates amyloid, dystrophic neurite, and synaptic pathology in the APP/PS1 transgenic model of Alzheimer's disease.* Neurobiol Aging, 2015. **36**(10): p. 2757-67.

79. Berg, D., C. Holzmann, and O. Riess, *14-3-3 proteins in the nervous system.* Nat Rev Neurosci, 2003. **4**(9): p. 752-62.
80. Peyrl, A., et al., *Aberrant expression of signaling-related proteins 14-3-3 gamma and RACK1 in fetal Down syndrome brain (trisomy 21).* Electrophoresis, 2002. **23**(1): p. 152-7.
81. Pang, Z.P., et al., *Calmodulin suppresses synaptotagmin-2 transcription in cortical neurons.* J Biol Chem, 2010. **285**(44): p. 33930-9.
82. Wang, B., et al., *FMRP-Mediated Axonal Delivery of miR-181d Regulates Axon Elongation by Locally Targeting Map1b and Calm1.* Cell Rep, 2015. **13**(12): p. 2794-807.
83. Chen, S., et al., *Quantitative proteomic analysis of human substantia nigra in Alzheimer's disease, Huntington's disease and Multiple sclerosis.* Neurochem Res, 2012. **37**(12): p. 2805-13.
84. DeGeer, J., et al., *Hsc70 chaperone activity underlies Trio GEF function in axon growth and guidance induced by netrin-1.* J Cell Biol, 2015. **210**(5): p. 817-32.
85. Marin-Vicente, C., et al., *ATP enhances neuronal differentiation of PC12 cells by activating PKCalpha interactions with cytoskeletal proteins.* J Proteome Res, 2011. **10**(2): p. 529-40.
86. Sonnenberg, A. and R.K. Liem, *Plakins in development and disease.* Exp Cell Res, 2007. **313**(10): p. 2189-203.
87. Proepper, C., et al., *Heterogeneous nuclear ribonucleoprotein k interacts with Abi-1 at postsynaptic sites and modulates dendritic spine morphology.* PLoS One, 2011. **6**(11): p. e27045.
88. Liu, Y. and B.G. Szaro, *hnRNP K post-transcriptionally co-regulates multiple cytoskeletal genes needed for axonogenesis.* Development, 2011. **138**(14): p. 3079-90.
89. Dickson, H.M., et al., *Targeted inhibition of the Shroom3-Rho kinase protein-protein interaction circumvents Nogo66 to promote axon outgrowth.* BMC Neurosci, 2015. **16**: p. 34.
90. Ernst, S., et al., *Shroom3 is required downstream of FGF signalling to mediate proneuromast assembly in zebrafish.* Development, 2012. **139**(24): p. 4571-81.
91. Nishimura, T. and M. Takeichi, *Shroom3-mediated recruitment of Rho kinases to the apical cell junctions regulates epithelial and neuroepithelial planar remodeling.* Development, 2008. **135**(8): p. 1493-502.
92. Hildebrand, J.D. and P. Soriano, *Shroom, a PDZ domain-containing actin-binding protein, is required for neural tube morphogenesis in mice.* Cell, 1999. **99**(5): p. 485-97.
93. Walch, L., *Emerging role of the scaffolding protein Dlg1 in vesicle trafficking.* Traffic, 2013. **14**(9): p. 964-73.
94. Zhou, W., et al., *GluR1 controls dendrite growth through its binding partner, SAP97.* J Neurosci, 2008. **28**(41): p. 10220-33.
95. Herradon, G. and C. Perez-Garcia, *Targeting midkine and pleiotrophin signalling pathways in addiction and neurodegenerative disorders: recent progress and perspectives.* Br J Pharmacol, 2014. **171**(4): p. 837-48.
96. Yoshida, Y., et al., *Midkine in repair of the injured nervous system.* Br J Pharmacol, 2014. **171**(4): p. 924-30.
97. Horiba, M., et al., *Neointima formation in a restenosis model is suppressed in midkine-deficient mice.* J Clin Invest, 2000. **105**(4): p. 489-95.
98. Ka, M., et al., *Essential Roles for ARID1B in Dendritic Arborization and Spine Morphology of Developing Pyramidal Neurons.* J Neurosci, 2016. **36**(9): p. 2723-42.
99. Um, J.W., *Synaptic functions of the IQSEC family of ADP-ribosylation factor guanine nucleotide exchange factors.* Neuroscience Research.
100. Boekhoorn, K., et al., *The microtubule destabilizing protein stathmin controls the transition from dividing neuronal precursors to postmitotic neurons during adult hippocampal neurogenesis.* Dev Neurobiol, 2014. **74**(12): p. 1226-42.
101. Liedtke, W., et al., *Stathmin-deficient mice develop an age-dependent axonopathy of the central and peripheral nervous systems.* Am J Pathol, 2002. **160**(2): p. 469-80.
102. Wu, G., et al., *Functional interplay between ganglioside GM1 and cross-linking galectin-1 induces axon-like neuritogenesis via integrin-based signaling and TRPC5-dependent Ca(2)(+) influx.* J Neurochem, 2016. **136**(3): p. 550-63.
103. McGraw, J., et al., *Altered primary afferent anatomy and reduced thermal sensitivity in mice lacking galectin-1.* Pain, 2005. **114**(1-2): p. 7-18.
104. Puche, A.C., et al., *Role of galectin-1 in the developing mouse olfactory system.* Dev Biol, 1996. **179**(1): p. 274-87.
105. Imaizumi, Y., et al., *Galectin-1 is expressed in early-type neural progenitor cells and down-regulates neurogenesis in the adult hippocampus.* Mol Brain, 2011. **4**: p. 7.

106. Sepp, K.J., et al., *Identification of neural outgrowth genes using genome-wide RNAi.* PLoS Genet, 2008. **4**(7): p. e1000111.
107. Comery, T.A., et al., *Abnormal dendritic spines in fragile X knockout mice: maturation and pruning deficits.* Proc Natl Acad Sci U S A, 1997. **94**(10): p. 5401-4.
108. Han, K., et al., *Fragile X-like behaviors and abnormal cortical dendritic spines in cytoplasmic FMR1-interacting protein 2-mutant mice.* Hum Mol Genet, 2015. **24**(7): p. 1813-23.
109. Qin, M., et al., *A mouse model of the fragile X premutation: effects on behavior, dendrite morphology, and regional rates of cerebral protein synthesis.* Neurobiol Dis, 2011. **42**(1): p. 85-98.
110. Toyo-oka, K., et al., *14-3-3epsilon and zeta regulate neurogenesis and differentiation of neuronal progenitor cells in the developing brain.* J Neurosci, 2014. **34**(36): p. 12168-81.
111. Toyo-oka, K., et al., *14-3-3epsilon is important for neuronal migration by binding to NUDEL: a molecular explanation for Miller-Dieker syndrome.* Nat Genet, 2003. **34**(3): p. 274-85.
112. Cheah, P.S., et al., *Neurodevelopmental and neuropsychiatric behaviour defects arise from 14-3-3zeta deficiency.* Mol Psychiatry, 2012. **17**(4): p. 451-66.
113. Shih, Y.Y., et al., *Calreticulin mediates nerve growth factor-induced neuronal differentiation.* J Mol Neurosci, 2012. **47**(3): p. 571-81.
114. Rauch, F., et al., *Heart, brain, and body wall defects in mice lacking calreticulin.* Exp Cell Res, 2000. **256**(1): p. 105-11.
115. Villarroel-Campos, D., et al., *Rab35 Functions in Axon Elongation Are Regulated by P53-Related Protein Kinase in a Mechanism That Involves Rab35 Protein Degradation and the Microtubule-Associated Protein 1B.* J Neurosci, 2016. **36**(27): p. 7298-313.
116. Korshunova, I., et al., *Characterization of BASP1-mediated neurite outgrowth.* J Neurosci Res, 2008. **86**(10): p. 2201-13.
117. Frey, D., et al., *Shared and unique roles of CAP23 and GAP43 in actin regulation, neurite outgrowth, and anatomical plasticity.* J Cell Biol, 2000. **149**(7): p. 1443-54.
118. Gurniak, C.B., E. Perlas, and W. Witke, *The actin depolymerizing factor n-cofilin is essential for neural tube morphogenesis and neural crest cell migration.* Dev Biol, 2005. **278**(1): p. 231-41.
119. Bellenchi, G.C., et al., *N-cofilin is associated with neuronal migration disorders and cell cycle control in the cerebral cortex.* Genes Dev, 2007. **21**(18): p. 2347-57.
120. Kinoshita, M.O., et al., *Selective upregulation of 3-phosphoglycerate dehydrogenase (Phgdh) expression in adult subventricular zone neurogenic niche.* Neurosci Lett, 2009. **453**(1): p. 21-6.
121. Yoshida, K., et al., *Targeted disruption of the mouse 3-phosphoglycerate dehydrogenase gene causes severe neurodevelopmental defects and results in embryonic lethality.* J Biol Chem, 2004. **279**(5): p. 3573-7.
122. Storbeck, M., et al., *Neuronal-specific deficiency of the splicing factor Tra2b causes apoptosis in neurogenic areas of the developing mouse brain.* PLoS One, 2014. **9**(2): p. e89020.
123. Roberts, J.M., et al., *Splicing factor TRA2B is required for neural progenitor survival.* J Comp Neurol, 2014. **522**(2): p. 372-92.
124. Pfister, J.A. and S.R. D'Mello, *Regulation of Neuronal Survival by Nucleophosmin 1 (NPM1) Is Dependent on Its Expression Level, Subcellular Localization, and Oligomerization Status.* Journal of Biological Chemistry, 2016. **291**(39): p. 20787-20797.
125. Grisendi, S., et al., *Role of nucleophosmin in embryonic development and tumorigenesis.* Nature, 2005. **437**(7055): p. 147-53.
126. Gau, B.H., et al., *FUBP3 interacts with FGF9 3' microsatellite and positively regulates FGF9 translation.* Nucleic Acids Res, 2011. **39**(9): p. 3582-93.
127. Paulus, J.D. and B.A. Link, *Loss of optineurin in vivo results in elevated cell death and alters axonal trafficking dynamics.* PLoS One, 2014. **9**(10): p. e109922.
128. Chibalina, M.V., et al., *Myosin VI and Optineurin Are Required for Polarized EGFR Delivery and Directed Migration.* Traffic (Copenhagen, Denmark), 2010. **11**(10): p. 1290-1303.
129. Korac, J., et al., *Ubiquitin-independent function of optineurin in autophagic clearance of protein aggregates.* J Cell Sci, 2013. **126**(Pt 2): p. 580-92.
130. Osawa, T., et al., *Optineurin in neurodegenerative diseases.* Neuropathology, 2011. **31**(6): p. 569-74.
131. Gess, B., et al., *Desmoplakin is involved in organization of an adhesion complex in peripheral nerve regeneration after injury.* Exp Neurol, 2015. **264**: p. 55-66.
132. Margarit, E., et al., *CNBP modulates the transcription of Wnt signaling pathway components.* Biochim Biophys Acta, 2014. **1839**(11): p. 1151-60.

133. Weiner, A.M., et al., *CNBP mediates neural crest cell expansion by controlling cell proliferation and cell survival during rostral head development.* J Cell Biochem, 2007. **102**(6): p. 1553-70.
134. Chen, W., et al., *The zinc-finger protein CNBP is required for forebrain formation in the mouse.* Development, 2003. **130**(7): p. 1367-79.
135. Weitzer, S., et al., *CLP1 as a novel player in linking tRNA splicing to neurodegenerative disorders.* Wiley Interdiscip Rev RNA, 2015. **6**(1): p. 47-63.
136. Hanada, T., et al., *CLP1 links tRNA metabolism to progressive motor-neuron loss.* Nature, 2013. **495**(7442): p. 474-80.
137. Karaca, E., et al., *Human CLP1 mutations alter tRNA biogenesis, affecting both peripheral and central nervous system function.* Cell, 2014. **157**(3): p. 636-50.
138. Kosacka, J., et al., *Apolipoproteins D and E3 exert neurotrophic and synaptogenic effects in dorsal root ganglion cell cultures.* Neuroscience, 2009. **162**(2): p. 282-91.
139. Ruiz, M., et al., *Lipid-binding properties of human ApoD and Lazarillo-related lipocalins: functional implications for cell differentiation.* FEBS J, 2013. **280**(16): p. 3928-43.
140. Ganfornina, M.D., et al., *Apolipoprotein D is involved in the mechanisms regulating protection from oxidative stress.* Aging Cell, 2008. **7**(4): p. 506-15.
141. Dassati, S., A. Waldner, and R. Schweigreiter, *Apolipoprotein D takes center stage in the stress response of the aging and degenerative brain().* Neurobiology of Aging, 2014. **35**(7): p. 1632-1642.
142. Loerch, P.M., et al., *Evolution of the aging brain transcriptome and synaptic regulation.* PLoS One, 2008. **3**(10): p. e3329.
143. Wu, Y., et al., *Regulation of global gene expression and cell proliferation by APP.* Scientific Reports, 2016. **6**: p. 22460.
144. Cao, X. and T.C. Sudhof, *A transcriptionally [correction of transcriptively] active complex of APP with Fe65 and histone acetyltransferase Tip60.* Science, 2001. **293**(5527): p. 115-20.
145. Gao, Y. and S.W. Pimplikar, *The gamma -secretase-cleaved C-terminal fragment of amyloid precursor protein mediates signaling to the nucleus.* Proc Natl Acad Sci U S A, 2001. **98**(26): p. 14979-84.
146. Konietzko, U., et al., *Co-localization of the amyloid precursor protein and the Notch intracellular domains in nuclear transcription factories.* Neurobiology of aging, 2010. **31**(1): p. 58-73.
147. Muresan, Z. and V. Muresan, *A phosphorylated, carboxy-terminal fragment of β-amyloid precursor protein localizes to the splicing factor compartment.* Human Molecular Genetics, 2004. **13**(5): p. 475-488.
148. Johnson, M.B., et al., *Functional and Evolutionary Insights Into Human Brain Development Through Global Transcriptome Analysis.* Neuron, 2009. **62**(4): p. 494-509.
149. Kapeli, K. and G.W. Yeo, *Genome-wide approaches to dissect the roles of RNA binding proteins in translational control: implications for neurological diseases.* Front Neurosci, 2012. **6**: p. 144.
150. Vuong, C.K., D.L. Black, and S. Zheng, *The neurogenetics of alternative splicing.* Nat Rev Neurosci, 2016. **17**(5): p. 265-81.
151. Zheng, S. and D.L. Black, *Alternative pre-mRNA splicing in neurons: growing up and extending its reach.* Trends Genet, 2013. **29**(8): p. 442-8.
152. Azuma, M., et al., *Ewing sarcoma protein ewsr1 maintains mitotic integrity and proneural cell survival in the zebrafish embryo.* PLoS One, 2007. **2**(10): p. e979.
153. Martin, S., et al., *Preferential binding of a stable G3BP ribonucleoprotein complex to intron-retaining transcripts in mouse brain and modulation of their expression in the cerebellum.* J Neurochem, 2016. **139**(3): p. 349-368.
154. Folsom, T.D., P.D. Thuras, and S.H. Fatemi, *Protein expression of targets of the FMRP regulon is altered in brains of subjects with schizophrenia and mood disorders.* Schizophr Res, 2015. **165**(2-3): p. 201-11.
155. Domingues, S.C., et al., *RanBP9 modulates AICD localization and transcriptional activity via direct interaction with Tip60.* J Alzheimers Dis, 2014. **42**(4): p. 1415-33.
156. Menon, R.P., T.J. Gibson, and A. Pastore, *The C terminus of fragile X mental retardation protein interacts with the multi-domain Ran-binding protein in the microtubule-organising centre.* J Mol Biol, 2004. **343**(1): p. 43-53.
157. Amadio, M., et al., *nELAV proteins alteration in Alzheimer's disease brain: a novel putative target for amyloid-beta reverberating on AbetaPP processing.* J Alzheimers Dis, 2009. **16**(2): p. 409-19.
158. Tam, J.H., et al., *Tyrosine Binding Protein Sites Regulate the Intracellular Trafficking and Processing of Amyloid Precursor Protein through a Novel Lysosome-Directed Pathway.* PLoS One, 2016. **11**(10): p. e0161445.

159. Freund, A., et al., *Proteostatic control of telomerase function through TRiC-mediated folding of TCAB1.* Cell, 2014. **159**(6): p. 1389-403.
160. de Bittencourt Pasquali, M.A., et al., *Gene Expression Profile of NF-kappaB, Nrf2, Glycolytic, and p53 Pathways During the SH-SY5Y Neuronal Differentiation Mediated by Retinoic Acid.* Mol Neurobiol, 2016. **53**(1): p. 423-35.
161. Zheng, X., et al., *Metabolic reprogramming during neuronal differentiation from aerobic glycolysis to neuronal oxidative phosphorylation.* Elife, 2016. **5**.
162. Witte, H. and F. Bradke, *The role of the cytoskeleton during neuronal polarization.* Current Opinion in Neurobiology, 2008. **18**(5): p. 479-487.
163. Flynn, K.C., *The cytoskeleton and neurite initiation.* BioArchitecture, 2013. **3**(4): p. 86-109.
164. Sabo, S.L., et al., *The Alzheimer Amyloid Precursor Protein (APP) and Fe65, an APP-Binding Protein, Regulate Cell Movement.* The Journal of Cell Biology, 2001. **153**(7): p. 1403-1414.
165. Sabo, S.L., et al., *The Amyloid Precursor Protein and Its Regulatory Protein, FE65, in Growth Cones and Synapses In Vitro and In Vivo.* The Journal of Neuroscience, 2003. **23**(13): p. 5407-5415.
166. Chauvin, S. and A. Sobel, *Neuronal stathmins: a family of phosphoproteins cooperating for neuronal development, plasticity and regeneration.* Prog Neurobiol, 2015. **126**: p. 1-18.
167. Yamada, K., et al., *Increased Stathmin1 Expression in the Dentate Gyrus of Mice Causes Abnormal Axonal Arborizations.* PLOS ONE, 2010. **5**(1): p. e8596.
168. Simon, R., et al., *A dual function of Bcl11b/Ctip2 in hippocampal neurogenesis.* The EMBO Journal, 2012. **31**(13): p. 2922-2936.
169. Hu, X., et al., *Peroxiredoxin-2 protects against 6-hydroxydopamine-induced dopaminergic neurodegeneration via attenuation of the ASK1 signaling cascade.* The Journal of neuroscience : the official journal of the Society for Neuroscience, 2011. **31**(1): p. 247-261.
170. Sippl, C., et al., *Depletion of optineurin in RGC-5 cells derived from retinal neurons causes apoptosis and reduces the secretion of neurotrophins.* Exp Eye Res, 2011. **93**(5): p. 669-80.
171. Calcaterra, N.B., et al., *CNBP: a multifunctional nucleic acid chaperone involved in cell death and proliferation control.* IUBMB Life, 2010. **62**(10): p. 707-14.
172. Rickhag, M., et al., *Apolipoprotein D is elevated in oligodendrocytes in the peri-infarct region after experimental stroke: influence of enriched environment.* J Cereb Blood Flow Metab, 2008. **28**(3): p. 551-62.
173. Sasaki, Y., et al., *p53 Family Members Regulate the Expression of the Apolipoprotein D Gene.* Journal of Biological Chemistry, 2009. **284**(2): p. 872-883.
174. Wen, Q., et al., *Forkhead family transcription factor FoxO and neural differentiation.* Neurogenetics, 2012. **13**(2): p. 105-13.
175. Garcia-Campmany, L. and E. Marti, *The TGFbeta intracellular effector Smad3 regulates neuronal differentiation and cell fate specification in the developing spinal cord.* Development, 2007. **134**(1): p. 65-75.
176. Vogel, T., et al., *Transforming growth factor beta promotes neuronal cell fate of mouse cortical and hippocampal progenitors in vitro and in vivo: identification of Nedd9 as an essential signaling component.* Cereb Cortex, 2010. **20**(3): p. 661-71.
177. Bernardino, L., et al., *Tumor necrosis factor-alpha modulates survival, proliferation, and neuronal differentiation in neonatal subventricular zone cell cultures.* Stem Cells, 2008. **26**(9): p. 2361-71.
178. Wang, L., et al., *Estrogen receptor (ER)beta knockout mice reveal a role for ERbeta in migration of cortical neurons in the developing brain.* Proc Natl Acad Sci U S A, 2003. **100**(2): p. 703-8.
179. Vezzali, R., et al., *The FOXG1/FOXO/SMAD network balances proliferation and differentiation of cortical progenitors and activates Kcnh3 expression in mature neurons.* Oncotarget, 2016. **7**(25): p. 37436-37455.

7.7. Supplementary Data

Supplementary Table B.2 - **MS data for the identified proteins.** Each condition was performed in duplicate (b indicates the duplicate). 3D, differentiation day3. 7D, differentiation day 7. #pep, indicates the number of unique peptides identified for each protein. # PSM, indicates the number of peptide-spectrum matches.

		N1b		N1		N1b		APP-WT		APP-WTb		APP-WT		APP-WTb		APP-SA		APP-SAb		APP-SA		APP-SAb		APP-SE		APP-SEb		APP-SE		APP-SEb	
		3D		7D		7D		3D		3D		7D		7D		3D		3D		7D		7D		3D		3D		7D		7D	
Uniprot ID	**Gene name**	**# pep**	**# PSM**	**# pep**	**# PSM**	**# pep**	**# PSM**	**# pep**	**# PSM**	**# pep**	**# PSM**	**# pep**	**# PSM**	**# pep**	**# PSM**	**# pep**	**# PSM**	**# pep**	**# PSM**	**# pep**	**# PSM**	**# pep**	**# PSM**	**# pep**	**# PSM**	**# pep**	**# PSM**	**# pep**	**# PSM**	**# pep**	**# PSM**
Present in both differentiation days																															
Q92841	DDX17			7	10	7	31	8	52	3	20	9	61	7	38	10	66	4	14	6	55	3	9	4	9	2	9	4	32	1	3
Q15459	SF3A1			3	3	2	2	12	43	2	2	9	32	5	21	10	26	3	3	4	17	3	3	3	3	1	1	3	3		
Q13283	G3BP1			7	17	5	15	7	36	3	8	10	67	5	18	11	82	4	8	5	44	2	6	2	2	4	6	3	35	2	8
P11940	PABPC1			5	7	4	11	7	25	1	1	10	30	6	26	10	29	1	1	3	14	3	5	1	1	3	3	2	7		
Q13310	PABPC4			3	3	2	4	4	14	1	1	5	16	3	13	5	14			4	10	2	3	1	1	2	2	2	2		
Q14444	CAPRIN1			4	8	2	14	5	14	2	6	3	10	2	7	5	15	2	3	4	11	2	1	3	7	2	6	3	21		
P0DMV8/P08107	HSPA1A			1	1	2	2	4	11	1	2	2	2	2	2	3	6	1	1	2	2	5	21			2	3	1	1		
Q15365	PCBP1			1	1	3	6	3	10	1	8	3	15	2	15	2	31			2	8	2	13	1	1			3	21	2	13
Q15637	SF1			1	1	1	3	3	10	1	8	1	6	1	8	1	7	1	2	1	16	1	9	1	1	1	1	1	13	1	4
P09012	SNRPA			4	9	3	4	5	8	1	3	7	27	2	6	4	10	1	1	4	15	3	5	1	1	1	1	4	17	3	17
P08670	VIM			3	6	4	12	5	5	2	3	5	6	6	32	5	6	4	7	8	11	10	57	2	72	3	3	5	10	2	8
Q9NXV6	CDKN2AIP			1	1	2	2	4	4	1	2	5	5	3	4	4	4	3	3	5	5	2	2	3	3	2	2	4	4		
Q9Y383	LUC7L2							3	4	1	1	1	1			2	2			1	1	2	2	1	1	1	1	1	1		
Q8WWM7	ATXN2L			1	1	1	1	4	4	1	1	3	3			4	4	2	2	3	3	2	2	2	2	1	1	1	1		
P08579	SNRPB2			2	2	1	2	3	3	1	3	3	4	1	5	3	5	1	1	2	3	2	4	2	2			2	3	2	4
O75525	KHDRBS3			1	1	1	2	2	2	1	1	1	2	2	3	2	2			1	1	1	1	1	1	1	1	1	1	1	3
P26378	ELAVL4					2	11	1	1	2	21	1	5	4	11	1	2	1	4	2	8	1	12			1	4	2	19	2	24
Q96PK6	RBM14			1	1	4	11	1	1	3	5	2	3	1	1	2	2			1	1	1	1	1	1	1	1	3	11		
P50402	EMD			1	1	1	1	1	1	1	2	2	2	1	1	1	1			1	1	1	1	1	1	1	1	1	1	1	1
O43933	PEX1			1	3	1	10	1	1	1	5	1	1	1	1	1	2	1	2	1	8	1	3	1	13	1	1	1	1	1	1
P46782	RPS5			1	1	1	1	6	8			2	3			7	9			2	2	1	1	3	3	1	1	1	1	2	2
Q8NC51	SERBP1			1	2			5	8			4	11	2	3	7	27	2	3	3	14	2	6	3	4					2	3
P62316	SNRPD2					1	1	2	8			1	1	1	2	2	9	1	1	2	19	1	1			1	1	1	2	1	1
Q96AG4	LRRC59							4	8			2	2			2	2			1	1	1	1	1	1						
O00571	DDX3X			2	2	3	7	6	7			9	10	4	14	6	6	3	3	4	4	3	3	3	3	2	2	3	4	1	1
P52272	HNRNPM			4	4	4	4	5	5			9	9			11	11	2	2	5	5	2	2	1	1	1	1	4	7		

		N1b		N1		N1b		APP-WT		APP-WTb		APP-WT		APP-WTb		APP-SA		APP-SAb		APP-SA		APP-SAb		APP-SE		APP-SEb		APP-SE		APP-SEb	
		3D		7D		7D		3D		3D		7D		7D		3D		3D		7D		7D		3D		3D		7D		7D	
Uniprot ID	**Gene name**	**# pep**	**# PSM**	**# pep**	**# PSM**	**# pep**	**# PSM**	**# pep**	**# PSM**	**# pep**	**# PSM**	**# pep**	**# PSM**	**# pep**	**# PSM**	**# pep**	**# PSM**	**# pep**	**# PSM**	**# pep**	**# PSM**	**# pep**	**# PSM**	**# pep**	**# PSM**	**# pep**	**# PSM**	**# pep**	**# PSM**	**# pep**	**# PSM**
O94906	PRPF6							4	5			5	5	1	1	2	2	2	2					1	1						
P02545	LMNA							4	4			2	2			3	3			1	1	9	14	1	1						
P23396	RPS3			1	1			3	3			5	8			3	3			2	2	2	3	2	2			2	2	3	3
P60468	SEC61B							2	3			2	2			2	2							1	1						
O43143	DHX15			1	1	1	1	3	3			2	3			3	3			3	3	1	1	1	1			1	2		
Q9P2N5	RBM27			1	1	1	1	3	3			2	2	2	2	2	2	1	1	1	1	1	1			1	1	1	1		
P62269	RPS18			1	1	1	4	2	2			1	1	1	2	1	1			1	1	2	2	1	1						
P55081	MFAP1			1	1	1	1	2	2			1	2			1	1	1	1	1	1	1	1	1	1	1	1	1	1	1	1
O00425	IGF2BP3			1	1	1	1	2	2			3	3	1	1	3	3			2	2	2	2			1	1	2	2		
Q5T8P6	RBM26			2	2	2	2	2	2			3	3			3	3	1	1	3	8	1	1	1	1	1	1	2	5		
Q06830	PRDX1			1	1			1	1							1	1					4	26	1	5						
P37108	SRP14							1	1							2	2			1	1	1	1	1	1			1	1		
P10809	HSPD1							1	1			1	1			1	1			1	1	7	37	1	1			1	1		
P62851	RPS25							1	1							1	1			1	1	1	2	1	1						
P62701	RPS4X							1	1							1	1			1	1	1	1	1	1						
P38646	HSPA9							1	1			2	2			2	2	1	1	1	1	4	5	1	1			1	1		
P42677	RPS27			1	1	1	2	1	1			1	1	1	2	1	1			1	1	1	1	1	1			1	4	1	1
O95639	CPSF4			1	1			1	1			2	2			2	2			1	1			1	1			1	1		
Q9BZ01	FRG1B							1	1			1	1			1	1	1	1	1	1	1	1	1	1			1	1	1	1
Q96CT7	CCDC124							1	1			1	1			1	1			1	1			1	1						
Q96LL9	DNAJC30							1	1							1	1			1	1			1	1						
Q5T749	KPRP			1	1	1	1	1	1			1	1			1	1	1	1	1	1	1	1	1	1	1	1	2	2	2	3
P48634	PRRC2A					1	1	1	1			2	2			2	2			1	1	1	1			1	1	1	1		
P23246	SFPQ	4	9	13	101	11	64	24	197	6	23	20	128	8	107	22	194	6	51	14	97	7	68	9	42	7	18	10	62	2	7
Q15393	SF3B3	2	4	9	28	3	26	22	80	5	19	17	113	10	72	13	82	6	13	13	64	4	29	9	21	5	16	6	46		
Q16630	CPSF6	2	3	6	21	5	31	8	52			10	59	7	63	12	79	5	23	5	46	5	25	5	12	4	24	5	26	2	10
Q7RTV0	PHF5A	1	1	2	2	2	7	5	13			3	12	1	12	4	15	3	6	4	33	1	1	4	10	1	1	3	20	3	14
P62318	SNRPD3	1	3	3	7	1	15	2	17			2	2	2	15	2	16			2	16	1	6	2	8	1	1	1	4	1	1
Q01081	U2AF1	1	1	1	1	1	2	2	4	1	1	2	4	1	1	2	4	1	1	2	3	2	2	2	2	1	1	2	13	2	7
P35637	FUS	4	22	5	72	4	29	6	77	3	13	4	51	6	80	7	85	4	30	4	30	3	19	4	16	4	41	5	26	3	10
Q92804	TAF15	1	9	2	18	1	14	3	18	3	11	2	22	3	42	3	20	1	12	3	27	1	14	1	2	1	19	4	17	3	17
P04083	ANXA1							2	2			1	1																		
Q03252	LMNB2							2	2													1	1								

		N1b		N1		N1b		APP-WT		APP-WTb		APP-WT		APP-WTb		APP-SA		APP-SAb		APP-SA		APP-SAb		APP-SE		APP-SEb		APP-SE		APP-SEb	
		3D		7D		7D		3D		3D		7D		7D		3D		3D		7D		7D		3D		3D		7D		7D	
Uniprot ID	**Gene name**	**# pep**	**# PSM**	**# pep**	**# PSM**	**# pep**	**# PSM**	**# pep**	**# PSM**	**# pep**	**# PSM**	**# pep**	**# PSM**	**# pep**	**# PSM**	**# pep**	**# PSM**	**# pep**	**# PSM**	**# pep**	**# PSM**	**# pep**	**# PSM**	**# pep**	**# PSM**	**# pep**	**# PSM**	**# pep**	**# PSM**	**# pep**	**# PSM**
O75323	GBAS							1	2			1	1																		
P07900	HSP90AA1							1	1													6	19								
P08238	HSP90AB1							1	1													5	21								
P13639	EEF2							1	1											1	1	7	9								
P20700	LMNB1							1	1													2	2								
Q00325	SLC25A3							1	1			1	1																		
P51114	FXR1					1	1	1	1			3	8	2	9					1	1										
Q96AE4	FUBP1							1	1			1	1																		
Q9BY77	POLDIP3							1	1											1	1							1	1		
Q9HBH1	PDF							1	1			1	1																		
Q14974	KPNB1							1	1													1	1								
Q15366	PCBP2					1	1	1	8	1	8	2	13	1	13	1	20			1	5	2	5					1	7	1	6
P07910	HNRNPC							1	3	1	3	1	1	1	1	1	3			1	2	1	10					1	5	1	6
Q6Y7W6	GIGYF2							2	2	1	1	1	1	1	1	5	7	1	1	2	2							1	1		
Q3MHD2	LSM12							1	1	1	2	1	1			1	1											1	1		
P49750	YLPM1			2	2	1	1	1	1	1	1	2	2	2	2	2	2			1	1	1	1					1	1		
O43719	HTATSF1							4	17			1	6			1	2														
Q9UN86	G3BP2			1	1	1	6	3	14			4	26	1	8	2	25			2	11	1	1					1	12		
Q9Y3B4	SF3B6							2	11							1	5			1	14										
P26368	U2AF2							6	9			3	4	1	1	3	3	1	1												
Q13435	SF3B2			2	2			6	9			5	17			4	14			3	6	1	1					2	2		
Q9Y2H5	PLEKHA6							3	8			1	8			3	8			1	9							1	1		
P63173	RPL38							4	6							3	13			1	4										
O60506	SYNCRIP					1	9	4	5			5	14	2	23	4	8	1	4	1	4	1	5								
O75533	SF3B1			1	1			4	4			6	12	2	2	5	6			6	19							3	5		
Q8IWX8	CHERP			1	1	1	1	2	4			3	4			4	4			2	2							2	2		
Q7L014	DDX46							4	4			2	2			3	3			2	2										
Q9NVI7	ATAD3A							2	3			2	2			2	3			2	2							2	2		
P15880	RPS2							3	3			1	1	2	12	2	2			3	5										
Q96GY0	ZC2HC1A							3	3			1	1			2	2														
P62263	RPS14			1	1	1	6	1	3			1	1	1	5	1	1			1	1							1	6	1	4
P31943	HNRNPH1			1	1			1	3			1	2			2	2														
Q13573	SNW1							2	3			1	1			1	1	2	2	1	1										

		N1b		N1		N1b		APP-WT		APP-WTb		APP-WT		APP-WTb		APP-SA		APP-SAb		APP-SA		APP-SAb		APP-SE		APP-SEb		APP-SE		APP-SEb	
		3D		7D		7D		3D		3D		7D		7D		3D		3D		7D		7D		3D		3D		7D		7D	
Uniprot ID	**Gene name**	**# pep**	**# PSM**	**# pep**	**# PSM**	**# pep**	**# PSM**	**# pep**	**# PSM**	**# pep**	**# PSM**	**# pep**	**# PSM**	**# pep**	**# PSM**	**# pep**	**# PSM**	**# pep**	**# PSM**	**# pep**	**# PSM**	**# pep**	**# PSM**	**# pep**	**# PSM**	**# pep**	**# PSM**	**# pep**	**# PSM**	**# pep**	**# PSM**
P05067	**APP**							2	3			2	2	1	1	2	3			1	1	1	1					1	1		
Q5T6F2	UBAP2							3	3			2	2			2	2	1	1	2	2										
P35268	RPL22							2	2							2	3			2	5	1	1								
P09661	SNRPA1							2	2			1	1			1	1			1	1										
Q16352	INA							2	2			1	1			1	1			1	1	1	8					2	2		
P02765	AHSG							2	2			1	1			2	2			2	2							1	1		
P42167	TMPO							2	2			1	1			1	1			1	1										
Q15428	SF3A2							2	2			2	2			1	1			1	1										
Q9Y2W2	WBP11							2	2			1	1			1	1	2	2												
Q5VT52	RPRD2							2	2			1	1			1	1			1	1							1	1		
P62987	UBA52							1	1					1	1	1	1			1	3							1	1		
P31946	YWHAB					1	1	1	1			1	1			1	1					3	5								
P31947	SFN					1	1	1	1			1	1			1	1					2	4								
P27348	YWHAQ					1	1	1	1			1	1			1	1					4	10								
P61981	YWHAG					1	1	1	1			1	1			1	1					2	4								
P11021	HSPA5							1	1					1	1	2	2					4	8								
P62158	CALM1							1	1							1	1			1	1	1	1								
Q07955	SRSF1							1	1			1	1	1	1	1	1			2	2	1	1								
Q9Y224	C14orf166			1	1	1	5	1	1			2	2			2	2			1	1	1	1								
P14866	HNRNPL							1	1			1	1			2	2					2	2								
P51116	FXR2							1	1			2	6	3	10	1	1			2	2							1	3		
Q15149	PLEC							1	1							1	1					8	8								
P61626	LYZ							1	1							1	1			1	1										
Q14498	RBM39							1	1							1	1					1	1								
P43243	MATR3							1	1			1	1			2	2														
Q8N954	GPATCH11							1	1			1	1			1	1			1	1							1	1		
P50416	CPT1A			1	1			1	1			2	2	1	1	1	1			1	1										
P62140	PPP1CB			1	1	1	2	1	1			1	1			1	1			1	1							1	11	1	1
Q92945	KHSRP							1	1					1	2	1	1	1	1	1	3										
Q9HC52	CBX8							1	1			1	1			1	1			1	1										
Q08211	DHX9							1	1			3	3			1	1			1	1										
Q96DI7	SNRNP40							1	1			1	1			1	1			1	1										
Q8NC56	LEMD2							1	1			1	1			1	1			1	1							1	1		

		N1b		N1		N1b		APP-WT		APP-WTb		APP-WT		APP-WTb		APP-SA		APP-SAb		APP-SA		APP-SAb		APP-SE		APP-SEb		APP-SE		APP-SEb	
		3D		7D		7D		3D		3D		7D		7D		3D		3D		7D		7D		3D		3D		7D		7D	
Uniprot ID	**Gene name**	**# pep**	**# PSM**	**# pep**	**# PSM**	**# pep**	**# PSM**	**# pep**	**# PSM**	**# pep**	**# PSM**	**# pep**	**# PSM**	**# pep**	**# PSM**	**# pep**	**# PSM**	**# pep**	**# PSM**	**# pep**	**# PSM**	**# pep**	**# PSM**	**# pep**	**# PSM**	**# pep**	**# PSM**	**# pep**	**# PSM**	**# pep**	**# PSM**
Q5VW36	FOCAD			1	1	1	1	1	1			3	3			3	3			1	1							1	1		
Q75N03	CBLL1							1	1			1	1			1	1														
Q9H7E2	TDRD3							1	1			1	1			1	1														
Q9H0D6	XRN2							1	1			1	1			1	1			1	1										
Q14694	USP10							1	1			1	1			1	1	1	1									1	1		
O94973	AP2A2							1	1			1	1			1	1														
Q07065	CKAP4	1	1					10	20			2	2			9	20	1	1	1	1			1	1						
P17844	DDX5	3	7	6	9	9	30	19	85	3	19	15	74	11	70	16	84	7	22	10	55	4	15	5	10	4	11	3	25	2	4
P11142	HSPA8	1	3	2	2	1	1	8	25	2	3	7	14	3	4	12	25	2	3	4	7	6	21	2	3	3	5				
Q9BWJ5	SF3B5	1	1			1	1	1	6			1	2	1	8	1	7			1	13							1	7		
Q12874	SF3A3	1	1	1	1			4	6			3	7	3	3	5	5	1	1	2	2					1	1				
Q00839	HNRNPU	1	3			1	1	6	16	1	1	3	12			5	14			4	12	2	2	1	1						
Q9UHX1	PUF60	3	6	2	2	3	7	14	31			9	17	4	10	11	29	2	2	5	11	3	4	2	2	2	2	5	8	1	1
P68363	TUBA1B	3	7	3	4	3	11	11	33	2	6	3	8	2	16	5	10	1	1	3	16	3	33	3	3	2	2	3	21	2	2
P68371	TUBB4B	2	8	1	6	1	1	4	31	1	1	5	15	2	10	5	13	2	15	2	2	4	26	1	5	2	13	2	2		
Q14011	CIRBP	2	2			1	2	4	7	1	2	3	10	1	3	2	2	1	1	1	2	1	1	2	3	1	1	1	1		
O15240	VGF	6	73	16	147	11	86	25	230	7	63	20	216	12	152	22	243	11	84	16	141	11	83	10	82	8	49	12	124	4	28
P07437	TUBB	3	15	2	13			7	41	1	1	6	22	3	15	7	18	2	15	3	3	5	39	2	10	3	23	2	2		
Q13885	TUBB2A	2	14	2	13			6	38	1	1	5	21	3	15	5	16	2	15	3	3	4	26	2	10	3	23	2	2		
P84103	SRSF3	2	3			1	1	3	8			2	4			1	1	1	1	1	2	1	1	2	3			1	1	1	1
P68104	EEF1A1	2	24	2	15	1	12	13	58	1	23	5	25	1	17	7	36	1	14	1	12	5	37	2	5	1	10	1	19	1	20
P62304	SNRPE	2	5					3	12			2	4	1	3	2	7			2	4										
P60709	ACTB	5	43	5	27	4	25	12	96	3	20	8	30	4	40	13	108	3	42	4	36	9	153	2	4	2	13	6	35	4	16
P38159	RBMX	2	3	1	1	3	4	3	4	1	1	7	7	4	8	6	6			4	4	1	1			1	1	2	2	3	15
P62913	RPL11	1	1	1	1	2	2	1	1			1	1			2	3			2	4	2	3					1	1		
Q5VUA4	ZNF318											1	1			3	3			1	1										
A8MWD9	SNRPGP15	2	5	1	1			1	5			1	1			2	2			2	2			1	1			1	1		
Q6DN90	IQSEC1											2	2			2	2														
O60814	HIST1H2BK	1	2	1	10			2	2	1	1	2	2			1	1			3	24	3	41	2	3			1	1	1	1
P22626	HNRNPA2B1											1	1			1	1			1	1	3	8								
P01764/ P01765	IGHV3-23	1	1													1	1													1	1
P09651	HNRNPA1	1	1	2	2	1	1	1	1			2	4			1	1			1	1	1	1	1	1	1	1	1	1	1	2
P35579	MYH9															1	1					5	5								

		N1b		N1		N1b		APP-WT		APP-WTb		APP-WT		APP-WTb		APP-SA		APP-SAb		APP-SA		APP-SAb		APP-SE		APP-SEb		APP-SE		APP-SEb	
		3D		7D		7D		3D		3D		7D		7D		3D		3D		7D		7D		3D		3D		7D		7D	
Uniprot ID	**Gene name**	**# pep**	**# PSM**	**# pep**	**# PSM**	**# pep**	**# PSM**	**# pep**	**# PSM**	**# pep**	**# PSM**	**# pep**	**# PSM**	**# pep**	**# PSM**	**# pep**	**# PSM**	**# pep**	**# PSM**	**# pep**	**# PSM**	**# pep**	**# PSM**	**# pep**	**# PSM**	**# pep**	**# PSM**	**# pep**	**# PSM**	**# pep**	**# PSM**
P62820	RAB1A															1	1					2	2								
Q6UXN9	WDR82	1	1									1	1	1	1	1	1														
P07196	NEFL															1	1					1	8								
P35580	MYH10															1	1					1	1								
P15884	TCF4											1	1			1	1			1	1										
Q9H2U1	DHX36															1	1			1	1										
Q9BTC0	DIDO1											1	1			1	1														
O94913	PCF11											1	1			1	1														
P61978	HNRNPK	16	154	14	90	9	108	25	278	9	111	15	173	13	224	17	278	12	175	10	157	8	105	11	73	10	82	8	118	7	88
Q8N684	CPSF7	3	37	6	41	3	29	8	50	4	16	9	50	5	76	9	65	7	59	6	55	5	52	3	3	6	42	6	64	5	54
O43809	NUDT21	4	25	3	4	3	28	9	46	4	36	5	41	3	23	5	42	1	1	4	35	3	22	6	32	2	5	2	11	3	25
Q8NFD5	ARID1B			1	1							2	2			1	1	1	1												
Q8TF72	SHROOM3													1	5			1	1											1	11
P02768	ALB	3	11	3	11	1	3	5	14	1	4	5	17	3	5	6	76			5	10	3	7	4	5	8	53	4	9	2	2
O75643	SNRNP200			1	1	1	1					6	6			5	5			2	2	1	1			1	1	1	1		
P62888	RPL30															1	1			1	1			1	1						
P14678	SNRPB	1	1					1	1			3	7			1	1			1	1			1	2						
P62306	SNRPF	2	7	1	2	3	58	1	5	1	1	1	3	2	16	1	13	1	1	2	65	1	1	2	16	2	2	2	18	1	14
P02795	MT2A											1	1							1	1			1	1	1	1	1	1		
P62805	HIST1H4A																			2	4			2	5						
P32119	PRDX2																					3	17	1	5						
P16403	HIST1H1C																			1	2			1	1			1	6		
Present only in differentiation day 3																															
Q96KK5	HIST1H2AH							1	2	1	1					1	3							1	6						
P81605	DCD							1	1	1	8					1	1	1	1					1	1	1	1				
Q8WXF1	PSPC1							1	1	1	1					2	2									1	1				
P62829	RPL23							2	2							2	2									1	1				
Q9UPT8	ZC3H4							2	2							3	3							1	1						
P39019	RPS19							1	1							2	2							1	1						
P05109	S100A8							1	1							1	1							2	4	2	2				
Q02413	DSG1							1	1							1	1	1	1					1	1	1	1				
P14923	JUP							1	1							1	1							1	1	1	1				
Q01844	EWSR1	1	1					3	27	1	14					4	47	2	12							3	10				

		N1b		N1		N1b		APP-WT		APP-WTb		APP-WT		APP-WTb		APP-SA		APP-SAb		APP-SA		APP-SAb		APP-SE		APP-SEb		APP-SE		APP-SEb	
		3D		7D		7D		3D		3D		7D		7D		3D		3D		7D		7D		3D		3D		7D		7D	
Uniprot ID	**Gene name**	**# pep**	**# PSM**	**# pep**	**# PSM**	**# pep**	**# PSM**	**# pep**	**# PSM**	**# pep**	**# PSM**	**# pep**	**# PSM**	**# pep**	**# PSM**	**# pep**	**# PSM**	**# pep**	**# PSM**	**# pep**	**# PSM**	**# pep**	**# PSM**	**# pep**	**# PSM**	**# pep**	**# PSM**	**# pep**	**# PSM**	**# pep**	**# PSM**
Q14157	UBAP2L	2	13					18	89	3	15					18	126	4	37					4	22	4	38				
Q92499	DDX1							1	2	1	3																				
O94874	UFL1							2	2																						
O15294	OGT							2	2																						
Q9UMS6	SYNPO2							2	2																						
Q04837	SSBP1							1	1																						
P05388	RPLP0							1	1																						
P0CG12	CHTF8							1	1																						
Q9Y3D7	PAM16							1	1																						
P60866	RPS20							1	1																						
Q6P5R6	RPL22L1							1	1																						
P59780	AP3S2							1	1																						
Q9UKK6	NXT1							1	1																						
Q8ND56	LSM14A							1	1																						
Q9UEU0	VTI1B							1	1																						
Q96GD4	AURKB							1	1																						
P27816	MAP4							1	1																						
P19387	POLR2C							1	1																						
Q96I25	RBM17							1	1																						
Q9BUU2	METTL22							1	1																						
P24539	ATP5F1							1	1																						
O95400	CD2BP2							1	1																						
Q9Y265	RUVBL1							1	1																						
P05141	SLC25A5							1	1																						
O43679	LDB2							1	1																						
Q9Y5U2	TSSC4							1	1																						
Q9NZB2	FAM120A							1	1																						
Q15007	WTAP							1	1																						
Q99700	ATXN2							1	1																						
O60313	OPA1							1	1																						
Q9UPN4	CEP131							1	1																						
Q9NRA8	EIF4ENIF1							1	1																						
Q9UQE7	SMC3							1	1																						

		N1b		N1		N1b		APP-WT		APP-WTb		APP-WT		APP-WTb		APP-SA		APP-SAb		APP-SA		APP-SAb		APP-SE		APP-SEb		APP-SE		APP-SEb	
		3D		7D		7D		3D		3D		7D		7D		3D		3D		7D		7D		3D		3D		7D		7D	
Uniprot ID	**Gene name**	**# pep**	**# PSM**	**# pep**	**# PSM**	**# pep**	**# PSM**	**# pep**	**# PSM**	**# pep**	**# PSM**	**# pep**	**# PSM**	**# pep**	**# PSM**	**# pep**	**# PSM**	**# pep**	**# PSM**	**# pep**	**# PSM**	**# pep**	**# PSM**	**# pep**	**# PSM**	**# pep**	**# PSM**	**# pep**	**# PSM**	**# pep**	**# PSM**
Q9P1Y5	CAMSAP3							1	1																						
Q12866	MERTK							1	1																						
O43795	MYO1B							1	1																						
Q9H6K5	PRR36							1	1																						
Q96QZ7	MAGI1							1	1																						
Q08AD1	CAMSAP2							1	1																						
Q5SW79	CEP170							1	1																						
P0DMR2	SCGB1C2									1	1																				
P39060	COL18A1									1	1																				
Q99623	PHB2							2	2							1	1														
Q15029	EFTUD2							2	2							2	2														
Q9Y520	PRRC2C							2	2							3	3	1	1												
P62273	RPS29							1	1							2	2														
Q9Y3C6	PPIL1							1	1							1	1														
P21741	MDK							1	1							1	1														
P30048	PRDX3							1	1							1	1														
Q9UI30	TRMT112							1	1							1	1														
Q96QR8	PURB							1	1							1	1														
O43174	CYP26A1							1	1							1	1														
Q86UP2	KTN1							1	1							1	1														
Q13263	TRIM28							1	1							1	1														
Q8WWY3	PRPF31							1	1							2	2														
O60884	DNAJA2							1	1							1	1														
Q8WYQ5	DGCR8							1	1							1	1														
Q10570	CPSF1							1	1							1	1														
O75420	GIGYF1							1	1							1	1														
P30153	PPP2R1A							1	1							1	1														
Q9BUJ2	HNRNPUL1							1	1							1	1														
Q12959	DLG1							1	1							1	1														
Q9BWU0	SLC4A1AP							1	1							1	1														
P56730	PRSS12							1	1							1	1														
O75400	PRPF40A							1	1							1	1														
Q8TB72	PUM2							1	1							1	1														

		N1b		N1		N1b		APP-WT		APP-WTb		APP-WT		APP-WTb		APP-SA		APP-SAb		APP-SA		APP-SAb		APP-SE		APP-SEb		APP-SE		APP-SEb	
		3D		7D		7D		3D		3D		7D		7D		3D		3D		7D		7D		3D		3D		7D		7D	
Uniprot ID	**Gene name**	**# pep**	**# PSM**	**# pep**	**# PSM**	**# pep**	**# PSM**	**# pep**	**# PSM**	**# pep**	**# PSM**	**# pep**	**# PSM**	**# pep**	**# PSM**	**# pep**	**# PSM**	**# pep**	**# PSM**	**# pep**	**# PSM**	**# pep**	**# PSM**	**# pep**	**# PSM**	**# pep**	**# PSM**	**# pep**	**# PSM**	**# pep**	**# PSM**
P09874	PARP1							1	1							1	1														
Q01804	OTUD4							1	1							1	1														
Q15233	NONO	6	14					17	111	2	7					22	160	4	18					5	12	5	20				
Q07666	KHDRBS1	4	12					7	92	3	26					7	89	4	38					4	8	4	13				
Q86V81	ALYREF	5	14					8	35	2	4					5	19	2	2					2	2	3	6				
Q9Y3I0	RTCB	1	2					2	2	1	1					2	2														
Q9BPW8	NIPSNAP1	1	7					1	3							2	2							1	4						
O43172	PRPF4															2	2														
Q9Y421	FAM32A															1	1														
P62244	RPS15A															1	1														
Q9Y4Z0	LSM4															1	1														
P31944	CASP14															1	1														
Q5JVS0	HABP4															1	1														
Q5JVF3	PCID2															1	1														
Q6PKG0	LARP1															1	1														
Q9BYJ9	YTHDF1															1	1														
P11171	EPB41															1	1														
Q12872	SFSWAP															1	1														
O94964	SOGA1															1	1														
P05783	KRT18	1	39					1	32	1	8					1	40	1	37					1	47	1	39				
Q9P2I0	CPSF2																	1	1												
P48668	KRT6C	4	28					12	51	4	17					6	52	7	47					5	106	13	100				
Q14D04	VEPH1																	1	1							1	1				
Q9UBC9	SPRR3																							1	1						
O43447	PPIH																							1	1						
Q9BRX5	GINS3																							1	1						
Q9UBG3	CRNN																							1	1						
Q96CV9	OPTN																							1	1						
A6NCW0	USP17L3																							1	1						
Q8NB25	FAM184A																							1	1						
Q96QA5	GSDMA																									1	1				
P62633	CNBP							1	1															1	1						
P15924	DSP							1	1															1	1	1	1				

		N1b		N1		N1b		APP-WT		APP-WTb		APP-WT		APP-WTb		APP-SA		APP-SAb		APP-SA		APP-SAb		APP-SE		APP-SEb		APP-SE		APP-SEb	
		3D		7D		7D		3D		3D		7D		7D		3D		3D		7D		7D		3D		3D		7D		7D	
Uniprot ID	**Gene name**	**# pep**	**# PSM**	**# pep**	**# PSM**	**# pep**	**# PSM**	**# pep**	**# PSM**	**# pep**	**# PSM**	**# pep**	**# PSM**	**# pep**	**# PSM**	**# pep**	**# PSM**	**# pep**	**# PSM**	**# pep**	**# PSM**	**# pep**	**# PSM**	**# pep**	**# PSM**	**# pep**	**# PSM**	**# pep**	**# PSM**	**# pep**	**# PSM**
Q05707	COL14A1							1	1															1	1						
Present only in differentiation day 7																															
Q9HCD5	NCOA5					1	1							1	12					2	2							3	5		
Q14966	ZNF638											1	1	1	1																
Q9NVH0	EXD2											2	2																		
Q9BYR8	KRTAP3-1											1	1																		
Q99816	TSG101											1	1																		
Q9NYF8	BCLAF1											1	1																		
Q9NX05	FAM120C											1	1																		
Q99959	PKP2											1	1																		
O15042	U2SURP											1	1																		
Q07157	TJP1											1	1																		
Q9ULI4	KIF26A											1	1																		
Q5JSZ5	PRRC2B											1	1																		
Q06787	FMR1											2	5	1	7					1	1	1	1								
P07355	ANXA2											1	1									4	24								
P00338	LDHA											1	1							1	1	3	39								
P08237	PFKM											1	1									1	1								
P46779	RPL28																			1	1	1	1								
P06748	NPM1																			1	1	2	20								
P16949	STMN1																			1	1	1	1								
P84098	RPL19																			1	1	1	1								
P08621	SNRNP70													1	1					2	2										
Q6P2Q9	PRPF8													1	1					2	2										
P62081	RPS7																			1	1										
P53007	SLC25A1																			1	1										
O75955	FLOT1																			1	1										
Q08188	TGM3																			1	1										
Q7L2E3	DHX30																			1	1										
P07195	LDHB																					4	46								
P29401	TKT																					8	45								
P80723	BASP1																					7	35								
P21333	FLNA																					13	27								

		N1b		N1		N1b		APP-WT		APP-WTb		APP-WT		APP-WTb		APP-SA		APP-SAb		APP-SA		APP-SAb		APP-SE		APP-SEb		APP-SE		APP-SEb	
		3D		7D		7D		3D		3D		7D		7D		3D		3D		7D		7D		3D		3D		7D		7D	
Uniprot ID	**Gene name**	**# pep**	**# PSM**	**# pep**	**# PSM**	**# pep**	**# PSM**	**# pep**	**# PSM**	**# pep**	**# PSM**	**# pep**	**# PSM**	**# pep**	**# PSM**	**# pep**	**# PSM**	**# pep**	**# PSM**	**# pep**	**# PSM**	**# pep**	**# PSM**	**# pep**	**# PSM**	**# pep**	**# PSM**	**# pep**	**# PSM**	**# pep**	**# PSM**
P60174	TPI1																					4	17								
P06454	PTMA																					1	17								
P61604	HSPE1																					2	16								
P63104	YWHAZ																					4	13								
P06703	S100A6																					2	12								
P07737	PFN1																					1	11								
P00558	PGK1																					3	8								
P62826	RAN																					2	7								
Q14103	HNRNPD																					1	6								
P31327	CPS1																					4	5								
P04075	ALDOA																					4	4								
O75369	FLNB																					4	4								
P62258	YWHAE																					3	3								
P31949	S100A11																					2	3								
P26038	MSN																					2	3								
P25705	ATP5A1																					2	3								
P13929	ENO3																					1	3								
P47914	RPL29																					1	3								
P62328	TMSB4X																					2	2								
P04792	HSPB1																					2	2								
P23284	PPIB																					2	2								
P37802	TAGLN2																					1	2								
P26639	TARS																					2	2								
P07237	P4HB																					2	2								
P29692	EEF1D																					1	2								
P67936	TPM4																					2	2								
P31948	STIP1																					2	2								
Q9Y266	NUDC																					2	2								
Q02790	FKBP4																					2	2								
Q01105	SET																					1	2								
P06744	GPI																					2	2								
P49588	AARS																					2	2								
P50990	CCT8																					2	2								

		N1b		N1		N1b		APP-WT		APP-WTb		APP-WT		APP-WTb		APP-SA		APP-SAb		APP-SA		APP-SAb		APP-SE		APP-SEb		APP-SE		APP-SEb	
		3D		7D		7D		3D		3D		7D		7D		3D		3D		7D		7D		3D		3D		7D		7D	
Uniprot ID	**Gene name**	**# pep**	**# PSM**	**# pep**	**# PSM**	**# pep**	**# PSM**	**# pep**	**# PSM**	**# pep**	**# PSM**	**# pep**	**# PSM**	**# pep**	**# PSM**	**# pep**	**# PSM**	**# pep**	**# PSM**	**# pep**	**# PSM**	**# pep**	**# PSM**	**# pep**	**# PSM**	**# pep**	**# PSM**	**# pep**	**# PSM**	**# pep**	**# PSM**
P13010	XRCC5																					2	2								
P12268	IMPDH2																					2	2								
P53396	ACLY																					2	2								
P11586	MTHFD1																					2	2								
P58107	EPPK1																					2	2								
O43707	ACTN4																					2	2								
Q9Y490	TLN1																					2	2								
Q14978	NOLC1																					2	2								
P05387	RPLP2																					1	1								
P23528	CFL1																					1	1								
P62937	PPIA																					1	1								
P06576	ATP5B																					1	1								
P62241	RPS8																					1	1								
Q9UBI6	GNG12																					1	1								
P26641	EEF1G																					1	1								
Q14847	LASP1																					1	1								
P40926	MDH2																					1	1								
P63241	EIF5A																					1	1								
O43175	PHGDH																					1	1								
P78371	CCT2																					1	1								
P61247	RPS3A																					1	1								
P48047	ATP5O																					1	1								
P37837	TALDO1																					1	1								
P10599	TXN																					1	1								
P30086	PEBP1																					1	1								
P83881	RPL36A																					1	1								
P12004	PCNA																					1	1								
P26447	S100A4																					1	1								
P49207	RPL34																					1	1								
P09382	LGALS1																					1	1								
P30101	PDIA3																					1	1								
P62995	TRA2B																					1	1								
P13987	CD59																					1	1								

		N1b		N1		N1b		APP-WT		APP-WTb		APP-WT		APP-WTb		APP-SA		APP-SAb		APP-SA		APP-SAb		APP-SE		APP-SEb		APP-SE		APP-SEb	
		3D		7D		7D		3D		3D		7D		7D		3D		3D		7D		7D		3D		3D		7D		7D	
Uniprot ID	**Gene name**	**# pep**	**# PSM**	**# pep**	**# PSM**	**# pep**	**# PSM**	**# pep**	**# PSM**	**# pep**	**# PSM**	**# pep**	**# PSM**	**# pep**	**# PSM**	**# pep**	**# PSM**	**# pep**	**# PSM**	**# pep**	**# PSM**	**# pep**	**# PSM**	**# pep**	**# PSM**	**# pep**	**# PSM**	**# pep**	**# PSM**	**# pep**	**# PSM**
P26373	RPL13																					1	1								
P14625	HSP90B1																					1	1								
Q99733	NAP1L4																					1	1								
P84085	ARF5																					1	1								
P62847	RPS24																					1	1								
P11413	G6PD																					1	1								
P48643	CCT5																					1	1								
Q16836	HADH																					1	1								
P31040	SDHA																					1	1								
P12277	CKB																					1	1								
P60842	EIF4A1																					1	1								
P27635	RPL10																					1	1								
P28072	PSMB6																					1	1								
P09622	DLD																					1	1								
Q12931	TRAP1																					1	1								
P27797	CALR																					1	1								
P15259	PGAM2																					1	1								
Q16186	ADRM1																					1	1								
P30040	ERP29																					1	1								
Q7L1Q6	BZW1																					1	1								
Q9H1E3	NUCKS1																					1	1								
Q05682	CALD1																					1	1								
Q7KZF4	SND1																					1	1								
P55809	OXCT1																					1	1								
Q6UVW9	CLEC2A																					1	1								
Q99436	PSMB7																					1	1								
P62753	RPS6																					1	1								
Q01130	SRSF2																					1	1								
P47756	CAPZB																					1	1								
P27695	APEX1																					1	1								
O75821	EIF3G																					1	1								
P13667	PDIA4													1	1							1	1								
Q09666	AHNAK																					1	1								

		N1b		N1		N1b		APP-WT		APP-WTb		APP-WT		APP-WTb		APP-SA		APP-SAb		APP-SA		APP-SAb		APP-SE		APP-SEb		APP-SE		APP-SEb	
		3D		7D		7D		3D		3D		7D		7D		3D		3D		7D		7D		3D		3D		7D		7D	
Uniprot ID	**Gene name**	**# pep**	**# PSM**	**# pep**	**# PSM**	**# pep**	**# PSM**	**# pep**	**# PSM**	**# pep**	**# PSM**	**# pep**	**# PSM**	**# pep**	**# PSM**	**# pep**	**# PSM**	**# pep**	**# PSM**	**# pep**	**# PSM**	**# pep**	**# PSM**	**# pep**	**# PSM**	**# pep**	**# PSM**	**# pep**	**# PSM**	**# pep**	**# PSM**
P25786	PSMA1																					1	1								
Q16881	TXNRD1																					1	1								
P12814	ACTN1																					1	1								
P22234	PAICS																					1	1								
Q15645	TRIP13																					1	1								
Q92973	TNPO1																					1	1								
P14324	FDPS																					1	1								
Q6ZV70	LANCL3																					1	1								
P55072	VCP																					1	1								
P23526	AHCY																					1	1								
P08195	SLC3A2																					1	1								
Q9Y5B9	SUPT16H																					1	1								
Q15019	SEPT2																					1	1								
Q09028	RBBP4																					1	1								
P50991	CCT4																					1	1								
Q08J23	NSUN2																					1	1								
P16070	CD44																					1	1								
P11498	PC																					1	1								
P46821	MAP1B																					1	1								
P06733	ENO1			1	1															1	1	9	85								
P14618	PKM			1	1																	7	45								
P39023	RPL3			1	1																	3	4								
P18206	VCL			1	1																	2	2								
P19338	NCL			1	1																	2	2								
P04406	GAPDH					1	1													1	1	4	47								
Q9UNN5	FAF1																			1	1	1	1					1	1		
P62979	RPS27A													1	1					1	3							1	1		
Q92989	CLP1																											1	3		
Q8IY26	PLPP6																											1	1		
Q96I24	FUBP3																											1	1		
Q92797	SYMPK																											1	1		
A3KMH1	VWA8																											1	1		
P05090	APOD																													1	1

		N1b		N1		N1b		APP-WT		APP-WTb		APP-WT		APP-WTb		APP-SA		APP-SAb		APP-SA		APP-SAb		APP-SE		APP-SEb		APP-SE		APP-SEb	
		3D		7D		7D		3D		3D		7D		7D		3D		3D		7D		7D		3D		3D		7D		7D	
Uniprot ID	**Gene name**	**# pep**	**# PSM**	**# pep**	**# PSM**	**# pep**	**# PSM**	**# pep**	**# PSM**	**# pep**	**# PSM**	**# pep**	**# PSM**	**# pep**	**# PSM**	**# pep**	**# PSM**	**# pep**	**# PSM**	**# pep**	**# PSM**	**# pep**	**# PSM**	**# pep**	**# PSM**	**# pep**	**# PSM**	**# pep**	**# PSM**	**# pep**	**# PSM**
Q6ZR08	DNAH12																													1	1
P30050	RPL12					2	3					2	3	1	4					1	1	1	1					2	6		
O75063	FAM20B											1	1																	1	1

Supplementary Table B.3 - **Proteins that were placed at different APPS655 phosphorylation categories in each differentiation day (D3 vs D7).** Might indicate that such proteins during differentiation and/or in different APP backgrounds suffer alterations in protein expression and consequently are/are not detected by MS. In bold are proteins that were selected as potential interesting for neuronal differentiation studies.

Condition	UniProt nr	Gene name	Condition	UniProt nr	Gene name
D3 dephospho and D7 independent	**P51116**	**FXR2**	D3 independent and D3 dephospho	O43933	PEX1
	P07910	HNRNPC		Q8NC51	SERBP1
	Q6Y7W6	**GIGYF2**		Q96AG4	LRRC59
	Q9NVI7	ATAD3A		**P02545**	**LMNA**
	Q16352	**INA**		P62269	RPS18
	P02765	AHSG		Q06830	PRDX1
	Q9Y2H5	PLEKHA6		P62851	RPS25
	Q8N954	GPATCH11		P62701	RPS4X
	Q8NC56	**LEMD2**		Q96CT7	CCDC124
	Q5VT52	RPRD2		Q96LL9	DNAJC30
	Q9UN86	G3BP2		Q15393	SF3B3
	Q9UHX1	PUF60		Q16630	CPSF6
	P17844	DDX5		P62318	SNRPD3
	P68371	TUBB4B		O75643	SNRNP200
	O75533	SF3B1		P62888	RPL30
	O43809	NUDT21		P14678	SNRPB
	P38159	RBMX	D3 phospho and D7 independent	P02795	MT2A
	P68363	**TUBA1B**		P16403	HIST1H1C
	Q15366	PCBP2	D3 phospho and D7 dephospho	P62805	HIST1H4A, …
	Q9BWJ5	SF3B5		P32119	PRDX2
	Q8IWX8	CHERP	D3 dephospho and D7 phospho	**Q8TF72**	**SHROOM3**
	P62987	UBA52		P01764	IGHV3-23
D3 independent and D7 dephospho	Q15459	SF3A1		P62140	PPP1CB
	P11940	PABPC1		Q3MHD2	LSM12
	Q13310	PABPC4		Q14694	USP10
	P0DMV8	HSPA1A		P09651	HNRNPA1
	P08670	**VIM**		P62263	RPS14
	Q8WWM7	ATXN2L		Q8N684	CPSF7

Supplementary Table B.4 - **Additional cell differentiation related functions retrieved using Panther overrepresentation test for "Total" APP protein interactors.** Dif. day, indicates the differentiation day. GO term, the enriched gene ontology term attributed. GO source, the gene ontology sources, namely molecular function (MF), biological processes (BP), and pathways. # proteins, number of proteins associated to the attributed enriched term. Pvalue, calculated pvalue with Bonferroni correction.

Dif. day	GO source	GO term	# proteins	pvalue
D3	BP	MT-based process	25	5.18E-03
	BP	cell-cell adhesion	39	7.81E-06
	BP	cell adhesion	44	1.22E-03
	MF	cadherin binding involved in cell-cell adhesion	29	6.03E-13
	MF	structural constituent of cytoskeleton	10	1.45E-02
	Pathways	Parkinson disease	8	1.91E-02
D7	BP	homotypic cell-cell adhesion	8	4.70E-02
	BP	cell-cell adhesion	64	1.34E-18
	BP	cell adhesion	67	3.20E-12
	MF	cadherin binding involved in cell-cell adhesion	55	3.51E-37
	Pathways	cytoskeleton regulation by Rho GTPases	9	2.41E-03
	Pathways	Parkinson disease	13	4.06E-06

Supplementary Table B.5 - **Examples of enriched functions attributed to the combined list of APP S655 phosphorylation-independent interactors (Figure 4) plus the list of APPWt interactors.** The enrichment analysis was performed using the Cytoscape app ClueGO, comparing differentiation day 3 and differentiation day 7. Pvalue, calculated p value with Bonferroni correction; GO term, the enriched term attributed. GO source, the gene ontology sources, namely biological processes (BP) and KEGG pathways. % genes, percentage of proteins (here by the gene name) associated to the attributed enriched term; ID, the gene names of the proteins associated with the attributed enriched terms.

Go Term	Go source	Enriched at *(Pvalue)*	Genes Cluster at D3	Genes Cluster at D7	% Genes D3	% Genes D7
translation	BP	**D3** *(630.0E-15)*	[ATXN2, CAPRIN1, DDX1, DDX3X, EEF2, EIF4ENIF1, FXR1, IGF2BP3, LSM14A, PABPC1, PABPC4, PDF, POLDIP3, RPL22L1, RPL23, RPL30, RPLP0, RPS18, RPS19, RPS20, RPS25, RPS27, RPS3, RPS4X, RPS5, SEC61B, SLC25A3, SLC25A5, SRP14]	[DDX3X, FXR1, FXR2, GIGYF2, IGF2BP3, PDF, POLDIP3, RPS27A, RPS3, RPS5, SEC61B, SLC25A3, SRP14, SYNCRIP, UBA52]	79.48	41.11
negative regulation of translation	BP	**D7** *(390.0E-6)*	[CAPRIN1, DDX3X, EIF4ENIF1, FXR1, IGF2BP3, RPS3]	[DDX3X, FXR1, FXR2, GIGYF2, IGF2BP3, RPS3, SYNCRIP]	57.11	66.63
positive regulation of translation	BP	**D3** *(2.2E-3)*	[DDX3X, EEF2, IGF2BP3, PABPC1, POLDIP3, RPS4X]	[DDX3X, IGF2BP3, POLDIP3, SYNCRIP]	72.44	48.29
RNA splicing	BP	**D7** *(38.0E-33)*	[CD2BP2, DDX1, DHX15, HNRNPM, HSPA1A, LUC7L2, PABPC1, PCBP1, PHF5A, POLR2C, PRPF6, PSPC1, RBM17, SF1, SF3A1, SF3B3, SFPQ, SNRNP200, SNRPA, SNRPB, SNRPB2, SNRPD2, SNRPD3, SNRPF, U2AF1, WTAP]	[C14orf166, DDX5, DHX15, FUS, HNRNPC, HNRNPH1, HNRNPK, HNRNPM, HTATSF1, LUC7L2, NUDT21, PCBP1, PCBP2, PCF11, PHF5A, PRPF6, PUF60, RBMX, SF1, SF3B1, SF3B5, SFPQ, SNRPA, SNRPB2, SNRPD2, SNRPF, SYNCRIP, U2AF1, U2AF2, WBP11, ZNF638]	55.31	65.94
ribonucleoprotein complex assembly	BP	**D3** *(250.0E-15)*	[ATXN2, ATXN2L, CD2BP2, DDX1, DDX3X, LSM14A, LUC7L2, PRPF6, RPS19, RPS27, RPS5, SF1, SF3A1, SNRNP200, SNRPB, SNRPD2, SNRPD3, SNRPF]	[DDX3X, HNRNPC, LUC7L2, PRPF6, RPS5, SF1, SF3B1, SNRPD2, SNRPF, U2AF2]	78.31	43.51
spliceosomal complex assembly	BP	**D3** *(580.0E-12)*	[DDX1, LUC7L2, PRPF6, SF1, SF3A1, SNRNP200, SNRPD2, SNRPD3]	[HNRNPC, LUC7L2, PRPF6, SF1, SF3B1, SNRPD2, U2AF2]	64.40	56.35
spliceosomal snRNP assembly	BP	**D3** *(11.0E-6)*	[CD2BP2, PRPF6, SNRPB, SNRPD2, SNRPD3, SNRPF]	[HNRNPC, PRPF6, SNRPD2, SNRPF]	72.44	48.29
stress granule assembly	BP	**D3** *(4.8E-3)*	[ATXN2, ATXN2L, DDX3X]	[DDX3X]	79.25	26.42
positive regulation of RNA splicing	BP	**D7** *(5.7E-3)*	[HSPA1A]	[HNRNPK, RBMX, U2AF2]	25.00	75.00
alternative mRNA splicing, via spliceosome	BP	**None specific** *(170.0E-6)*	[HNRNPM, RBM17, SFPQ, WTAP]	[DDX5, HNRNPM, RBMX, SFPQ]	57.44	57.44
negative regulation of mRNA metabolic process	BP	**D7** *(1.4E-3)*	[PABPC1]	[HNRNPK, RBMX, SYNCRIP, U2AF2]	20.00	80.00
negative regulation of mRNA splicing, via spliceosome	BP	**D7** *(32.0E-3)*	[]	[HNRNPK, RBMX, U2AF2]	0.00	100.00
Ribosome	KEGG	**D3** *(8.7E-9)*	[RPL22L1, RPL23, RPL30, RPLP0, RPS18, RPS19, RPS20, RPS25, RPS27, RPS3, RPS4X, RPS5]	[RPS27A, RPS3, RPS5, UBA52]	81.59	27.20
mRNA surveillance pathway	KEGG	**None specific** (*69.0E-6)*	[CPSF4, CPSF6, NXT1, PABPC1, PABPC4]	[CPSF4, NUDT21, PCF11, WDR82]	59.15	47.32

Go Term	Go source	Enriched at *(Pvalue)*	Genes Cluster at D3	Genes Cluster at D7	% Genes D3	% Genes D7
RNA degradation	KEGG	**D3** *(18.0E-3)*	[HSPA9, HSPD1, PABPC1, PABPC4]	[HSPA9, HSPD1]	77.37	38.69
Spliceosome	KEGG	**D7** *(26.0E-27)*	[DHX15, HNRNPM, HSPA1A, PCBP1, PHF5A, PRPF6, RBM17, SF3A1, SF3B3, SNRNP200, SNRPA, SNRPB, SNRPB2, SNRPD2, SNRPD3, SNRPF, U2AF1]	[CHERP, DDX5, DHX15, HNRNPC, HNRNPK, HNRNPM, PCBP1, PHF5A, PRPF6, PUF60, RBMX, SF3B1, SF3B5, SNRPA, SNRPB2, SNRPD2, SNRPF, U2AF1, U2AF2, U2SURP, WBP11]	55.62	68.70

Supplementary Table B.6 - **Additional cell differentiation-related functions retrieved using Panther overrepresentation test for the dephosphoS655 APP interactome.** 'Dif. day', differentiation day. 'GO term', the enriched term attributed. 'GO source', the gene ontology sources, namely molecular function (MF), biological processes (BP), and pathways. '# proteins', number of proteins associated to the attributed enriched term. 'Pvalue', calculated pvalue with Bonferroni correction; 'ID', the gene names of the proteins associated with the attributed enriched terms.

Dif. day	GO term	GO source	# proteins	pvalue	ID
D3	structural constituent of cytoskeleton	MF	8	3.00E-03	[TUBA1A, ACTB, TUBB, EPB41, TUBB4B, NEFL, TUBB2A, INA]
	cadherin binding involved in cell-cell adhesion	MF	16	3.54E-07	[GIGYF2, PLEC, RAB1A, HSPA5, KTN1, RPS2, YWHAB, LARP1, SFN, HSPA8, UBAP2, PUF60, HNRNPK, DLG1, MYH9, KRT18]
	cytoskeletal regulation by Rho GTPases	pathways	6	4.41E-03	[MYH10, ACTB, TUBB, TUBB4B, TUBB2A, MYH9]
	Parkinson disease	pathways	6	1.23E-02	[HSPA5, YWHAB, SFN, HSPA8, YWHAG, YWHAQ]
D7	substantia nigra development	BP	10	1.47E-06	[ACTB, BASP1, CALM1, CKB, ENO3, G6PD, HSPA5, LDHA, YWHAE, YWHAQ]
	cytoskeleton organization	BP	28	1.99E-02	[EPPK1, PFN1, HSP90B1, KPNB1, MYH10, STMN1, RAN, MSN, FLNA, NPM1, ACTB, TUBB, CALR, FLNB, GAPDH, MAP1B, NEFL, TUBB2A, LMNA, CFL1, CAPZB, TLN1, ACTN1, ACTN4, ALDOA, TMSB4X, MYH9, VIM]
	PKC inhibitor activity	MF	3	1.58E-02	[HSPB1, SFN, YWHAG]
	cadherin binding involved in cell-cell adhesion	MF	45	1.90E-34	[PSMB6, PFN1, SEPT2, CCT8, YWHAZ, PAICS, PLEC, RAB1A, HSPA5, BZW1, EEF1G, PKM, AHNAK, RAN, RPS2, FLNA, NUDC, YWHAB, S100A11, SFN, EEF2, YWHAE, FLNB, HSPA8, UBAP2, SND1, LDHA, SLC3A2, CAPZB, TLN1, RPL29, SERBP1, ANXA2, ALDOA, RPL34, CALD1, TAGLN2, MYH9, PRDX1, LASP1, ENO1, HSP90AB1, ATXN2, EEF1D, VCL]
	actin filament binding	MF	11	9.87E-04	[MYH10, FLNA, EEF2, CFL1, CAPZB, TLN1, ACTN1, ACTN4, MYH9, LASP1, VCL]
	actin bindidng	MF	20	1.25E-04	[PFN1, PLEC, MYH10, MSN, FLNA, EEF2, FLNB, CFL1, CAPZB, TPM4, TLN1, S100A4, ACTN1, ACTN4, ALDOA, TMSB4X, CALD1, MYH9, LASP1, VCL]
	glycolysis	Pathways	10	9.38E-10	[ALDOA, ENO1, ENO3, GAPDH, GPI, PFKM, PGAM2, PGK1, PKM, TPI1]
	cytoskeletal regulation by Rho GTPases	Pathways	8	8.24E-04	[PFN1, MYH10, STM1, ACTB, TUBB, TUBB2A, CFL1, MYH9]
	Parkinson disease	Pathways	11	3.76E-06	[SEPT2, HSPA5, PSMB7, HSPA8, PSMA1, SFN, YWHAZ, YWHAB, YWHAE, YWHAQ, YWHAG]

Supplementary Table B.7 - **Additional dephosphoS655 APP associated protein interactors present only in differentiation day 7 (D7).** Proteins were selected based on functional annotations directly related to brain development, neuron function, neurogenesis, and/or neuronal differentiation related events (cytoskeleton organization, cell adhesion, and cell migration) and signaling pathways. In bold are the UniProt accession number representing newly identified APP interactors. The gene ontology (GO) terms determinant for the selection are described in the biological process column. Node degree ('k'), is the number of interactors the protein presents and refers to the position of the protein inside the protein-protein interaction network that includes all the interactors identified for each differentiation day. 'Ref', indicates references retrieved from the PubMed supporting the role in neuronal differentiation. 'Mammalian phenotype/human diseases', KO mouse phenotypes were searched on Jackson Laboratories mouse knockout database, and human diseases retrieved from UniProt and other indicated references. 'Expression', brain enrichment or altered expression in RA-differentiated SH-SY5Y cells are indicated. 'Dif.' – differentiation; 'Reg.' – regulation; 'PM' – plasma membrane.

Uniprot nr	gene name and symbol	k	Biological Process	REF	Mammalian Phenotype	Expression
O75955	Flotillin-1; FLOT1	4	axonogenesis (GO:0007409); positive reg. of synaptic transmission, dopaminergic (GO:0032226); ECM disassembly (GO:0022617); positive reg. of heterotypic cell-cell adhesion (GO:0034116), of cell-cell adhesion mediated by cadherin (GO:2000049), and of cell adhesion molecule production (GO:0060355); reg. of receptor internalization (GO:0002090); reg. of Rho protein (GO:0035023), and PKC signaling (GO:0070528); positive reg. of cell junction assembly (GO:1901890)	[1, 2]		
Q9Y490	Talin-1; TLN1	5	movement of cell or subcellular component (GO:0006928); cytoskeletal anchoring at PM (GO:0007016); cell-cell (GO:0007043) and cell-substrate (GO:0007044) junction assembly; cortical actin cytoskeleton organization (GO:0030866); cell adhesion (GO:0007155)	[3, 4]		
P18206	Vinculin; VCL	3	axon extension (GO:0048675); movement of cell or subcellular component (GO:0006928); cell-matrix adhesion (GO:0007160); lamellipodium assembly (GO:0030032); negative reg. of cell migration(GO:0030336); adherens junction assembly (GO:0034333)	[4]	embryonic lethality during organogenesis, complete penetrance; incomplete rostral neuropore closure; exencephaly; absent brain ventricles; increased embryonic neuroepithelium apoptosis [5].	
P07737	Profilin-1; PFN1	2	actin cytoskeleton organization (GO:0030036); neural tube closure (GO:0001843); negative (GO:0030837) and positive (GO:0030838) reg. of actin filament polymerization; negative (GO:0032232) and positive (GO:0032233) reg. of actin filament bundle assembly; positive (GO:0051496) and negative (GO:0051497) reg. of stress fiber assembly; Wnt signaling pathway, planar cell polarity pathway (GO:0060071); cell-cell adhesion(GO:0098609)	[6, 7]	Amyotrophic lateral sclerosis 18.	
P62328	Thymosin beta-4; TMSB4X	1	actin filament organization (GO:0007015); reg. of cell migration (GO:0030334); actin cytoskeleton organization (GO:0030036); sequestering of actin monomers(GO:0042989)	[8, 9]		
P47756	F-actin-capping protein subunit beta; CAPZB	0	neuron projection development (GO:0031175); cell projection organization (GO:0030030); reg. of cell morphogenesis (GO:0022604); actin cytoskeleton organization (GO:0030036); barbed-end actin filament capping (GO:0051016); negative reg. of MT polymerization (GO:0031115); reg. of PKC signaling (GO:0090036); movement of cell or subcellular component	[10, 11]		

Uniprot nr	gene name and symbol	k	Biological Process	REF	Mammalian Phenotype	Expression
			(GO:0006928); negative reg. of filopodium assembly (GO:0051490); cell-cell adhesion (GO:0098609)			
Q09666	Neuroblast differentiation-associated protein AHNAK; AHNAK	5	cell-cell adhesion (GO:0098609)	-	*increased cell proliferation and neuronal differentiation in the hippocampal dentate gyrus [12].*	RA dif SH-SY5Y regulated gene [13, 14].
P26038	Moesin; MSN	2	movement of cell or subcellular component (GO:0006928); reg. of cell shape (GO:0008360); reg. of cell size (GO:0008361); positive reg. of protein localization to early endosome (GO:1902966), and of early endosome to late endosome transport (GO:2000643); cytoskeleton organization (GO:0007010)	[15, 16]		
P21333	Filamin-A; FLNA	15	cell projection organization (GO:0030030); adenylate cyclase-inhibiting dopamine receptor signaling (GO:0007195); reg. of cell migration (GO:0030334); actin cytoskeleton reorganization (GO:0031532); cell junction assembly (GO:0034329); negative reg. of apoptotic process (GO:0043066); positive reg. of I-kB kinase/NF-kB signaling(GO:0043123); actin crosslink formation (GO:0051764); semaphorin-plexin signaling (GO:0071526); positive reg. of substrate adhesion-dependent cell spreading (GO:1900026); positive reg. of integrin-mediated signaling (GO:2001046)	[17, 18]	abnormal brain size [19]; Frontometaphyseal dysplasia 1 (intelectual disability); Periventricular nodular heterotopia 1 (abnomal neuronal migration).	
P16070	CD44 antigen; CD44	3	cell-matrix adhesion (GO:0007160); ECM disassembly(GO:0022617), and organization(GO:0030198); positive reg. of heterotypic cell-cell adhesion (GO:0034116); negative reg. of apoptotic process (GO:0043066); cellular response to FGF (GO:0044344); positive reg. of ERK1 and ERK2 (GO:0070374)	[20]	abnormal miniature excitatory postsynaptic currents [21].	RA dif SH-SY5Y regulated gene [13, 14].

References – Supplementary Table 6

1. Swanwick, C.C., et al., *Flotillin-1 mediates neurite branching induced by synaptic adhesion-like molecule 4 in hippocampal neurons.* Mol Cell Neurosci, 2010. **45**(3): p. 213-25.
2. Chen, T.Y., et al., *The intracellular domain of amyloid precursor protein interacts with flotillin-1, a lipid raft protein.* Biochem Biophys Res Commun, 2006. **342**(1): p. 266-72.
3. Tan, C.L., et al., *Full length talin stimulates integrin activation and axon regeneration.* Mol Cell Neurosci, 2015. **68**: p. 1-8.
4. Dingyu, W., et al., *Regulation of Intracellular Structural Tension by Talin in the Axon Growth and Regeneration.* Mol Neurobiol, 2016. **53**(7): p. 4582-95.
5. Marg, S., et al., *The vinculin-DeltaIn20/21 mouse: characteristics of a constitutive, actin-binding deficient splice variant of vinculin.* PLoS One, 2010. **5**(7): p. e11530.
6. Brettle, M., et al., *Amyotrophic lateral sclerosis-associated mutant profilin 1 increases dendritic arborisation and spine formation in primary hippocampal neurons.* Neurosci Lett, 2015. **609**: p. 223-8.
7. Michaelsen-Preusse, K., et al., *Neuronal profilins in health and disease: Relevance for spine plasticity and Fragile X syndrome.* Proceedings of the National Academy of Sciences, 2016. **113**(12): p. 3365-3370.
8. Kim, D.H., et al., *Peptide fragment of thymosin β4 increases hippocampal neurogenesis and facilitates spatial memory.* Neuroscience, 2015. **310**: p. 51-62.
9. van Kesteren, R.E., et al., *Local synthesis of actin-binding protein beta-thymosin regulates neurite outgrowth.* J Neurosci, 2006. **26**(1): p. 152-7.
10. Delalle, I., et al., *Mutations in the Drosophila orthologs of the F-actin capping protein alpha- and beta-subunits cause actin accumulation and subsequent retinal degeneration.* Genetics, 2005. **171**(4): p. 1757-65.
11. Davis, D.A., et al., *Capzb2 interacts with beta-tubulin to regulate growth cone morphology and neurite outgrowth.* PLoS Biol, 2009. **7**(10): p. e1000208.
12. Shin, J.H., et al., *Increased Cell Proliferations and Neurogenesis in the Hippocampal Dentate Gyrus of Ahnak Deficient Mice.* Neurochem Res, 2015. **40**(7): p. 1457-62.
13. Korecka, J.A., et al., *Phenotypic characterization of retinoic acid differentiated SH-SY5Y cells by transcriptional profiling.* PLoS One, 2013. **8**(5): p. e63862.
14. Pezzini, F., et al., *Transcriptomic Profiling Discloses Molecular and Cellular Events Related to Neuronal Differentiation in SH-SY5Y Neuroblastoma Cells.* Cell Mol Neurobiol, 2016.
15. Parisiadou, L., et al., *Phosphorylation of ezrin/radixin/moesin proteins by LRRK2 promotes the rearrangement of actin cytoskeleton in neuronal morphogenesis.* J Neurosci, 2009. **29**(44): p. 13971-80.
16. Paglini, G., et al., *Suppression of radixin and moesin alters growth cone morphology, motility, and process formation in primary cultured neurons.* J Cell Biol, 1998. **143**(2): p. 443-55.
17. Sheen, V.L., et al., *Filamin A and Filamin B are co-expressed within neurons during periods of neuronal migration and can physically interact.* Hum Mol Genet, 2002. **11**(23): p. 2845-54.
18. Zhang, J., et al., *Filamin A regulates neuronal migration through brefeldin A-inhibited guanine exchange factor 2-dependent Arf1 activation.* J Neurosci, 2013. **33**(40): p. 15735-46.
19. Feng, Y., et al., *Filamin A (FLNA) is required for cell-cell contact in vascular development and cardiac morphogenesis.* Proc Natl Acad Sci U S A, 2006. **103**(52): p. 19836-41.
20. Roszkowska, M., et al., *CD44 - a novel synaptic cell adhesion molecule regulating structural and functional plasticity of dendritic spines.* Mol Biol Cell, 2016.
21. Matzke, A., et al., *Haploinsufficiency of c-Met in cd44-/- mice identifies a collaboration of CD44 and c-Met in vivo.* Mol Cell Biol, 2007. **27**(24): p. 8797-806.

C. General Discussion and Future Perspectives

General Discussion and Future Perspectives

The Amyloid precursor protein (APP) is a ubiquitously expressed type 1 transmembrane glycoprotein. For long APP was mainly studied for its association with Alzheimer's disease (AD), since it is the precursor protein of the amyloid β-peptide (Aβ), the main component of the senile plaques, one of the histopathological hallmarks of this neurodegenerative disease. Nevertheless, APP is highly enriched in neurons and has been established as a neuromodulator of developing and mature nervous system. Attributed physiological roles include cell adherence, survival, migration, differentiation, axon guidance, dendritogenesis, synaptogenesis, and synaptic plasticity. However, this protein has proved to be very complex due to its elaborate intracellular trafficking, posttranslational modifications (for instance, several phosphorylation sites that modulate APP fate and function), proteolytic cleavage (with the production of several bioactive peptides), and the existence of multiple protein interactors. Importantly, several of the APP protein interactors are highly involved in nervous system related functions, namely neuronal development, synaptic signaling, synapse organization, and neuron death. In addition, the APP interactor's share several nervous system diseases and mental disorders with APP.

The main aim of this thesis was to contribute to the characterization of the APP physiological role in the cellular alterations underlying neuronal differentiation events. Particularly, we focused on mechanisms mediated by APP, its proteolytic fragment sAPP, and APP phosphorylation at serine 655. Figure C.1 schematizes the main findings of the present work.

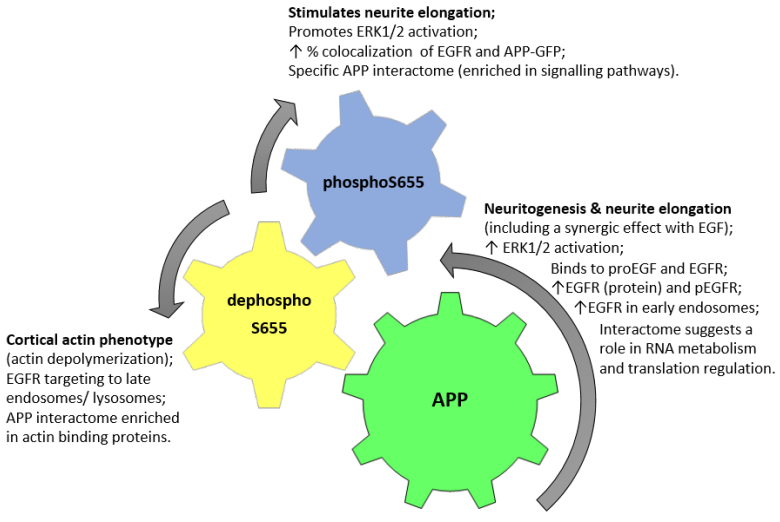

Figure C.1 - APP S655 phosphorylation and neuronal differentiation mechanism.

We started by establishing a comprehensive model of the neuritogenic-related alterations in RA-mediated SH-SY5Y neuronal-like differentiation, namely cell morphology and neurite outgrowth,

and cytoskeleton related biochemical parameters (especially tubulin acetylation) and APP protein levels. The comprehensive analysis of this model pointed to a biphasic temporal differentiation response induced by 10 μM RA treatment on SH-SY5Y cells: a first early phase (D0-D4, D4 excluded), where a sAPP/APP peak assists the emergence of new processes and their elongation into neurites; and a second phase (D4-D8) where increased holoAPP protein levels are necessary to sustain neuritic elongation and stabilization.

In this first study, we focused on APP full-length protein levels and medium secreted APP. A more complete study could involve further characterization of the levels of additional APP fragments, namely C-terminal fragments (CTFs), intracellular domain (AICD), and Aβ with cell differentiation. More specifically, it would be very interesting to monitor the production of non-amyloidogenic pathway-resulting fragments versus the ones resulting from the amyloidogenic pathway, potentially in association with expression studies and activity assays of the corresponding secretases. It would be also very important to fully address the changes in the different APP isoforms with differentiation time, potentially by combination of mRNA expression analysis with proteomic studies using specific antibodies.

The SH-SY5Y cell line was chosen for our studies because it has some advantages when compared to other extensively used models, like primary neuronal cells and neural stem cells. Its usefulness as an in vitro model relates to its human origin, the cells ability to rapidly divide, to be cultured and subcultured for relatively long periods of time, and its comparative low resource requirements. SH-SY5Y cells are easy to obtain, to grow and manipulate and, importantly, do not involve animal sacrifice. Moreover, once clonal-based, they are quite reproducible, exhibit relatively low genetic variability between seedings and can be scaled-up to perform a high number of multiple simultaneously analyses. The main limitation is that this model only mimics in some extent neuronal differentiation events [1, 2]. Nevertheless, it can constitute a useful starting point model to screen important players for brain development and disease. In our work this model has been useful to distinguish between neuritogenesis and neurite outgrowth/elongation events.

We used the knowledge gathered during the characterization of the RA-mediated SH-SY5Y neuronal-like differentiation to delineate two specific differentiation time points for APP modulation. Subsequent work focused on the discovery of potential APP protein effectors and regulators involved in neuronal differentiation events, and the role played by a specific APP posttranslational modification in the establishment of protein-protein interactions – APP phosphorylation at its serine 655. To this end, we used RA-differentiated SH-SY5Y cells for 3 or 7 days (comprising the two differentiation phases). Cells were transfected with Wt or S655 phosphomutants APP-GFP cDNAs in the last 24h, and used as the protein pool. The GFPTrap

assay was used to immunoprecipitate the specific APP proteins (Wt, S655A, and S655E) and their respective interacting partners, which were subsequently identified by mass spectrometry (MS).

In general, we found a special enrichment in RNA-binding proteins linking APP role in neuronal differentiation with regulation of mRNA processing (splicing, decay and translation). These RNA regulatory proteins were found for both the phosphoS655 and dephosphoS655 categories, but particularly enriched in the latter. The hypothesis that APP can bind different RBPs to modulate their function and/or that APP can be part of messenger ribonucleoprotein complexes, influencing the cellular fates of different mRNAs is very curious and should be further studied. These aspects are very important in neurons where alternative splicing events, and the correct transport, target, and local translation of mRNA are determinant for neuronal development (e.g. neuronal polarity) and function (e.g. synaptic plasticity) [3].

The dephosphoS655 APP (S655A) interactome was also enriched in energy metabolism related proteins, and in cytoskeleton-related proteins, especially from the actin family, which translated in an overrepresentation of functions like cytoskeleton organization, actin and actin filament binding. Concordantly, upon 4 days of RA exposure, APP-S655A overexpression could be particularly associated with actin depolymerization and cortical actin distribution. The phophoS655 APP (S655E) interactome presented a reduced number of protein interactors, when compared to the other categories, possibly denoting a higher degree of functional specificity. The phosphoS655 APP interactome included proteins involved in the regulation of proliferation, survival and differentiation, and in various signaling pathways that appear to promote cell fate, neurite outgrowth and neuronal maturation. Concordantly, we could demonstrate that overexpression of the APP phosphomimetic mutant from differentiation day 6 to day 7 promotes SH-SY5Y neurite outgrowth. Although we have detected several functional interesting new APP protein interactors, validity of the interactions is imperative. Each new interaction should be demonstrated using different assays, preferably including techniques that would allow to distinguish direct protein-protein interactions. The interpretation of the protein-protein interactions, at this point, can only be speculative. Nevertheless, this study allowed to start to characterize the biological/molecular context of APP S655 phosphorylation during neuronal-like differentiation, and substantiates the hypothesis that this phosphorylation could be acting as a ‘‘biochemical switch’’ changing the molecular composition of APP complexes to perform specific functions. The APP-S655 phosphorylation interactome follow-up studies could be further supplemented with the study of transcriptome alterations under the different APP backgrounds [2, 4], and/or with the study of overall cell proteome changes [5, 6].

In line with our main aim, we pursed the APP physiological role in neuronal differentiation by characterizing APP relationship with a specific growth-factor signaling pathway – the EGF-EGFR-

ERK signaling. We showed, for the first time, that APP interacts with the proEGF, and with endogenous EGFR in rat cortex lysates. We have also showed that combined APP and EGF have a synergistic effect on ERK1/2 activation and on neuronal-like differentiation. The APP ability to activate ERK1/2 was further associated with APP phosphorylation at S655, and we collected data supporting the involvement of APP and its S655 phosphorylation in the modulation of EGFR expression levels and trafficking. All the three APP species tested increased EGFR colocalization with the early endocytic marker Rab5, and all increased total EGFR protein levels. Nevertheless, we hypothesize that the fate of the increased half-lived EGFR protein may be different: on one hand, the APP-S655E phosphomutant presented the highest colocalization of EGFR and APP-GFP, the highest increase of EGFR colocalization with Rab5, and increased promotion of ERK signaling; on the other hand, the dephosphomimetic mutant APP-S655A increased the presence of EGFR in LAMP2-positive vesicles, failed to increase the total level of EGFR phosphorylation, and failed to induce ERK1/2 activation. Such results raise the hypothesis that APP-S655E increases EGFR residence in the endosomal outer membrane and diverts EGFR from being sorted into intraluminal vesicles (ILVs) during multivesicular body (MVB)'s formation, in this way contributing to ERK1/2 signaling promotion. Previous work from our lab showed that the APP-S655E enhanced APP retrieval via retromer (and decreased its lysosomal targeting) [7], and recent evidences extended the functions of the retromer complex beyond regulating endosome-to-Golgi retrieval to include mediation of the endosome-to-plasma membrane recycling pathway [8]. In this direction, we soon plan to test if overexpression of the APP-S655E phosphomutant increases EGFR colocalization with the recycling endosome (RE; identified as Rab11 positive vesicles). The use of high-resolution imaging techniques (electronic microscopy, or super-resolution light microscopy techniques) would be helpful to define if there are specific sorting events occurring at the endosome favored by each of the APP S655 mutants. For example, it would help to distinguish between the tubular extensions emerging from the outer membranes of the sorting endosomes characteristic of recycling events, and the ILVs, from where cargo is generally targeted for lysosomal degradation [9].

The spatio-temporal distribution of tyrosine kinase receptors along the endosomal system seems to be tightly associated to signaling specificity, signaling amplitude and duration. Changing how the phosphorylated EGFR is distributed between endosomes can, thus, alter signal properties and lead to differential cell responses after exposure to receptor ligands [10]. Our findings that the different APP S655 phosphomimetic mutants alter the dynamic of EGFR endocytosis and are associated with differential ERK1/2 activation correlates well with such arguments.

We are currently addressing how the different APP species influence EGFR trafficking after EGF stimulation, and we need to further consolidate the effects of APP phosphomutants on EGFR

activation. As shown, we tried to perform a first general evaluation of the EGFR phosphorylation status using the phos-tag assay. Although results appear to show a differential level of total EGFR phosphorylation depending on the APP S655 phosphorylation status, the assay has proven to be very difficult to perform and analyze, due to the high molecular weight of the receptor, and we recognize a need for validation by a different assay. A simple approach would be to immunoprecipitate EGFR and, after SDS-PAGE, probe the immunoblot with an antibody specific for tyrosine phosphorylation sites (an indirect measure of the activation of the EGFR tyrosine-kinase domain). Such approach would further allow to use antibodies against other posttranslational modifications, like ubiquitination, that can as well provide important clues regarding EGFR fate. A complementary approach could involve flow cytometry studies using an EGFR phospho-specific antibody (a first possible residue of choice would be the T1068, previously implicated in Ras-ERK1/2 downstream signaling). Flow cytometry would offer the additional advantages of distinguish between transfected cells and non-transfected ones, and would allow to evaluate the expression levels of the APP-GFP exogenous protein. MS techniques would also allow to map phosphorylated residues and to study protein phosphorylation (and other relevant posttranslational modifications) patterns [11, 12]. Additionally, MS techniques would allow to characterize (at least in part) the “topology”, and possibly the dynamics, of the EGFR signaling network elicited by the two APP S655 phosphomutants [13].

Another interesting point, based on the different percentages of colocalization that we have obtained between EGFR and the different APP-GFP species, would be to evaluate if the strength (and subcellular location) of the interaction between APP and the EGFR changes with the state of APP phosphorylation at S655. EGFR is activated by the formation of ligand-dependent dimers. The receptors dimerization, through contacts between the two receptor molecules, allows trans- and auto-phosphorylation of tyrosine residues within the cytoplasmic (C-terminal) domain of both receptors. The process of dimerization has proven to be very complex, with the formation of homo-dimers, heterodimers with other EGFR family members, and even heterodimers with other more distantly related tyrosine kinase receptors (TKRs). The type of dimers formed has important effects on the downstream signaling events due to the distinct adaptor binding profile of each receptor. The main mechanisms of receptor dimerization seem to depend on a conformational change that exposes the "dimerization arm" located in the extracellular domain of the receptors. Additionally, the transmembrane alpha helices of EGFR family receptors which include GxxxG motifs, have been implicated in both ligand-dependent and-independent interactions, and it has been proposed that such motifs may also facilitate the formation of heterodimers between TKRs [14]. APP transmembrane domains can also form homodimers and the interaction is primarily mediated by the three consecutive GxxxG motifs, similar to the transmembrane domains of ErbB-receptors (the

EGFR protein family) [15]. These transmembrane motifs might also be mediating the APP interaction with EGFR, assuming it is a direct interaction. Since APP contains a conserved ^{682}YENPTY^{687} cytoplasmic motif similar to nonreceptor tyrosine kinases which may be involved in propagating signaling responses, the formation of a functional EGFR:APP dimer, as mentioned above for EGFR and other TKRs, is a very attractive hypothesis. The formation of heterodimers between TKRs could be also mediated through interactions at the intracellular region [14]. In the particular case of the interaction between APP and EGFR, this would also be an attractive possibility as it would intuitively explain how the APP phosphorylation at S655 could be modulating the strength of such interaction, since this phosphorylation is described to induce structural alterations to the APP C-terminus [16].

APP shares several protein interactors with the EGFR (as indirectly demonstrated in the previous chapters of this work), any of each could be mediating the interaction between both proteins. Interestingly, some of these shared interactors can also provide clues on the APP ability to modulate EGFR expression levels and trafficking, as the previously discussed interaction with the Rab5 effector APPL1 (or DCC-interacting protein 13-alpha); the interaction with Grb2, LRP1, or c-Src that could modulate, in turn, the interaction of the ubiquitin-protein ligase CBL with EGFR; and the interaction with the deubiquitinating enzyme UCH-L1. There are several other possibilities (see Figure C.2) since APP can be trafficked in the same population of endosomes/MVBs that delivers EGFR to the lysosome for degradation, as shown by our results and results from other [17]. Based on our results with the APP-S655E phosphomutant, it would be interesting to investigate if APP can be also recycled in the same vesicles as EGFR.

In our APP S655 phosphorylation interactome we detected the protein optineurin (OPTN) as a potential APP phosphoS655 exclusive protein interactor (on the earlier differentiation phase, at day 3). Interestingly, OPTN has been extensively related to membrane trafficking events, namely in post-Golgi membrane trafficking to the plasma membrane, membrane trafficking at the RE, and lysosome function, especially by its ability to interact with huntingtin, myosin IV, and Rab8 and its GTPase-activating protein, TBC1D17 [18-20]. The fact that OPTN is present in the RE, is able to bind both Rab8 (a regulator of the endocytic traffic to the RE) and Rab11 (regulator of the transport of cargo from the RE to plasma membrane) [21], and the results showing that the interaction TBC1D17:OPTN regulates the Rab8-mediated endocytic recycling of transferrin receptor [22], provide a molecular hypothesis on how the APP-S655E could be promoting (as we propose) EGFR recycling. Noteworthy, OPTN was already implicated in the polarized distribution of EGFR at the plasma membrane [23].

The biological importance of APP and proEGF should be also pursued, including if APP is also able to interact with the mature EGF, and what protein domains are involved in such interactions.

There are a considerable amount of evidences showing how EGF affects APP processing, and it would be noteworthy to test how APP affects EGF. Since EGF is part of a large family of ligands, it would be interesting to also test the ability of APP to interact with other EGF family members. Data from our lab shows that APP also interacts with HB-EGF.

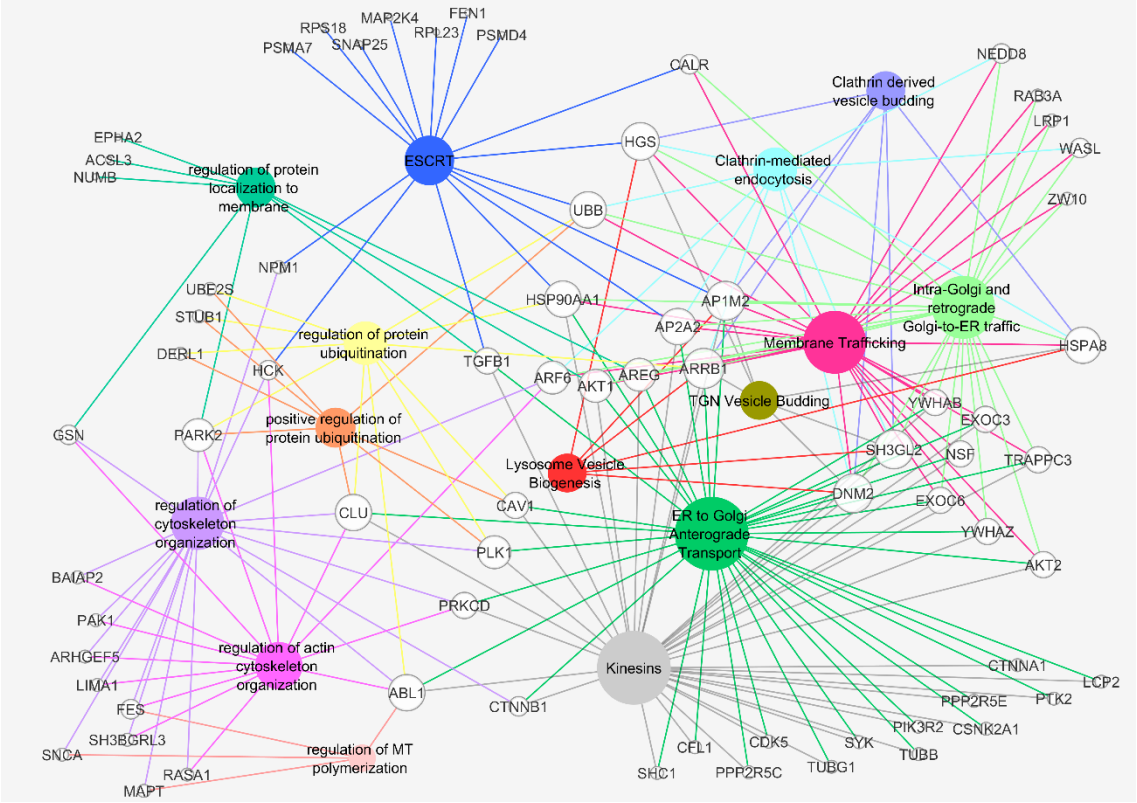

Figure C.2 - **APP and EGFR common interactors implicated in intracellular trafficking events.** Interactors shared by APP and EGFR were retrieved from the HIPPIE database (March 2017). Functional enrichment analysis was performed using the Cytoscape app ClueGO, and restricted to $p < 0.05$. Functional terms of interest to intracellular trafficking and the respective proteins were selected. Ontologies' sources included the Reactome and Gene Ontology Biological Process. Interactors are represented by their gene symbol (white nodes, grey outlined) and functions by coloured nodes. Nodes are configured by size accordingly to degree (low values to small sizes). ESCRT: Endosomal Sorting Complex Required for Transport; ER: endoplasmic-reticulum; TGN: trans-Golgi network; MT: microtubules.

Regarding ERK1/2 activation, its involvement in APP-induced neurite outgrowth must be confirmed in the presence of a specific inhibitor of the ERK1/2 pathway, like the commonly used MEK (mitogen-activated protein kinase kinase or ERK activator kinase) inhibitor and/or under knock-down conditions. It should be considered that other upstream effectors could lead to ERK1/2 activation and/or other signaling pathways could be leading to neurite outgrowth, under the APP modulation. For instance, APP has been shown to be a positive modulator of the Wnt-PCP pathway required for axonal outgrowth [24], and our lab has gathered evidences that the interaction between APP and Gαo can influence neuritogenesis via modulation of the STAT3 and ERK signaling (Dias R et al, submitted).

During this work, we have faced reproducible problems when translating SH-SY5Y differentiation studies to mice cortical primary neurons. While in SH-SY5Y cells APP seems to have a synergistic effect with the EGF-EGFR signaling to promote cell differentiation, in cortical primary cultures the combination of APP overexpression and EGF stimulation seems detrimental. We are currently analyzing data on identical studies using a different growth factor (NGF). Nevertheless, in cortical primary neurons we were able to demonstrate that APP overexpression tends to induce increases in the number of primary dendrites and dendritic branches, in a S655 phosphorylation-dependent manner. The APP-S655A overexpression was always associated with decreased neuronal differentiation parameters, while the APPWt overexpression and the phosphomimetic mutant APP-S655E presented similar neuritogenic results.

A detailed study of the endogenous APP S655 phosphorylation during neuronal differentiation events is, at this point, imperative. This is of most importance since our studies stem from APP transient overexpression using cDNAs under the control of a strong promoter, what may induce overwhelmed and dysregulated APP processing and/or localization [25], and may also affect protein folding and protein interactions [26]. Furthermore, the phosphomimetic mutants generated can only mimic to some extent the mechanism of phosphorylation, a biological process that *in vivo* most certainly occurs as dynamic cycles of phosphorylation and dephosphorylation. In addition, a phosphate group imposes to the local protein backbone two negative charges and a high electronic density, while glutamate has only one negative charge and much less valence electrons [27]. It would be important to test how APP phosphorylation levels changes in response to specific known neurogenic stimulus, for example EGF, or upon specific insults. An increased APP phosphorylation at S655 was previously detected in AD brain lysates [28], a likely result of the deregulation of the cellular phosphorylation system that has been reported to occur in AD or a result of a compensatory response. The difficulty to study endogenous APP S655 phosphorylation levels resides in the absence of a specific anti-phospho-S655 APP antibody. Our studies using the unique available commercial antibody failed due to lack of specificity in mice. Although this sequence is predicted to have high similarity between species, studies with human cell lines could be further conducted. Indeed, using the anti-phospho-S655 APP antibody in WB assays, we were able to detect increases in the signal of transfected AICD-DsRed peptides (human AICD sequence), in cells exposed to the PKC activator PDBu (data not shown). Endogenous APP S655 phosphorylation could be also pursued by quantitative mass spectrometry proteomics using for instance rodent primary neuronal cultures of different differentiation days, and tissue samples from different brain areas of different embryonic stages [29, 30]. Nevertheless, one as to expect that transduction signals like phosphorylation could operate in an acute and transient mode or could function in low levels that would fail to be detected by even the most sensitive proteomic

approaches. If such approach proved to be possible, it would be valuable to detect the levels of S655 in relation to other described APP phosphosites like T668, Y682 and Y687 [31]. An indirect approach using transgenic knock-in mice for these APP phosphomutants could also be of interest [32, 33], and would further allow *in vivo* behavior and functional studies, or other *in vitro* detailed characterizations of neuronal progenitor's proliferation, migration and differentiation. Ultimately, it would be interesting to test the neuroregenerative potential of the APPS655 phosphorylation in specific brain injury models.

App KO mice are viable and fertile indicating that APP is not essential. Only the combined KO of all the *APP* family members (*App*/*Aplp2*/*Aplp1* triple KO) or the mice haploinsufficient for *Aplp2* are lethal (during gestation period or early postnatal). Although the described phenotypes for *App* KO mice might be considered, in general, subtle, one should consider that in the human brain a lack or a dysfunction of APP might have more dramatic implications. For example, animals with higher encephalization, and more specifically humans, have more expanded subventricular zones, with higher numbers and diversity of intermediate progenitors, which in turn correlate with increased number of neurons and thicker cortical layers [34, 35]. Thus, APP can have "expanded"/specific effects in human neuronal differentiation events. Additional differences in species should also be considered. A study using species-specific genome scale microarrays to compare the protein-coding transcriptome of the aging cerebral cortex in mice, rhesus monkeys, and humans showed that a relatively small subset of age-regulated gene expression changes are conserved from mouse to man. The study also shows that age-related downregulation of neuronal genes has increased dramatically from mouse to man, and might be a particularity of humans [36]. Furthermore, humans have unique cognitive processes in which APP might be specifically involved. The effects of APP will most probable depend on the brain area/cell type and on the brain development and maturation stage. Noteworthy, completion of brain development is only accomplished around the 3rd decade of life: axon/dendrite outgrowth and synaptogenesis extend into early childhood, while the refinement of synaptic connections and dendritic pruning (and, curiously, myelination) can last until the 3rd decade of life. On the other hand, the time-course for each neuronal differentiation and maturation event, in the human brain, varies enormously by brain region [37]. In humans, the degree of vulnerability of a neuronal system seems to correlate with the degree of plasticity throughout life, and the last systems to mature - the ones associated with more advanced functions – are also among the first to degenerate in disorders such as Alzheimer's disease [38], and might represent areas where APP can be particularly important.

The molecular mechanisms of APP might include a role in RBP modulation and alternative splicing control, so important for neuronal function, and the regulation of gene transcription. It might also include modulation of intracellular signaling pathways: as a receptor, APP could trigger

signaling cascades in response to specific stimulus; or APP could be functioning as a co-receptor, e.g. for EGFR and other growth factor receptors, for integrin, or for GPCRs; APP can be a modulator of intermediate signaling cascade steps, sequestering, blocking, or enhancing different signaling players. In addition, APP might be an active player in the endocytic pathway. This last aspect is of particular interest, since it can relate well with a role in the modulation of signaling pathways, a role in neuritogenesis and neurite outgrowth (membrane trafficking events are necessary for the increase of the plasma membrane surface area), and a role in modulation of synaptogenesis and synaptic plasticity (for example the regulated addition and removal of synaptic receptors at the post-synaptic membrane influences synaptic strength).Several studies show that APP has a role in endosomal transport, and that increased gene dose for APP (associated to an increase in both APP full-length and βCTFs) leads to endosomal abnormalities and reduces the endosomal trafficking and signaling of specific cargo, namely of the nerve growth factor leading to degeneration of basal forebrain cholinergic neurons, and of the EGFR [39-42]. Furthermore, a dysfunction of the neuronal endocytic system has been identified in the earliest stages of sporadic AD, before the onset of dementia and before the formation of plaques and tangles, and in Down's syndrome [39-42].

APP studies were for long centered in Aβ production and in the amyloid cascade hypothesis as the AD origins. APP involvement in several other human diseases calls for ponderation of important physiological functions carried by APP, including in central nervous system development and function. APP has been associated, both with the trajectory of brain development in normal conditions, and with neurodevelopmental disorders (like schizophrenia, fragile x syndrome, autism) and neurodegenerative disorders associated with aging (like Alzheimer’s disease and Parkinson’s disease) [43]. Furthermore, the involvement of APP in adult neurogenesis, axonal outgrowth and dendritogenesis during neuronal regeneration after brain injury and disease, has also been pointed out [44]. The role of APP in such events most probable includes complex interactions with several other, functionally related (and probably functionally redundant), molecules. A dysregulation in the interaction networks of such molecules might be the common molecular basis of several nervous system diseases and mental disorders [45], and might particularly affect the human brain (including specific areas and/or brain circuits). It might also implicate that the treatment of such pathologies should involve rescue of an entire network of interacting molecules [46].

Concluding, with the present work we hope to have advanced the knowledge on the physiological role of APP, particularly on the functions it plays on neuronal differentiation when phosphorylated on its elusive S655 residue, and hope that this knowledge will help to assist future therapies targeting neurological diseases and injury.

References

1. Goldie, B.J., M.M. Barnett, and M.J. Cairns, *BDNF and the maturation of posttranscriptional regulatory networks in human SH-SY5Y neuroblast differentiation.* Front Cell Neurosci, 2014. **8**: p. 325.
2. Korecka, J.A., et al., *Phenotypic characterization of retinoic acid differentiated SH-SY5Y cells by transcriptional profiling.* PLoS One, 2013. **8**(5): p. e63862.
3. Pilaz, L.-J. and D.L. Silver, *Post-transcriptional regulation in corticogenesis: how RNA-binding proteins help build the brain.* Wiley Interdisciplinary Reviews: RNA, 2015. **6**(5): p. 501-515.
4. Pezzini, F., et al., *Transcriptomic Profiling Discloses Molecular and Cellular Events Related to Neuronal Differentiation in SH-SY5Y Neuroblastoma Cells.* Cell Mol Neurobiol, 2016.
5. Sutinen, E.M., et al., *Interleukin-18 alters protein expressions of neurodegenerative diseases-linked proteins in human SH-SY5Y neuron-like cells.* Front Cell Neurosci, 2014. **8**: p. 214.
6. Park, S. and J. Lee, *Proteome profile changes in SH-SY5y neuronal cells after treatment with neurotrophic factors.* J Cell Biochem, 2011. **112**(12): p. 3845-55.
7. Vieira, S., et al., *Retrieval of the Alzheimer's amyloid precursor protein from the endosome to the TGN is S655 phosphorylation state-dependent and retromer-mediated.* Molecular Neurodegeneration, 2010. **5**(1): p. 40.
8. Seaman, M.N., *The retromer complex - endosomal protein recycling and beyond.* J Cell Sci, 2012. **125**(Pt 20): p. 4693-702.
9. Chia, P.Z.C. and P.A. Gleeson, *Imaging and Quantitation Techniques for Tracking Cargo along Endosome-to-Golgi Transport Pathways.* Cells, 2013. **2**(1): p. 105-123.
10. Villaseñor, R., et al., *Regulation of EGFR signal transduction by analogue-to-digital conversion in endosomes.* eLife, 2015. **4**: p. e06156.
11. Tong, J., P. Taylor, and M.F. Moran, *Proteomic analysis of the epidermal growth factor receptor (EGFR) interactome and post-translational modifications associated with receptor endocytosis in response to EGF and stress.* Mol Cell Proteomics, 2014. **13**(7): p. 1644-58.
12. Morandell, S., et al., *Quantitative proteomics and phosphoproteomics reveal novel insights into complexity and dynamics of the EGFR signaling network.* Proteomics, 2008. **8**(21): p. 4383-401.
13. Shi, T., et al., *Conservation of protein abundance patterns reveals the regulatory architecture of the EGFR-MAPK pathway.* Sci Signal, 2016. **9**(436): p. rs6.
14. Kennedy, S.P., et al., *The Under-Appreciated Promiscuity of the Epidermal Growth Factor Receptor Family.* Frontiers in Cell and Developmental Biology, 2016. **4**(88).
15. Munter, L.M., et al., *GxxxG motifs within the amyloid precursor protein transmembrane sequence are critical for the etiology of Aβ42.* The EMBO Journal, 2007. **26**(6): p. 1702-1712.
16. Ramelot, T.A. and L.K. Nicholson, *Phosphorylation-induced structural changes in the amyloid precursor protein cytoplasmic tail detected by NMR.* Journal of Molecular Biology, 2001. **307**(3): p. 871-884.
17. Edgar, J.R., et al., *ESCRTs regulate amyloid precursor protein sorting in multivesicular bodies and intracellular amyloid-beta accumulation.* J Cell Sci, 2015. **128**(14): p. 2520-8.
18. Vaibhava, V., et al., *Optineurin mediates a negative regulation of Rab8 by the GTPase-activating protein TBC1D17.* J Cell Sci, 2012. **125**(Pt 21): p. 5026-39.
19. Sahlender, D.A., et al., *Optineurin links myosin VI to the Golgi complex and is involved in Golgi organization and exocytosis.* The Journal of Cell Biology, 2005. **169**(2): p. 285-295.
20. del Toro, D., et al., *Mutant Huntingtin Impairs Post-Golgi Trafficking to Lysosomes by Delocalizing Optineurin/Rab8 Complex from the Golgi Apparatus.* Molecular Biology of the Cell, 2009. **20**(5): p. 1478-1492.
21. Li, X., et al., *A function of huntingtin in guanine nucleotide exchange on Rab11.* Neuroreport, 2008. **19**(16): p. 1643-7.
22. Nagabhushana, A., et al., *Regulation of endocytic trafficking of transferrin receptor by optineurin and its impairment by a glaucoma-associated mutant.* BMC Cell Biology, 2010. **11**(1): p. 4.
23. Chibalina, M.V., et al., *Myosin VI and Optineurin Are Required for Polarized EGFR Delivery and Directed Migration.* Traffic (Copenhagen, Denmark), 2010. **11**(10): p. 1290-1303.
24. Soldano, A., et al., *The Drosophila homologue of the amyloid precursor protein is a conserved modulator of Wnt PCP signaling.* PLoS Biol, 2013. **11**(5): p. e1001562.
25. Villegas, C., V. Muresan, and Z. Ladescu Muresan, *Dual-tagged amyloid-beta precursor protein reveals distinct transport pathways of its N- and C-terminal fragments.* Hum Mol Genet, 2014. **23**(6): p. 1631-43.

26. Gibson, T.J., M. Seiler, and R.A. Veitia, *The transience of transient overexpression.* Nat Methods, 2013. **10**(8): p. 715-21.
27. Sieracki, N.A. and Y.A. Komarova, *Studying Cell Signal Transduction with Biomimetic Point Mutations*. Genetic Manipulation of DNA and Protein - Examples from Current Research. 2013.
28. Lee, M.-S., et al., *APP processing is regulated by cytoplasmic phosphorylation.* The Journal of Cell Biology, 2003. **163**(1): p. 83-95.
29. Dephoure, N., et al., *Mapping and analysis of phosphorylation sites: a quick guide for cell biologists.* Molecular Biology of the Cell, 2013. **24**(5): p. 535-542.
30. Veraksa, A., *Regulation of developmental processes: insights from mass spectrometry-based proteomics.* Wiley Interdiscip Rev Dev Biol, 2013. **2**(5): p. 723-34.
31. Xu, F., et al., *Simultaneous quantification of protein phosphorylation sites using liquid chromatography-tandem mass spectrometry-based targeted proteomics: a linear algebra approach for isobaric phosphopeptides.* J Proteome Res, 2014. **13**(12): p. 5452-60.
32. Barbagallo, A.P., et al., *The intracellular threonine of amyloid precursor protein that is essential for docking of Pin1 is dispensable for developmental function.* PLoS One, 2011. **6**(3): p. e18006.
33. Barbagallo, A.P., et al., *Tyr(682) in the intracellular domain of APP regulates amyloidogenic APP processing in vivo.* PLoS One, 2010. **5**(11): p. e15503.
34. Silbereis, John C., et al., *The Cellular and Molecular Landscapes of the Developing Human Central Nervous System.* Neuron. **89**(2): p. 248-268.
35. Taverna, E., M. Gotz, and W.B. Huttner, *The cell biology of neurogenesis: toward an understanding of the development and evolution of the neocortex.* Annu Rev Cell Dev Biol, 2014. **30**: p. 465-502.
36. Loerch, P.M., et al., *Evolution of the aging brain transcriptome and synaptic regulation.* PLoS One, 2008. **3**(10): p. e3329.
37. Sowell, E.R., P.M. Thompson, and A.W. Toga, *Mapping changes in the human cortex throughout the span of life.* Neuroscientist, 2004. **10**(4): p. 372-92.
38. Mesulam, M.M., *A plasticity-based theory of the pathogenesis of Alzheimer's disease.* Ann N Y Acad Sci, 2000. **924**: p. 42-52.
39. Cataldo, A.M., et al., *Down syndrome fibroblast model of Alzheimer-related endosome pathology: accelerated endocytosis promotes late endocytic defects.* Am J Pathol, 2008. **173**(2): p. 370-84.
40. Salehi, A., et al., *Increased App expression in a mouse model of Down's syndrome disrupts NGF transport and causes cholinergic neuron degeneration.* Neuron, 2006. **51**(1): p. 29-42.
41. Laifenfeld, D., et al., *Rab5 mediates an amyloid precursor protein signaling pathway that leads to apoptosis.* J Neurosci, 2007. **27**(27): p. 7141-53.
42. Kim, S., et al., *Evidence that the rab5 effector APPL1 mediates APP-betaCTF-induced dysfunction of endosomes in Down syndrome and Alzheimer's disease.* Mol Psychiatry, 2016. **21**(5): p. 707-16.
43. Westmark, C.J., *What/'s hAPPening at synapses[quest] The role of amyloid [beta]-protein precursor and [beta]-amyloid in neurological disorders.* Mol Psychiatry, 2013. **18**(4): p. 425-434.
44. Plummer, S., et al., *The Neuroprotective Properties of the Amyloid Precursor Protein Following Traumatic Brain Injury.* Aging Dis, 2016. **7**(2): p. 163-79.
45. Darby, M.M., R.H. Yolken, and S. Sabunciyan, *Consistently altered expression of gene sets in postmortem brains of individuals with major psychiatric disorders.* Transl Psychiatry, 2016. **6**: p. e890.
46. Lee, S.-A., et al., *Construction and analysis of the protein-protein interaction networks for schizophrenia, bipolar disorder, and major depression.* BMC Bioinformatics, 2011. **12**(13): p. S20.